INFORMATION TO USERS

This manuscript has been reproduced from the microfilm master. UMI films the text directly from the original or copy submitted. Thus, some thesis and dissertation copies are in typewriter face, while others may be from any type of computer printer.

The quality of this reproduction is dependent upon the quality of the copy submitted. Broken or indistinct print, colored or poor quality illustrations and photographs, print bleedthrough, substandard margins, and improper alignment can adversely affect reproduction.

In the unlikely event that the author did not send UMI a complete manuscript and there are missing pages, these will be noted. Also, if unauthorized copyright material had to be removed, a note will indicate the deletion.

Oversize materials (e.g., maps, drawings, charts) are reproduced by sectioning the original, beginning at the upper left-hand corner and continuing from left to right in equal sections with small overlaps. Each original is also photographed in one exposure and is included in reduced form at the back of the book.

Photographs included in the original manuscript have been reproduced xerographically in this copy. Higher quality 6" x 9" black and white photographic prints are available for any photographs or illustrations appearing in this copy for an additional charge. Contact UMI directly to order.

UMI®

Bell & Howell Information and Learning
300 North Zeeb Road, Ann Arbor, MI 48106-1346 USA
800-521-0600

Université d'Ottawa · University of Ottawa

DEVELOPMENT AND CHARACTERIZATION OF DENSE MEMBRANES FOR GAS SEPARATION MADE FROM HIGH MOLECULAR WEIGHT SULFONATED POLY (PHENYLENE OXIDE). EFFECT OF CASTING CONDITIONS ON THE MORPHOLOGY AND PERFORMANCE OF THE MEMBRANES

by

Boguslaw Kruczek

A thesis submitted to the School of Graduate Studies and Research
In partial fulfillment of the requirements for the
degree of
DOCTOR OF PHILOSOPHY
in the Department of Chemical Engineering
University of Ottawa

August 1998

ABSTRACT

Membrane gas separation emerged as an alternative gas separation technology 20 years ago. Since that time membranes have made many inroads in the field of gas separation. In comparison with traditional gas separation technologies like cryogenic distillation, pressure swing adsorption and absorption, membranes offer a number of advantages, including low capital and operational costs along with simplicity and flexibility of operation. On the other hand, membranes cannot compete with the traditional technologies on the basis of product purity. Improvements in this area require development and characterization of new membrane materials with better gas separation properties compared to the existing polymers.

This research was focused on the improvement of gas transport properties of poly(2,6-dimethyl-1,4-phenylene oxide) (PPO) by chemical and physical modifications of the polymer. Another objective of this work was to recognize and investigate structure/property relationships governing gas transport in polymeric membranes. The study was divided into two parts: (1) chemical modifications of PPO along with characterization of the products; (2) investigation of the effect of casting conditions.

High molecular weight PPO was sulfonated to different ion exchange capacity (*IEC*) values with chlorosulfonic acid. The resulting polymer, sulfonated PPO in the acid form (HSPPO), was further modified by substituting the proton in sulfonic groups by various metal cations including Na^+, Mg^{2+}, and Al^{3+}. Sulfonated PPO in metal form (MeSPPO) and HSPPO were used for preparation of homogeneous membranes by complete evaporation of the solvent. Some physical properties such as density, thermal stability, and x-ray diffraction as well as the gas transport properties of the membranes were determined.

Sulfonation of PPO results in a linear increase of density with *IEC* while the average d-spacing in polymer remains constant. HSPPO is not thermally stable. Sulfonic groups decompose at temperatures above 175°C. They may decompose at even lower temperatures after a longer exposure time. HSPPO membranes show a stable performance in a long-term permeation tests with CO_2 at room temperature. An increase in the *IEC* value of HSPPO results in an increase in O_2/N_2 and CO_2/CH_4 permeability ratios and a decrease in O_2 and CO_2 permeabilities. The

combination of permeability and permeability ratio, for both gas pairs, places HSPPO membranes above the respective tradeoff lines for standard commercial polymers but below the respective upper-bound lines for polymers. An increase in the *IEC* value; however, brings the permeability versus permeability ratio relationship closer to the upper bound line, especially for the O_2/N_2 gas pair.

Substitution of the proton in sulfonic groups by metal cations increases polarity and density of the polymer. In some instances, a small increase in d-spacing and X-ray diffraction is also observed. Introduction of metal cation into the polymer backbone improves its thermal stability. Despite a greater density, MeSPPO is more permeable to gases compared to the corresponding HSPPO. The increase in gas permeability depends on the *IEC* value of the polymer and the valence of the metal cation. MeSPPO with greater d-spacing and X-ray diffraction intensity compared to the original polymer shows no change or increase in O_2/N_2 and CO_2/CH_4 permeability ratios. This represents an improvement in gas transport properties of the polymer. The combination of O_2 permeability and O_2/N_2 permeability ratio of MgSPPO-1.37 and MgSPPO-1.80, places these polymers above the upper-bound line. The actual separation factors for O_2/N_2 and CO_2/CH_4 are lower than the ideal values. The maximum difference is; however, not greater than 13%. Gas transport properties of high molecular weight HSPPO and MeSPPO have never been reported.

To investigate the effect of casting conditions dense membranes were prepared using different solvents in casting solution. In addition two series of dense membranes were prepared in which solution temperature and the film casting temperature were controlled separately. The changes in gas transport properties and surface morphology observed by atomic force microscope were monitored.

The change of solvent in casting solution results in changes of more than two-fold in gas permeability and changes of up to 12% in permeability ratio of the membrane. The changes in gas transport properties are associated with significant changes in the surface morphology of the membrane. Although no direct relationship between surface morphology in the achieved resolutions and gas transport properties is observed, it is evident that very high surface roughness, resulting from the presence of large nodule aggregates, is not desirable. Membranes with such

morphologies are less selective and usually less permeable than the membranes with relatively smooth surfaces. Weak polymer-solvent interactions and high volatility of casting solution enhance high surface roughness of the membrane.

This study has also revealed some interesting relationship between the testing system and the obtained gas transport data. In particular, membranes tested in a system in which permeate side is open to atmosphere are influenced by relative humidity in the atmosphere. An increase in relative humidity in the atmosphere increases the apparent CO_2 permeability and CO_2/CH_4 permeability ratio and decreases the apparent O_2 permeability and O_2/N_2 permeability ratio. The change in gas transport properties under different relative humidities of the atmosphere was as high as 25%. The effect of relative humidity in the atmosphere on the permeation properties of membranes has never been reported.

SOMMAIRE

La séparation des gaz par membranes est devenue un moyen viable il y a 20 ans. Depuis ce temps, les membranes sont devenus populaires dans le domaine de la séparation des gaz. En comparaison avec d'autres moyens plus traditionnels, entre autres, la distillation à basse température, adsorption et absorption avec forte décompression, les membranes offrent plusieurs avantages, incluant coûts réduits de mise en chantier et d'opération suivit d'une simplicité et flexibilité d'opération. Par contre, les membranes ne peuvent pas competitionner en terme de pureté avec les technologies traditionnelles. Afin d'améliorer la situation, il faudrait developper et caractériser des nouveaux matériaux offrants une meilleure séparation des gaz à comparer avec les polymères de ce jour.

La recherche dont on fait l'objet ici visa l'amélioration des propriétés du transport des gaz du poly(2,6-diméthyl-1,4-oxide phénylique) (POP) en modifiant le polymère d'une façon chimique et physique. Un autre objectif de ce travail était de reconnaitre et étudier les relations structures/propriété gouvernant le transport des gaz à l'intérieur des membranes polymèriques. L'étude fut divisée en deux parties : (1) modification chimique de POP avec caractérisations des produits, et puis; (2) étude des effets des différentes conditions du moulage.

Du POP avec un poid moléculaire élevé fut sulfoné pour atteindre certaines valeurs de capacité d'échange d'ion différentes (CEI) utilisant l'acide chlorosulfonique. Les polymères obtenus, POP sulfoné en forme acide (HSPOP), furent additionnellement modifiés en substituant le proton dans le groupe sulfonique par des cations incluant Na^{+}, Mg^{2+}, et Al^{3+}. Le POP sulfoné sous forme métallique (MéSPOP) et (HSPOP) furent utilisés dans la préparation de membranes homogène par évaporation complète du solvant. Quelques propriétés physiques incluant la densité, la stabilité thermique et la diffraction au rayon X, avec ceux des propriétés de transport des membranes, furent déterminées.

La sulfonication du POP produit une augmentation linéaire de la densité avec le CEI, pendant que l'espace demeure constant. Le HSPOP n'est pas stable thermiquement. Le groupe sulfonique se décompose à des températures dépassants 175 °C. Il peut se decomposer à des températures plus basses après une durée de temps plus longue. Par contre, les membranes

HSPOP démontrent une performance stable durant des essaies de perméation avec le CO_2 à température ambiante. Une augmentation de la valeure de CEI a pour effet d'augmenter les rapports de perméabilité d'O_2/N_2 et CO_2/CH_4 et une réduction de la perméabilité d'O_2 et CO_2.

La combinaison de la perméabilité et du rapport de perméabilité, pour les deux paires, place les membranes HSPOP au dessus du seuil d'utilité respectif pour les polymères de base commercials et en dessous du seuil maximal respectif des polymères. Par contre, une augmentation de la valeur du CEI apporte la relation perméabilité vis à vis le rapport de perméabilité plus proche de la ligne maximale, spéciallement pour la paire de gaz O_2/N_2.

La substitution de proton du groupe sulfonique par des cations métalliques augmente la polarité et la densité du polymère. Dans quelques cas, une petite augmentation dans l'espacement d et dans la diffraction du rayon X sont aussi observés. L'introduction du cation métallique dans la structure centrale améliore la stabilité thermique. Malgré une densité plus élevé, le MéSPOP est plus perméable aux gaz comparativement au HSPOP qui lui correspond. L'augmentation de la perméabilité du gaz dépend de la valeur CEI du polymère et la valence de cation métallique. Le MéSPOP avec une plus grande espace d et plus grande diffraction du rayon X comparé au polymère original ne démontre aucun changement ou augmentation du rapport de perméabilité O_2/N_2 et CO_2/CH_4. Ceci représente une amélioration des propriétés de transport du gaz du polymère. La combinaison de la perméabilité d'O_2 et du rapport de perméabilité O_2/N_2 du MgSPOP – 1.37 et du MgSPOP – 1.80 place ces polymères au dessus de la ligne maximale. Les facteurs de séparation actuel pour le O_2/N_2 et le CO_2/CH_4 sont plus bas que les valeurs idéales. Par contre, la différence maximale n'est pas plus grand que 13%. Les propriétés de transport de gaz pour les HSPOP et MeSPOP à haut poid moléculaire n'ont jamais été rapportées.

Afin d'étudier les effets de changement des conditions sur le moulage, des membranes à haute densité furent préparées avec différents solvant dans la solution de moulage. En plus, deux séries de membranes à haute densité furent préparées avec un control séparé de la température de la solution et du moulage de la mince couche. Les changements des propriétés du transport du gaz et de la morphologie de la surface furent observés par microscope à force atomique.

Le changement du solvant dans la solution du moulage a eu comme résultat un doublage de perméabilité des gaz et une augmentation jusqu'à 12% du rapport de perméabilité de la membrane. Les changments des propriétés de transport des gaz sont associés avec des changements important de la morphologie de la surface de la membrane. Bien qu'il n'y ait pas de relation direct observé entre la morphologie de la surface à la résolution atteinte et aux propriétés de transport des gaz, il est évident qu'une rudesse très élevée de la surface résultant de la présence d'aggrégats de nodules a forte diamètre n'est pas désirable. Les membranes avec ces morphologies sont moins selectives et habituellement moins perméable que les membranes avec une surface lisse. Les intéractions faibles polymèrs-solvant et la volatilité élevée de la solution de moulage accroit la possibilité d'obtenir des membranes avec une surface très rude.

Cette étude a aussi révélée des relations intéressantes entre le système d'essaie et les données obtenues sur le transport des gaz. En particulier, les membranes testées dans un système dont la sortie est ouverte à l'atomosphère sont influencées par l'humidité relative de l'atmosphère. Une augmentation de l'humidité relative de l'atmosphère augmente la permeabilité apparente du CO_2 et de la perméabilité de rapport CO_2/CH_4 et reduit la perméabilité apparente de O_2 et du rapport de permeabilité du O_2/N_2. Le changement des propriétés du transport des gaz sous différents conditions d'humidité relative atteignèrent le 30%. Les effets de l'humidité relative de l'atmosphère sur les propriétés de perméation des membranes n'a jamais été rapportés.

Acknowledgements

The author wishes to express his gratitude to Prof. T. Matsuura for his guidance and financial assistance throughout the course of this work. The financial support of NSERC Canada is also greatly appreciated. This work would not have been completed without the encouragement, endless patience and understanding of the author's wife, Anna Kruczek. Also, this work would had never begun without the inspiration from the author's parents, late Mrs. Albina Kruczek and Mr. Michal Kruczek.

The author would like to thank to Dr. G. Chowdhury for her help and assistance at the beginning of this work, Dr. G. Facey for the H NMR analysis, Mr. R. Hartree for the X-ray diffraction spectra, Dr. Z. Y. Wang and his students Ms. J. Douglas and Mr. T. Bender for the TGA analysis, Dr. P. Handa for letting to use his laboratory and equipment for the measurements of the polymer density, and Dr. D. Mathieu for the EDX analysis.

The technical assistance and help of Mr. L. Tremblay, Mr. F. Ziroldo, and Mr. G. Nina during the course of this work is greatly appreciated. Much is owed to the colleagues from IMRI for their help and valuable discussions.

Finally, the author would like to thank Mr. S. Mortazavi for helping in correction of this thesis, Mr. L. Tremblay and Ms. A. Boucher Sharma for preparation of the French version of the abstract, and Mr. and Mrs. Kowalczyk for lending me their computer, which helped put together this thesis.

Table of Contents

List of Tables

List of Figures

Nomenclature

ABBREVIATIONS

AFM	- Atomic Force Microscope (Microscopy)
AlSPPO	- Sulfonated Poly(2,6-dimethyl-1,4-phenylene oxide) in Aluminum Form
AMU	- Atomic Mass Unit
AV	- Air Actuated Valve
Avg.	- Average
BrPPO	- Brominated poly(2,6-dimethyl-1,4-phenylene oxide)
BSV	- Bellows Sealed Valve
CP	- Constant Pressure testing system
CV	- Constant Volume testing system
CVL	- Check Valve
DMAC	- N,N-dimethylacetamide
DMF	- N,N-dimethylformamide
DS	- Degree of sulfonation $\Leftrightarrow$ degree of substitution
EDX	- Energy Dispersive X-ray spectroscopy
^{1}H NMR	- Proton Nuclear Magnetic Resonance spectroscopy
HSPPO	- Sulfonated Poly(2,6-dimethyl-1,4-phenylene oxide) in Acid Form
IEC	- Ion exchange capacity
IR	- Infrared spectroscopy
LgC	- Large Cylinder
MeSPPO	- Sulfonated Poly(2,6-dimethyl-1,4-phenylene oxide) in Metal Form
MFC	- Mass Flow Controller
MgSPPO	- Sulfonated Poly(2,6-dimethyl-1,4-phenylene oxide) in Magnesium Form
MgSPS	- Sulfonated Polystyrene in Magnesium Form
NaSPPO	- Sulfonated Poly(2,6-dimethyl-1,4-phenylene oxide) in Sodium Form
NaSPS	- Sulfonated Polystyrene in Sodium Form
NMP	- 1-methyl-2-pyrrolidinone
P	- Rotary Vacuum Pump
PPO	- Poly(2,6-dimethyl-1,4-phenylene oxide)
PSS	- Sulfonated Polystyrene
PT	- Pressure Transducer
RGA	- Residual Gas Analyzer
RH	- Relative Humidity
SEM	- Scanning Electron Microscopy
SmC	- Small Cylinder

St.Dev. - Standard Deviation
STP - Standard Temperature and Pressure conditions
SPPO - Sulfonated Poly(2,6-dimethyl-1,4-phenylene oxide)
SPPO-XX - Sulfonated Poly(2,6-dimethyl-1,4-phenylene oxide) of *IEC* equal to XX
SR - Silicone Rubber
TCE - Trichloroethylene
TEM - Transmission Electron Microscopy
TGA - Thermogravimetric Analysis
THF - Tetrahydrofuran
TM AFM - Tapping Mode Atomic Force Microscope (Microscopy)
TP - Turbo Pump

SYMBOLS

a - constant in Mark-Houwink equation (Eq.6.1) ....[-]
A - permeation area of the membrane..... .....[cm^2]
A_{12} - difference between solubility parameters in polar systems ....[$Mpa^{1/2}$]
A_π - pre-exponential permachor permeability constant ....[Barrer[a]]
A_p - pre-exponential permeability constant in Eq.(2.22)..... .....[Barrer]
b - hole affinity constant .....[$cmHg^{-1}$]
B_p - constant in Eq.(2.22) ....[$kg\ m^{-3}$]
c - concentration of polymer solution ....[$g\ dL^{-1}$]
C - concentration of gas in polymer ....[$cm^3(STP)\ cm^{-3}$]
C_D - concentration of gas in the Henry sites of polymer..... .....[$cm^3(STP)\ cm^{-3}$]
CED - cohesive energy density ....[$J\ cm^{-3}$]
C_H - concentration of gas in the Langmuir sites of polymer .....[$cm^3(STP)\ cm^{-3}$]
C'_H - hole saturation constant .....[$cm^3(STP)\ cm^{-3}$]
d -d-spacing ....[Å]
d_n - average diameter of nodules ....[nm]
d_N - average diameter of nodule aggregates ....[nm]
D - diffusion coefficient ....[$cm^2\ s^{-1}$]
D_{eff} - effective diffusion coefficient ....[$cm^2\ s^{-1}$]
D_k - kinetic diameter of gas molecule ....[m]
D_o - pre-exponential diffusion coefficient ....[$cm^2\ s^{-1}$]
DS - degree of sulfonation ....[-]
ΔE - energy of vaporization ....[$J\ mol^{-1}$]
ΔG_m - Gibbs free energy of mixing ....[$J\ mol^{-1}$]
ΔH_m - enthalpy change on mixing ....[$J\ mol^{-1}$]

[a] 1 Barrer = 10^{-10} cm^3(STP) cm cm^{-2} s^{-1} $cmHg^{-1}$

Δp - pressure gradient across the membrane ..... [cmHg]

ΔS_m - entropy change on mixing ..... [J $mol^{-1}K^{-1}$]

$E_{coh,i}$ - structural component for the cohesive energy density ..... [J mol^{-1}]

E_d - activation energy ..... [J mol^{-1}]

E_h - structural component for the hydrogen bonding force..... [J mol^{-1}]

f - average jumping frequency of gas molecule ..... [s^{-1}]

F - permeation flux ..... [cm^3(STP) cm^{-2} s^{-1} $cmHg^{-1}$]

$F_{d,i}$ - structural component for the dispersion force ..... [J $cm^{3/2}$ mol^{-1}]

FFV - fractional free volume..... [-]

$F_{p,i}$ - structural component for the dipole force ..... [J $cm^{3/2}$ mol^{-1}]

h_{avg} - average peak height ..... [nm]

I_i - intensity of peak i on ^{1}H NMR spectrum ..... [-]

IEC - ion exchange capacity ..... [meq g^{-1}]

l - membrane thickness ..... [cm]

l_{12} - parameter characterizing intermolecular forces ..... [-]

K - capillary constant ..... [cSt s^{-1}]

K' - constant in Mark-Houwink equation (Eq.6.1) ..... [dL g^{-1}]

m - mass of dry polymer ..... [g]

M - molecular weight ..... [g mol^{-1}]

p - pressure ..... [cmHg =1.33 kPa]

P - permeability ..... [Barrer]

PI - partial immobilization coefficient ..... [-]

P_V - vapor pressure ..... [kPa]

r - pore radius..... [m]

R - universal gas constant ..... [J mol^{-1} K^{-1}]

R_a - mean Z value (mean roughness) ..... [nm]

R_m - resistance of the membrane ..... [cmHg s cm^{-3}(STP)]

R_q - root mean square of z values ..... [nm]

R_z - mean difference between 5 highest peaks and 5 lowest valleys . ..... [nm]

s_p - permachor permeability constant ..... [-]

S - solubility ..... [cm^3(STP) cm^{-3} $cmHg^{-1}$]

SFV - specific free volume ..... [m^3 kg^{-1}]

t - efflux time ..... [s]

T - temperature ..... [K]

T_c - critical temperature ..... [K]

$T_{casting}$ - casting temperature ..... [°C]

T_g - glass transition temperature ..... [°C]

T_{NBP} - normal boiling point ..... [°C]

v - volume of 0.1 N standard solution of HCl ..... [cm^3]

v_{STP} - volume of one mole of gas at STP conditions ..... [cm^3 mol^{-1}]

V - molar volume ..... [m^3 mol^{-1}]

V_f - free volume ..... [m^3 mol^{-1}]

V_o - volume occupied by polymer chains ..... [m^3 mol^{-1}]

V_p - volume of the permeate side ..... [cm^3]
V_W - van der Waals volume ..... [$m^3\ mol^{-1}$]
W_o - weight of polymer sample in air ..... [g]
W_1 - weight of polymer sample in water ..... [g]

GREEK SYMBOLS

$\alpha.$ - actual separation factor..... [-]
α_D - diffusivity selectivity..... [-]
α_o - ideal separation factor ⇔ permeability ratio ⇔ permselectivity. ..... [-]
α_S - solubility selectivity..... [-]
β - van der Waals volume constant depending on group *k* ..... [-]
χ - Flory-Huggins interaction parameter ..... [-]
χ_H - enthalpic component of the Flory-Huggins interaction parameter .. .. [-]
χ_S - entropic term of the Flory-Huggins interaction parameter..... [-]
δ - Hildebrand solubility parameter ..... [$Mpa^{1/2}$]
δ_d - dispersion force component of the solubility parameter ..... [$Mpa^{1/2}$]
δ_h - hydrogen bonding component of the solubility parameter ..... [$Mpa^{1/2}$]
δ_p - dipole component of the solubility parameter ..... [$Mpa^{1/2}$]
δ_t - total solubility parameter ..... [$Mpa^{1/2}$]
Δ - difference between Hildebrand solubility parameters ..... [$Mpa^{1/2}$]
Δ' - difference between Hansen solubility parameters ..... [$Mpa^{1/2}$]
θ - time lag ..... [s]
Φ - volume fraction ..... [-]
γ_{nk} - empirical factor depending on gas *n* and group *k* ..... [-]
λ - mean free path of gas molecule..... [m]
λ_d - length of diffusional jump of gas particle..... [m]
λ_X - wavelength of X-rays ..... [Å]
η - absolute viscosity ..... [$cP = 10^{-3}\ kg\ m^{-1}\ s^{-1}$]
η_{red} - reduced viscosity ..... [$dL\ g^{-1}$]
η_{rel} - relative viscosity ..... [-]
η_{sp} - specific viscosity ..... [-]
$[\eta]$ - intrinsic viscosity ..... [$dL\ g^{-1}$]
ν - kinematic viscosity ..... [$cSt = 10^{-6}\ m^2\ s^{-1}$]
π -polymer permachor value ..... [-]
υ - constant in Koningsveld equation, Eq. (4.15) ..... [K]
ω - constant in Koningsveld equation, Eq. (4.15) ..... [K^{-1}]
ψ - constant in Koningsveld equation, Eq. (4.15) ..... [K^{-1}]
ρ - density ..... [$g\ cm^{-3}$]

CHAPTER 1

Introduction

1.1 Motivation

Development of new chemical processes and increasing concerns about a clean environment increase the demand for gas separation. Today, gas separation is needed not only in large-scale chemical processes but also in a variety of small-scale operations. Traditional, well-developed technologies like cryogenic distillation, pressure-swing adsorption, and absorption are not always economically attractive in small-scale applications where capital cost, space, simplicity of operation, and power consumption are of concern. This opens an excellent opportunity for gas separation membranes [Prasad, 1994].

The concept of gas separation by permeation through polymeric membranes has been known for more than 160 years. It is; however, only during the last 20 years that the use of polymeric membranes has emerged as a new gas separation technique. Current membrane processes for gas separation include separation of N_2 from air, recovery of H_2 from NH_3 and CH_3OH purge gas, recovery of H_2 from refinery and petrochemical streams, separation of CO_2 from hydrocarbons in enhanced oil recovery operations, and separation of CO_2 and H_2S from natural gas. The development and potential applications of gas separation membranes include the removal of organic vapors from air, dehydration of air and natural gas, upgrading of low quality natural gas and landfill gas, desulfurization of flue gas, and separation of olefins from alkanes [Stern, 1994].

The future of membranes as an alternative gas separation technology strongly depends on the development of new membrane materials and advances in membrane formation. As pointed out by Kesting and Fritzsche (1993), until recently it was believed that permeability and

selectivity of gas separation membranes were invariably coupled, and that one could only be increased at the expense of the other. If it were true, the future of polymeric gas separation membranes would have been questionable.

The 1990's proved that it is possible to decouple permeability from selectivity. Koros and Fleming (1993) in their review paper demonstrated that tailoring the chemical structure of polymers allows improving permeability and selectivity simultaneously. On the other hand, Kesting *et al.* (1990a) demonstrated on the example of polysulfone hollow fiber membranes, that the same effect can be achieved by optimizing the physical structure of polymer (micropore size, rigidity and selective layer anisotropicity).

There were two major motivations for this research. The first motivation was improvement of gas transport properties of polymeric membranes by chemical modification of commercially available polymers. Chemical modification of commercially available polymers is easier than synthesizing entirely new polymers. The base polymer chosen in this study was poly(2,6-dimethyl-1,4-phenylene oxide) (PPO). The choice of PPO as a base polymer was dictated by its properties. Homogeneous membranes made from modified PPO were characterized.

It is generally believed in the membrane community that the properties of homogeneous membranes are entirely governed by the chemical structure of polymer. This is despite some literature evidence showing that the properties of homogeneous membranes depend on casting conditions. Consequently, the importance of the optimization of the physical structure of polymer has only been recognized in case of asymmetric membranes. The second motivation for this research was; therefore, to challenge the belief that the properties of homogeneous films are entirely governed by the chemical properties of polymer.

1.2 Scope of the Research

This research project consists of two major parts. The first part is focused on the chemical modification of high molecular weight PPO, which is a material known for its high permeability and low selectivity for gas separation. Improvement of the gas selectivity of PPO has been attempted by the aryl sulfonation of the polymer. The resulting polymer, sulfonated PPO in

protonated form (HSPPO), has been further modified by substituting the proton in sulfonic groups by various metal cations including Na^+, Mg^{2+}, Al^{3+}. Some physical properties along with gas transport properties of HSPPO and sulfonated PPO in metal form (MeSPPO) have been determined.

The second part of this study is focused on the effect of the solvent in the casting solution on the properties of membranes prepared by complete evaporation of the solvent. Assuming that the volatility of polymer solution and polymer-solvent interactions are the two dominating parameters governing the physical properties of homogeneous films, it has been attempted to decouple the effect of these parameters by changing the temperature of casting solution (solution temperature) and the temperature at which the films were cast (casting temperature). The effects of these parameters have been monitored by following the changes in gas transport properties and surface morphology of the membranes. Surface morphology was characterized using atomic force microscopy (AFM).

1.3 Objectives

The general objectives of this work were:

- To improve gas transport properties of PPO by aryl sulfonation and introduction of various metal cations into the polymer backbone.
- To investigate relationships between the type of modification and the gas transport and physical properties of modified PPO.
- To evaluate the effect of the solvent in the casting solution on the properties of homogeneous membranes.
- To decouple the effect of volatility of casting solution from the effect of polymer-solvent interactions.
- To develop a phenomenological relationship between surface morphology and gas transport properties of homogeneous membranes prepared from modified PPO.

These general objectives were achieved by fulfilling the following specific objectives which were:

- To modify high molecular weight PPO by sulfonation of the polymer by chlorosulfonic acid and subsequent conversion of the polymer into various metal forms.
- To characterize the sulfonated PPO by acid-base titration, proton nuclear magnetic resonance, infrared spectroscopy, density, thermal stability, and x-ray diffraction.
- To compare various methods for characterization of polymer-solvent interactions in polymer solutions.
- To prepare membranes by complete evaporation of the solvent using different solvents and different casting and solution temperatures.
- To implement atomic force microscopy for evaluation of surface morphology of the membranes.
- To characterize gas transport properties of the membranes by determination of pure gas permeabilities, permeability ratios, and the actual separation factors.

1.4 Organization of the Thesis

The thesis is divided into four parts. The literature review is presented in the first part. The literature review is divided into three chapters. The first chapter of the literature review focuses on the structure of polymeric membranes, transport mechanisms, and correlations for permeability prediction. The second chapter summarizes properties of PPO and PPO-based polymers. The third chapter provides an overview of the effect of casting parameters important in the preparation of homogeneous membranes and background on the application of atomic force microscopy in studies of surface morphology of polymeric membranes. The second part presents the reasoning, as well as details, of the experimental procedures and analytical techniques used in the study. In the third part, the results of the study are presented and discussed. The third part is divided into four chapters. The first two chapters are focused on the results pertaining to the chemical modification of PPO. The other two chapters present data on the effect of casting parameters. The fourth part consists of the conclusions and recommendations for future research along with list of contributions made, as a result of this work, to the fields of membrane science

and technology, polymer science, and chemical engineering. The additional results as well as details of some procedures employed in this study are presented in several appendices.

PART I

Literature Review

CHAPTER 2

Gas Transport in Polymeric Membranes

2.1 Structure of Polymeric Membranes

There are five mechanical states in which macromolecules can exist. In the order of increasing density these are liquid, rubber, leather, glass, and crystalline [Meares, 1965]. The lower the density of polymer, the greater the free volume. The free volume represents micropores available for polymer segment jumps and gas diffusion. In the case of liquids, rubbers and leathers, chain segments have sufficient mobility to undergo Brownian jumps. Consequently the micropores will be transient in nature, that is, their size and size distribution will change with time, temperature and pressure. Segmental mobility is much less pronounced in glassy and crystalline mechanical states where viscosity is essentially infinite [Kesting and Fritzsche, 1993].

For practical gas separation membranes only rubbery and glassy polymers have been considered. Rubbery polymers are particularly attractive for the separations involving condensable vapors. On the other hand, glassy polymers offer the best combination of gas permeability and gas selectivity [Kesting and Fritzsche, 1993]. Both rubbery and glassy polymers are amorphous. The latter; however, may exhibit some structural order. The existence of order in glassy polymer is indicated by the ratio of amorphous density to crystalline density. Robertson (1965) calculated that for completely amorphous polymer this ratio should be approximately 0.65. For most glassy polymers; however, this ratio ranges from 0.8 to 1.0.

Development of microscopic techniques allows direct observation of the membrane morphology. Using scanning electron microscopy Schultz and Asunmaa (1970) observed spherical particles in the surface of cellulose acetate reverse osmosis membranes. Similar spherical particles were observed on the surface of other glassy polymers. Kamide and Manabe (1985) presented evidence that nodules subsequently agglomerate into larger secondary particles. Further association of secondary particles leads ultimately to the formation of open cells.

Kesting (1990) proposed the four-tiers of structure of polymeric membranes, which systemized the observation of the surface morphology. The first tier of structure is formed by 2-5 Å intermolecular chain segment displacements in nodule interior. Macromolecules agglomerate to form nodules. The second tier of structure is formed by 3-10 Å holes in low-density regions between the nodules. The first and the second tiers of structure govern gas permeation through polymeric membranes. Nodules further agglomerate to form nodule aggregates, which correspond to secondary particles observed by Kamide and Manabe (1985). Interstices between incompletely coalesced nodule aggregates ranging from 10 to 200 Å represent the third tier of structure. The fourth tier of structure is formed by aggregates of nodule aggregates also called supernodular aggregates. The supernodular aggregates form sponge- or foamlike structures with μm-sized apertures (pores) between open cells [Kesting, 1990].

2.2 Mechanisms of Membrane-Based Gas Separation

According to Koros and Fleming (1993), gas separation through membranes is based on one of three general transport mechanisms: Knudsen-diffusion, solution-diffusion and molecular sieving. Schematic representation of these mechanisms is shown in Figure 2-1.

Permeation of gas through porous membranes, which is shown in Figure 2-1a, is governed by Knudsen-diffusion. This mechanism of gas permeation is applicable to microfiltration and ultrafiltration membranes where supernodular aggregates and interstices between nodule aggregates form pores. For a binary gas mixture the ideal selectivity (α_o) in Knudsen-diffusion is given by

$$\alpha_o = \left[\frac{M_A}{M_B}\right]^{1/2} \tag{2.1}$$

where M_A and M_B are the molecular weights of component A and B, respectively. It is clear from Eq. (2.1) that Knudsen diffusion does not offer attractive separation factors, especially for gases of comparable molecular weights. When the Poiseiulle flow represents a significant fraction of the total gas permeation through the porous membrane, the actual separation factor is lower than the ideal selectivity calculated by Eq. (2.1). In the Poiseuille flow, movement of each species in a gas mixture is coupled with all other species present. No separation is; therefore, possible [Uhlhorn *et al.*, 1989].

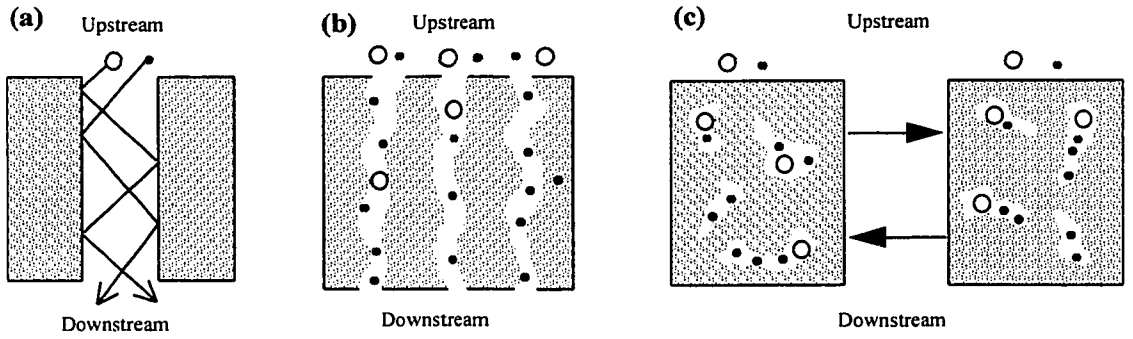

Figure 2-1. Mechanisms of membrane-based gas separation; (a) Knudsen flow; (b) molecular sieving; (c) solution-diffusion.

The proportions of Knudsen diffusion to Poiseuille flow are governed by the ratio of the pore radius (r) to the mean free path (λ) for the gas molecules. The mean free path is given by

$$\lambda = \frac{3\eta}{2p}\left(\frac{\pi RT}{2M}\right)^{1/2} \tag{2.2}$$

where p is the pressure, η is the viscosity of the gas, T is the temperature, R is the universal gas constant and M is the molecular weight of the gas. When r/λ is much less than 1, Knudsen diffusion is dominant. However, when r/λ becomes larger than 1 Poiseuille flow becomes dominant [Uhlhorn *et al.*, 1989].

Molecular sieving separation occurs through microporous materials with pores of diameter of less than 7 Å [Koros and Fleming, 1993]. The molecular sieving is based on the principle that a penetrant molecule smaller than a membrane pore can pass through the membrane while a penetrant molecule larger than a pore cannot. If the size of penetrants is similar, for example in case of O_2/N_2 separation, the difference in affinity to the membrane is

also an important factor. According to the four tier-structure proposed by Kesting (1990), gas permeation through the pores formed by interchain displacements and the holes in the low density regions between nodules should be governed by the mechanism shown in Figure 2-1b. Surprisingly, this mechanism is only recognized for carbon molecular sieves and glass hollow fiber membranes [Koros and Fleming, 1993].

The mechanism of gas transport through practical polymeric gas separation membranes is exclusively described by the solution-diffusion mechanism shown in Figure 2-1c. Effective solution-diffusion polymeric membranes have no continuous passages but rely upon thermally agitated motion of chain segments comprising polymer matrix to generate penetrant-scale transient gaps in the matrix, thereby allowing diffusion from the upstream to the downstream face of the membrane [Koros and Hellums, 1989]. Solution-diffusion separation is based on both solubility and mobility factors. Solubility selectivity favors the most condensable molecule, while mobility selectivity favors the smallest molecule.

The assumption that polymeric gas separation membranes have no continuous passages is justified for rubbery polymers and glassy polymers with low glass transition temperature (T_g). In case of rigid glassy polymers, particularly those with high T_g, a gas separation model should incorporate the concept of fixed micropores [Kesting and Fritzsche, 1993]. Moreover, in the related field of reverse osmosis, pore theory developed by Sourirajan has been successfully applied to describe performance of reverse osmosis membranes made of glassy polymers [Sourirajan, 1977; Sourirajan and Matsuura, 1985, Sourirajan, 1992]. Dismissal of the existence of pores in gas separation membranes leads to a simplified concept of intrinsic permeability and selectivity for a given polymer [Kesting and Fritzsche, 1993]. On the other hand, the solution-diffusion model with the modifications made by Petropoulos (1970) and Paul and Koros (1976) has been successfully applied to describe gas separation in various glassy polymers [Stern, 1994]. The details of the solution-diffusion model are presented in the following sections.

2.3 Gas Separation by Solution-Diffusion Mechanism

Permeability (P), which is the pressure-and-thickness-normalized flux, provides the overall measure of the ease of transporting a gas through the material. In the solution-diffusion

model, permeability is a fundamental property of the polymeric material. Permeability can be written as a product of a thermodynamic factor, S, called the solubility coefficient, and a kinetic parameter, D, called diffusion coefficient [Koros and Fleming, 1993]

$$P = SD . \tag{2.3}$$

Consequently, in the solution-diffusion model the ideal selectivity (α_o), which is the ratio of permeabilities of species A and B, can be written as a product of solubility selectivity (α_S) and diffusivity selectivity (α_D)

$$\alpha_o = \frac{P_A}{P_B} = \frac{S_A}{S_B}\frac{D_A}{D_B} = \alpha_S \alpha_D . \tag{2.4}$$

The coefficients in Eqs. (2.3) and (2.4) can themselves be complex functions of many variables. These coefficients are discussed in greater detail in the following subsections.

2.3.1 Solubility of gases in polymers

2.3.1.1 Rubbery polymers

Solubility of gases in polymer above T_g is well described by Henry's law

$$C = Sp \tag{2.5}$$

where C is the concentration of gas in polymer, S is the Henry's solubility constant for the polymer-gas pair, and p is the penetrant gas pressure, *i.e.*, partial pressure. The gas concentration in the polymer is linear to the external partial pressure. Both positive and negative deviations from this relationship have been observed at high pressure [Kesting and Fritzsche, 1993].

2.3.1.2 Glassy polymers

Sorption isotherms in glassy polymers are convex to the pressure axis. The deviation from the Henry's law in case of gas sorption in glassy polymers provides the basis for the dual mode sorption theory.

The dual mode sorption theory postulates the existence of two types of sorption sites in glassy polymers. One accommodates mobile gas molecules following Henry's law. The other sorption sites, Lagnmuir sites, are unique to the glassy polymers arising from the abrupt change in slope of the specific volume versus temperature curve as the T_g is traversed. The Langmuir

sorption sites are associated with microvoids or excess free volume formed from intersegmental packing defects. The penetrant molecules sorbed in the Langmuir sites are much less mobile than those in the Henry's law sorption sites [Kesting and Fritzsche, 1993].

Sorption of gases in glassy polymer is given by the following equation:

$$C = C_D + C_H = Sp + \frac{C_H' bp}{1 + bp} \tag{2.6}$$

where C_D is the concentration in the Henry type-sites, C_H is the concentration in the Langmuir sites, b is the hole affinity constant, and C_H' is the hole saturation constant. The variables C, S, and p were already defined. At low pressures when bp is much less than 1, Eq. (2.6) reduces to the linear expression consistent with modified Henry-like behavior

$$C = (S + C_H' b)p. \tag{2.7}$$

At sufficiently high pressures when bp is much greater than 1, additional penetrant can no longer be accommodated in the Langmuir sorption sites. The Langmuir sorption sites reach the saturation limit and the Eq. (2.6) further reduces to the linear form

$$C = Sp + C_H' \tag{2.8}$$

Total solubility of gases in glassy polymers is higher than that in rubbers, which is consistent with the existence of additional sorption sites in these polymers [Kesting and Fritzsche, 1993]. In the absence of groups that specifically attract a given penetrant, the solubility in a polymer is largely determined by condensibility of the penetrant. The critical temperature of a gas is a good indicator of its condensibility [Koros and Fleming, 1993].

2.3.2 Diffusion of gases in polymers

The movement of polymer segments and subsegments can be visualized as a rapidly flickering picture (Figure 2-1c). Exchanges between subtly different conformations occur over a characteristic time scale governed by the intrinsic rigidity of the polymer, intersegmental attractions, and temperature. The free space shown in Figure 2-1c is mobile, and exists as more or less disconnected pockets. The flickering process of the polymer is responsible for activated penetrant jumps [Koros and Fleming, 1993].

The diffusion coefficient shows an Arrhenius dependence on temperature

$$D = D_o \exp\left(\frac{-E_d}{RT}\right) \tag{2.9}$$

where D_o is a pre-exponential factor and E_d is activation energy. The activation energy can be interpreted as the energy required to open a path between pockets of free volume on Figure 2-1c. Meares (1965) proposed that

$$E_d = \frac{\pi \lambda_d D_k^2 CED}{4} \tag{2.10}$$

where CED is the cohesive energy density of the polymer, D_k is the kinetic diameter of penetrant, and λ_d is the jump length.

2.3.2.1 Rubbery polymers

Fick's first law of diffusion normally describes gaseous diffusion through rubbery polymers

$$F = -D\left(\frac{dC_D}{dx}\right) \tag{2.11}$$

where F is the permeation flux, D is the diffusion coefficient, C_D is the local concentration of gas in the membrane and x is the coordinate direction of permeation in the membrane. The diffusion coefficient of a penetrant in the membrane matrix can be written in terms of the average jump length (λ_d) and the average jumping frequency (f) as

$$D = \frac{f\lambda_d^2}{6} \tag{2.12}$$

The diffusion coefficient can be determined by measuring the "time lag" for the pressure increase on the low pressure side of the membrane after a high pressure has been applied to its other side. The time lag is related to the time required by the gas to establish a state of equilibrium in the degassed membrane and is given by

$$\theta = \frac{l^2}{6D} \tag{2.13}$$

where θ is the time lag, l is the membrane thickness. The time lag is found by extrapolating the linear portion of the pressure versus time curve to the time axis after the steady state permeation rate of the gas through the membrane has been reached [Kesting and Fritzsche, 1993].

The large-scale motions in rubbery polymers render them unable to produce sufficiently subtle size selective transient gaps. Hence, in the absence of extreme solubility selectivity, rubbery matrices are unable to provide high separation factors [Koros and Fleming, 1993].

2.3.2.2 Glassy polymers

Vieth and Sladek (1965) developed a model for kinetic diffusion of gases in glassy polymers on the basis of the dual sorption theory. They assumed that the penetrant sorbed in Langmuir sites does not contribute to the diffusive flux and; therefore, the diffusive flux is determined by the diffusion of the penetrant sorbed in Henry's sorption sites. There is a local equilibrium between mobile and immobilized species throughout the polymer. They also assumed that the diffusive flux is driven by the concentration gradient, and the diffusion coefficient is constant and independent of concentration or position in the membrane. With these assumptions the continuity equation for gas can be written as

$$D\frac{d^2C_D}{dx^2} = \frac{dC_D}{dt}\left[1 + \frac{C_H' \dfrac{b}{S}}{(1+bp)^2}\right]. \tag{2.14}$$

At very high pressures, $bp >> 1$, the second term in square bracket approaches zero. Equation (2.14), hence reduces to the Fick's second law of diffusion

$$D\frac{d^2C_D}{dx^2} = \frac{dC_D}{dt}. \tag{2.15}$$

At very low pressures, $bp << 1$, the denominator in the square bracket approaches unity. Dividing both sides of the Eq. (2.14) by the term in the square bracket yields

$$\left(\frac{D}{1+\dfrac{C_H' b}{S}}\right)\frac{d^2C_D}{dx^2} = \frac{dC_D}{dt}. \tag{2.16}$$

Defining

$$D_{eff} = \frac{D}{1+\dfrac{C_H' b}{S}}. \tag{2.17}$$

Eq. (2.16) can be expressed in a modified form of Fick's second law of

$$D_{eff}\frac{d^2C_D}{dx^2}=\frac{dC_D}{dt}. \tag{2.18}$$

In the limiting case of low pressure, the experimentally measured diffusion (D_{eff}) is reduced by the factor $1/(1+C'_H\, b/S)$ compared to the true diffusion coefficient (D). In other words, the attainment of sorption equilibrium is delayed by the immobilization process, which reduces the number of penetrant molecules in the diffusing species [Michaels *et al.*, 1963].

Petropoulos (1970), who allowed for partial immobilization of penetrant in Langmuir sorption sites, modified the above model for kinetic diffusion of gases in glassy polymers. The partial immobilization model, also referred to as the dual mobility model, accounts for two distinct molecular environments with different inherent mobilities D_D and D_H, where D_D and D_H are the diffusivity coefficients in Henry and Langmuir environments, respectively. Both coefficients are assumed to be independent of pressure [Petropoulos, 1970].

Paul and Koros (1976) modified the partial immobilization model. They assumed that the total gas concentration can be divided into a mobile part with a diffusion coefficient D and concentration C_m and the remainder, C - C_m, which is totally immobilized. The mobile part of the gas comprises all penetrant molecules sorbed in the Henry sorption sites and a fraction (PI) of penetrant molecules sorbed in the Langmuir sorption sites. The model developed by Paul and Koros reduces in one limit to the total immobilization model ($PI = 0$) and in the other limit to a situation with a linear isotherm with no distinction between sorption mechanism or transport behavior for any of the sorbed gases [Paul and Koros, 1976].

In the case of partial immobilization ($0< PI < 1$) the diffusion coefficient can not be determined by the time lag method, because both the time lag and permeability depend on pressure. Similarly, in case of complete immobilization ($PI = 0$), the diffusivity coefficient depends on pressure. Only when there is no immobilization ($PI = 1$), the diffusivity coefficient is constant. Permeability; however, depends on pressure [Paul and Koros, 1976].

2.4 Correlations for Prediction of Gas Permeability

A number of methods have been proposed for correlating permeability to different structural or physical properties of polymers and the penetrant gases. In general, the correlations can be divided into two groups. The first group includes the correlations for directly predicting

the permeability of gases in polymers. The second type of correlations provides prediction of solubility and diffusivity coefficients in polymers.

2.4.1 Direct estimation of permeability

Salame (1986) proposed that permeability of polymers could be predicted by a group contribution method. He assigned numerical values, called segmental "permachor" values, to various functional groups forming the backbone and side chains of a number of polymers. The segmental permachor values are obtained from correlations of the structure of different polymers with their cohesive energy density (*CED*) and fractional free volume (*FFV*). The fractional free volume is defined as a ratio of free volume (V_f) to the total volume (V) of polymer

$$FFV = \frac{V_f}{V} = \frac{V - V_o}{V}. \tag{2.19}$$

The area of white pockets represents the free volume in Figure 2-1c, while the area of the square represents the total volume. The difference between V and V_f represents the volume (V_o) occupied by polymer chains. All volume terms in Eq. (2.19) can be expressed in units of m^3/mol.

A polymer permachor (π) is calculated from the relation

$$\pi = \sum \frac{\pi_i}{n} \tag{2.20}$$

where π_i are the individual segmental permachor values, and n is the number of permachor values used. The permeability (P) for a gas/polymer system is then predicted from the relation

$$P = A_\pi \exp(-s_p \pi) \tag{2.21}$$

where A_π and s_p are constants which depend on the nature of the permeation gas [Salame, 1986].

Lee (1980) proposed another correlation

$$P = A_p \exp\left(\frac{-B_p}{SFV}\right) \tag{2.22}$$

where A_p and B_p are characteristic constants which are independent of the penetrant concentration and temperature. *SFV* is the specific free volume that is defined as

$$SFV = \frac{V - V_o}{M} \tag{2.23}$$

where M is the molecular weight of the polymer repeat unit. Other investigators used *FFV* in Eq. (2.22) instead of *SFV* [Stern, 1994]. The agreement between the values of permeability

determined from Eq. (2.22) and the experimental values is fair at high values of permeability, that is, for rubbery polymers. For glassy polymers the experimental data scatter considerably from the correlation [Stern, 1994].

Recently, Park and Paul (1997) proposed a correlation analogous to the Eq. (2.22) based on *FFV* of polymer. They considered that different penetrant species see different free volume (V_f) in a given polymer. This is justified because the size and the structure of the gas molecule may influence the amount of space the molecule can access inside the polymer. Consequently *FFV* depends not only on the polymer structure but also on the permeating gas. The model proposed by Park and Paul allows predicting *FFV* by predicting the total volume of polymer (V) and the volume occupied by polymer chains (V_o) by the group contribution method

$$V = \sum_{k=1}^{K} \beta_k (V_W)_k \tag{2.24}$$

and

$$(V_o)_n = \sum_{k=1}^{K} \gamma_{nk} (V_W)_k \tag{2.25}$$

where β_k is the constant depending on group k, $(V_w)_k$ is the van der Waals volume for group k, and γ_{nk} is the empirical factor depending on gas n and group k. The values of constants in the above equations were determined by analyzing 105 glassy polymers of known density and permeability for different gases [Park and Paul, 1997].

2.4.2 Prediction of solubility and diffusivity coefficients

The major advantage of the correlations discussed in the previous section is their simplicity. These correlations; however, neglect the complexity of gas transport in polymeric membranes. The models predicting solubility and diffusivity in a gas/polymer system separately address this issue.

An example of such model is given by correlations for the diffusion and solubility coefficients proposed by Teplyakov and Meares (1990). The diffusion coefficient is predicted by

$$\log D = K_1 - K_2 d_{eff}^2 \tag{2.26}$$

where K_1 and K_2 are the constants that depend on the nature of the polymer, and d_{eff} is the effective molecular diameter of the penetrant. Values of K_1 and K_2 for various polymers, as well

as of d_{eff} at temperatures above and below T_g for a large number of gases are provided by Teplyakov and Meares (1990).

The solubility coefficient is predicted by

$$\log S = K_3 + K_4(\varepsilon / k) \tag{2.27}$$

where K_3 and K_4 also depend on the nature of the polymer, and ε/k is the Lennard-Jones energy parameter of the penetrant gas. Values of K_3 and K_4 for polymers and copolymers, and values of ε/k for many gases were also provided by Teplyakov and Meares (1990). Combining Eqs. (2.26) and (2.27) permeability for a gas/ polymer system is given

$$\log P = K_1 + K_3 - K_2 d_{eff}^2 + K_4(\varepsilon / k) \tag{2.28}$$

The Eqs. (2.26)-(2.28) have not been tested with a sufficient number of experimental data to permit an assessment of their usefulness [Stern, 1994]. Moreover, the values of constants provided by Teplyakov and Meares (1990) cover only a limited number of polymers. In general, models for solubility and diffusivity coefficients are multi-parameter correlations. Determination of all required parameters may sometimes be more complicated than the actual gas permeation experiment.

There are many other empirical or semi-empirical correlations of permeability as well as diffusion and solubility coefficients. As shown by Robeson (1991) these correlations are generally useful for very specific groups of polymers.

CHAPTER 3

Properties of PPO and PPO-Based Polymers

3.1 Development of Polymers for Gas Separation Membranes

Development and characterization of new polymers for gas separation is an important factor for the future of membranes as an alternative gas separation technology. A review of the list of US patents on membrane materials from 1987 to 1992 reveals that polyimides dominate over other polymers as the material for gas separation membranes [Koros and Fleming, 1993]. The majority of the listed polyimides; however, have been specially prepared for the purpose of gas separation. As indicated by the closeness of polyimides to the upper bound line [Robeson, 1991], tailoring the chemical structure of this polymer has been successful in achieving promising materials for gas separation.

The alternative approach in tailoring chemical structure is modification of existing polymers, preferably commercial polymers. It is generally easier to increase selectivity than permeability of the polymer; therefore, the base polymer should be very permeable [Koros and Fleming, 1993]. Poly(2,6-dimethyl-1,4-phenylene oxide), which has one of the highest permeability for gases appears to be an excellent candidate for chemical modifications.

3.2 Properties of PPO

Poly(2,6-dimethyl-1,4-phenylene oxide), the base polymer in this research project, was first produced commercially by General Electric in 1965 under the trade name of PPO [Mahajan, 1991]. PPO is a glassy polymer with glass transition temperature (T_g) ranging from 212 to 218°C

[Toi *et al.*, 1982; Hay, 1986; Aguilar-Vega and Paul, 1993; Plate and Yampol'skii, 1994]. Among the glassy polymers PPO shows one of the highest permeability to gases [Plate and Yampol'skii, 1994]. This high permeability is attributed to the absence of polar groups in the main chain of PPO. There is; however, a significant scatter of permeability observed by different authors. For example, CO_2 permeability for PPO ranges from 42 [Story and Koros, 1992] to 200 Barrer[1] [Plate and Yampol'skii, 1994]. PPO has a relatively low selectivity for gases, although there are also differences between different sources. For example, CO_2/CH_4 permeability ratio for PPO membranes ranges from 12-13 [Plate and Yampol'skii, 1994] to 16.4 [Percec and Li, 1988]. These differences result from the fact that PPO can crystallize under some conditions and the variation of the crystallinity can cause considerable changes in permeability and permeability ratio of PPO membranes [Plate and Yampol'skii, 1994]. PPO isolated by precipitation in methanol could be up to 15% crystalline [Hay, 1986]. The degree of crystallinity; however, has not been indicated in most of the publications dealing with this material.

PPO possesses excellent mechanical and thermal properties. It has high impact strength; it is also stiff, hard, and extremely tough. The high impact strength of PPO is a result of the ability to undergo rapid conformational transitions by the phenyl rings rotating freely about C-O bonds. Stiffness of PPO is attributed to the rigidity of the phenol rings in the backbone. Phenyl rings also make PPO hydrophobic and resistant to many chemical environments including acids, bases, alcohol, and steam [Aycock, 1974]. High hydrophobicity of PPO also results in the lack of solubility in conventional membrane dipolar aprotic solvents. This lack of solubility along with a relatively low selectivity for gases prevents the facile preparation of PPO membrane systems for commercial use in gas separation [Percec and Li, 1988]. Hence, PPO needs to be chemically modified in order to overcome the inherent disadvantages of this otherwise very attractive membrane material.

3.3 Gas Separation Membranes from Modified PPO

Percec and Li (1988) modified PPO by aromatic bromination and studied the effect of the degree of substitution on the gas permeation properties of brominated PPO (BrPPO) membranes.

[1] 1 Barrer = 10^{-10} cm^3(STP) cm cm^{-2} s^{-1} $cmHg^{-1}$

They found that both CO_2 permeability and CO_2/CH_4 permeability ratio increased with an increase of the degree of bromination. For membranes prepared from 100% substituted BrPPO, they reported CO_2 permeability of 158.08 Barrer and CO_2/CH_4 permeability ratio of 23.73. On the other hand, CO_2 permeability and CO_2/CH_4 permeability ratio reported by Story and Koros (1992) for membranes from 100% substituted BrPPO were 104 Barrer and 15.0, respectively, although the trend between the degree of substitution and CO_2 permeability was the same as that observed by Percec and Li. Aryl bromination of PPO and the properties of BrPPO were also investigated by Chern *et al.* (1987).

Percec and Li (1988) also studied the permeation properties of sulfonylated PPO of different substitution degrees for different sulfonyl groups. Similar to BrPPO, sulfonylated PPO membranes, generally exhibited higher CO_2 permeabilities and CO_2/CH_4 permeability ratios compared to unmodified PPO. The nature of the sulfonylated groups; however, seemed to have a stronger influence on the permeation properties of the modified PPO membranes than the degree of substitution. Story and Koros (1992) investigated the properties of carboxylated PPO (CPPO). They reported a decrease in T_g from 208°C to 153.6°C when the substitution degree increased from 0 to 45%. At the same time, CO_2 permeability decreased from 42.0 to 12.9 Barrer while the CO_2/CH_4 permeability ratio increased from 15.8 to 23.2. Another type of chemical modification was investigated by Pedretti *et al.* (1992) who modified PPO with trialkyl-silyl, hydroxyethylene, and/or ethyleneoxytrialkyl-silyl groups. They reported that the CO_2 permeability for modified PPO membranes ranged between 24.0 and 29.7 Barrer, while the CO_2/CH_4 permeability ratio ranged between 13 and 20.

Another possible modification of PPO is achieved by attaching sulfonic groups to the main polymeric chain by means of sulfonation of PPO using chlorosulfonic acid. Sulfonation has been used to improve the gas selectivity of other polymeric materials. For example, Chiou and Paul (1988) showed that incorporation of sulfonic groups into Nafion improved gas transport selectivity of Nafion membranes, while Liu and Martin (1991) and Liu *et al.* (1992) observed a similar trend in the case of polystyrene membranes. Sulfonated polymers can be further modified by substitution of the proton in the sulfonic groups by different metal cations. Chen and Martin

(1994), who reported a significant improvement of permeability ratios of metal substituted membranes compared to unsubstituted ones, used this approach for sulfonated polystyrene.

3.3.1 Sulfonated PPO as a membrane material

The first report on sulfonation of PPO goes back to 1970; however, initially sulfonated PPO (SPPO) was considered only as a potential material for reverse osmosis membranes [Plumer *et al.*, 1970]. It was found that salt rejections for SPPO membranes were lower than those for cellulose acetate; however, SPPO membranes exhibited a few fold advantages in water flux compared to cellulose acetate membranes. Furthermore, SPPO membranes were relatively resistant to compaction. Huang and Kim (1984b) examined a potential of SPPO-polysulfone composite membranes for the purification of Alberta tar sand waste waters. The studies showed that membranes made from SPPO of *IEC* ranging from 2.1 to 2.3 meq/g exhibited excellent rejection of salts and an excellent production rate. Recently, Hamza *et al.* (1995) studied the effects of *IEC* of SPPO and solvent used for casting on the reverse osmosis performance of SPPO composite membranes. They found that the proper adjustment of the IEC of polymer and the composition of the solvent consisting of chloroform and methanol could optimize the membrane performance.

Percec and Li (1988) examined some gas permeation properties of SPPO and reported a relatively high CO_2/CH_4 permeability ratio of 38.80 and a moderate CO_2 permeability of 19.84 Barrer for this polymer. They also reported that SPPO was hygroscopic and unstable. They did not; however, provide the *IEC* or the degree of substitution of the polymer. The problem of instability of SPPO was also indicated earlier for the polymer of *IEC* of 3 meq/g or more [Plumer *et al.*, 1970]. Recently, Fu *et al.* (1994a) synthesized SPPO and characterized the physico-chemical properties of polymer. They found that the density and T_g of SPPO increased with an increasing degree of polymer substitution. Thermogravimetric analysis (TGA) showed that SPPO had lower thermal stability than PPO; however, thermal stability of SPPO was improved by substituting the proton in the sulfonic groups with sodium cation. The performance tests on dense SPPO membranes showed that an increase in the degree of electrophilic substitution resulted in a linear increase of O_2/N_2 permeability ratio along with a few-fold decrease in O_2 permeability.

Permeability ratio of 7.5 for O_2/N_2 was reported for the membranes prepared from SPPO of the highest degree of substitution of 37%. No significant differences were observed between the performance of the membranes made from the protonated and sodium forms of SPPO [Fu *et al.*, 1994b].

Bikson and Nelson (1994) prepared composite SPPO membranes for gas separation. The membranes were prepared by casting a dilute polymer solution containing SPPO along with an amino functional siloxane on a polysulfone substrate. They reported a high separation factor for O_2/N_2, particularly for SPPO in a lithium salt form. For example, for membranes prepared from the lithium form of SPPO of *IEC* equal to 2.14 meq/g, they reported a separation factor for O_2/N_2 of 5.7 and O_2 permeance of $2.2 \cdot 10^{-5}$ cm^3/cm^2 cmHg s. The separation data for O_2/N_2 reported by Bikson and Nelson was obtained in the air separation experiments. A high permeance combined with a high separation factor of composite SPPO membranes demonstrates that SPPO based membranes have a great potential as a gas separation material.

3.3.2 Influence of molecular weight on properties of polymeric membranes

Another important factor of the material aspect of membrane gas separation is the molecular weight of polymer. In general it is anticipated that an increase in molecular weight should improve mechanical integrity of membranes. Considering gas transport properties of polymers, there have been only few studies on the effect of molecular weight. For example, Smid *et al.* (1991) tested integrally skinned hollow fiber membranes prepared from PPO of different intrinsic viscosities, indicating different molecular weights of polymer. They reported that O_2 permeability increased while O_2/N_2 permeability ratio remained unchanged with increasing the molecular weight of PPO. A similar relationship between molecular weight and permeability was reported recently by Polotskaya *et al.* (1996). In addition to that, they showed that an increase in the molecular weight of the polymer also resulted in an increase in free volume in dense polymeric membranes.

Most of the studies on PPO and modified PPO membranes, including SPPO, were based on low molecular weight polymers. Up to date, there have been no data in the literature on the gas transport properties of high molecular weight SPPO.

CHAPTER 4

Effect of Casting Conditions on Properties of Homogeneous Membranes

A review of literature pertaining to PPO, which was presented in Chapter 3, revealed considerable variations in intrinsic gas transport properties of this polymer. It was shown that its CO_2 permeability ranges from 42 [Story and Koros, 1992] to 200 Barrer [Plate and Yampol'skii, 1994], while its CO_2/CH_4 permselectivity ranges from 12 [Plate and Yampol'skii, 1994] to 16.4 [Percec and Li, 1988]. A question arises, which values represent the true gas transport properties of PPO?

It is generally believed in the membrane community, that properties of homogeneous membranes are entirely determined by the polymer chemistry. The above example; however, clearly indicates that apart from polymer chemistry, there must be some other factors influencing the properties of homogeneous membranes. Furthermore, if the structure of a solution cast homogeneous membrane were entirely determined by the polymer chemistry, selectivity for gases of such a membrane would represent the maximum for a given type of polymer. Consequently, gas selectivity of integrally skinned asymmetric and thin film composite membranes could only approach that of homogeneous films. There are; however, examples in the literature which show that gas selectivity of asymmetric membranes can exceed that of homogeneous membranes when both are prepared from the same material [Pesek and Koros, 1993].

Kesting and Fritzsche (1993) listed factors which, apart from polymer type, purity and molecular weight, may influence the structure and function of a thin dense polymeric film when

the film is prepared by the complete evaporation of the solvent from a solution of polymer and solvent. These factors include solvent strength, solvent volatility, solvent molecular size, concentration of polymer solution, concentration of residual solvent, environmental temperature, solution temperature, relative humidity, air flow rate, concentration of solvent vapor above desolvating solution, nature of the casting surface, and desolvation and gelation kinetics. It can be noticed that most of the above factors either represent or are related to the properties of solvent in casting solution.

In this Chapter, the examples from literature documenting the influence of casting parameters, in particular the solvent in casting solution, on properties of homogeneous membranes is presented. Also a theoretical background pertaining to polymer-solvent interactions and the ways of their evaluation is discussed. Finally, the examples of application of atomic force microscopy (AFM) in membrane studies are reviewed, because AFM is used for characterization of surface morphology of membranes in this dissertation.

4.1 Effect of Casting Solvent

Kesting (1985) reviewed some literature examples showing the influence of casting the solution on the properties of the solution cast dense films. One of the first indications that properties of polymeric films depend on the nature of polymer solution came more than 60 years ago from Jones and Miles (1933). They found that the tensile strength and elongation of nitrocellulose films varied with the solvent from which they were prepared. Haas *et al.* (1952) reported that for solution-cast ethyl cellulose membranes the film birefrigency, density and toughness decreased with increasing power of solvent, i.e., benzene < chlorobenzene < 2-nitropropane, whereas Doolitle (1954) reported that cellulose films from toluene solvent had three times higher elongation than similar films cast from ethanol solution. The tensile strength and water vapor permeation of former films was also higher. Katz and Munk (1969) extended the effect of the casting solution to the membrane permeability. Studying the effect of solvent polarity on the permeability of water vapor of nitrocellulose, chlorinated rubber and an alkyd membranes, they suggested that the closer the structural similarity between polymer and solvent, the lower water vapor permeability.

Packter and Nerurkar (1968) investigated the development of the membrane crystallinity in polyvinyl alcohol films prepared by controlled evaporation of aqueous solution. They observed a delay in the beginning of rapid crystallization with a decreasing rate of evaporation of solvent; however, the final crystallinity remained practically independent of the evaporation rate. On the other hand, addition of 2 - 20% high boiling point solvents to the polymer solution resulted in higher final crystallinity of membranes. The effect of the solvent on the morphology of dense atactic polystyrene films prepared from xylene, carbon tetrachloride, and mixtures of aromatic hydrocarbon solutions was studied by Zubov *et al.* (1968) using electron microscopy. They reported different sizes of "globules" and different extents of oriented structures on the surfaces, depending on the solvent used.

Okuno *et al.* (1993), studied the effect of the casting solution on the properties of poly(vinyl chloride) membranes. The casting solutions were modified by changing the concentration of polymer and by addition of different nonsolvents into the polymer solution. They reported that density and crystallinity of poly(vinyl chloride) membranes increased with an increasing relative viscosity of casting solution. They also reported that the permeation rate of water vapor increased, while the separation factor of water-ethanol system decreased with a decrease in the crystallinity [Okuno *et al.*, 1993]. On the other hand, Mohr and Paul (1991) reported a six-fold greater gas permeability of dense poly(4-methyl-1-pentane) films prepared from cyclopentane solution compared to those prepared from chloroform solution. Despite that, there were no significant differences in the degree of crystallinity between membranes prepared from these two solvents. X-ray diffraction photographs; however, showed that crystallites in the films cast from chloroform solution had strongly preferred orientation, while the film cast from cyclopentane solution was nearly isotropic, with only a slight tendency for crystallite orientation [Mohr and Paul, 1991].

4.2 Effect of Residual Solvent

The influence of residual solvent on gas transport properties of homogeneous membranes is probably best understood among the effects of factors listed by Kesting and Fritzsche (1993). The effect of concentration of various residual solvents on properties of PPO

and polysulfone films was studied by Maeda and Paul (1987), while a similar study involving a fluorinated polyimide membranes was done by Moe *et al.* (1988). In general, the effect of residual solvent is concentration dependent. When trace amounts of residual solvent are left in a membrane made from a glassy polymer, the molecules of residual solvent occupy Langmuir sorption sites in the polymer, decreasing its free volume and permeability, while increasing its selectivity. In such cases the residual solvent acts as an antiplasticizer. Above a certain threshold concentration, when all Langmuir sites are occupied, the excess of residual solvent acts as a plasticizer, that is, it causes a decrease in polymer-polymer interactions which leads to an increase in chain mobility and free volume of polymer. Consequently, membrane permeability increases while the membrane selectivity decreases [Kesting and Fritzsche, 1993].

The removal of residual solvent from a polymeric membrane in glassy state is not easy. Joly *et al.* (1996), who studied polyimide films, reported a weight loss of 4% at around 300°C and attributed it to the loss of residual solvent, irrespective of the solvent. The solvents considered by Joly *et al.* were dioxane, N,N-dimethylacetamide (DMAC) and 1-methyl-2-pyrrolidinone (NMP), which had boiling points well below 300°C. On the other hand, a similar analysis using Ultem 1000, a commercial polyetherimide, showed a weight loss at around 200°C. The authors attributed the difference in the temperature at which the weight loss occurred to the difference in the glass transition temperature (T_g) of polymers. T_g of the studied polyimide was equal to 306°C while T_g of Ultem 1000 was equal to 210°C. Polymer chains slide against one another when the temperature is close to T_g which enhances evaporation of solvent entrapped in the membrane structure [Joly *et al.*, 1996].

4.3 Other Casting Factors

O'Brien *et al.* (1987), who investigated the influence of casting and curing conditions on gas transport and sorption of polyimide films. Laboratory prepared polyimide films were compared with chemically identical, commercially available Kapton (DuPont) films. The Kapton films were more oriented, aggregated and denser than isotropic laboratory made membranes. Also Kapton membranes were one order of magnitude less permeable to CO_2 and considerably more CO_2/CH_4 selective than the laboratory made membranes. Similarly, both CO_2 and CH_4 were

considerably less soluble in the oriented and aggregated Kapton films than in the isotropic polyimide membranes [O'Brien *et al.*, 1987].

Khulbe *et al.* (1996a), studied the effect of volatility of solvent in casting solution. Considering chloroform and trichloroethylene (TCE) as solvents for PPO, they observed under AFM different morphologies of membrane surfaces. In general, membranes prepared from the more volatile solvent - chloroform showed larger dimension of nodules than those prepared from the less volatile solvent - TCE. Since chloroform and TCE have similar solubility parameters, they attributed the difference in surface morphology to the difference in volatility of chloroform and TCE. The difference in surface morphology was associated with the difference in permeability for gases, that is, the chloroform membranes were more permeable than the TCE membranes [Khulbe *et al.*, 1996a].

Khulbe *et al.* (1997) considered the effect of temperature of casting solution. Using PPO with chloroform as casting solvent, they reported that membranes prepared at -10°C had roughness parameters one order of magnitude greater than the membranes prepared at 4 and 22°C. At the same time, membranes prepared at -10°C were slightly more permeable and significantly less selective than the membranes prepared at higher temperatures.

Kesting *et al.* (1990a&b) postulated the importance of solvent size on free volume and permeability of graded skin density of asymmetric membranes. They observed that permeability of polysulfone asymmetric hollow fibers increased with an increase in the size of solvent. He suggested that solvent acts as a transient template which increases the spacing between macromolecules in polymer solution. When the solvent is rapidly removed during the membrane formation process, the structure present in the polymer solution might be preserved in a dry membrane [Kesting *et al.*, 1990a&b]. Similar phenomenon could occur during formation of dense films; however, there is no evidence in the literature that solvent size affects the properties of homogeneous membranes.

4.4 Polymer-Solvent Interactions and Their Evaluation

Most of the literature examples showing the importance of casting conditions on properties of homogeneous membranes were directly related to the solvent in casting solution. A

change in solvent results in simultaneous changes in a number of properties of casting solutions, for example solution volatility and polymer-solvent interactions. Volatility of casting solution, although different from the volatility of pure solvent, can be approximated by the vapor pressure of pure solvent. On the other hand, interpretation and evaluation of polymer-solvent interactions is not straightforward.

The interaction force acting between molecules is often expressed by solubility parameter. The solubility parameter is a measure of secondary forces working between separate molecules. These forces are much weaker than covalent bonds - the primary forces, which hold molecules together. Nevertheless, the secondary forces have a strong effect on the physical properties of substances. The interaction forces are intrinsic to the chemical structure, that is, the interaction force measured by solubility parameter is uniquely determined when the molecular formula of the molecules involved in the interaction is given [Matsuura, 1994].

In case of a binary system such as polymer solution, there are three types of interactions: polymer-polymer, solvent-solvent and polymer-solvent interactions. If the attractive forces working between solvent molecules and those acting between polymer macromolecules are similar in their nature and magnitude, the polymer will be dissolved in the solvent. The relative strength of polymer-solvent interactions determines the properties of casting solution and presumably the properties of the final membrane. For convenience, the polymer-solvent interactions relative to the polymer-polymer interactions, will be referred to from now as the polymer-solvent interactions.

4.4.1 Solubility parameter

The process of dissolving an amorphous polymer in a solvent is governed by the free energy of mixing

$$\Delta G_m = \Delta H_m - T\Delta S_m \tag{4.1}$$

where ΔG_m is the Gibbs free energy of mixing, ΔH_m is the enthalpy change on mixing, T is the absolute temperature, and ΔS_m is the entropy change on mixing. A negative ΔG_m predicts that a process will occur spontaneously. The dissolution of a high-molecular polymer is always associated with a large increase in entropy; therefore, the enthalpy term is the deciding factor in

determining the sign of the Gibbs free energy of change. Hildebrand and Scott (1950) proposed that

$$\Delta H_m = V\left(\left(\frac{\Delta E_1}{V_1}\right)^{1/2} - \left(\frac{\Delta E_2}{V_2}\right)^{1/2}\right)^2 \Phi_1\Phi_2 \tag{4.2}$$

where V is the volume of mixture, ΔE_i is the energy of vaporization of species i, also called the cohesive energy, V_i is the molar volume of species i, and Φ_i is the volume fraction of i in the mixture. A physical interpretation of ΔE is the degree of attraction between molecules in a liquid. The solubility parameter, often called the Hildebrand parameter, defined as

$$\delta_i = \left(\frac{\Delta E_i}{V_i}\right)^{1/2} \tag{4.3}$$

describes the attractive strength between molecules of the material. Eq. (4.2) can be rewritten to give the enthalpy of mixing per unit volume for a binary mixture

$$\frac{\Delta H_m}{V} = (\delta_1 - \delta_2)^2 \Phi_1\Phi_2 . \tag{4.4}$$

It is clear from this equation that ΔH_m is always positive. In order for ΔG_m in Eq. (4.1) to be negative, the enthalpic term must be smaller than the entropic term. Heat of mixing is minimized and hence polymer is soluble in a solvent when the difference between their solubility parameters, $(\delta_1 - \delta_2)$, is minimized.

4.4.1.1 Multi-component solubility parameters

Solubility parameter represents the sum of all secondary intermolecular forces. There are; however, several types of interactions working between molecules. These include, dispersion forces, dipole forces, and hydrogen bonding forces. Hansen (1969) and Hoy (1970) proposed that the Hildebrand parameter could be divided into three components arising from the dispersive, permanent dipole-dipole interactions and hydrogen bonding forces

$$\delta^2 = \delta_d^2 + \delta_p^2 + \delta_h^2 \tag{4.5}$$

where δ_d is the dispersive term, δ_p is the polar term, and δ_h is the hydrogen bond term. Hansen and Hoy; however, used different approaches to determine the components of solubility parameter. Consequently, there are some differences between the values listed by Hansen and Hoy.

Solubility parameter and its components for a low molecular weight liquid, can be correlated to a number of physical properties of the liquid, including: enthalpy of vaporization, internal pressure, van der Waals constant, surface tension, critical pressure, index of refraction, and dipole moment. In case of polymers, the available methods include: solvency testing, swelling values, refractive index, dipole moment, intrinsic viscosity, and inverse phase gas chromatography [Grulke, 1989]. The solubility parameter and its components for both low molecular weight solvents and polymers can also be estimated by a group contribution method. This method requires application of additivity rules to the structural components of the solvent molecule, or the repeat unit of the polymer. Van Krevelen (1976) proposed equations for estimation of the solubility parameter and its components. These equations are presented in Appendix B. Matsuura (1994) put together a comprehensive list of group contributions, which allows estimation of solubility parameter and its components for a wide variety of polymers using Van Krevelen equations.

There are other multi-component models for the solubility parameter which are available in the literature, including two, four, and five-component models [Barton, 1983]. The three component models proposed by Hansen and Hoy, provide good predictions of the interactions between polymer and solvent for a wide variety of polymer solutions without going into the complexity of the four and five-component models.

4.4.1.2 Relation between polymer-solvent interaction and solubility parameter

The universally used measure of solvent power is (χ). The change in free energy of mixing defined in Eq. (4.1) has been related with the polymer-solvent interaction parameter [Flory, 1953] by

$$\Delta G_m = RT\left[n_1 \ln \Phi_1 + n_2 \ln \Phi_2 + \chi n_1 \Phi_2\right] \tag{4.6}$$

where R is the universal gas constant, n_1 and n_2 are the number of moles of solvent and polymer, respectively, and χ is the Flory-Huggins parameter, which is a measure of solvent power. In case of polymer solutions χ is also called the polymer-solvent interaction parameter. Because the first two terms in Eq. (4.6) are negative, the strongest solvent will be the one with the smallest value

of χ. The Flory-Huggins parameter can be represented as a sum of entropic and enthalpic components

$$\chi = \chi_S + \chi_H \tag{4.7}$$

where χ_S is the entropic term and χ_H is the enthalpic term. The entropic contribution to the interaction parameter is determined considering only the size and shape of molecules and ignoring enthalpic interactions between the molecules. This assumption is accurate at high temperatures when the kinetic energy of molecules is large compared to any interaction energies between molecules [Danner and High, 1993]. The entropic term is usually taken to be a constant between 0.3 and 0.4 [Blanks and Prausnitz, 1964]. The enthalpic contribution to the interaction parameter arises from the difference in interaction energies, which are directly related with the heat of mixing. Bristow and Watson (1958) proposed a semiempirical equation that relates the enthalpic component of the interaction parameter to the solubility parameter:

$$\chi_H = \frac{V_1}{RT}(\delta_1 - \delta_2)^2 \tag{4.8}$$

For polymer and solvent to be completely miscible over the entire composition range, χ should be smaller than 0.5 [Burrell, 1955].

For polar systems, the geometric mean assumption of regular solution theory is not appropriate; therefore, $(\delta_1 - \delta_2)^2$ term is replaced by the A_{12} defined

$$A_{12} = \delta_1^2 + \delta_2^2 - 2l_{12}\delta_1\delta_2 \tag{4.9}$$

where l_{12} characterizes the intermolecular forces between molecules. This extra term describes the interchange energy density for the solvent-solute pair [Grulke, 1989].

4.4.2 Solution viscosity

Viscosity is a measure of the energy dissipated by a fluid in motion as it resists an applied shearing force [Rodriguez, 1989]. The polymer-solvent interactions have strong influence on the physical properties of the polymer solution, including its viscosity. The exact effect of polymer-solvent interactions on the viscosity of polymer solution depends on the concentration of polymer in the solution. Furthermore, a very dilute polymer solution can be considered as a Newtonian liquid, while a concentrated polymer solution behaves as a non-

Newtonian liquid, that is, its viscosity is not constant, changing with the shear stress and shear rate.

4.4.2.1 Dilute polymer solutions

Equilibrium configuration of molecular chains in polymer solution depends on the balance between the Gibbs free energy change due to mixing and that due to elastic deformation [Barton, 1983]. The extent of deformation depends on the relative strengths of polymer-polymer and polymer-solvent interactions. In a good solvent the polymer is unfolded, obtaining to the maximum extent the more favorable polymer-solvent interactions. On the other hand, in a poor solvent the polymer molecules remain folded because of more favorable polymer-polymer interactions. Consequently, the viscosity of a dilute solution of polymer is maximum in the best solvent, that is, in one where the solubility parameters of solvent and polymer are comparable.

The intrinsic viscosity, [η], of a polymer-solvent system is defined as:

$$[\eta] = \lim_{c \to 0} \left(\frac{\eta - \eta_o}{c\eta_o} \right) \tag{4.10}$$

where η and η_o are the absolute viscosities of the solution and solvent, respectively, and c is the concentration of polymer solution.

The intrinsic viscosity is often correlated to solubility parameters. A variety of equations exist, however, they all have the following form [Grulke, 1989]

$$[\eta] = K_I - K_{II} V_i'' \Delta^2 \tag{4.11}$$

where K_I and K_{II} are the constants, n is either 0.5 or 1, and Δ is the difference between solubility parameters of polymer and solvent. Knowing the solubility parameter of the solvent and the values of constants, Eq. (4.11) can be used for estimation of the solubility parameter of polymer [Van Dyk *et al.*, 1985].

4.4.2.2 Concentrated polymer solutions

Although the viscosities of dilute polymer solutions show a minimum in poor solvents because the polymer macromolecules remain coiled, there is a "changeover" in behavior: the viscosity at higher concentrations is greater in poor than in strong solvents [Ferry *et al.*, 1951;

Gandhi and Williams, 1971]. Barton (1983) suggests that there is an aggregation or clustering of polymer macromolecules preliminary to phase separation, not only in solvents that have solubility parameters near the limits of the miscibility range for the polymer, but also in good solvents from the middle of the miscibility range for polymer. According to Kesting (1990), macromolecular aggregates (nodules), which are observed on the surface of dry polymeric membranes, originate from the clusters of individual macromolecules present in the polymer solution. The presence of the nodules in all but the most dilute polymer solutions is a consequence of interaction between macromolecules in a crowded environment of polymer solution [Kesting and Fritzsche, 1993].

Naturally, the tendency to form aggregates in polymer solutions should be enhanced by the strong polymer-polymer and weak polymer-solvent interactions as well as the concentration of polymer. Considering that the flow of polymer solution involves sliding of individual macromolecules upon one another, it is clear that such sliding will be resisted more within the nodule consisting of entangled macromolecules than in a solution consisting of individual macromolecules. Hence, for a given concentration of polymer solution, the viscosity should increase with an increase in tendency for macromolecular aggregation in the solution and hence with a decrease in solvent strength.

This qualitative consideration is supported by the experimental data provided by Hoernschemeyer (1974), who showed that specific viscosity (η_{sp})

$$\eta_{sp} = \frac{\eta - \eta_o}{\eta_o} \tag{4.12}$$

of concentrated polymer solution decreased with a decrease in partial molar free energy of mixing. The same applies to the relative viscosity (η_{rel}) defined

$$\eta_{rel} = \frac{\eta}{\eta_o} \tag{4.13}$$

The change in the partial molar free energy of mixing is related to the Flory-Huggins interaction parameter (χ) in a similar fashion as the change in the free energy of mixing defined in Eq. (4.6). A decrease in the partial free energy of mixing hence indicates an increase in polymer-solvent interactions. Hoernschemeyer (1974) also showed that a decrease in specific viscosity was directly related to an increase in tolerance of polymer solution for a nonsolvent. This observation

confirms that solvent strength and hence polymer-solvent interactions are directly related to the specific and relative viscosities of concentrated polymer solution.

4.4.3 Effect of temperature

The effect of temperature on the absolute polymer-solvent and polymer-polymer interactions is quite obvious, that is, these interactions decrease with an increase in temperature. This is because of an increase in kinetic energy of molecules with temperature. At high temperatures kinetic energy of molecules predominates any inter-molecular interactions [Danner and High, 1993]. On the other hand, the effect of temperature on the polymer-solvent interactions relative to those between polymers is not obvious.

The behavior of the molecules in polymer solution is described as a sum of two terms, the enthalpic and entropic contributions. In the most general form it is expressed by the free energy of mixing defined by Eq. (4.1). It is clear from Eq. (4.1) that an increase in temperature should result in more negative ΔG_m since ΔS_m is always positive. On the other hand, the enthalpic term is also a function of temperature; therefore, the relationship between ΔG_m and T is not obvious.

The free energy of mixing is also defined by Eq. (4.6). According to this equation, it also appears, at the first glance that the free energy of mixing becomes more negative when the temperature increases. The interaction parameter in Eq. (4.6) is; however, not a constant and dependents on the volume fraction of polymer in the solution and temperature of the solution [Danner and High, 1993]. The interaction parameter can be written as

$$\chi = f_1(\Phi_2) f_2(T). \tag{4.14}$$

The dependence of the interaction parameter on temperature is quite complex. Koningsveld (1975) proposed a three-parameter expression to adequately correlate the interaction parameter to temperature

$$f_2(T) = 1 + \frac{\upsilon}{T} + \omega T + \psi \ln T \tag{4.15}$$

where υ, ω, and ψ are the constants characteristic for a given polymer-solvent system. It is clear that the actual dependence of χ on temperature depends on the values of these constants. On the other hand, even when χ increases with temperature, ΔG_m may still become more negative, since

the terms involving logarithm of volume fractions are always negative and they become even more negative as the temperature increases. It can; therefore, be concluded that although the inter-molecular interactions for both polymer-solvent and polymer-polymer are expected to decrease with an increase in temperature, the change in the relative intensity of the former to the latter interactions is theoretically unpredictable.

4.5 Application of Atomic Force Microscopy in Membrane Studies

Development of microscopic techniques such as scanning electron microscopy (SEM), transmission electron microscopy (TEM), and recently atomic force microscopy, has allowed direct examination of surface and cross-section of polymeric membranes. Studies on membrane structure using SEM provided basis for the four tier structure model of integrally skinned polymeric membranes [Kesting, 1990].

Although SEM and TEM are very powerful tools to investigate the structure of polymeric membranes, they possess some inherent disadvantages. For example, the utilization of an electron beam under high vacuum in SEM requires coating of the membrane surface with a heavy metal such as gold, palladium, or platinum. The coating process itself might be destructive and may obscure fine details of membrane morphology. Another problem in the study of polymeric membranes by SEM, is beam-induced damage [Fritzsche, *et al.*, 1992a]. Use of TEM, on the other hand, requires preparation of a replica. Consequently, the structure of polymeric membranes, as revealed by SEM and TEM, may not be identical to that which existed before its conversion into a specimen suitable for microscopic examinations.

The newly developed atomic force microscopy techniques have circumvented the limitation of SEM and TEM techniques [Binning *et al.*, 1986]. AFM, which operates as an ultra-low-force imaging surface profiler has been recognized as a very useful tool for studying surface morphology of ultrafiltration and microfiltration membranes. Fritzsche *et al.* (1992b) studied the surface structure and topography of commercially available polyvinylidene fluoride microfiltration membranes. They observed, by the AFM technique, uniform nodule aggregates with small pores in their interstitial regions. The nodule aggregates assembled to form supernodular aggregates whose boundaries could also be delineated by AFM. Larger pores

existed in these boundary regions [Fritzsche *et al.*, 1992b]. Dietz *et al.* (1992) studied the images of the surface of various commercial microfiltration and ultrafiltration membranes prepared from polycarbonate, polysulfone and polyethersulfone by AFM. They reported pore sizes of ultrafiltration membranes to be between 7.2 and 36.6 nm which were considerably smaller than those for microfiltration membranes, and pore densities ranging from 88 to 482 pores/μm^2. AFM was also successfully applied to measure pore diameters of polyethersulfone ultrafiltration membranes with molecular weight cut off 30,000 and 100,000, respectively. When the latter membranes were immersed in water, pore diameters were 15 to 25 nm and 50 to 60 nm, respectively. These values were larger than those obtained by SEM because the solvent exchange procedure used during the sample preparation for SEM examination caused a diminution in pore dimensions [Fritzsche *et al.*, 1992a]. On the other hand, when ethanol was substituted for water as the immersion medium, pores in the surface of polyethersulfone ultrafiltration membranes with diameters of 7 to 9 nm were observed. This image enhancement was attributed to an increased damping and concomitant noise reduction resulting from the higher viscosity of ethanol compared to water [Fritzsche *et al.*, 1992c].

In the above examples, surface images were obtained using contact mode AFM. In this mode, the tip is very close to the surface being imaged and is responding to short range repulsive interactions with the sample. In more recently developed non-contact mode AFM, the tip instead responds to attractive van der Waals interactions with the sample [Digital Instruments, 1993].

Bowen *et al.* (1996a & b) applied non-contact AFM in studies of surface morphology of the polymeric membrane. The resolution obtained in non-contact mode AFM compares favorably with that of contact mode AFM. For example, they observed pores of diameter as small as 3 nm on the surface of ultrafiltration membranes prepared from polyethersulfone [Bowen *et al.*, 1996a]. On the other hand, using Cyclopore and Anopore microfiltration membranes which have significantly larger pores than ultrafiltration membranes, Bowen *et al.* (1996b) showed that the mean pore size determined using both contact and non-contact mode AFM were similar.

Another development in atomic force microscopy was the introduction of the tapping mode (TM) AFM. In this mode of operation, the probe oscillates close to the sample surface and

touches the surface at a given frequency while scanning. The energy applied to the surface is more than that in the non-contact mode AFM, which prevents the probe from stacking in the surface. On the other hand, the energy applied to the sample is less than in the contact mode AFM, which prevents distortion of the sample surface by the probe. In principal, the resolution in tapping mode and non-contact mode AFM should be comparable [Digital Instruments, 1993].

Despite developments in atomic force microscopy, there have been only a few attempts to extend applicability of AFM to the investigation of surface morphology of polymeric gas separation membranes [White *et al.*, 1995; Kruczek *et al.*, 1995; Khulbe *et al.*, 1996a & b; Khulbe *et al*, 1997]. The major reason for this is the fact that the maximum achievable resolution by AFM, although considerably higher than that for other ultramicroscopic techniques, is still not sufficient to image pores in gas separation membranes or to distinguish individual macromolecules inside macromolecular aggregates. On the other hand, considering that the gas permeation is governed not only by the spacing between macromolecules inside the nodules, but also by the spacing between the nodules, the size and distribution of nodules, which are observable under AFM, might be related to gas transport properties of membranes. In fact, Khulbe *et al.* (1996a), reported that membranes with larger nodules on the top surface were more permeable to gases than those with smaller nodules. A systematic study of surface morphology of membranes in conjunction with evaluation of gas transport properties may; therefore, provide some interesting relationships between them.

PART II

Methodology and Experimental

CHAPTER 5

Methodology and Experimental

This chapter includes the description of experimental setups and some details of analytical methods used in this work along with some theoretical considerations and definitions. The description follows the development of this work from polymer modifications to characterization of membranes. The list of chemicals used in this project is presented at the end of the chapter.

5.1 Preparation of Polymer

5.1 1 Sulfonation of PPO

Sulfonation of poly (2,6-dimethyl-1,4-phenylene oxide) (PPO) was carried out using chlorosulfonic acid as a sulfonating agent following the reaction shown in Figure 5-1. Another alternative for sulfonation of PPO is the reaction with sulfuric acid. The reaction with sulfuric acid is; however, slow and leads to relatively low conversions [Fu *et al.*, 1994a]. On the other hand, sulfonation with chlorosulfonic acid is an easy, one-step chemical reaction, which leads to high conversions [Plummer *et al.*, 1970; Huang and Kim, 1984a; Fu *et al.*, 1994a]. The product, sulfonated PPO, is abbreviated as SPPO or more accurately as HSPPO to indicate the protonated form of the polymer. millimeter

Ion exchange capacity (*IEC*) or degree of sulfonation (*DS*) can express the extent of sulfonation of polymer. The *IEC* indicates the number of milli-equivalents of ions in one gram of the dry polymer. The *DS* indicates the average number of sulfonic groups per repeat unit of the polymer. For sulfonated PPO *IEC* and *DS* are related by the following equation

$$IEC = \frac{1000DS}{200DS + 120(1 - DS)} \tag{5.1}$$

where, 200 and 120 are the molecular weights of substituted and unsubstituted PPO units, respectively. The extent of sulfonation of PPO will be expressed by *IEC* throughout this work.

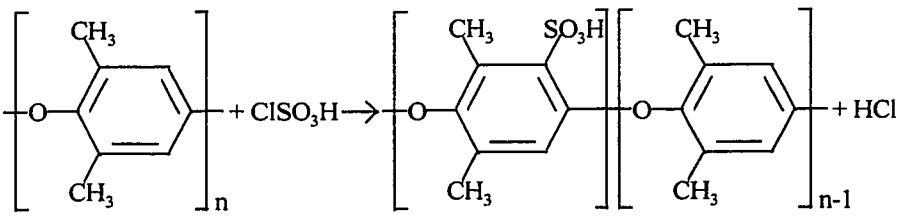

Figure 5-1. Sulfonation of PPO with chlorosulfonic acid.

Sulfonation of PPO was carried out in a reactor shown in Figure 5-2. Batches of 10 g of dry polymer (PPO was dried in vacuum at 40°C for at least two days prior to sulfonation) were dissolved in 600 cm^3 of anhydrous chloroform in a 1000 cm^3 3-neck reaction flask. Mechanical stirring and continuous purging of the reactor with nitrogen speeded-up dissolution of PPO in chloroform. The dissolution step, which was carried out for one hour, was followed by addition of a sulfonating solution (pre-calculated amount of chlorosulfonic acid in 100 cm^3 anhydrous chloroform). The sulfonating solution was added into the reactor via an addition funnel equipped with a pressure equalizer arm, over a period of five minutes, while the reactor content was vigorously stirred and purged with nitrogen. Stirring and purging were continued for half an hour after addition of chlorosulfonic acid. Purging of the reactor with nitrogen before and during sulfonation allowed to minimize the influence of atmospheric moisture on the reaction and to enhance removal of hydrochloric acid formed during the sulfonation reaction. In the case of preparation of HSPPO of *IEC* equal to 1.37 meq/g or greater, the sulfonated polymer precipitated from the chloroform solution. The liquid phase containing unreacted PPO and/or fractions of HSPPO of low *IEC* values was poured out from the reactor and 500 cm^3 of methanol was added to the reactor to dissolve the precipitated HSPPO.

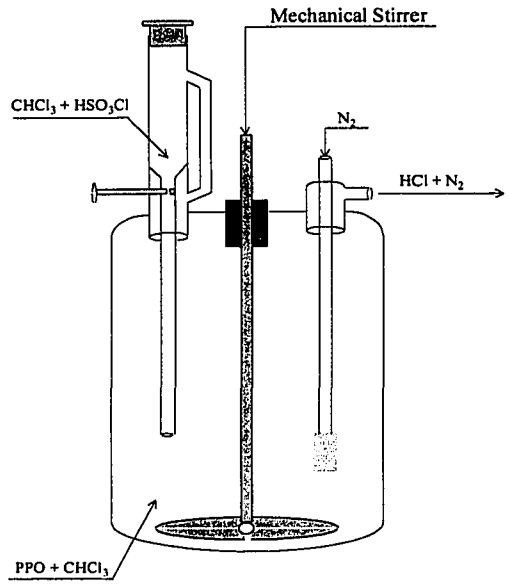

Figure 5-2. Experimental setup for sulfonation of PPO with chlorosulfonic acid.

A homogeneous solution of HSPPO in chloroform or methanol-chloroform mixture was poured into a Pyrex glass tray to form a film and was allowed to dry in air for one day. The dried polymer sheet was shredded into small pieces and washed with distilled water until the pH of washed water was the same in three consecutive washings. After water washing the polymer was air-dried. The air-dried polymer was stored in vacuum at the absolute pressure less than 1.0 cmHg.

PPO was sulfonated to *IEC* of 0.72, 1.01, 1.37 and 1.80 meq/g, respectively. For convenience the value of *IEC* will be incorporated into the abbreviation of the polymer. For example, HSPPO-1.37 indicates sulfonated PPO in acid form with *IEC* equal to 1.37 meq/g.

5.1.2 Conversion into metal form

Some HSPPO batches were further modified by substitution of the proton in sulfonic groups by various metal cations. Sulfonated PPO in metal form will be abbreviated as MeSPPO to distinguish from the polymer in acid form. After substitution of the proton in sulfonic groups by metal cations, the polymer loses its ion exchange capacity. The *IEC* of the original polymer will be included in the abbreviation of the modified polymer. For example, NaSPPO-1.37 indicates sulfonated PPO in sodium form obtained from HSPPO of *IEC* equal to 1.37 meq/g. The metal cations considered in this study were Na^+, Mg^{2+}, and Al^{3+}.

Sulfonated PPO in sodium form (NaSPPO) was obtained by soaking HSPPO in a dilute aqueous solution of NaOH for two days. After soaking, the polymer was washed with deionized

water in order to remove excess of NaOH. The polymers in magnesium (MgSPPO) and aluminum (AlSPPO) forms were obtained by two-day soaking of NaSPPO in dilute aqueous solutions of $Mg(NO_3)_2$ and $Al(NO_3)_3$, respectively. Similar to NaSPPO, the excess of metal cations was removed by washing the polymers with deionized water. After washing and air-drying the polymers were stored in vacuum with an absolute pressure less than 1.0 cmHg.

The conversion of NaSPPO into MgSPPO and AlSPPO was confirmed by energy dispersive X-ray (EDX) analysis. The EDX analysis did not provide quantitative results; however, they showed only the magnesium and aluminum peaks in the spectra of MgSPPO and AlSPPO, respectively. The lack of the sodium peaks in these spectra indicated that magnesium and aluminum replaced all sodium in the respective polymers.

5.2 Determination of Ion Exchange Capacity

The acid-base titration and proton nuclear magnetic resonance (^{1}H NMR) techniques determined *IEC* of sulfonated PPO batches.

5.2.1 Acid-base titration

For acid-base titration, a sample of dry polymer was soaked in a 10 cm^3 of 0.1N NaOH standard solution for two days, followed by the titration of the soaked solution with a 0.1N HCl standard solution, in the presence of phenolphthalein as an indicator. At least three samples from each batch of HSPPO were examined and *IEC* [meq/g] was calculated using the following equation

$$IEC = \frac{(10 - v)}{m} 0.1 \tag{5.2}$$

where v is the volume [cm^3] of 0.1N HCl standard, and m is the mass [g] of polymer.

5.2.2 ^{1}H NMR

For ^{1}H NMR analysis, a 50 to 100 mg sample of HSPPO was dissolved in a mixture of methyl-d_3 alcohol-*d* and chloroform-*d* the composition of which depended on the anticipated *IEC* of polymer. All ^{1}H NMR spectra were acquired on a Bruker AMX-500 NMR spectrometer using

a standard one-pulse sequence employing 45-degree pulses. Considering a repeat unit of PPO (Figure 5-1), it can be noticed that there are eight hydrogen atoms (protons) in each unit, two of which are attached to the aromatic carbons and six of which are attached to the methyl carbons. Consequently, hydrogen atoms attached to the aromatic and methyl carbons give two different signals on the ^{1}H NMR spectrum of PPO. Presence of the sulfonic group in the PPO repeat unit results in shift of the signal from the protons attached to the methyl group, which is in the *ortho* position to the sulfonic group, and that from the aromatic proton of the substituted unit. The ^{1}NMR spectrum of HSPPO shows two extra signals in addition to that of PPO and the degree of substitution (*DS*) of HSPPO can be determined considering the relative intensities of the shifted signals. Consequently, *IEC* of polymer can be calculated from Eq. (5.1). More details on the determination of *DS* from the ^{1}H NMR spectra along with an example of the ^{1}H NMR spectrum of HSPPO are provided in Appendix A.

Since the determination of *IEC* by ^{1}H NMR did not require large samples of polymer, this technique was particularly useful in evaluation of *IEC* of membranes after long-term-permeation tests or heat treatments. Moreover, unlike the acid-base titration, the ^{1}H NMR technique could also be used for determination of *DS* of MeSPPO.

5.2.3 Infrared spectroscopy

In addition to ^{1}H NMR and acid-base titration, infrared (IR) spectra were obtained for PPO and some HSPPO polymers using a Perkin-Elmer Infrared Spectrophotometer 267. Before obtaining IR spectra, the calibration of the instrument was checked by obtaining the spectrum of a 0.05 mm standard polystyrene film. The IR spectroscopy could be used for determination of *IEC* of HSPPO and MeSPPO [Fu *et al.*, 1994a]. In this study; however, IR spectroscopy was only used for qualitative analysis, *i.e.*, for the confirmation of the aryl sulfonation of PPO. The IR spectroscopy was particularly useful when a discrepancy occurred between *IEC* values determined by ^{1}H NMR and acid-base titration.

5.3 Characterization of Polymer Solutions

A polymer solution of concentration 4.0 g/dL was prepared by dissolving polymer in solvent at room temperature. Magnetic stirring speeded-up the dissolution of polymer in solvent. Polymer solution was filtered through 0.2 μm-pore size Teflon filters. If necessary, it was prefiltered using 1.0 μm-pore size Teflon filters. The polymer solution so prepared was subsequently used for preparation of polymeric membranes; therefore, it is sometimes referred to as the casting solution. The polymer solution was characterized in terms of solvent size, volatility, and polymer-solvent interactions.

5.3.1 Solvent size

Following the approach proposed by Kesting *et al.*, (1990a), the size of solvent was evaluated by the molar volume of the solvent.

5.3.2 Volatility of polymer solution

Volatility of polymer solution was evaluated by the vapor pressure of the pure solvent at a given temperature.

5.3.3 Polymer-solvent interactions

Polymer-solvent interactions in polymer solutions were evaluated on the basis of the difference between solubility parameters of polymer and solvent, with the intrinsic viscosity of polymer-solvent system and the relative viscosity of polymer solution.

5.3.3.1 Comparison of solubility parameters

The difference between solubility parameters of polymer and solvent is a measure of polymer-solvent interactions in polymer solution. Considering Hildebrand parameters this difference (Δ) is expressed as

$$\Delta = |\delta_P - \delta_S| \tag{5.3}$$

where subscripts P and S refer to the polymer and solvent, respectively. Examples of calculating Hildebrand and Hansen solubility parameters of HSPPO of different *IEC* values

along with the solubility parameters of solvents used in this work are presented in Appendix B. As shown in Appendix B, it is possible that the Hildebrand parameters of polymer and solvent are similar, while the components of the Hansen parameters of polymer and solvent are different. The difference in solubility parameters was also calculated using the Hansen solubility parameters

$$\Delta' = \sqrt{(\delta_{P,d} - \delta_{S,d})^2 + (\delta_{P,p} - \delta_{S,p})^2 + (\delta_{P,h} - \delta_{S,h})^2} \tag{5.4}$$

where subscripts *d*, *p*, and *h* indicate dispersive, polar, and hydrogen bonding components of Hansen solubility parameters.

5.3.3.2 Viscosity measurements

Polymer-solvent interactions were also evaluated by means of the intrinsic viscosity of the polymer-solvent system and the relative viscosity of the polymer solution. These parameters are based on experimentally determined kinematic viscosities of solvents and polymer solutions.

Kinematic viscosities of solvents and polymer solutions were determined using Cannon-Fenske viscometers. The efflux times of polymer solutions of concentration 4.0 g/dL were measured in the viscometer with capillary size 150, while the efflux times of solvents and dilute polymer solutions were measured in the viscometers with capillary sizes 50 and 75, respectively. The kinematic viscosity (ν) was determined by

$$\nu = Kt \tag{5.5}$$

where K is the capillary constant and in [cSt/s] and t is the efflux time in [s]. The kinematic viscosity represents the absolute viscosity (η) divided by density (ρ)

$$\nu = \frac{\eta}{\rho}. \tag{5.6}$$

Table 5-1 shows the values of capillary constants for different capillary sizes at different temperatures.

5.3.3.3 Intrinsic viscosity

Intrinsic viscosity of polymer-solvent system was determined at 25°C. To maintain the constant temperature, the viscometer was placed in a water bath. In the first step, the efflux time

Table 5-1. Capillary constants of Cannon-Fenske viscometers of different sizes.

Temperature	Capillary constant		
°C	Size 50	Size 75	Size 150
25	0.003635	0.01530	0.036706
40	0.00363	0.01528	0.03667
100	0.00361	0.01521	0.03648

was determined for pure solvent using the viscometers with capillary sizes 50 and 75, respectively. This is to determine the optimum capillary size in measuring the efflux time of dilute polymer solutions.

A dilute polymer solution of concentration 0.6 g/dL was prepared and filtered through a 0.2-μm pore-size Teflon filter. A polymer solution sample of 4 cm^3 and of a known weight was placed in a viscometer. The sample was kept in the viscometer for 10 minutes to allow it to reach the temperature of the water bath. Then, suction was applied to the viscometer leg containing the capillary. To measure the efflux time, the sample was allowed to flow freely between the upper and lower marks indicated on the leg. The time for the meniscus to pass from the upper to the lower mark was recorded as the efflux time. After measuring the efflux time three times, the sample was diluted by adding a known weight of the solvent. Sucking the sample to the capillary leg and allowing it to flow freely in the viscometer at least twice before the efflux time was measured ensured mixing of the solvent and polymer solution. The initial polymer solution sample was diluted at least four times, and three efflux time measurements were undertaken for each concentration.

To determine the intrinsic viscosity, $[\eta]$, the reduced viscosity (η_{red}) was plotted versus concentration (c). Since the concentrations of all polymer solutions used in the determination of the intrinsic viscosity were very low, it was assumed that the density of all polymer solutions was the same and equal to the density of solvent. Moreover, the efflux times were measured for a given series of progressively diluted polymer solutions and pure solvent using a viscometer of the same capillary size. The η_{red} can be calculated from one of the following relationships

$$\eta_{red} = \frac{\eta - \eta_o}{\eta_o c} = \frac{\nu - \nu_o}{\nu_o c} = \frac{t - t_o}{t_o c} \tag{5.7}$$

where t and ν are the efflux time and kinematic viscosity of polymer solution; subscript o refers to the solvent. The η_{red} was calculated considering efflux times. The intrinsic viscosity, $[\eta]$, was estimated by a linear extrapolation of η_{red} to zero concentration. A linear regression was applied.

5.3.3.4 Relative viscosity

The relative viscosity (η_{rel}), is the ratio of the absolute viscosities of a polymer solution and the solvent (Eq. 4.13). Because of relatively high concentration of casting solutions (4.0 g/dL), the efflux times of solutions were measured in a viscometer with a larger capillary (capillary size 150). The procedure to measure the efflux times of casting solutions was exactly the same as that of dilute polymer solutions.

To determine the effect of temperature on polymer-solvent interactions, the relative viscosity of some polymer solutions was also obtained at elevated temperatures (40, 60, and 80°C). The capillary constants at 60 and 80°C were evaluated by a linear interpolation between the given values at 40 and 100°C. The temperature of the polymer solution was controlled by means of a water bath. The maximum variation of the temperature of the water bath was ± 0.1°C.

5.4 Preparation of Membranes

Homogeneous membranes were prepared by complete evaporation of solvent from cast films. A fixed amount (4 cm^3) of casting solution was poured inside a 9 cm diameter aluminum ring, which was placed on a leveled glass plate. Polymer solution on the glass plate was covered by a filter paper and the solvent was allowed to evaporate for two days. The membranes from THF were prepared in a dust-free casting box at room temperature, while all the other membranes were prepared in a forced air convection oven at temperatures ranging from 40 to 120°C. Immersing the plate together with the polymer film into distilled water facilitated removal of the membrane from the plate.

Membrane drying was a multi-stage process. After removal of membranes from the casting plate, the free standing films were air dried at room temperature for one day, followed by

air drying at 60 °C for another day. Air dried membranes were then dried in vacuum at pressure of 1 cmHg (absolute) and room temperature for at least two days before they were placed in a testing cell. The final membrane-drying step took place in the testing cell; however, its characteristics depended on the testing system in which the membrane was to be tested for gas permeation.

The membranes to be tested in the constant volume system were dried in the final membrane-drying step at 0.0003 cmHg (absolute) and room temperature for one day. The pressure of 0.0003 cmHg (absolute) was the highest vacuum that could be achieved in the constant volume testing system with or without the membrane inside the cell. When the membrane was placed in the testing cell, it took a maximum of 4 hours before the pressure reached the constant value of 0.0003 cmHg (absolute). During evacuation of the testing cell, the system was connected to the residual gas analyzer (RGA). This allowed monitoring and identifying residual vapors evaporating from the membrane.

The membranes to be tested in the constant pressure testing system were conditioned with dry CO_2 for 8 days in the final membrane-drying step. The conditioning was performed at the pressure gradient of 517 cmHg (688 kPa) while the permeate-side was at atmospheric pressure.

The above description indicates that there are a number of factors involved in the membrane preparation process. Those considered in this study include the solvent in the casting solution, the temperature at which evaporation of solvent takes place (casting temperature), and the temperature of polymer solution before it is cast in the oven (solution temperature).

5.5 Characterization of Membranes

5.5.1 Film thickness

The thickness of a membrane was determined by calculating the average from at least 10 thickness readings taken by a micrometer from the entire permeation area of the membrane.

5.5.2 Measurement of film density

The density of a polymeric film was determined by measuring the weight of polymer film in air and in a non-swelling liquid using a Mettler Kit, Model 163. The density (ρ) was calculated using an equation

$$\rho = \frac{W_o \rho_1}{W_o - W_1} \tag{5.8}$$

where ρ_1 is the density of liquid, W_o and W_1 are the weights of the sample in air and in the liquid, respectively. The weight measurements were done at 25°C, and water was used as a non-swelling liquid.

5.5.3 X-ray diffraction

The X-ray diffraction spectra of HSPPO and MeSPPO were obtained from the polymer films on a Philips Diffractometer PW370 BASED in a continuous scan with a scan step of 2Θ equal to 0.020° and a scan speed of 0.020°/s between 2Θ equal to 5 and 40°. The polymer films were mounted on a sample-holder disk without using any glycerin or back-up tape. Fitted profiles of the spectra were obtained using PC-APD diffraction software.

The values of 2Θ at the center of peaks on the spectra were used for calculation of d-spacing (d) using the Bragg equation:

$$d = \frac{\lambda_X}{2 \sin \Theta} \tag{5.9}$$

where λ_X is a wavelength of X-rays. A copper cathode generated monochromatic beam of X-rays of λ_X equal to 1.54 Å.

5.5.4 Thermal analysis

Thermal stability of the polymer films was examined using a Seiko 220TG/DTA analyzer run from 25 to 600°C heated at 10°C/min. Tests were done in nitrogen flushed at 200 cm^3/min.

5.5.5 Microscopic analysis

The surface morphology of membrane was investigated using a Nanoscope III atomic force microscope (AFM), operating in the tapping mode (TM). The AFM equipment was purchased from the Digital Instruments, Santa Barbara, CA.

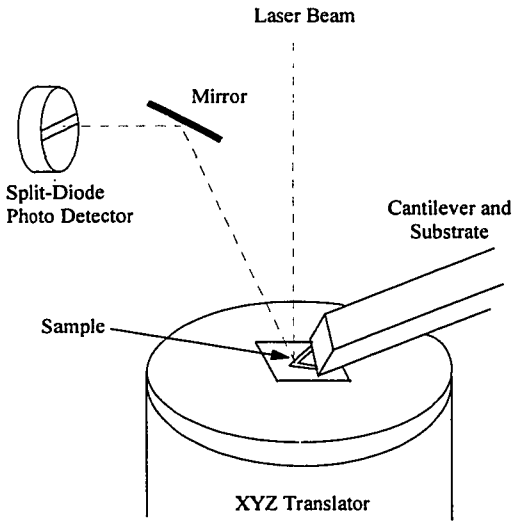

Figure 5-3. Schematic diagram of TM AFM utilizing an optical lever technique for sensing cantilever deflection.

Figure 5-3 shows a schematic diagram of an AFM utilizing an optical lever technique for sensing cantilever deflection. An extremely sharp tip, attached to a micro-cantilever arm is vibrated and brought near the sample surface. The cantilever oscillation is modified by interactions between the tip and the surface of the sample. Changes in the cantilever oscillation are detected by a split-diode photo-detector, which monitors a laser beam reflected off the cantilever. The signal from the photo-detector is sent to a control system, which maps the sample surface by adjusting the piezo height to maintain constant vibrational amplitude of the cantilever.

Before imaging the membrane surface, the calibration of the microscope was examined. The distances in X and Y directions measured on a 1 μm gold calibration grating differed less than 2%, while the distance in Z direction measured on a 180 nm step height calibration standard differed less than 10% from the values provided by the manufacturer. The images were obtained using etched silicon probes having tip diameter between 5 to 10 nm and half cone angle of $17 \pm 2°$.

In this study only the top surface of membrane, that is the surface formed on the solution-air interface, was observed. Small squares of approximately 0.5 cm^2 area were cut from

the dry membranes and glued on metal disks. Samples so prepared were ready for AFM investigation. The membrane surface was first imaged in a large scan size (12.0 x 12.0 μm) followed by a gradual zooming in a uniform section of the first image. The smallest scan size considered was 0.75 x 0.75 or 0.65 x 0.65μm.

5.5.5.1 Roughness parameters

The surfaces of the membranes were compared in terms of various roughness parameters, such as the mean roughness (R_a), the root mean square of the Z data (R_q), the mean difference between the five highest peaks and the five lowest valleys (R_z), the average peak height (h_{avg}), and the peak count. The roughness parameters were calculated using an image analysis software supplied with the AFM equipment [Digital Instruments, 1993]. The comparison was based on representative images of each of the studied surfaces. The roughness parameters depend on the curvature and size of the sensing probe, as well as on the treatment of the captured surface data (planefitting, flattening, filtering etc.). The comparison of the roughness data obtained in this study with a literature data might; therefore, not be appropriate. All the surface images; however, which will be discussed in the later part of this thesis, were obtained using the same type of the scanning probes and following the same protocol for the image treatment.

The mean roughness is the mean value of the surface (Z data) relative to the center plane, the plane for which the volume enclosed in the image above and bellow this plane are equal, and is calculated as

$$R_a = \frac{1}{L_x L_y} \int_0^{L_y} \int_0^{L_x} |f(x,y)| dx dy \tag{5.10}$$

where $f(x,y)$ is the surface (Z value) relative to the center plane and L_x and L_y are the dimensions of the surface.

The root mean square of the Z values is the standard deviation of the Z values within the given area and is calculated as:

$$R_q = \sqrt{\frac{\sum (Z_i - Z_{avg})^2}{N}} \tag{5.11}$$

where Z_{avg} is the average of Z values within the given area; Z_i is the current Z value; and N, the number of points within given area.

5.5.5.2 Measurement of features on images

The dimensions of nodules and nodule aggregates observed on images were estimated from cross-sectional profiles of the data along the reference line. An example of the measurement of the diameter and the height of the nodule aggregates is shown in Figure 5-4. For each pair of cursors, the horizontal and vertical distances as well as the angle between the cursors are given in the right window. The reference line can be placed anywhere on the image. The cursors can be placed anywhere on the reference line.

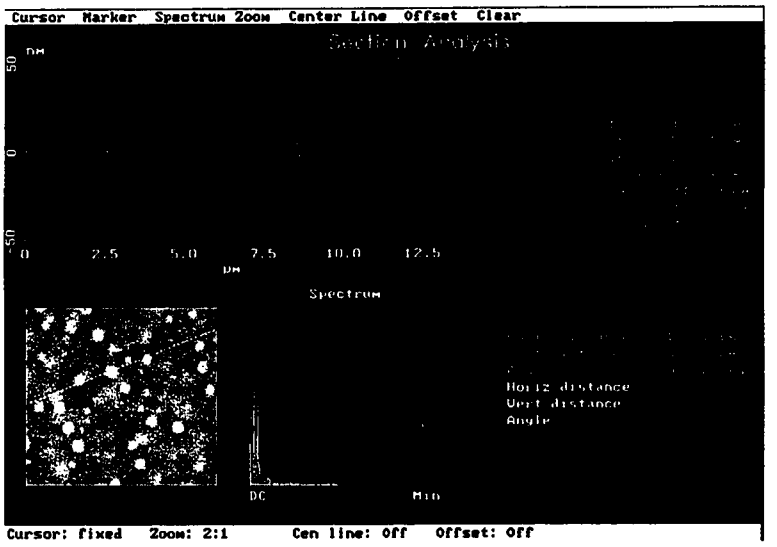

Figure 5-4. Example of determination of the size of the features on the membrane surface using AFM image software.

5.5.6 Gas permeation testing

Single gas permeation tests with N_2, O_2, CH_4, and CO_2 were performed in the constant volume (CV) and the constant pressure (CP) testing systems. In addition, gas separation experiments with O_2/N_2 and CO_2/CH_4 mixtures were performed in the CV testing system connected to the residual gas analyzer (RGA).

The details of the testing cell used in both testing systems are shown in Figure 5-5. A membrane is sandwiched between the feed and permeate sides of the cell. The sealing in the cell

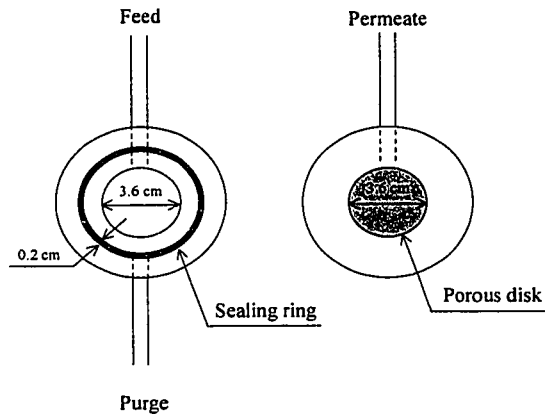

Figure 5-5. Details of the testing cell used in CV and CP gas permeation testing systems.

is provided by the contact of the membrane with a 2 mm wide and 0.2 mm high flat metal ring on the upstream part of the cell and a flat metal surface on the downstream part of the cell.

To prevent a potential damage of membrane by the edge of the sealing ring, the feed side of the membrane is laminated with a paraffin film ring of inner diameter equal to the diameter of the porous metal disk on the permeate side of the cell (3.6 cm). A filter paper is also placed on the porous plate to prevent a possible damage of the membrane when contacted with a rough surface of the porous disk. The permeation area of the cell (10.2 cm^2) is determined by the inner diameter of the paraffin film, because the paraffin film is impermeable for gases.

5.5.6.1 Single gas permeation test in the CV system

Permeation rate in the CV system is determined from the rate of pressure rise (*dp/dt)* in a known permeate side volume (V_p)

$$Q = \frac{V_p v_{STP}}{RT}\frac{dp}{dt} \tag{5.12}$$

where Q is the permeation rate of gas at standard temperature and pressure (STP) conditions. The STP conditions refer to T equal to 273.15 K and p equal to 101.3 kPa. The volume of one mole of any gas at the STP conditions (v_{STP}) is 22,415 cm^3/mol. R is the universal gas constant, and T is the absolute temperature in the testing cell.

Figure 5-6 shows the diagram of the CV testing system. Tabe Mohammadi (1995) described the details of this system. The following describes the procedure of gas permeation experiments performed in the CV testing system.

The pressure transducer PT2 monitors the pressure in the permeate side of the system and the computer records it. This allows continuous monitoring of *dp/dt* and hence permeation rates through the membrane. The permeate side volume of the system can be varied depending on the permeation rate. For low permeation rates, only the permeate side volume of tubing is utilized. The permeate side volume of tubing is the volume enclosed between AV2, AV5, BSV1, BSV2, BSV3 and the membrane. As the permeation rate increases, the permeate side volume can be increased by incorporating small (SmC), large (LgC) or both cylinders.

After placing membrane in the testing cell, the cell with the membrane was evacuated for one day as described in Section 5.4. Following evacuation, the valves AV1 and AV2 were opened to purge the gas supply line, which is the line connecting a gas cylinder with the mass flow controller MFC1, with the testing gas. During the purging process closing the valves AV3 and AV4 isolated the cell and the retentate line. Purging was necessary to remove air and the gas tested in the previous experiment from the supply line. The purge gas was removed from the system by the rotary vacuum pump P1. The RGA analyzer analyzed the composition of the purge

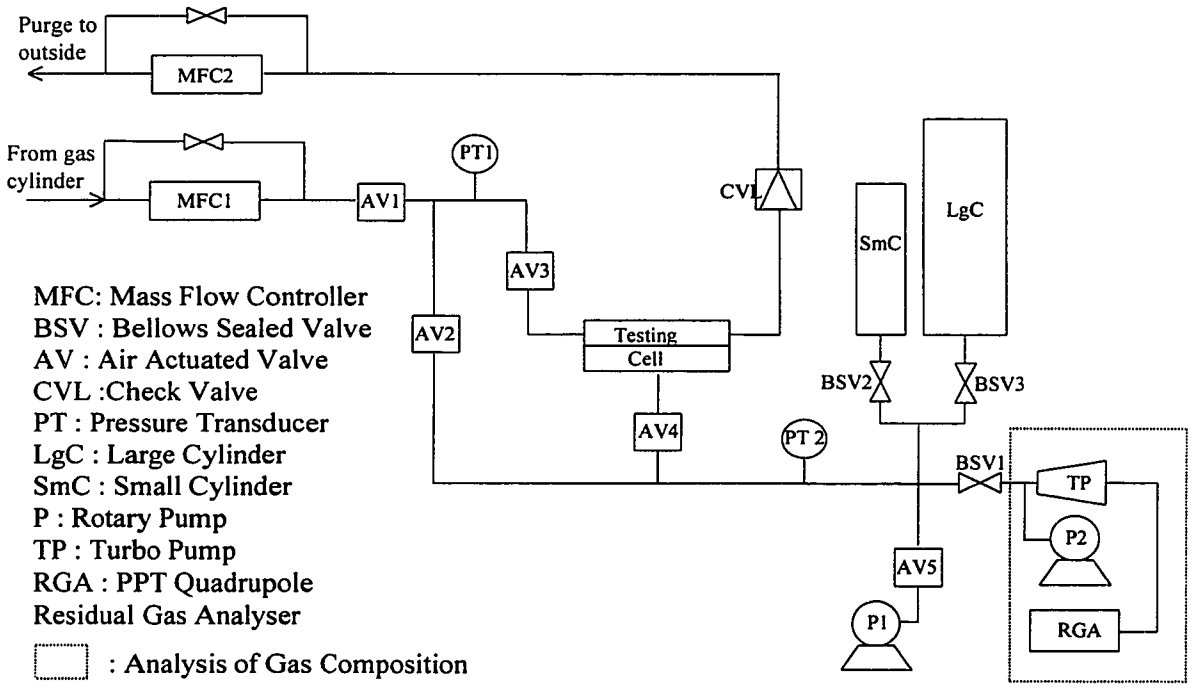

Figure 5-6. Schematic diagram of the constant volume testing system along with the residual gas analyzer.

gas. When the analyzer indicated no impurities in the purge gas, the cell and the retentate line were connected to the system by opening the valves AV3 and AV4. Following the purging process, the valve AV2, which connects the feed and permeate sides of the system, was closed. This initiated pressurization of the feed side and evacuation of the permeate side of the system. The pressurization of the feed side continued until the pressure reached the set value. When the pressure reached the set value the gas continued to flow into the feed side of the system. To maintain the constant feed side pressure the excess of the gas was continuously removed via the mass flow controller MFC2. Isolating the permeate side of the system from the pump P1 and the RGA analyzer by closing the valves AV5 and BSV2 commenced the gas permeation experiment.

Gas permeation experiments were performed at feed side pressure of 500 cmHg (665 kPa), while the permeate side pressure varied from 0.001 to 1.0 cmHg. When the feed side pressure reached 1.0 cmHg (end of a cycle), the valve AV5 was automatically opened, connecting the permeate side of the system to the vacuum pump P1. When the pressure dropped below 0.001 cmHg, the valve AV5 was automatically closed. Permeation tests were carried out over at least several cycles until the average permeation rate in a few consecutive cycles reached a constant value. The tests with N_2, O_2, and CH_4 were carried out for one day, while the tests with CO_2 were carried out for two days. Some membranes were tested with CO_2 for up to five days. The tests were performed in the following order; N_2, O_2, CH_4, and CO_2. In case of some membranes, after the test with CO_2, the test with CH_4 or N_2 was repeated.

5.5.6.2 Single gas permeation test in the CP testing system

In addition to the single gas permeation tests in the constant volume testing system, some membranes were tested in the constant pressure (CP) testing system. The constant pressure testing system consisted of six cells, so that six membranes could be tested simultaneously. The arrangement of the CP testing system for one of the testing cells is shown in Figure 5-7. The permeation rate was measured manually using a bubble flow meter attached to the permeate side of the system. The pressure gradient across the membrane during gas permeation test was 517 cmHg (688 kPa). The permeate side was at atmospheric pressure. The gases were tested in the following order: CO_2, N_2, O_2, and CH_4. The test with CO_2 was carried out for eight days, while

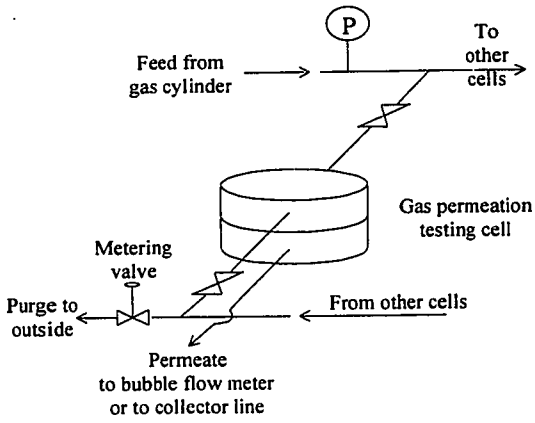

Figure 5-7. Arrangement of a cell in the constant pressure testing system.

each of the other gasses was tested for at least two days. The eight-day permeation test with CO_2 (CO_2 conditioning) represents an alternative for the final membrane-drying step. Some membranes were tested with CO_2 for more than 2 months to evaluate their stability in CO_2 at room temperature.

Permeability (P) of a membrane is calculated from

$$P = \frac{Ql}{A\Delta p} 10^{10} \qquad (5.13)$$

where Q is the steady state permeation rate (cm^3(STP)/s), l (cm) is the membrane thickness, A (cm^2) is the permeation area of the membrane, and Δp (cmHg) is the pressure gradient across the membrane. Permeability calculated from Eq. (5.13) has the unit of Barrer, which is defined as

$$1\text{Barrer} = 10^{-10}\, cm^3(STP)\ cm/(cm^2 s\ cmHg). \qquad (5.14)$$

This unit is widely used in the field of gas separation membranes in recognition of the major contributions of R.M. Barrer to this field.

Permeabilities obtained in single gas permeation tests were used to calculate permeability ratios. The permeability ratio (α_o) is also called permselectivity or ideal selectivity. The permeability ratios considered in this work were for O_2/N_2 and CO_2/CH_4.

5.5.6.3 Separation experiments

The actual separation factor (α) for the separation of gas A from gas B is given by

$$\alpha = \frac{[A]_p [B]_f}{[A]_f [B]_p} \qquad (5.15)$$

where square brackets indicate the concentration of gas and subscripts p and f refer to the feed and permeate, respectively.

Gas separation tests were performed in the CV testing system connected to the RGA analyzer as shown in Figure 5-6. The RGA is capable of analyzing the composition of gas

samples at pressures ranging from 10^{-5} to 10^{-9} cmHg (absolute). This is why the RGA analyzer is preceded by the rotary vacuum pump P2 and the turbo pump TP. The rotary vacuum pump brings down the pressure to a level of 10^{-4} cmHg (absolute). The turbo pump further reduces the pressure down to 10^{-9} cmHg (absolute). At these pressures high-energy electron beam ionizes and partly atomizes gas molecules present in the RGA chamber. This gives rise to characteristic peaks on the RGA spectrum. The location of the peak on the spectrum indicates the atomic mass of the ionized atom or molecule. For example, O_2 shows two peaks, one at 16 and the other one at 32 atomic mass units (AMU). When a sample contains some N_2, in addition to O_2, the RGA spectrum shows two extra peaks at 14 and 28 AMU. The composition of gas mixture is determined from the intensities of characteristic peaks.

The procedure of gas separation experiments is similar to the procedure of gas permeation experiments described in the previous subsection. Before the feed side of the system was pressurized, several spectra of the feed mixture were obtained. The separation experiment was carried out over at least several permeation cycles. When the average permeation rate in a few consecutive cycles reached a constant value, the system was connected to the RGA analyzer to determine the composition of the permeate. Several RGA spectra were obtained over at least two permeation cycles. After depressurization of the system, the composition of the feed mixture was verified.

The actual separation factor for O_2/N_2 separation was determined using air as a feed. The actual separation factor for CO_2/CH_4 separation was determined using two feed streams, one containing 20.4% of CO_2 in CH_4 and the other one containing 50% of CO_2 in CH_4.

5.6 Chemicals

The alphabetical list of the chemicals used in this study along with their suppliers is given in Table 5.2.

Table 5-2. List of chemicals used during the course of this research.

	Chemical	Specifications	Source [a]
A	Acetone	Reagent Grade	Fisher
	Aluminum Nitrate	99.99% Purity	Aldrich
B	Buffer Solution	pH = 4.0	BDH
C	Carbon Dioxide	Gas Cylinder, 99.5% Purity	Air Products
	Carbon Dioxide in Methane (1)	Gas Cylinder, 50% CO_2 in CH_4	Air Products
	Carbon Dioxide in Methane (2)	Gas Cyl., 20.4% CO_2 in CH_4	Air Products
	Chloroform	Anhydrous	Aldrich
	Chloroform	Hydrocarbon stabilized	BDH
	Chloroform-*d*	100 atom % D	Aldrich
	Chlorosulfonic acid	99% Purity	Aldrich
D	N,N-Dimethylacetamide (DMAC)	HPLC Grade	BDH, Fisher
	N,N-Dimethylformamide (DMF)	Analytical Grade	BDH
H	Hydrochloric Acid	0.1 N Standard	BDH
M	Magnesium Nitrate	99.995% Purity	Aldrich
	Methane	Gas Cylinder, 99% Purity	Air Products
	Methyl Alcohol	Reagent Grade	BDH
	Methyl-d_3 Alcohol-*d*	99.95 atom % D	Aldrich
	N-methyl-2-Pyrrolidone (NMP)	HPLC Grade	Aldrich, BDH
N	Nitrogen	Gas Cylinder, 99.95% Purity	Air Products
	Nitroethane	Reagent Grade	Fisher
O	Oxygen	Gas Cylinder, 99.5 Purity	Air Products
P	Phenolphthalein	Alcohol Solution	BDH
	PPO	Powder, $[\eta]$=1.78 dL/g @25°C	GE
	Pyridine	Reagent Grade	Fisher
S	Silicone Rubber	Film, thickness = 50.4μm	GE
	Sodium Hydroxide	0.1 N Standard	BDH
T	Tetrahydrofuran (THF)	Reagent Grade	BDH
	Trichloroethylene (TCE)	Reagent Grade	BDH

[a] Full names of suppliers: Air Products Canada, Nepean, ON; Aldrich Chemical Company, Inc., Milwaukee, WI; BDH Chemicals Canada Limited, Toronto ON; Fisher Scientific, Ottawa, ON, General Electric Company, Selkirk, NY

PART III

RESULTS AND DISCUSSION

CHAPTER 6

Development and Characterization of HSPPO Films

6.1 Sulfonation of PPO

During chemical modification of PPO via sulfonation to a target *IEC* equal to 1.4 meq/g, the polymer precipitated prior to complete addition of chlorosulfonic acid solution. Similarly, while sulfonating PPO to the targeted *IEC* value of 2.0 meq/g, precipitation of HSPPO from the chloroform solution was observed when approximately 60 - 70% of the chlorosulfonic acid solution was added to the reactor. Consequently, the maximum achieved *IEC* was only 1.80 meq/g, which was considerably lower than the *IEC* values reported in the literature. For example, Plummer *et al.* (1970) prepared HSPPO of an *IEC* value above 3.0 meq/g while Fu *et al.* (1994a) prepared HSPPO of *IEC* equal to 2.5 meq/g. It is important to emphasize that PPO used for sulfonation in this work had an intrinsic viscosity equal to 1.78 dL/g, which was considerably greater than that 0.4 - 0.5 dL/g of PPO used in the earlier works [Plummer *et al.*, 1970; Percec, 1987; Percec and Li, 1988; Huang and Kim, 1984a; Fu *et al.*, 1994a].

The relationship between intrinsic viscosity [η] and molecular weight (*MW*) is described by the Mark-Houwink equation

$$[\eta] = K' MW^{a} \tag{6.1}$$

where K' and a are constants. For PPO-chloroform system at 25°C the values of K' and a are 0.00048 and 0.64, respectively, [Industrial Membrane Research Institute, 1995]; therefore, the molecular weigh of PPO having [η] equal to 1.78 dL/g is more than 7 times greater than the molecular weight of PPO having [η] equal to 0.5 dL/g.

An increase in the molecular weight of PPO results in a decrease in solubility of PPO in chloroform and enhances early precipitation of HSPPO out of the chloroform solution. After precipitation of HSPPO, further sulfonation is restricted to the interface between the solution and the precipitated polymer. It would probably be possible to sulfonate PPO to an *IEC* above 1.80 meq/g by using a large excess of cholrosulfonic acid; however, such HSPPO may not have a uniform distribution of sulfonic groups within the polymer batch.

The targeted *IEC* values are compared in Table 6-1 with the values determined experimentally by acid-base titration and ^{1}H NMR. It can be noticed that, in general, the achieved *IEC* values were close to the anticipated values. Apart from the deviation between targeted and achieved *IEC* values for batches 8 and 9, which has already been discussed, it is interesting to note that *IEC* determined by ^{1}H NMR was higher than that determined by acid-base

Table 6-1. Comparison of the targeted and actual *IEC* values of SPPO batches prepared by sulfonation of PPO using chlorosulfonic acid.

Batch No.	Press. in purge line, psig	Target *IEC* meq/g	Actual *IEC*, meq/g	
			Titration	^{1}H NMR
1	< 2	1.0	0.47	0.96
2	8	1.0	1.01	1.03
3	< 2	1.4	1.18	1.42
4	8	1.0	0.98	1.02
5	8	1.4	1.36	1.39
6	8	1.4	1.37	1.35
7	8	0.75	0.72	0.77
8	8	2.0	1.80	1.83
9	8	2.0	1.78	1.80

titration for batches 1 and 3. The infrared (IR) spectrum of the films prepared from batches 1 and 3 showed two extra peaks at 635 and 780 cm^{-1} in addition to the IR spectrum of the film prepared from PPO polymer. On the other hand, films prepared from other HSPPO batches showed only one extra peak at 635 cm^{-1}. The peak at 635 cm^{-1} can be assigned to C-S bond [Rao, 1963] resulting from the attachment of the sulfonic group to the aromatic carbon. The second peak at

780 cm^{-1} was probably due to C-Cl bond resulting from the attachment of Cl to the benzene ring [Rao, 1963]. This indicates that sulfonation of batches 1 and 3 resulted in a sulfonated-chlorinated PPO, rather than in sulfonated PPO.

The *IEC* value determined by acid-base titration indicates the degree of polymer substitution with sulfonic groups because sodium hydroxide can only react with the proton on the sulfonic groups. On the other hand, the *IEC* value determined by ^1H NMR indicates the total degree of polymer substitution, including both sulfonic and chlorine substituents because, the shifts caused by these substituents could not be distinguished by the resolution of the ^1H NMR equipment used in this study. Therefore, the difference between the degree of substitution determined by ^1H NMR and that determined by acid-base titration should correspond to the degree of chlorination of polymer.

The only difference in the sulfonation procedure of batches 1 and 3 from other batches of PPO was the rate of N_2 gas purging of the reactor content during sulfonation. In case of batches 1 and 3, the pressure in the N_2 line was set at less than 2 psig, while in case of sulfonation of other PPO batches, the pressure in the N_2 line was set at 8 psig. A decrease in the purge rate of the reactor content with N_2 led to a less efficient removal of hydrochloric acid, formed during sulfonation, from the polymer solution. In turn, this resulted in an increase in concentration of hydrochloric acid in the polymer solution and might have consequently enhanced the reaction between PPO and hydrochloric acid. In this work, however, the possibility of simultaneous sulfonation and chlorination of PPO was not further pursued, although this could be a valuable material for gas separation membranes. Polymer solutions for casting films were prepared only from sulfonated PPO batches.

6.2 Film Density

The density of HSPPO film increased with an increase in the *IEC* value of polymer as shown in Figure 6-1. The experimentally measured densities are slightly larger than densities calculated by the modified free volume model proposed by Park and Paul (1997). The numerical values of the predicted and experimental densities of HSPPO films can be found in Appendix C. The deviation between experimental and calculated densities increased with an

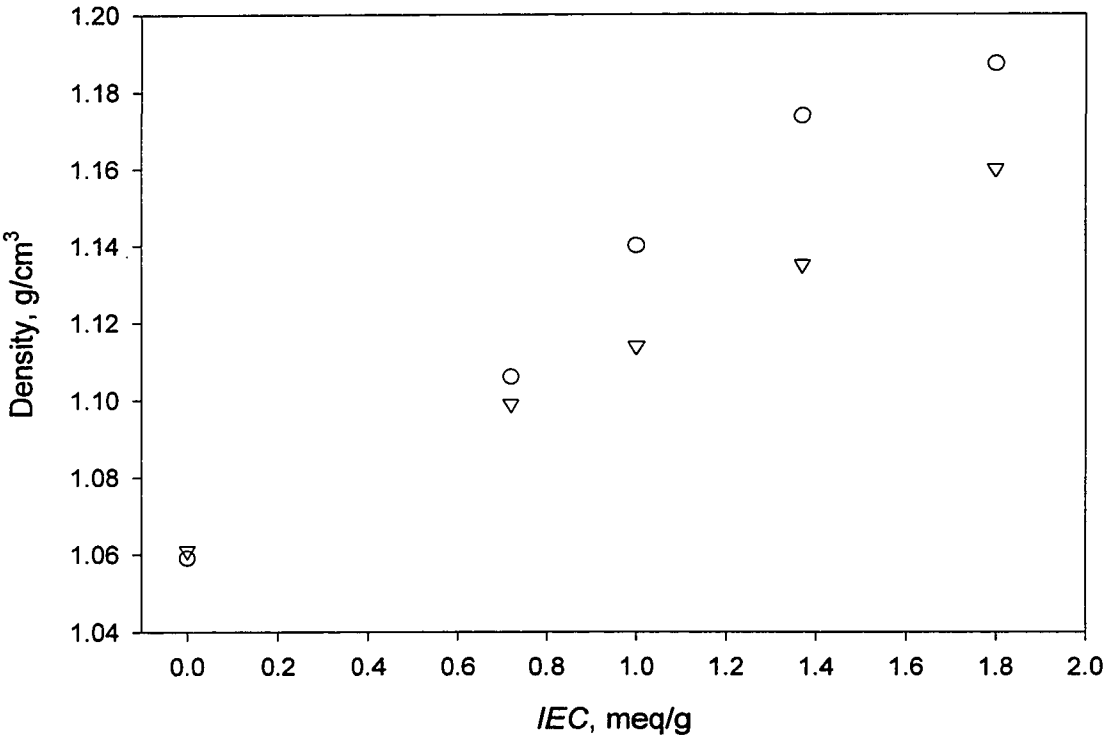

Figure 6-1. Effect of *IEC* on density of HSPPO films; (o) experimental; (∇) calculated by the modified free volume model [Park and Paul, 1997].

increase of sulfonic content in the polymer. It should be emphasized; however, that the weight of film was measured in water, which was a non-swelling liquid required for determination of experimental density. An increase in *IEC* resulted in an increase of the hydrophilicity of polymer. Consequently, more water can penetrate into the microporous structure of the polymer, thus increasing the apparent weight of the sample in water, and hence its experimental density [Volkov *et al.*, 1997]. An increase in affinity for water with increasing *IEC* was confirmed by TGA analysis of films with *IEC* values equal to 1.37 and 1.80 meq/g, which is discussed in more detail later in Section 6.4.

6.3 X-ray Diffraction Spectra

The X-ray diffraction spectra of the films made of PPO and HSPPO of various degrees of sulfonation are very similar. Figure 6-2 shows the X-ray diffraction spectrum of an HSPPO film whose *IEC* value is equal to 1.80 meq/g. The major feature of this spectrum is a broad peak at 2Θ of 14.4°, which corresponds to a d-spacing of 6.15Å. This value of d-spacing does not change with the degree of sulfonation and is close to the value of 6.1Å reported by Story and Koros (1992) for PPO and carboxylated PPO.

The peak in Figure 6-2, however, does not have a Gaussian shape. The right shoulder of the peak is higher in its intensity than the left one, which suggests the presence of a lower intensity peak at 2Θ equal to about 21 - 22°. Using a profile fitting software, the X-ray diffraction spectrum of HSPPO films can be resolved into two overlapping peaks, the first one located at 2Θ ranging from 14.04 to 14.12° and the second one located at 2Θ ranging from 21.15 to 21.60°. The difference in positions of the first peak on the fitted and actual profiles is a result of the interference from the second peak, which shifts the center of the first peak towards a higher 2Θ angle. A summary of the analysis of the X-ray diffraction spectra of PPO and HSPPO films is shown in Table 6-2. The spectra were compared in terms of peak position, peak width, peak intensity and intensity ratio. None of the above parameters changes significantly as *IEC* increased from 0 to 1.80 meq/g. Some variation in absolute intensities of the peaks from sample to sample may be attributed to the differences in the thickness of samples.

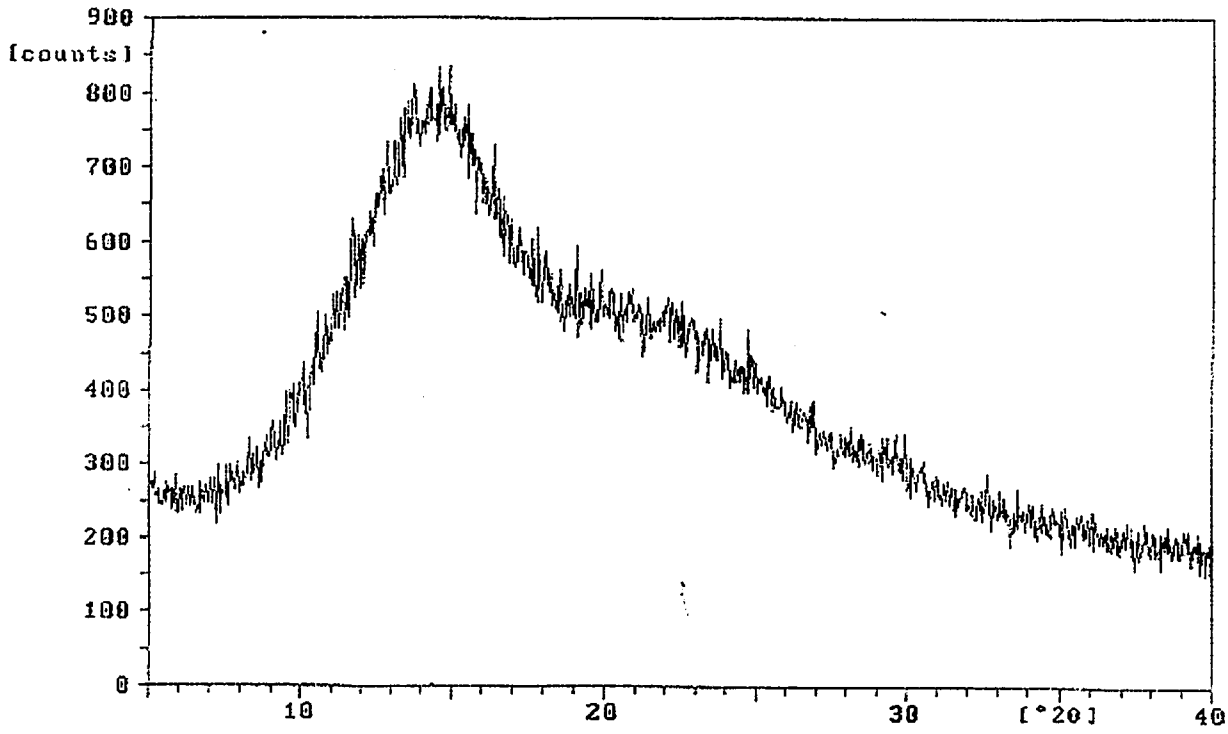

Figure 6-2. X-ray diffraction spectrum of HSPPO-1.80 film prepared using DMAC as a solvent.

Table 6.2 Summary of the analysis of X-ray diffraction spectra of HSPPO membranes.

IEC meq/g	Peak	Position, 2Θ° actual	Position, 2Θ° fitted	Width, 2Θ°	Peak Intensity[a]	Intensity ratio
0	1	14.3	14.07	5.81	321	1.91
	2	-	21.01	11.42	168	
0.72	1	14.4	14.04	5.00	280	1.92
	2	-	21.15	10.98	146	
1.00	1	14.4	14.10	5.49	255	1.97
	2	-	21.07	12.99	129	
1.37	1	14.4	14.12	5.91	419	2.23
	2	-	21.06	10.05	188	
1.80	1	14.3	14.05	5.67	339	1.95
	2	-	21.52	11.19	174	

[a] From the spectra resolved using a profile fitting software

6.4 Thermal Stability

Figure 6-3 presents TGA spectra of HSPPO-1.37 and HSPPO-1.80 films prepared from DMAC solutions. The films were dried at pressures less than 10 Torr and room temperature for several days. Before TGA analysis the films were exposed to air at atmospheric conditions. Three weight loss stages followed by the final decomposition of polymer can be distinguished in Figure 6-3. For the HSPPO-1.37 film the weight loss stages were located at 30 to 100°C, 175 to 297°C and 297 °C up to the final decomposition of polymer. For the HSPPO-1.80 film the weight loss stages were located at 30 to 100°C, 175 to 275°C and 300 °C up to the final decomposition of polymer. For both films the final decomposition of polymer begins just above 400°C. The location of the weight loss stages observed here is almost identical to the location of weight loss stages in low molecular weight HSPPO reported by Fu *et al.* (1994a). The weight losses at the three weight loss stages for the HSPPO-1.37 film were 2.0, 10.7 and 3.0% of the original weight of the polymer, while for the HSPPO-1.80 film these were 3.0, 11.8 and 4.5% of

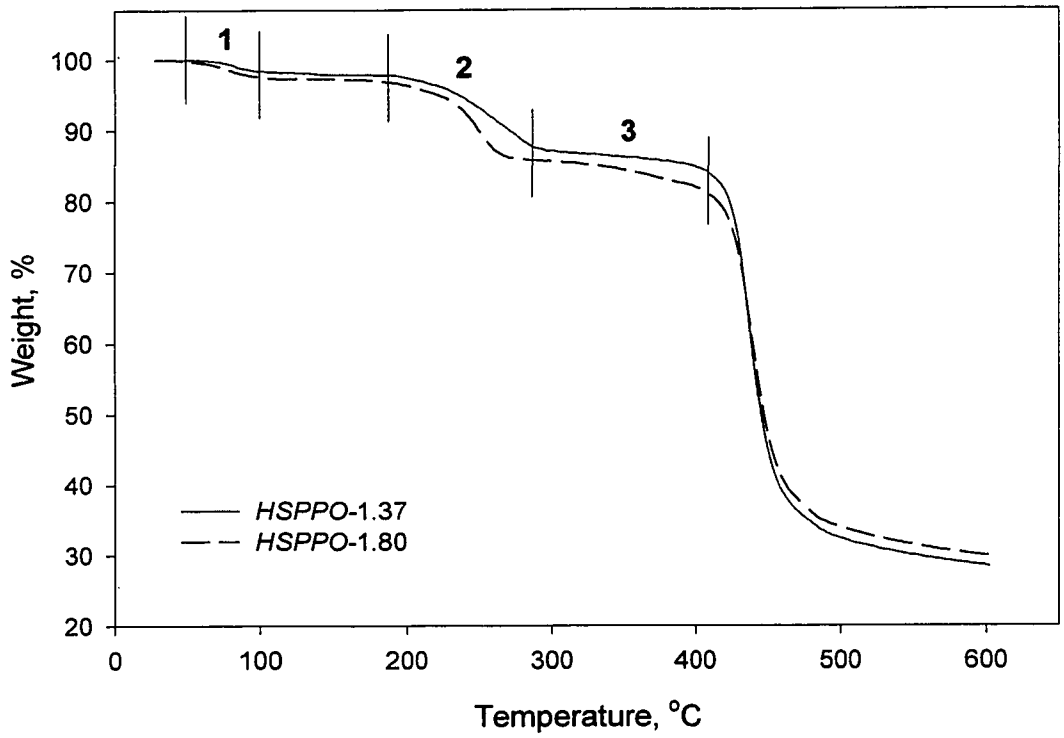

Figure 6-3. Thermogravimetric analysis of HSPPO films prepared using DMAC as a solvent.

the original weight of polymer. This comparison indicates that the weight loss increases with an increase in *IEC* of polymer. Similar relation between *IEC* and the weight loss was reported by Fu *et al.* (1994a) for low molecular weight HSPPO.

Considering that prior to TGA analysis the films were exposed to air and hence to the atmospheric moisture, the weight loss in the first stage can be attributed to the loss of moisture adsorbed from air. This weight loss increased with an increase in the *IEC* value, *i.e.* with an increase in sulfonic content. This is not surprising considering the fact that sulfonic groups are very hydrophilic. The loss in the second stage can be attributed to the decomposition of sulfonic groups. The observed weight losses in the second stage; *i.e.* of 10.7 and 11.8 % of the original weight of the films of *IEC* values equal to 1.37 and 1.80 meq/g, respectively, are comparable to the corresponding weight percent of sulfonic groups in these polymers; *i.e.* to 11.0 and 14.3 wt.% respectively. The decomposition of sulfonic groups at high temperatures was confirmed by the measurement of *IEC* of HSPPO by ^{1}H NMR after annealing polymer samples in an oven at 120 and 140°C, respectively. Annealing polymer samples of the initial *IEC* equal to 1.37 meq/g for 24 hrs at these temperatures resulted in a decrease in *IEC* to 0.87 and 0.62 meq/g, respectively.

Following the second stage, the weight of the membranes continues to decrease at a much slower rate than in the second stage. According to Fu *et al.* (1994a), the weight loss in the third stage is related to the beginning of the splitting of the main chains. The weight loss in this stage may also be related to the evaporation of residual DMAC. Following decomposition of sulfonic groups in the second stage, the polymer becomes more hydrophobic (PPO); therefore, DMAC, if still present, becomes a residual non-solvent. Because of the lack of strong interactions between the polymer and non-solvent, the latter should be easily removed form the polymer. Furthermore, in the third weight loss stage HSPPO is already in a rubbery state [Fu *et al.*, 1994a] and the temperatures are well above the boiling point of DMAC of 162°C. Consequently, DMAC should leave the polymer in a relatively narrow temperature range. However, a decrease in the weight of the polymer in the third stage is spread over a wide temperature range, up to the final decomposition of polymer. This indicates that the weight loss in the third stage is not likely associated with the evaporation of residual DMAC.

The possibility of existence of residual solvent in films after drying is further discussed in Chapter 8 when the properties of films prepared from different casting solutions are considered.

6.5 Gas Transport Properties

To facilitate the process of testing, gas permeation experiments were performed in two different testing systems, a constant volume (CV) and a constant pressure (CP) testing system. The details of testing systems are described in Chapter 5.

6.5.1 Properties of gases

Table 6.3 shows some properties of gases used in this study. The solubility parameters (δ) for O_2 and N_2 are not available, however their values should be close to the solubility parameter of CH_4 of 11.0 $MPa^{1/2}$ and considerably lower than the solubility parameter of CO_2 of 21.9 $Mpa^{1/2}$ [Grulke, 1989]. CO_2 has not only the highest δ, but also is the most condensable and has the smallest molecule among gases used in this study. Critical temperature (T_c) of CO_2 is 31.1°C (304.1 K) [Linde, 1992] and the kinetic diameter (D_k) of CO_2 is 3.3 Å [Kesting and Fritzsche, 1993].

Table 6-3. Some properties of gases used for testing membranes.

Gas	T_c, K	δ, $Mpa^{1/2}$	D_k, Å
N_2	126.2	-	3.64
O_2	154.6	-	3.46
CH_4	190.5	11.0	3.80
CO_2	304.1	21.9	3.30

6.5.2 Conditioning of HSPPO films by CO_2

Testing conditions, in particular the duration of gas permeation experiments and the order in which gases were tested, rarely accompany gas separation data available in the literature. These factors; however, are very important, especially when an experiment involves a gas with high solubility parameter such as CO_2 that can condition [Maeda and Paul, 1987] or plasticize polymeric membranes [Puelo and Paul, 1989].

(a)

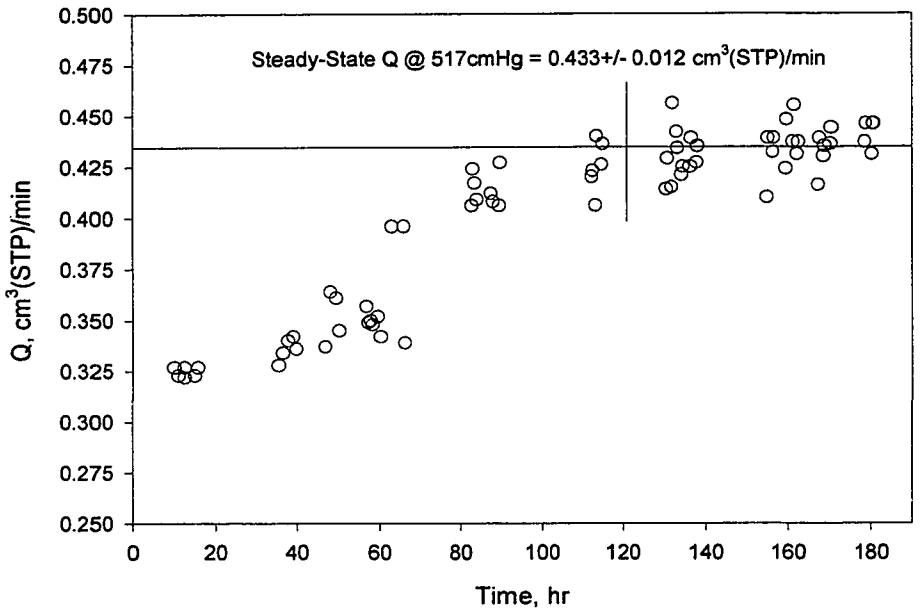

(b)

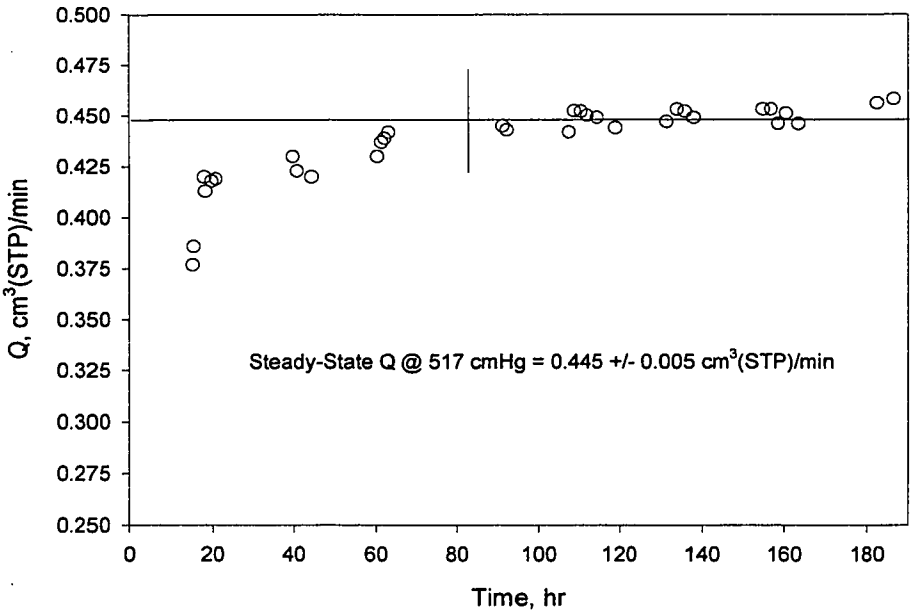

Figure 6-4. Progress of CO_2 permeation experiment in the constant pressure testing system at 517 cmHg trans-membrane pressure using HSPPO-1.01 membrane prepared from THF solution; **(a)** first test; **(b)** repeated test with the same membrane.

Figure 6-4a shows the progress of a permeation experiment with CO_2 at a 517 cmHg pressure gradient across the membrane in the CP system. It can be noticed that after a relatively constant permeation rate in the first day, the permeation rate continued to increase from the second day until it leveled off after the fifth day. The average rate of permeation after 120 hrs was found to be 0.433 cm^3(STP)/min with a standard deviation of 0.012 cm^3(STP)/min.

Permeation rates of N_2, O_2, and CH_4 increased by 20 – 40% after the test with CO_2. The CO_2 permeation experiment was repeated after N_2, O_2, and CH_4 permeation experiments. The results are shown in Figure 6-4b. The permeation rate of CO_2 leveled off again after the initial increase. The permeation rate became 0.445 ± 0.005 cm^3(STP)/min) when the steady state was reached. Comparing Figures 6-4a and 6-4b one can notice that initial permeation rate was higher and the steady state was reached more rapidly in the second test. It should also be noted that, unlike the CO_2 tests, no increasing trend in permeation rate was observed for other gases in experiments lasting four days.

Some HSPPO films were tested with CO_2 for two months. The progress of a 63-day permeation test with CO_2 is shown in Figure 6-5. The experiment was carried out between December 1996 and February 1997 in the CP system at a 517 cmHg trans-membrane pressure. It can be noticed that CO_2 permeation rate increased approximately by 20% during the first 3 days and after that it remained constant. The trend observed in Figure 6-5 is similar to that observed in the 8-day permeation experiments (Figure 6-4). The results shown in Figure 6-6 are indicative of the long-term stability of HSPPO at room temperature.

The above stability effect can be considered as a means for conditioning of polymeric films with CO_2. Jordan *et al.* (1990), who studied properties of aromatic polyimides, emphasized the importance of CO_2 conditioning. They reported up to 100% increase in O_2 permeability and negligible changes in O_2/N_2 permselectivity resulting from conditioning of hollow fibers with CO_2 at 646 cmHg for two days. On the other hand, conditioning of homogeneous films prepared from the same polymer resulted in much smaller (13.5%) increase in O_2 permeability [Jordan *et al.*, 1990].

Concurrently to the tests in the CP system, HSPPO films were also tested in the CV system. Figure 6-6 shows the progress of a five-day permeation test with CO_2 in the CV system.

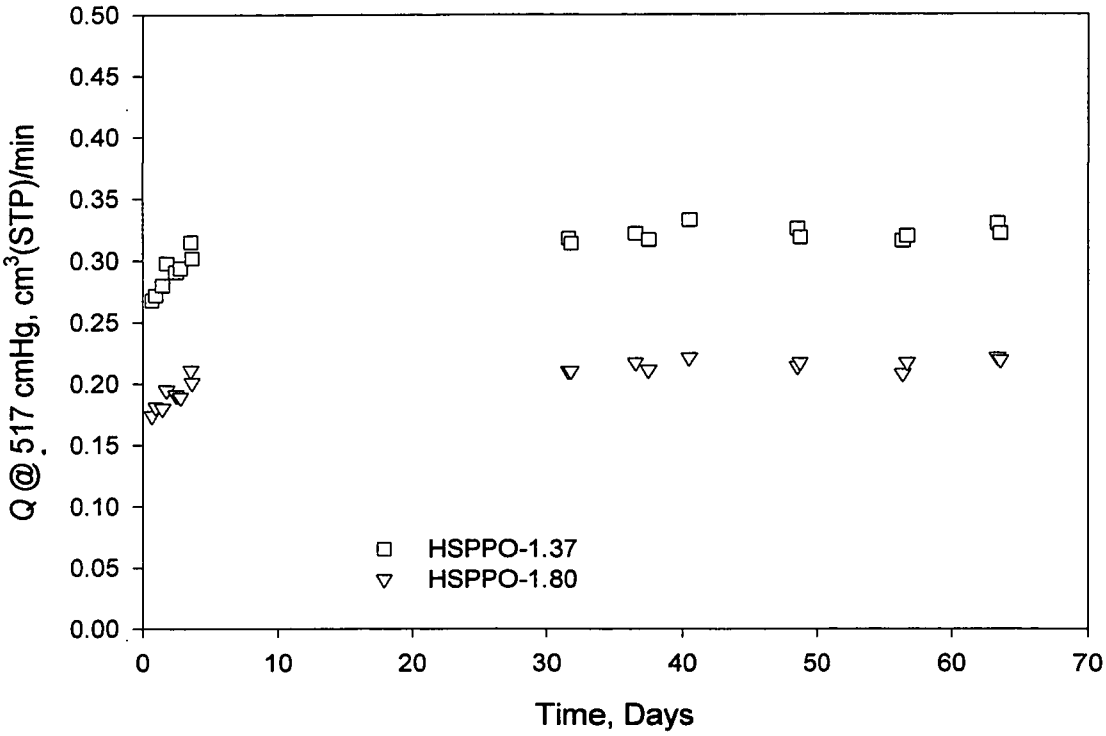

Figure 6-5. Progress of long-term permeation tests with CO_2 in the constant pressure testing system at 517 cmHg trans-membrane pressure using HSPPO films prepared from DMAC solutions.

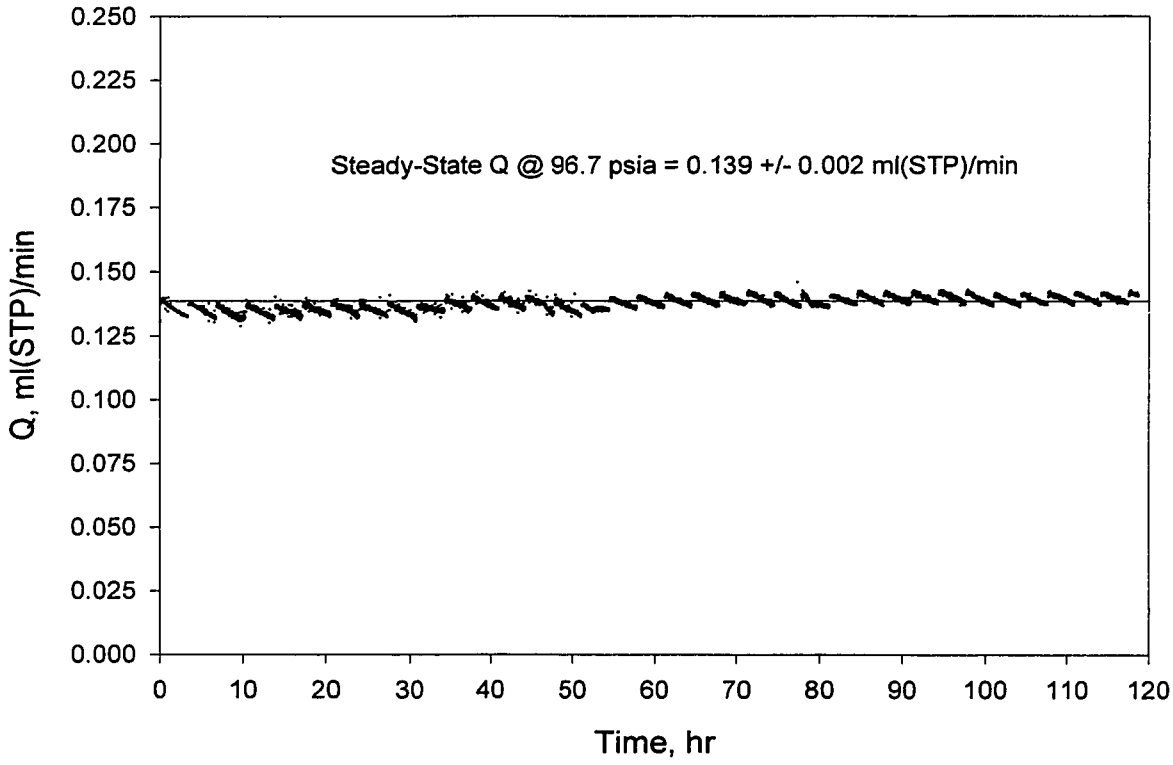

Figure 6-6. Progress of CO_2 permeation experiment in the constant volume testing system using HSPPO-1.80 membrane prepared from DMAC solution; upstream pressure equal to 96.7 psia, downstream at vacuum.

It can be noticed that, unlike the tests in the CP system, CO_2 permeation did not change significantly during the experiment. In addition, the conditioning effect observed in the CP system, that is an increase in permeation rate of N_2, O_2, and CH_4 after the test with CO_2, was not observed in the CV system.

6.5.3 Comparison of data obtained in CV and CP systems

Table 6-4 shows gas permeabilities of HSPPO-1.37 membranes prepared from DMAC solution measured by the CV and CP systems. Three membranes were tested in each of the testing systems.

Table 6-4. Gas permeabilities of HSPPO-1.37 tested in constant volume (CV) and constant pressure (CP) testing systems.

System	Permeability, Barrer				Permselectivity			
	N_2	O_2	CH_4	CO_2	O_2/N_2	CO_2/CH_4	CO_2/O_2	N_2/CH_4
	0.45	2.85	0.34	13.15	6.29	37.10	5.06	1.32
CV	0.54	3.38	0.45	16.29	6.30	36.28	4.88	1.19
	0.51	3.24	0.46	16.04	6.40	34.81	4.95	1.10
Avg.	0.50	3.16	0.42	15.16	6.33	36.06	4.96	1.20
St.Dev.	0.05	0.27	0.07	1.75	0.07	1.16	0.09	0.11
	0.46	2.54	0.37	16.09	5.58	43.55	6.33	1.23
CP	0.53	2.96	0.39	16.44	5.35	42.82	5.82	1.38
	0.62	3.23	0.47	18.06	5.22	38.43	5.60	1.31
Avg.	0.54	2.91	0.41	16.86	5.38	41.6	5.92	1.31
St.Dev.	0.08	0.35	0.05	1.05	0.18	2.77	0.37	0.08

It can be noticed in Table 6-4 that polymer films behave differently in different testing systems. On one hand, permeabilities for N_2 and CH_4 obtained in both systems are comparable. On the other hand, O_2 permeability obtained in the CV system is greater, while CO_2 permeability is smaller than that obtained in the CP system.

The difference in gas transport properties obtained in the two testing systems is more evident when permeability ratios are compared. For example, O_2/N_2 permeability ratio of 6.33

obtained in the CV system was considerably greater than 5.38 obtained in the CP system. On the other hand, CO_2/CH_4 permeability ratio of 36.06 obtained in the CV system was less than 41.6 obtained in the CP system.

The films tested in the CV system were dried at an ultra-high vacuum in the testing cell for one day, whereas the films tested in the CP system were conditioned with CO_2 for eight days in the testing cell prior to permeation experiments. While the film was subjected to an ultra high vacuum, the CV system was connected to the residual gas analyzer (RGA), which allowed monitoring of species evaporating from the film. As already mentioned in Chapter 5, it took up to four hours before the system reached the maximum vacuum of 0.0003 cmHg absolute. Immediately after starting evacuation, the peaks characteristic to air appeared in the RGA spectrum. Their presence was a result of exposing the system to the atmosphere when placing the film in the cell. While the air peaks were quickly disappearing, the peaks characteristic to water started to appear on the spectrum. The presence of water peaks in the RGA spectra was also a result of the exposure of films and the testing system to the atmosphere. The presence of water (2-3 wt%) was also observed in the TGA spectra of HSPPO films (Figure 6-3). The water peaks; however, were gradually diminishing over the course of the system evacuation. No peaks, which could be associated with DMAC, were observed during evacuation.

As a result, gas permeation experiments in the CV system were performed in a completely dry environment because all moisture was removed prior to the beginning of gas permeation tests. As for the CP system, on the other hand, while the CO_2 gas used for conditioning of films in the CP system was dry, the permeate side of the CP system was opened to atmosphere. Consequently, the atmospheric humidity could have prevented the purging of all moisture from the films during their conditioning with CO_2, and therefore, some moisture could have been present in films during their gas permeation tests.

All permeation experiments in the CP system were carried out in the second half of November 1996. During the above period, the relative humidity in the laboratory oscillated between 25 and 35 % while the temperature oscillated between 21.5 and 22.5°C.

6.5.4 Effect of relative humidity on gas permeation test in constant pressure system

Permeability of HSPPO-1.37 prepared from the DMAC solution was re-examined in the CP system using new films. Two series of tests were performed. In each series at least three membranes were tested. The first series was carried out in the second half of February 1997, whereas the second series was carried out in the second half of July 1997. The temperature in the laboratory throughout the year was approximately constant ranging from 21 to 23°C. On the other hand, the relative humidity during the winter test oscillated between 11 and 17%, while during the summer test it oscillated between 42 and 55%. Table 6-5 summarizes permeability data in the two series of experiments.

It can be noticed in Table 6-5 that there are significant differences in permeabilities of the same type of films measured in the same testing system at different times of the year. It should be emphasized that in both testing series only freshly prepared films were used, and that all films in the respective series were tested simultaneously.

Table 6-5. Permeability of HSPPO-1.37 films prepared from the DMAC solution determined in the CP system during winter and summer tests.

Test Time	Permeability, Barrer				Permselectivity			
	N_2	O_2	CH_4	CO_2	O_2/N_2	CO_2/CH_4	CO_2/O_2	N_2/CH_4
Winter	0.50	3.00	0.41	15.85	5.95	38.53	5.26	1.23
	0.58	3.29	0.48	17.69	5.47	36.71	5.37	1.23
	0.45	2.81	0.38	14.56	6.30	39.02	5.18	1.21
	0.53	3.20	0.45	17.19	6.02	37.97	5.37	1.18
Avg.	0.52	3.08	0.43	16.32	5.94	38.06	5.30	1.21
St.Dev.	0.05	0.21	0.04	1.41	0.34	1.00	0.09	0.02
Summer	0.56	2.65	0.40	20.26	4.83	50.18	7.65	1.36
	0.50	2.33	0.33	15.75	4.61	47.96	6.76	1.54
	0.56	2.75	0.43	19.99	4.88	46.91	7.26	1.32
Avg.	0.54	2.58	0.39	18.67	4.77	48.35	7.22	1.41
St.Dev.	0.03	0.22	0.05	2.53	0.14	1.67	0.45	0.12

It can be noticed that O_2 permeability of the winter test is greater than that in the summer test. In case of CO_2 permeability the order is reversed. As a result, CO_2/O_2 permeability ratio increased by 36% from winter to summer. There are also significant changes in O_2/N_2 and

CO_2/CH_4 permselectivities. The former decreased by 20%, while the latter increased by 27% from winter to summer.

The fact that, for a given type of membrane, the change in permeability occurs not only in different systems but also in the same testing system, suggests that gas permeability is affected by the permeate side conditions. As already mentioned the temperature in the laboratory remained almost constant throughout the year; however, the water vapor pressure varied considerably. Since temperature in the laboratory was constant, the changes in water vapor pressure in the laboratory can be represented by the change in the relative humidity (RH).

The effect of RH in the atmosphere on permeability of HSPPO-1.37 films is summarized in Table 6-6. The data obtained in the CV system are also included in this table. It is assumed that the RH in the CV system is zero, since all water was removed completely from the system prior to gas permeation tests. Permeabilities shown in Table 6-6 are the average values for a given RH range.

Table 6-6 shows clearly that permeability of HSPPO-1.37 films is affected by relative humidity in the atmosphere. In particular, O_2 permeability decreases while CO_2 permeability

Table 6-6. Effect of relative humidity in the atmosphere on permeability of dense high molecular weight HSPPO-1.37 membranes prepared from the DMAC solution[a].

RH, %	Permeability, Barrer				Permselectivity			
	N_2	O_2	CH_4	CO_2	O_2/N_2	CO_2/CH_4	CO_2/O_2	N_2/CH_4
0[b]	0.50	3.16	0.42	15.16	6.33	36.06	4.96	1.20
11 - 17	0.52	3.08	0.43	16.32	5.94	38.06	5.30	1.21
25 - 35	0.54	2.91	0.41	16.86	5.38	41.6	5.92	1.31
42 - 55	0.54	2.58	0.39	18.67	4.77	48.35	7.22	1.41

[a] Test done by CP system
[b] Test done by CV system

increases with an increase in RH. Consequently, O_2/N_2 permselectivity decreases while CO_2/CH_4 permselectivity increases with an increase in RH. Considering that an increase in the relative humidity results in a higher equilibrium concentration of water in a film, an increase in CO_2 permeability can be interpreted as a consequence of higher solubility of CO_2 in water compared to other gases. Presence of water in the film has probably enhanced adsorption of CO_2 on the

film surface and a subsequent transport of this gas through the membrane. On the other hand, a decrease in O_2 permeability with an increase in the RH cannot be explained considering the solubility of gases in water.

Although the exact mechanism for the change in film permeability is not clear, the effect of relative humidity is evident. Even for tests performed in winter, there are some differences between data obtained in the CV and CP systems. The influence of RH does not allow for comparison of permeability of different membranes when the data are obtained in different testing systems. The data obtained in the CV system appears to be, at least, better defined since the permeate side humidity is known to be at a zero level; therefore, all gas permeability data reported hereafter, are those obtained in the CV system, unless otherwise stated.

The dependence of gas permeability on relative humidity has been rarely indicated in the literature. It would be interesting to design a systematic study on the effect of RH on gas transport properties of membranes. This would require a use of testing system with a controllable permeate side RH, as well as testing of different hydrophilic and hydrophobic films. Such studies could provide some insight on the gas transport in polymeric membranes. However, because of the time constraint, the effect of relative humidity on gas permeability was not further studied in this work.

6.5.5 Effect of *IEC* on permeation properties of HSPPO films

The summary of gas permeation properties along with some physical properties of HSPPO films of different *IEC* values are presented in Table 6-7. The average and standard deviation values for permeabilities and permeability ratios respectively, were determined from at least 3 films of the same type. All gas permeation tests were performed in the CV system. It can be observed that in all cases standard deviation of permeability ratios was small (less than 4% of the corresponding average permeability ratio). On the other hand, standard deviation of permeabilities was as high as 20% of the corresponding average permeability. The values of standard deviations for permeability and permeability ratios reported in Table 6-7 are similar to those reported earlier in Tables 6-4 and 6-5 for HSPPO-1.37 films.

Table 6-7. Summary of gas transport properties of dense high molecular HSPPO membranes.

IEC meq/g	Solvent		Permeability, Barrer				Permeability Ratio	
			N_2	O_2	CH_4	CO_2	O_2/N_2	CO_2/CH_4
0.72	THF	Avg.	1.38	8.03	1.43	37.58	5.01	22.77
		St.Dev.	0.13	0.48	0.21	2.57	0.15	2.07
1.00	THF	Avg.	0.89	5.22	0.84	24.94	5.84	29.86
		St.Dev.	0.14	0.85	0.14	4.41	0.20	1.29
1.37	DMAC	Avg.	0.49	3.09	0.42	15.03	6.33	36.09
		St.Dev.	0.05	0.31	0.05	1.36	0.16	1.31
1.80	DMAC	Avg.	0.32	2.11	0.25	10.78	6.69	43.38
		St.Dev.	0.13	0.82	0.10	4.05	0.04	1.23

The variation in membrane permeability can be attributed to an error associated with determination of the thickness of the membrane. In general dry thickness of membranes ranged from 10 to 20 μm. Some films; however, showed considerable differences in the thickness within the permeation area. In extreme cases these differences were ± 25% of the average thickness of the film. It is important to emphasize; however, that in spite of some variation in permeability, membranes prepared at certain conditions showed very consistent values of O_2/N_2 and CO_2/CH_4 permselectivities.

The effect of *IEC* on O_2 and CO_2 permeabilities of HSPPO films is shown in Figures 6-7a and 6-7b, respectively. The data in these figures include permeability of a PPO film. The PPO film was prepared from the same batch of polymer that was used in the sulfonation reactions and its permeability was determined in the CV testing system [Annual Progress Report for British Gas, 1995]. Along with the experimental permeabilities, Figures 6-7a and 6-7b show permeabilities at different *IEC* values predicted from the modified free volume model proposed recently by Park and Paul (1997). The same model was used in Section 6.2 for prediction of HSPPO density. The details of the modified free volume model along with the calculations and numerical values for the predicted permeabilities shown in Figure 6-7 can be found in Appendix C.

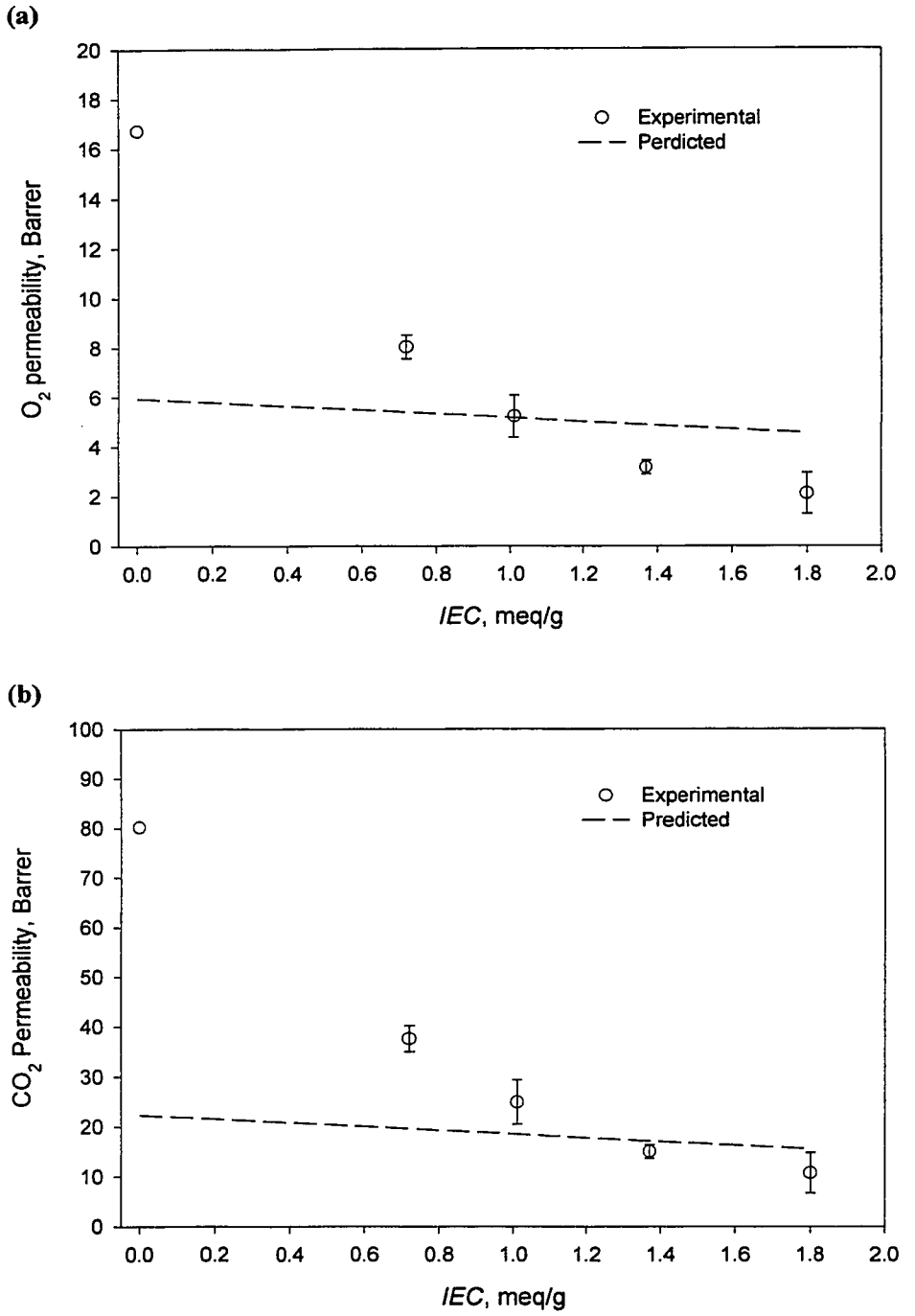

Figure 6-7. Effect of *IEC* on **(a)** O_2 and **(b)** CO_2 permeability of HSPPO membranes. Comparison of the experimental data with the values calculated by the modified group contribution method [Park and Paul, 1997].

Considering that an increase in *IEC* results in an increase in polymer density (Figure 6-1), a decrease in film permeability with an increase in *IEC* was anticipated. However, the effect of *IEC* on the experimental permeability was considerably greater than the prediction. It should be emphasized that film permeabilities were calculated based on the predicted rather than experimental fractional free volume (*FFV*). According to Eq. (2.22), permeability decreases with a decrease in the *SFV* and hence *FFV* of polymer. In turn, *FFV* decreases with an increase in polymer density. The experimentally measured densities were greater than those predicted by the modified group contribution model and the difference between experimental and predicted densities increased with an increase in *IEC* (Figure 6-1). The use of the experimental rather than estimated *FFV* of polymer would improve the agreement, especially for HSPPO of higher *IEC*.

The effect of *IEC* on O_2/N_2 and CO_2/CH_4 permeability ratios of HSPPO films is shown in Figures 6-8a and 6-8b, respectively. The experimental permeability ratios in these figures are compared with the permeability ratios calculated by the modified free volume model [Park and Paul, 1997]. The numerical values of the predicted permeability ratios are included in Appendix C. It can be noticed that the experimental permeability ratios increase with an increase in *IEC* of polymer. On the other hand, the predicted permeability ratios are virtually constant over the entire range of *IEC* values.

In general, the modified free volume model predicts only little changes in permeability and permselectivity of HSPPO films with *IEC*. The *FFV* of polymer is an important factor determining gas transport properties of glassy polymers. It does not, however, include distribution of free volume in the polymer. It does not also include the changes in the interactions between gas species and polymeric materials as a result of the introduction of strong electrophilic substituents into the polymer backbone. Sulfonic groups are one of the strongest electrophilic substituents. Therefore, at even very low degree of polymer substitution they can profoundly change the properties of the polymer as is evident from the example of HSPPO. It should be emphasized that the effect of sulfonation of PPO on its permeation properties is similar to the effect of sulfonation of other polymers, for example, those of Nafion [Chiou and Paul, 1988], polysulfone [Bikson *et al.*, 1991] and polystyrene [Chen and Martin, 1994].

(a)

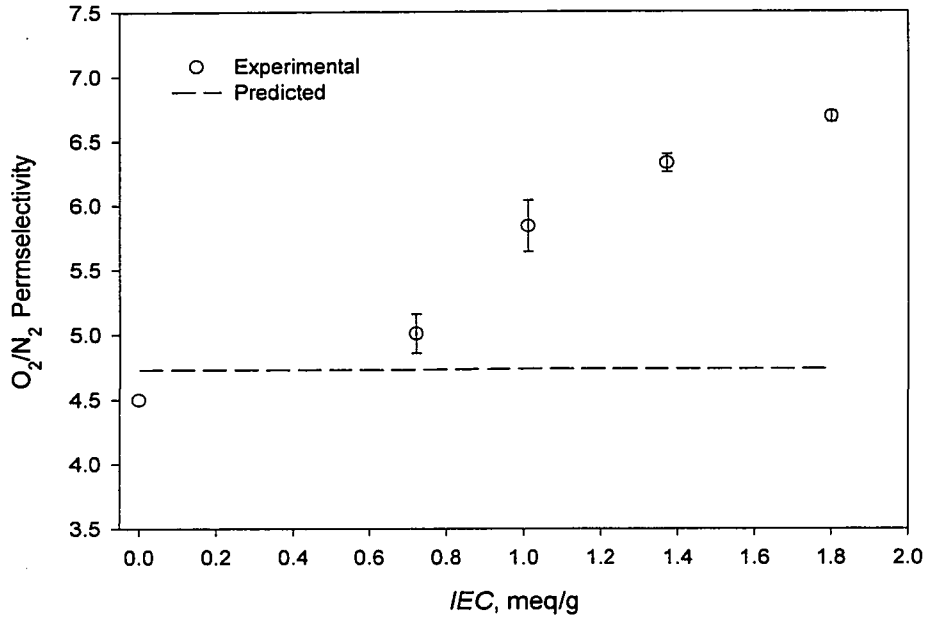

(b)

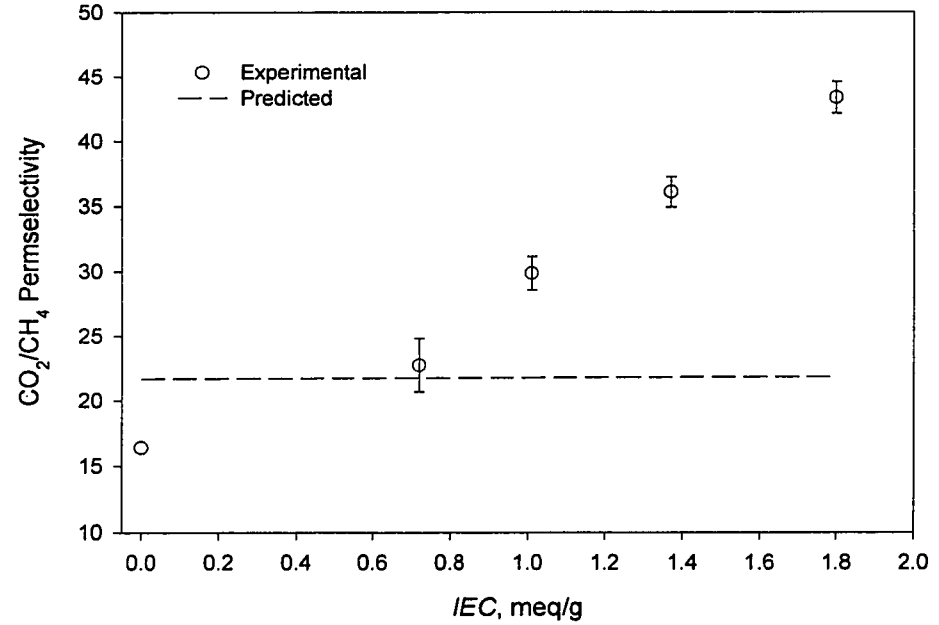

Figure 6-8. Effect of *IEC* on **(a)** O_2/N_2 and **(b)** CO_2/CH_4 permeability ratios of HSPPO membranes. Comparison of the experimental data with values calculated by the modified group contribution method [Park and Paul, 1997].

It is interesting to note that while changes in polymer density, in gas permeability and in permeability ratios occurred with a change in *IEC* of polymer, the d-spacing of polymer remained constant. This is rather surprising considering the fact that incorporation of ionic groups into a polymer is known to cause electrostatic cross-linking [Mattera and Risen, 1986]. Such electrostatic cross-linking should lead to a decrease in d-spacing, which was not observed here (Table 6-2). It should be emphasized; however, that HSPPO of the highest *IEC* value considered in this study was equal to 1.80 meq/g, which corresponded to the degree of substitution equal to 25%. This means that in the polymer of the highest degree of substitution, sulfonic groups appeared approximately only on every fourth repeat unit. Therefore, while the electrostatic cross-linking between sulfonic groups may exist, their presence does not lead to a measurable change in d-spacing because of relatively low degree of polymer substitution. Since polymer density increased with the degree of sulfonation while the d-spacing remained constant, it can be concluded that sulfonic groups fitted well in an open arrangement of macromolecules created by nonlinear ether linkages of the PPO backbone. Similar effect of electrophilic substitution of PPO on the d-spacing, density and permeability was reported by Story and Koros (1992), who studied carboxylated and methyl esterified carboxylated PPO. In their case; however, the electrophilic groups were introduced on methyl groups, whereas sulfonic groups in HSPPO were introduced on aromatic rings.

6.5.6 Comparison of HSPPO with other polymers

It is important to compare gas permeation properties of HSPPO membranes with data for other polymers that are of interest for gas separation. With respect to standard commercial polymers, which included polysulfone and polycarbonates, Zolandz and Fleming (1992) compiled a tradeoff between permeability and permeability ratio for several gas pairs. On the other hand, Robeson (1991) compiled permeability and permeability ratio data for several gas pairs in a number of polymer materials. Robeson's analysis revealed an upper-bound relationship for permeability and permeability ratio.

Figure 6-9a presents a relationship between O_2 permeability and O_2/N_2 permeability ratio for HSPPO membranes in a log-log domain in comparison with standard tradeoff and upper-

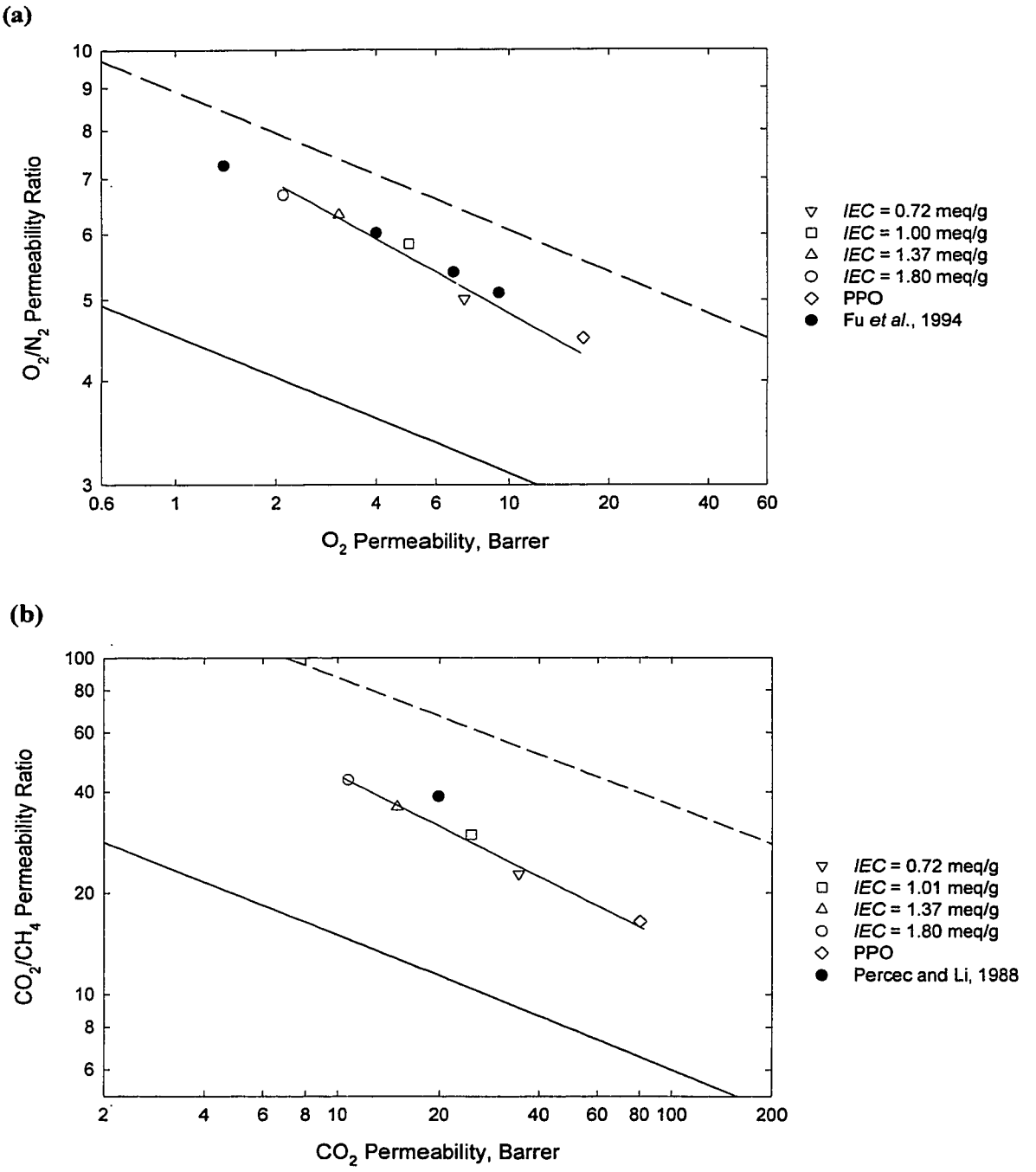

Figure 6-9. Gas transport properties of high molecular weight HSPPO membranes in comparison to tradeoff line for standard commercial polymers (—) [Zoladz and Fleming, 1992] and upper-bound line (----) [Robeson, 1991] for **(a)** O_2/N_2 gas pair and **(b)** CO_2/CH_4 gas pair.

bound lines for this pair of gases. Similar relationship for the CO_2/CH_4 gas pair is shown in Figure 6-9b. It can be noticed that in both cases the combination of permeability and permeability ratio places the HSPPO membranes above the respective tradeoff lines for standard commercial polymers but below the respective upper-bound lines. It can also be noticed that in O_2 permeability versus O_2/N_2 permeability ratio, the HSPPO membranes are closer to the upper-bound line than in CO_2 permeability versus CO_2/CH_4 permeability ratio. It is also apparent that the permeability versus permeability ratio plot obtained in this work for higher molecular weight HSPPO, forms a straight line in the log-log domain for both O_2/N_2 and CO_2/CH_4 gas pairs. Furthermore, the slope of the straight line is steeper than the upper-bound line for both cases. This indicates that the higher degree of sulfonation brings the permeability versus permeability ratio relationship closer to the upper-bound line. It is more apparent for O_2/N_2 than for CO_2/CH_4 [Kruczek and Matsuura, 1998].

It can be noticed that the O_2/N_2 gas transport data reported by Fu *et al.* (1994b) for low molecular weight HSPPO, fits well to the straight line determined by the data for high molecular weight HSPPO. On the other hand, the experimental data reported by Percec and Li (1988) for CO_2/CH_4 lies above the line for high molecular weight HSPPO. It should be emphasized; however, that the data reported by Percec and Li (1988) probably represented a single experiment rather than the average of several membrane samples. This is significant considering variation in permeability data for a given type of membrane, due to an error associated with determination of the membrane thickness. As already stated, considerable variation in permeability data was observed for a given type of membrane.

6.6 Chapter Summary

The highest achievable degree of sulfonation of high molecular weight PPO (*IEC* = 1.80 meq/g) is lower than that of low molecular PPO (*IEC* $\geq$ 2.5 meq/g), because of the lower solubility of high molecular weight polymer in chloroform. Sulfonation with chlorosulfonic acid may lead to a sulfonated-chlorinated product when the hydrochloric acid formed during sulfonation is not effectively removed from the reactor.

Sulfonic groups attached to the aromatic ring in the PPO backbone are not thermally stable. Sulfonic groups decompose at temperatures above 175°C. They may decompose even at

lower temperatures after a longer exposure time. On the other hand, a two-month conditioning with CO_2 at 517 cmHg indicated stability of the polymer at room temperature. The final decomposition of the polymer begins at above 400°C.

Sulfonation of PPO results in an increase in density linearly with respect to the *IEC* value while the average d-spacing in polymer remains constant. This indicates that sulfonic groups fit well in an open arrangement of macromolecules created by kink ether linkages of the PPO backbone.

Gas transport properties of membranes tested in the constant pressure testing system (downstream open to atmosphere) are influenced by relative humidity in the atmosphere. On the other hand, relative humidity in the atmosphere does not affect gas transport properties obtained in the constant volume testing system (downstream at vacuum). An increase in relative humidity in the atmosphere increases the apparent CO_2 permeability and CO_2/CH_4 permeability ratio and decreases the apparent O_2 permeability and O_2/N_2 permeability ratio. The change in gas transport properties may be as high as 25% when the relative humidity is changed form 10 to 50%.

The modified fractional free volume model proposed recently by Park and Paul (1997) fails to predict permeability of HSPPO. An increase in *IEC* results in a decrease in permeability and an increase in ideal selectivity of HSPPO.

The combination of permeability and ideal selectivity for both O_2/N_2 and CO_2/CH_4 places the HSPPO above the respective tradeoff lines for standard commercial polymers but below the respective upper-bound lines. An increase in *IEC* brings the permeability versus ideal selectivity relationship closer to the upper-bound line. This improvement in gas transport is more apparent for the O_2/N_2 gas pair than for the CO_2/CH_4 gas pair.

CHAPTER 7

Effect of Metal Cation on Properties of SPPO Membranes

7.1 Solubility in Organic Solvents

The effect of introduction of metal cation on solubility of polymer in organic solvents is presented in Table 7-1. This effect is illustrated by the example of solubility of HSPPO and MeSPPO in THF and DMAC, respectively. The Hildebrand solubility parameters of THF and DMAC are equal to 19.4 $MPa^{1/2}$ and 22.7 $MPa^{1/2}$, respectively [Grulke, 1989].

Table 7-1. Effect of metal cation on solubility of high molecular weight SPPO in organic solvents[a].

Solvent	*IEC* = 1.01		*IEC* = 1.37				*IEC* = 1.80		
	H	Na	H	Na	Mg	Al	H	Na	Mg
THF	+	-	+	-	-	-	-	-	-
DMAC	-	+	+	+	+	s	+	+	+

[a] + : polymer soluble in solvent
s : polymer swollen in solvent
- : polymer insoluble in solvent

It can be noticed that HSPPO-1.01 is soluble in THF but not in more polar DMAC. On the other hand, when the proton in sulfonic groups is replaced by the Na^+ cation, the polymer (NaSPPO-1.01) becomes insoluble in THF, but soluble in more polar DMAC. This comparison indicates that for the same *IEC*, the polymer in a metal form is more polar than the polymer in the acid form. The magnitude of polarity increase can be illustrated by the fact that HSPPO-1.37

is soluble, while NaSPPO-1.01 is insoluble in THF. This indicates that NaSPPO-1.01 is more polar than HSPPO-1.37. It is shown in Table B-4 in Appendix B that an increase in *IEC* of HSPPO from 1.01 to 1.37 meq/g results in an increase in the Hildebrand parameter from 24.84 to 25.54 $MPa^{1/2}$. Since THF dissolves HSPPO-1.37, while it does not dissolve NaSPPO-1.01, the Hildebrand solubility parameter of the latter should be greater than 25.54 $Mpa^{1/2}$.

Except for AlSPPO-1.37, all polymers listed in Table 7-1 were soluble in either THF or DMAC. In fact, AlSPPO-1.37 was not soluble in any of the solvents listed in Table B-1. in Appendix B. A vigorous stirring of small chunks of AlSPPO in DMAC for one day resulted in only some swelling of the polymer. Insolubility of AlSPPO in organic solvents can be explained by cross-linking of the polymer by Al^{3+} cations. Each Al^{3+} cation can attach to three sulfonic groups thus making a polymer network. On the other hand, MgSPPO-1.37 and even MgSPPO-1.80 were soluble in DMAC. Similar to Al^{3+}, Mg^{2+} cation can attach to more than one sulfonic group and hence cross-link the polymer. Apparently, the polymer network in MgSPPO (if any) was not as strong as that in AlSPPO so MgSPPO was soluble in DMAC.

7.2 Thermal Stability

Figure 7-1 presents the TGA spectra of HSPPO, NaSPPO and MgSPPO. All films had the same *IEC* value of 1.80 meq/g. It can be noticed that substitution of the proton in sulfonic groups by the metal cation had a significant effect on the TGA spectrum of the film. The weight loss below 100°C, which indicates the amount of moisture adsorbed on a film, increased from 3.0% for HSPPO-1.80 to 5.3 and 7.5% for NaSPPO-1.80 and MgSPPO-1.80, respectively. The increase in the weight loss below 100°C indicates an increase in hydrophilicity of the polymer. This result is consistent with a higher polarity of NaSPPO-1.01 compared to HSPPO-1.01, which was reported in the previous section based on the solubility tests in THF and DMAC. The higher water content in MgSPPO compared to NaSPPO is probably due to the higher valence of Mg^{2+} compared to Na^{+} cation. The extra charge of Mg^{2+} can attract more water into the polymer.

Unlike the TGA spectrum of HSPPO-1.80, which showed 11.8% weight loss in a 175 - 275°C temperature interval due to removal of sulfonic groups, the TGA spectra of NaSPPO-1.80 and MgSPPO-1.80 showed a constant weight in this temperature range. The substitution of the

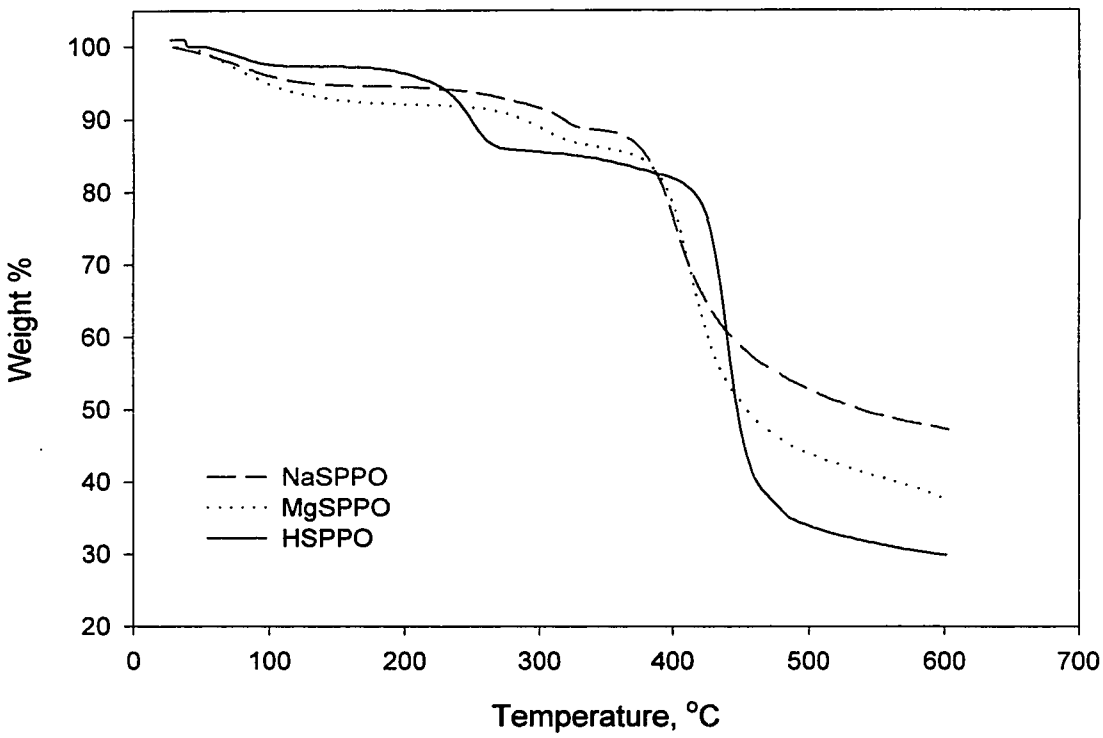

Figure 7-1. Effect of metal cation on thermal stability of dense high molecular weight SPPO-1.80 films prepared from DMAC solutions.

proton in sulfonic groups with a metal cation; therefore, increased thermal stability of the sulfonic groups. It can be observed that NaSPPO-1.80 and MgSPPO-1.80 showed approximately 5% weight loss above 300°C. This was probably due to removal of some sulfonic groups. It is; however, important to emphasize that this weight loss was significantly lower and occurred at significantly higher temperatures than in case of HSPPO-1.80. The final decomposition of NaSPPO-1.80 and MgSPPO-1.80 began around 390°C, which is approximately 20°C below the decomposition temperature of HSPPO-1.80. Despite this fact, it is clear that NaSPPO-1.80 and MgSPPO-1.80 show a better thermal stability than HSPPO-1.80.

7.3 Density and X-ray Diffraction Spectra

Table 7-2 shows the effect of metal cation on polymer density and on d-spacing and peak intensity determined from the X-ray diffraction spectra. It can be noticed that for given *IEC*, the density of polymer increased in the order of H < Na < Mg. Interestingly, the density of AlSPPO-1.37 was lower than the density of MgSPPO-1.37. It should, however, be emphasized that AlSPPO-1.37 film used for the measurement of polymer density was prepared in a different way than the other films. Since AlSPPO-1.37 was not soluble in any solvent, the membrane was prepared by soaking NaSPPO-1.80 film in a dilute aqueous solution of $Al(NO_3)_3$. All other films were prepared directly from appropriate polymer solutions.

The X-ray diffraction spectra of MeSPPO were generally similar to the X-ray diffraction spectrum of HSPPO-1.80 shown in Figure 6-2. In case of NaSPPO and MgSPPO of *IEC* values equal to 1.37 and 1.80 meq/g; however, the major peak was slightly shifted to a lower 2Θ. Consequently the calculated d-spacing for these polymers was slightly larger than for HSPPO. It is interesting to note that the increase in d-spacing was associated with an increase in peak intensity. In turn, an increase in peak intensity indicates more diffraction coming from the sample and hence a greater order of macromolecular orientation within the polymer and a more rigid structure.

AlSPPO-1.37 shows the lowest d-spacing and the second lowest peak intensity. On the other hand, NaSPPO-1.37 and MgSPPO-1.37 show an increase in both d-spacing and peak

Table 7-2. Effect of metal cation on density and X-ray diffraction spectrum of dense high molecular weight SPPO membranes.

IEC, meq/g	Cation	Density, g/cm^3	d-spacing, Å	Peak Intensity
1.01	H	1.14	6.15	255
1.01	Na	1.16	6.15	213
1.37	H	1.17	6.15	419
1.37	Na	1.19	6.33	594
1.37	Mg	1.20	6.33	629
1.37	Al	1.19	6.09	217
1.80	H	1.19	6.19	339
1.80	Na	1.22	6.29	576
1.80	Mg	1.24	6.33	529

intensity compared to HSPPO-1.37. These unexpected properties of AlSPPO-1.37 were probably due to the different preparation procedure of AlSPPO-1.37 compared to the other films.

7.4 Gas Transport Properties

7.4.1 Effect of membrane preparation method

When testing AlSPPO-1.37 with single gases, it became apparent that the membranes were defective. They showed at least two-orders of magnitude greater permeability than HSPPO-1.37 membranes. Moreover, the AlSPPO-1.37 membranes had no selectivity, which was indicated by similar permeation rates for O_2 and N_2. The membranes were laminated with a silicone rubber film and the single gas permeation experiments were repeated. Other membranes in a metal form did not require lamination with the silicone rubber film. Permeability of AlSPPO-1.37 membrane was calculated by the following equation which was derived from a resistance model for resistances in series [Henis and Tripodi, 1981]:

$$P_2 = \frac{l_2 P_1 Q}{P_1 A - Q l_1} \tag{7.1}$$

where Q is the steady state permeation rate through a laminated membrane, l is the membrane thickness, P is the membrane permeability, and A is the permeation area which is the same for the AlSPPO-1.37 membrane and the silicone rubber film. Subscript 1 refers to the silicone rubber membrane, while subscript 2 refers to the AlSPPO-1.37 membrane. Permeability data for

silicone rubber was obtained from the manufacturer (General Electric). Derivation of Eq. (7.1) and permeability data for the silicone rubber (SR) membrane can be found in Appendix D.

To determine whether the defects in AlSPPO-1.37 films were inherent to the polymer or resulted from the preparation procedure, some NaSPPO-1.37 and MgSPPO-1.37 membranes were prepared by soaking HSPPO-1.37 films in dilute aqueous solutions of NaOH and $Mg(NO_3)_2$, respectively. The performance of these membranes is summarized in Table 7-3. The table also presents the performance of NaSPPO-1.37 and MgSPPO-1.37 membranes prepared directly from the polymer solution.

Similar to AlSPPO-1.37, MgSPPO-1.37 membranes prepared by soaking in a dilute aqueous solution of $Mg(NO_3)_2$ were defective and required lamination of the surface with the silicone rubber film. On the other hand, NaSPPO-1.37 membranes prepared by soaking in a dilute aqueous solution of NaOH did not require lamination. Furthermore, the performance of all NaSPPO-1.37 membranes was very consistent as indicated by the permeability data in Table 7-3.

It is known that drying of hydrophilic integrally skinned asymmetric membranes may result in pore collapse, densification and brittleness of the membranes. Kesting and Fritzsche

Table 7-3. Effect of film preparation procedure on gas transport properties of dense high molecular weight MeSPPO-1.37.

Cation	Preparation Method[a]	Permeability, Barrer		Permselectivity	
		O_2	CO_2	O_2/N_2	CO_2/CH_4
Na	1	7.70	39.34	6.22	35.03
Na	1	6.86	34.24	6.44	36.89
Na	2	7.92	39.73	5.97	34.87
Na	2	7.08	35.03	6.55	37.49
Mg	1	4.20	21.66	7.28	45.14
Mg	1	5.28	27.28	6.64	41.06
Mg[b]	2	7.21	36.81	6.40	40.17
Mg[b]	2	6.21	30.99	6.62	41.11

[a] 1 - membranes prepared directly form polymer solution
2 - membranes prepared by soaking in aqueous solution of metal cation
[b] membranes laminated with SR film of thickness equal to 50.8 μm

(1993) described the mechanism of this phenomenon. As already discussed, SPPO is a hydrophilic material. For the highest *IEC* of 1.80 meq/g, the sulfonic groups are attached on approximately every fourth repeat unit. The distribution of the substituent groups is; however, not necessarily uniform as indicated by Chiou and Paul (1988). They reported that sulfonic groups in Nafion, which is a sulfonated fluorohydrocarbon, form clusters. Similar phenomenon can be expected for SPPO. The presence of such clusters would result in the existence of hydrophilic and hydrophobic regions in the SPPO membranes. During evaporation of high surface tension liquid such as water, the collapsing force is exerted only on the walls of hydrophilic pores [Kesting and Fritzsche, 1993]. At the same time, a stretching force in the hydrophobic regions surrounded by the hydrophilic regions could develop. This stretching force could lead to an enlargement of pores and defects in the hydrophobic regions. The simultaneous densification and defect formation should be enhanced by an increase in polarity of electrophilic substituents.

Figure 7-1 shows that substitution of the proton in sulfonic groups by metal cations increases polarity and hence hydrophilicity of the polymer. Furthermore, MgSPPO-1.80 is more hydrophilic than NaSPPO-1.80. The higher hydrophilicity of MgSPPO is a result of the higher valence of Mg^{2+} compared to Na^{+}. Using the same argument, AlSPPO should be the most hydrophilic among the polymers of the same *IEC*. The existence of defects in MgSPPO-1.37 and AlSPPO-1.37 can; therefore, be attributed to higher polarity of sulfonic groups in Mg and Al forms compared to those in acid and Na forms. The above argumentation; however, does not explain why the defects were present in MgSPPO-1.37 prepared by soaking in a dilute aqueous solution of $Mg(NO_3)_2$ but not in MgSPPO-1.37 prepared directly from the polymer solution.

Substitution of the proton in sulfonic groups by multivalent metal cations such as Mg^{2+} and Al^{3+} may result in formation of bonds with more than one sulfonic group. When MeSPPO membranes are prepared by soaking the membrane in acid form in a dilute aqueous solution of metal cation, the polymer is in a glassy state. Consequently, steric hindrance may restrict the formation of bonds with more than one sulfonic group. As a result, the polymer can be positively charged. The presence of positive charge can attract water molecules to the polymer. On the other hand, dissolution of MgSPPO-1.37 in DMAC allows the polymer to rearrange itself and

hence to minimize its positive charge. The expected higher hydrophilicity of MgSPPO-1.37 membranes prepared by soaking in a dilute aqueous solution of $Mg(NO_3)_2$ compared to those prepared directly from the polymer solution could be responsible for the existence of defects in the former membranes.

7.4.2 Improvement of gas transport properties

Table 7-4 presents the summary of gas transport properties of MeSPPO membranes. For comparison, the gas transport data of the corresponding HSPPO membranes are also provided. Permeabilities and permeability ratios shown in Table 7-4 represent the average values for at least two membranes of the same type. The number of membranes (n) used for calculation of the average and the standard deviation for a given type is shown in a separate column.

As shown in Table 7-1, HSPPO-1.01 was not soluble in DMAC. All other polymers except for AlSPPO-1.37, which was not soluble in any solvent, were soluble in DMAC. All SPPO-1.37 and SPPO-1.80 membranes were; therefore, prepared from polymer solutions in DMAC. On the other hand, HSPPO-1.01 and NaSPPO-1.01 membranes were prepared from solutions in NMP, in which both polymers were soluble. All permeation experiments were performed in the CV testing systems.

The effects of the metal cations on permeability and permselectivity of SPPO membranes are discussed separately. This is followed by the discussion of the performance of MeSPPO with reference to the upper-bound line for polymeric materials [Robeson, 1991].

7.4.2.1 Permeability of MeSPPO membranes

Introduction of a metal cation results in an increase in permeability of the membrane regardless of the valence of the cation and *IEC* of the polymer as indicated in Table 7-4. Considering all membranes presented in the table, AlSPPO-1.37 shows the highest permeability for gases, but as already discussed, AlSPPO membranes were defective and the permeation data was obtained after lamination of the membranes with a silicone rubber film. It is interesting to note that a higher permeability of MeSPPO compared to HSPPO is associated with an increase in polymer density. According to the modified free volume model, permeability should decrease

Table 7-4. Summary of gas transport properties of dense high molecular weight HSPPO and MeSPPO membranes.

IEC meq/g	Cation	*n*		Permeability, Barrer O_2	CO_2	Permselectivity O_2/N_2	CO_2/CH_4
1.01	H	3	Avg.	4.16	20.03	6.00	31.55
			St.Dev.	1.07	4.90	0.13	2.88
1.01	Na	3	Avg.	5.60	27.68	5.54	29.02
			St.Dev.	0.74	2.56	0.16	1.34
1.37	H	3	Avg.	3.09	15.03	6.33	36.09
			St.Dev.	0.31	1.36	0.16	1.31
1.37	Na	4	Avg.	7.39	37.09	6.30	36.07
			St.Dev.	0.43	2.46	0.22	1.14
1.37	Mg	2	Avg.	4.74	24.47	6.96	43.10
			St.Dev.	0.54	2.81	0.32	2.04
1.37	Al[b]	2	Avg.	8.58	42.60	6.10	35.98
			St.Dev.	1.08	5.90	0.16	1.49
1.80	H	4	Avg.	2.11	10.78	6.69	43.38
			St.Dev.	0.82	4.05	0.04	1.23
1.80	Na	3	Avg.	3.47	17.41	7.06	42.85
			St.Dev.	0.69	3.48	0.31	1.74
1.80	Mg	3	Avg.	2.33	11.98	8.36	54.13
			St.Dev.	0.45	2.51	0.64	3.94

[a] Number of tested membranes
[b] Laminated with silicone rubber film of thickness equal to 50.8 μm

with an increase in polymer density [Park and Paul, 1997]. It is; therefore, clear that the free volume model is not applicable for the prediction of permeability of MeSPPO membranes. Fu *et al.* (1994b), who studied properties of low molecular weight SPPO, also reported an increase O_2 permeability after substitution of the proton in sulfonic groups by Na^+ cations.

The comparison of the performance data of HSPPO and NaSPPO reveals that an increase in membrane permeability depends on the *IEC* of polymer. The maximum increase in permeability was observed for the polymer of *IEC* equal to 1.37 meq/g. For example, the average CO_2 permeability increased from 15.03 to 37.16 Barrer. On the other hand, in case of the

polymer of *IEC* equal to 1.01 meq/g, the average permeability increased only from 20.03 to 27.68 Barrer. The substitution of Na^+ by Mg^{2+} in sulfonic groups decreased permeability of the membranes. The difference between the average permeabilities of NaSPPO and MgSPPO was approximately 50%. Despite this decrease, MgSPPO was more permeable than the corresponding HSPPO membranes.

The increase in permeability of SPPO membrane after substitution of the proton in sulfonic groups by metal cations can be explained using the analogy with brominated PPO (BrPPO). It was reported that aryl bromination of PPO resulted in more than two-fold increase in CO_2 permeability [Percec and Li, 1988; Story and Koros, 1992]. The increase in permeability by bromination was associated with an increase in polymer density. Furthermore, bromination of PPO also led to a decrease in d-spacing [Story and Koros, 1992]. According Story and Koros (1992), an increase in permeability of BrPPO was due to an increase in diffusivity. They argued that bromine substituents at the ring position inhibit rotation of individual polymer segments due to interference of bromine substituents with methyl groups on adjoining PPO segments. As a result, any rotational motion in BrPPO must involve several repeat units as opposed to only one or two units in PPO, thus increasing the diffusional jump length. Considering that diffusivity is proportional to the square of the length of diffusional jumps (Eq. 2.12), the diffusivity and hence permeability of BrPPO should increase. It should be noted; however, that an increase in permeability was observed only for a 100% substituted polymer, that is, for BrPPO with bromine groups on every repeat unit. On the other hand, permeability of a 36% substituted BrPPO was not significantly different from that of PPO [Story and Koros, 1992].

In case of SPPO, sulfonic groups in aryl position reduced significantly permeability of the membranes. The effect of *IEC* on permeability of HSPPO has been discussed in Chapter 6. When the proton in sulfonic groups is replaced by a metal cation, polarity of the sulfonic groups increases, as indicated by the solubility test in organic solvents (Table 7-1) and TGA analysis (Figure 7-1). It is believed that the higher polarity of sulfonic groups in metal form causes electrostatic cross-linking between neighboring substituents on the same chain. The electrostatic cross-linking between neighboring sulfonic groups on the same chain would inhibit rotation of single PPO units while enhancing simultaneous rotation of all PPO units between substituents.

Recalling Figure 2-1c, the free volume of polymer is represented by the free space in that figure. An improvement in gas permeability resulting from inhibition of the rotation of individual PPO units can be visualized as an increase in the length of free volume pockets in Figure 2-1c.

The above discussion assumes that there is a simultaneous rotation of all PPO units between sulfonic groups. Such a rotation of several repeat units in a rigid glassy polymer like MeSPPO would require very high activation energies. The electrostatic cross-linking between neighboring sulfonic groups on the same chain; therefore, may inhibit not only the rotation of single PPO units but also any rotation at all. This would lead to the formation of continuous passages through the polymer. In this case the mechanism of gas transport through the polymer would be governed by molecular sieving (Figure 2-1b) rather than by solution-diffusion (Figure 2-1c).

The increase in permeability caused by substitution of the proton in sulfonic groups by metal cations depends on the *IEC* of the polymer. For example, an increase in permeability of NaSPPO-1.37 from HSPPO-1.37 was approximately 140%, while an increase in permeability of NaSPPO-1.80 from HSPPO-1.80 was only approximately 60%. In the polymer of *IEC* equal to 1.37 meq/g, the sulfonic groups are attached to every fifth repeat unit, while in case of the polymer of *IEC* equal to 1.80 meq/g, the sulfonic groups are on every fourth repeat unit. Assuming that gas transport is governed by the solution-diffusion mechanism, the lower increase (in permeability resulting from the replacement of the proton in sulfonic groups by metal cations) in the polymer of higher *IEC* value would be a result of lower increase in the diffusional jump length. On the other hand, considering SPPO of *IEC* equal to 1.01 meq/g (sulfonic groups on every seventh repeat unit), permeability of NaSPPO-1.01 was only 35% greater than that of HSPPO-1.01. This was probably because the neighboring sulfonic groups were too far apart, which prevented formation of electrostatic cross-linking between them. It is interesting to note that d-spacing and diffraction from HSPPO-1.01 and NaSPPO-1.01 were comparable (Table 7-2). On the other hand, for the polymers of *IEC*s equal to 1.37 and 1.80 meq/g, respectively, d-spacing and diffraction increased after replacement of the proton in sulfonic groups by Na^+ cations.

Sulfonic groups in the Mg form are even more polar than sulfonic groups in the Na form. However, as already noted, permeabilities of NaSPPO were approximately 50% greater than those of MgSPPO. In case of the latter, the extra charge of the cation may have resulted in formation of bonds with more than one sulfonic groups and consequently densification of the polymer. In fact MgSPPO has slightly higher density than the corresponding NaSPPO (Table 7-2) and consequently lower free volume, which explains lower permeability of MgSPPO compared to NaSPPO. In addition to this, considering the molecular sieving mechanism, formation of bonds with more than one sulfonic groups by Mg^{2+} cations would lead to an increase in tortuosity of the polymer and hence a decrease in gas permeability.

7.4.2.2 Effect of molecular weight on permeability

The increase in permeability of NaSPPO compared to the corresponding HSPPO is considerably greater than that reported by Fu *et al.* (1994b) for low molecular polymer. In case of SPPO prepared from PPO of the intrinsic viscosity equal to 0.5 dL/g, substitution of the proton in sulfonic groups by sodium cations resulted only in a 20-40% increase in O_2 permeability, regardless of the *IEC* of the polymer [Fu *et al.*, 1994b].

Kesting and Fritzsche (1993) postulated the importance of molecular weight of polymer on its gas transport properties. They argued that an increase in the molecular weight of polymer results in an increase in chain stiffness. Packing of long and stiff chains should result in a higher free volume and hence a higher permeability of the membrane compared with the membrane made of short and flexible polymer chains [Kesting and Fritzsche, 1993]. The postulated effect of molecular weight was confirmed by Polotskaya *et al.* (1996), who reported an increase in free volume and O_2 permeability of homogeneous PPO membranes with an increase in the molecular weight of polymer. At the same time, O_2/N_2 permeability ratio did not change [Polotskaya, *et al.*, 1996].

The increase in permeability resulting from substitution of the proton in sulfonic groups by metal cations was explained in the previous section by an increase in the diffusional jump length (solution-diffusion) or by formation of continuous passages through the membrane (molecular sieving). However, as the molecular weight of polymer decreases, the number of

chain ends in a given volume increases. Chain ends are considered more mobile than the middle parts of the chain. The mobile chain ends can find their way into long free volume pockets (solution-diffusion) or micropores (molecular sieving). In either case this should lead to a decrease in permeability of the membrane. As discussed in Chapter 6, PPO of [η] equal to 1.78 dL/g used in this work has molecular weight more than 7 times greater than PPO of [η] equal to 0.5 dL/g used by Fu *et. al.*(1994b). There are; therefore, 7 times more of mobile chain ends in a given volume of low molecular polymer compared to the mobile chain ends of high molecular weight polymer. This is the reason why Fu *et al.* (1994b) did not notice a large effect of metal cation exchange on the permeability.

7.4.2.3 Permeability ratios of MeSPPO

As shown in Table 7-4, the effect of metal cation on permeability ratio of MeSPPO membranes depends on the valence of the cation and *IEC* of the polymer. In case of the polymer of *IEC* equal to 1.01 meq/g, the substitution of the proton by Na^+ cations results in a decrease in both O_2/N_2 and CO_2/CH_4 permeability ratios. On the other hand, the same substitution in polymers of *IEC*s equal to 1.37 and 1.80 meq/g does not result in significant changes in these permeability ratios. In case of low molecular weight SPPO, substitution of the proton in sulfonic groups by Na^+ cations decreased O_2/N_2 permeability ratio of the membranes. The difference; however, was small and the difference decreased with an increase in *IEC* of polymer [Fu *et al.*, 1994b].

The comparison of NaSPPO and MgSPPO of the same *IEC* reveals that the membranes from the latter polymer are considerably more selective. The increase in CO_2/CH_4 permeability ratio is more evident than the increase in O_2/N_2 permeability ratio. The former increased by 19.9 and 26.3% for *IEC*s of 1.37 and 1.80 meq/g, respectively. The latter increased by 10.4 and 18.4% for *IEC*s equal to 1.37 and 1.80 meq/g, respectively. The above comparison also indicates that the increase in permeability ratio was greater for the polymer of higher *IEC*. Introduction of Al^{3+} cations into sulfonic groups of SPPO-1.37, decreased the permeability ratio from MgSPPO-1.37. Permselectivities of AlSPPO-1.37 were comparable to those of HSPPO-1.37 and NaSPPO-1.37. It should be remembered that AlSPPO-1.37 membranes were laminated with a silicone rubber

film prior to gas permeation tests in order to seal the defects in the membrane.

Chen and Martin (1994), who studied gas transport properties of sulfonated polystyrenes (SPS) reported a similar relationship between permselectivities of the membranes in Na and Mg forms. For any *IEC* of the polymer, MgSPS membranes were more selective than the NaSPS membranes. The difference in permeability ratio increased with an increase in *IEC* of the polymer. The higher permselectivity of MgSPS compared to NaSPS was explained by the fact that the divalent Mg^{2+} counterion was a better cross-linking agent than the monovalent Na^{+} counterion [Chen and Martin, 1994]. The same argument can be used for the explanation of a higher permselectivity of MgSPPO compared to NaSPPO of the same *IEC*. Furthermore, it was already shown in Table 7-2, that for a given *IEC*, MgSPPO was slightly denser than NaSPPO. This increase in density and hence a decrease in free volume of polymer indicates that the former could in fact be cross-linked to a greater extend than the latter. Considering that a decrease in free volume usually results in an increase in polymer selectivity, the observed higher permeability ratios of MgSPPO compared to NaSPPO can be expected.

7.4.2.4 Summary of gas transport properties of MeSPPO

When evaluating usefulness of a polymer for gas separation membranes, it is important to consider its permeability and permselectivity simultaneously. The effect of metal cation on the combination of permeability and permselectivity of SPPO membranes is shown graphically in Figures 7-2 – 7-4. The gas transport properties of the membranes are compared with the upper-bound line for polymers considering O_2/N_2 and CO_2/CH_4 gas pairs [Robeson, 1991].

It can be noticed in Figures 7-2a and 7-2b that NaSPPO-1.01. is not any closer to the upper bound line than HSPPO-1.01. This is because an increase in permeability of NaSPPO-1.01 is compensated by its decrease in selectivity. It is evident that HSPPO-1.01 and NaSPPO-1.01 are closer to the upper-bound line for O_2/N_2 (Figure 7-2a) than CO_2/CH_4 (Figure 7-2b).

Unlike SPPO-1.01, introduction of metal cations into sulfonic groups of SPPO-1.37 results in a considerable improvement of gas transport properties. This improvement in gas transport properties is indicated by the position of MeSPPO-1.37 relative to the upper-bound line in Figures 7-3a and 7-3b. NaSPPO-1.37 and AlSPPO-1.37 fall just below the upper-bound line in

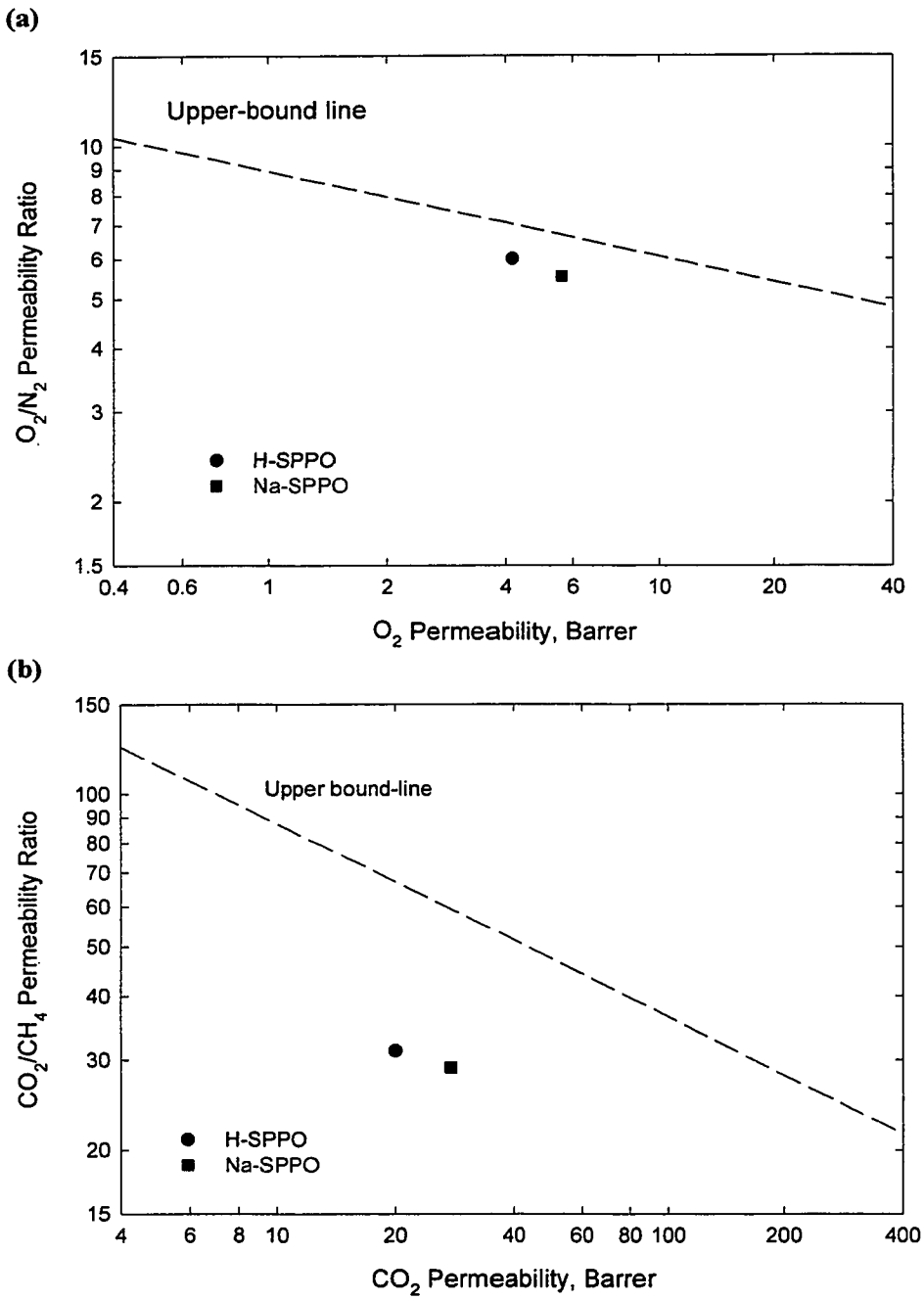

Figure 7-2. Effect of metal cation on the combination of **(a)** O_2 permeability and O_2/N_2 permeability ratio and **(b)** CO_2 permeability and CO_2/CH_4 permeability ratio of SPPO-1.01 membranes prepared from NMP solutions.

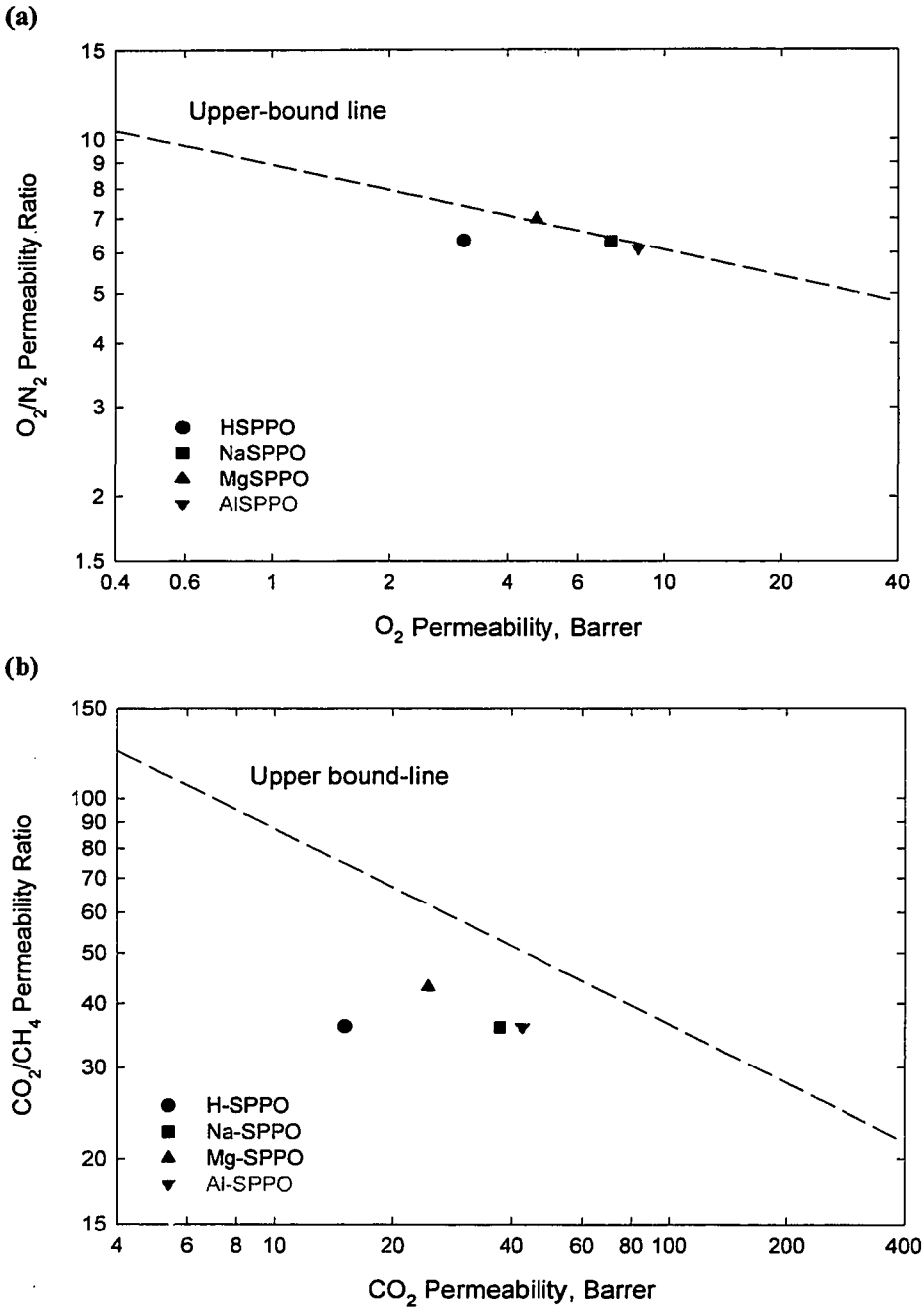

Figure 7-3. Effect of metal cation on the combination of **(a)** O_2 permeability and O_2/N_2 permeability ratio and **(b)** CO_2 permeability and CO_2/CH_4 permeability ratio of SPPO-1.37 membranes prepared from NMP solutions.

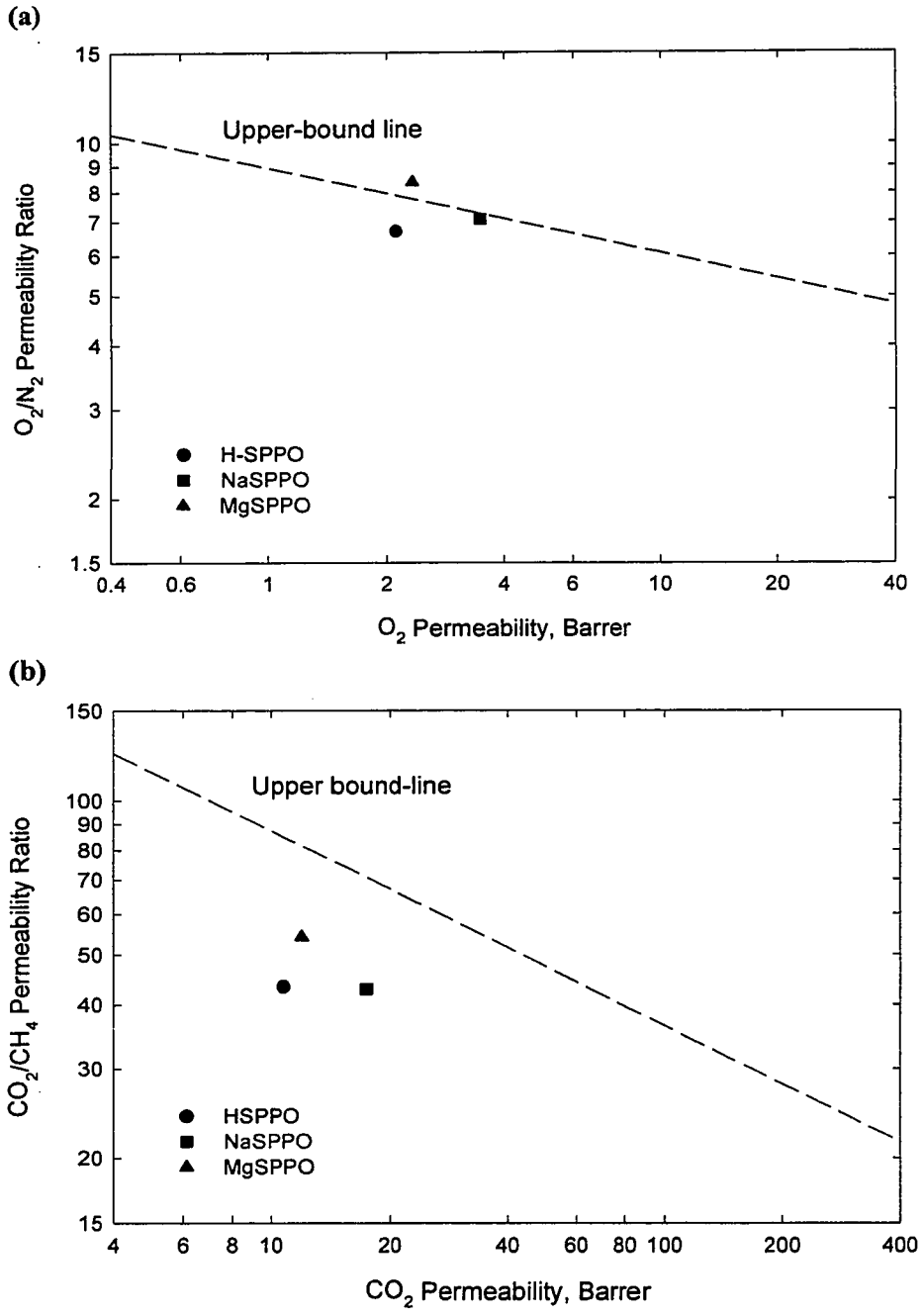

Figure 7-4. Effect of metal cation on the combination of **(a)** O_2 permeability and O_2/N_2 permeability ratio and **(b)** CO_2 permeability and CO_2/CH_4 permeability ratio of SPPO-1.80 membranes prepared from NMP solutions.

Figure 7-3a because of a considerable increase in O_2 permeability and almost no change in O_2/N_2 permselectivity compared to HSPPO-1.37. On the other hand, MgSPPO-1.37 falls just above the upper-bound line in Figure 7-3a despite a lower O_2 permeability compared to NaSPPO-1.37 and AlSPPO-1.37. The improvement in gas transport properties of MgSPPO-1.37 is mainly due to a considerable increase in its permselectivity. In Figure 7-3b, MeSPPO-1.37 membranes fall below the upper bound line for CO_2/CH_4 gas pair. This further reinforces the earlier conclusion that SPPO is a more promising material for the O_2/N_2 separation than for the CO_2/CH_4 separation.

The effect of metal cation on gas transport properties of SPPO-1.80 (Figures 7-4a and 7-4b) is very similar to that observed for SPPO-1.37. The increase in permeability of NaSPPO compared to HSPPO is not as significant as in case of SPPO-1.37. It can be noticed that MgSPPO-1.80 falls even more above the upper bound line for O_2/N_2 separation than MgSPPO-1.37. MgSPPO-1.80; therefore, appears to be the most attractive polymer for preparation of asymmetric integrally skinned or thin film composite membranes, especially for O_2/N_2 separation.

7.4.3 Effect of *IEC* on permeability of NaSPPO

Figure 7-5 shows the effect of *IEC* on O_2 permeability of high molecular weight NaSPPO membranes. For comparison, the figure also shows the effect of *IEC* on O_2 permeability of the corresponding HSPPO membranes and the low molecular weight NaSPPO membranes [Fu *et al.*, 1994b]. It can be noticed that unlike HSPPO and low molecular weight NaSPPO, high molecular weight NaSPPO shows the maximum O_2 permeability for the polymer of *IEC* equal to 1.37 meq/g.

An increase in *IEC* results in an increase in polarity of the polymer. It is well known that an increase in polarity of the polymer tends to decrease its permeability for gases [Chern *et al.*, 1985]. It is evident in Figure 7-5 that such a decrease in permeability with an increase in polarity of the polymer was observed for high molecular weight HSPPO and low molecular weight NaSPPO. A decrease in permeability with an increase in *IEC* was also observed for other polymers. For example, Chen and Martin (1994) reported a monotonic decrease in permeability of sulfonated polystyrene in Na and Mg forms with an increase in the sulfonic content of the

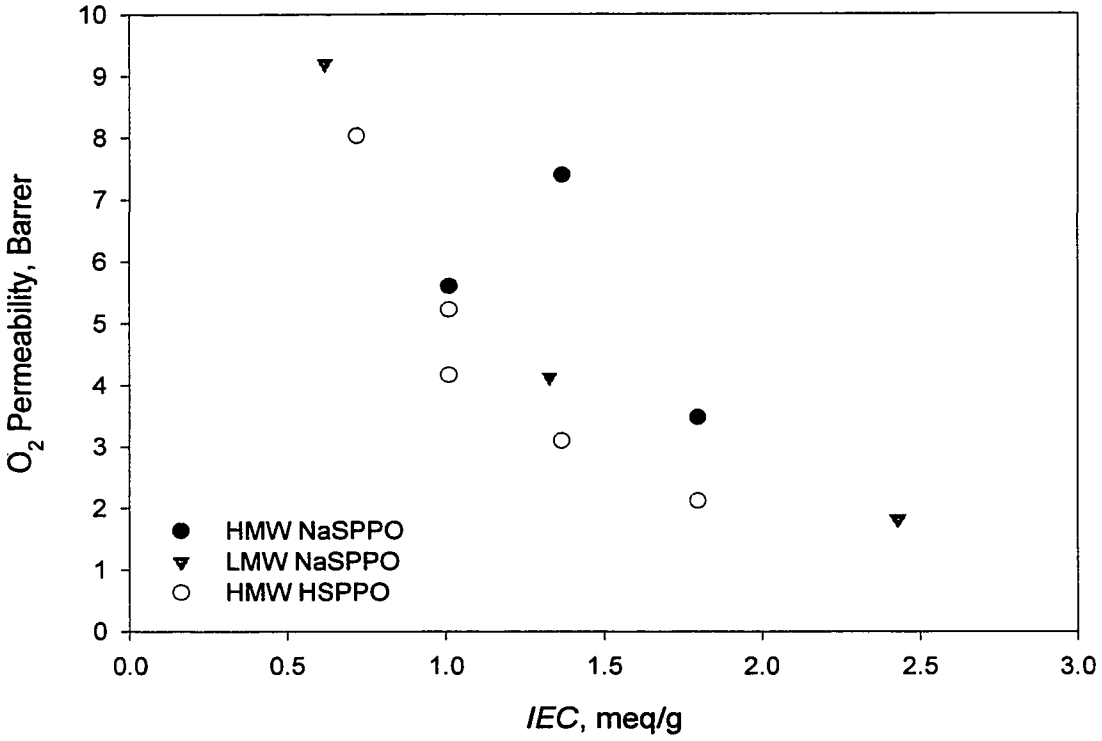

Figure 7-5. Effect of *IEC* on O_2 permeability of high molecular weight (HMW) NaSPPO, low molecular weight (LMW) NaSPPO and high molecular weight (HMW) HSPPO dense membranes.

polymer. The observed relationship between *IEC* and O_2 permeability for high molecular weight NaSPPO was; therefore, not expected.

Considering X-ray diffraction results summarized in Table 7-2, it can be noticed that d-spacing and peak intensity increased when *IEC* of NaSPPO increased from 1.01 to 1.37 meq/g. On the other hand, an increase in *IEC* did not result in any changes in the X-ray diffraction spectra of HSPPO films. This indicates that at some *IEC* between 1.01 and 1.37 meq/g, there was a change in the structure of high molecular weight NaSPPO. This change could be a result of inhibition of the rotation of individual PPO units resulting from electrostatic cross-links between the neighboring sulfonic groups. In turn, the inhibition of the rotation of individual PPO units may result in a more rigid structure of the polymer, which may explain the increase in peak intensity from NaSPPO-1.37, compared to NaSPPO-1.01.

It is postulated that the maximum permeability of NaSPPO-1.37 is a result of a transition in the membrane structure as *IEC* of polymer increases from 1.01 to 1.37 meq/g. When *IEC* increases the average distance between the neighboring sulfonic groups decreases, which results in an increase in the interactions between them. At some *IEC* these interactions become strong enough to immobilize rotation of individual PPO units between the neighboring sulfonic groups. When that happens, permeability of the polymer increases due to an increase in the length of diffusional jumps gas molecules can execute in the polymer [Story and Koros, 1992] or because of formation of fixed micropores in the membrane.

It is believed that there are three factors that are responsible for the unusual permeation properties of NaSPPO-1.37. These factors are high polarity of sulfonic groups in Na form, high molecular weight of polymer, and high free volume of the base polymer, PPO. When even one of these factors is missing, permeability will decrease with an increase in polarity of the polymer as for example in case of high molecular weight HSPPO, low molecular weight NaSPPO, and sulfonated polystyrene in sodium form. The last example represents the importance of the structure of the base polymer. On one hand, PPO is a polymer of high free volume and high permeability for gases because of an open arrangement of macromolecules created by nonlinear ether linkages [Story and Koros, 1992]. On the other hand, polystyrene has considerably lower

free volume and permeability than PPO because free rotation of repeat polystyrene units is restricted by side benzene rings [Chen and Martin, 1994].

Computer simulations of gas transport in SPPO and polystyrene of different IEC, cation and molecular weight could confirm the above hypothesis. Such computer simulations; however, were beyond the scope of this thesis. Furthermore, the computer simulations of gas transport in polymeric matrices are still in early stage of development and most of these studies have involved rubbery polymers [Stern, 1994].

7.4.4 Comparison of permeability ratios to actual gas separation factors

Table 7-5 shows the comparison of O_2/N_2 and CO_2/CH_4 permeability ratios with the actual separation factors of some MeSPPO membranes. The separation factors for O_2/N_2 were obtained using air as a feed, while the separation factors for CO_2/CH_4 were obtained using two different feed mixtures, feed 1 containing 50% CO_2 in CH_4 and feed 2 containing 20.4% of CO_2 in CH_4. The separation experiments were performed in the CV system connected to the RGA. Consequently, the permeate was collected at pressure no greater than 1 cmHg. The details of the system used in gas separation experiments along with the experimental procedure were described in Chapter 5.

Table 7-5. Comparison of ideal and actual separation factors for some dense high molecular weight MeSPPO membranes.

IEC meq/g	Cation	$P_{O2/N2}$	$\alpha^{a}_{O2/N2}$	$P_{CO2/CH4}$	$\alpha^{a}_{CO2/CH4}$ Feed1[b]	Feed2[c]
1.80	Mg	8.73	7.65	56.14	48.79	54.73
1.80	Mg	8.22	7.25	51.93	46.04	51.28
1.80	Na	7.21	6.24	42.79	38.43	42.70
1.01	Na	5.78	5.49	29.34	25.60	28.19

[a] determined in the CV system
[b] 50% of CO_2 in CH_4
[c] 20.4% of CO_2 in CH_4

It can be noticed that the actual separation factors are always lower than the corresponding permselectivities. This is not surprising because permselectivity (permeability

ratio), is often referred to as the ideal selectivity. The term ideal selectivity implies that its value represents the maximum separation factor for a given gas mixture by a given polymer. In case of the membranes presented in Table 7-5, the actual separation factors are less than the ideal values; however, the difference does not exceed 13%. It is interesting to note that CO_2/CH_4 separation factor depends on the composition of the feed. When the feed contains 50% of CO_2, the actual separation factor is 10-13% lower than its ideal value; however, when the feed contains 20.4% of CO_2 the actual separation factor is very close to the corresponding ideal value, the maximum difference being 2.5%. Considering composition of air and feed 2, both mixtures contain approximately 20% of the more permeable gas, that is 21% of O_2 in air and 20.4% CO_2 in feed 2. On the other hand, the difference between the actual separation factor and the ideal value is more significant for air compared to feed 2.

The results shown in Table 7.5 confirm a great potential of MeSPPO, especially that of MgSPPO, for gas separation. For example, the separation factor for O_2/N_2 of 7.65 corresponds to the 67.3% of O_2 in the permeate when the membrane is used for oxygen enrichment of air. The separation factor for CO_2/CH_4 of 48.79 obtained using the feed containing 50% of CO_2 in CH_4 corresponds to 98.0% of CO_2 in the permeate, while the separation factor of 54.73 obtained using the feed containing 20.4% of CO_2 in CH_4 corresponds to 93.3% of CO_2 in the permeate.

7.5 Chapter Summary

Sulfonic groups in a metal form are more polar than sulfonic groups in the acid form, consequently, MeSPPO is more hydrophilic than HSPPO of the same *IEC* value.

Substitution of the proton in sulfonic groups by a metal cation increases the thermal stability of this substituent. This is indicated by an increase of the decomposition temperature from 175 to 300°C.

Despite a greater density, MeSPPO is more permeable to gases than HSPPO. Increase in permeability resulting from the exchange of proton with a metal depends on the *IEC* of the polymer. The maximum increase is observed for the polymer of *IEC* equal to 1.37 meq/g.

As *IEC* increases, the distance between neighboring sulfonic groups decreases resulting in stronger intra-molecular interactions between them. The increase in interactions between

neighboring sulfonic groups inhibits rotation of individual PPO repeat units between those two sulfonic groups, thus increasing rigidity of the polymer chain. The increase in rigidity of polymer chain with an increase in *IEC* is indicated by higher peak intensity on the X-ray diffraction spectrum of NaSPPO-1.37 compared to NaSPPO-1.01. Inhibition of the rotation of PPO repeat units increases the length of the free volume pockets and possibly creates continues passages through the membrane matrix. As a result, despite a higher *IEC* value, permeability of NaSPPO-1.37 is greater than permeability of NaSPPO-1.01.

MeSPPO, which shows an increase in peak intensity on the X-ray diffraction spectrum and an increase in d-spacing compared to the corresponding HSPPO, shows no change or increase in ideal selectivity. This represents an improvement in gas transport properties. The combination of O_2 permeability and O_2/N_2 ideal selectivity of MgSPPO-1.37 and MgSPPO-1.80 places these polymers above the upper-bound line.

The actual separation factors for O_2/N_2 and CO_2/CH_4 obtained in the CV system are lower than the ideal values; however, the maximum difference is not greater than 13%.

CHAPTER 8

Effect of Solvent in Casting Solution

The results presented in Chapters 6 and 7 pertaining to the characterization of high molecular weight HSPPO and MeSPPO indicated some promising properties of these materials for gas separation. In particular, MgSPPO appears to be a very attractive material for O_2/N_2 separation. The properties of homogeneous membranes, such as those presented in Chapters 6 and 7, are often referred to as the intrinsic properties. The term intrinsic implies that these properties are unique to the polymer chemistry. This assumption is very convenient; however, it neglects all parameters involved in preparation of homogeneous membranes.

The literature review presented in Chapter 4 indicates that among the factors affecting properties of homogeneous membranes, solvent in the casting solution is the most obvious and probably the most important one. Despite that, there have been no systematic studies on the effect of the solvent on the properties of homogeneous membranes. As a result, in this chapter the effect of the solvent on the surface morphology and gas transport properties of HSPPO-1.37 membranes prepared by complete evaporation of solvent will be examined and discussed.

There are a number of physico-chemical properties that can be used for characterization of solvent; however, as discussed in Chapter 4, solvent strength, solvent volatility and solvent size appear to be the most important parameters.

8.1 Evaluation of Solvent Strength

Solvent strength governs the polymer-solvent interactions in the casting solution. There are several approaches that can be used for the evaluation of these interactions. In the following

discussion the solubility parameter, intrinsic viscosity, and relative viscosity approaches will be adopted.

8.1.1 Solubility parameter approach

The solubility parameter approach is based on comparison of solubility parameters of polymer and solvent. The smaller the difference between the solubility parameters of polymer and solvent, the stronger the polymer-solvent interactions. Table 8-1 summarizes the difference in the Hildebrand solubility parameters (Δ) and the difference in the Hansen solubility parameter (Δ') for various solvents when the polymer is HSPPO of *IEC* equal to 1.37 meq/g (HSPPO-1.37). The solubility of HSPPO-1.37 in these solvents at room temperature was also examined. The results are also presented in Table 8-1. The values of solubility parameters of solvents considered in this study and the solubility parameters of HSPPO of different *IEC* are shown in Appendix B.

According to the Hildebrand parameter approach, the strongest polymer-solvent interactions should occur in DMF followed by NMP. The same conclusion is drawn when the Hansen solubility parameters are considered. The third and fourth solvents are nitroethane and DMAC according to the Hildebrand parameter, respectively. On the other hand, when the Hansen parameters are considered, DMAC and nitroethane switch their positions. In general, with exceptions of THF and methanol, the solvents follow a similar pattern in both the Hildebrand and Hansen solubility parameter approaches.

Solubility tests of HSPPO-1.37 in solvents provide a first verification of the predicted order of the strength of these solvents. It can be noticed in Table 8-1 that, nitroethane, which is predicted to be a "good" solvent for HSPPO-1.37, does not even swell the polymer. On the other hand, THF, which according to the Hildebrand parameter approach exerts the weakest interaction on the polymer, actually dissolves the polymer. Considering the solubility test results, it can be noticed that the Hansen parameters provide a slightly better estimation of the polymer-solvent interactions than the Hildebrand parameters. Even the Hansen solubility parameter predicts that nitroethane and acetone have stronger interactions than pyridine and THF, whereas in reality the former solvents do not dissolve the polymer and the latter solvents do.

Table 8-1. Solubility of high molecular weight HSPPO-1.37 in organic solvents. Differences between the Hildebrand solubility parameter (Δ) and the Hansen solubility parameter (Δ').

Solvent	Solubility[a]	Δ, $MPa^{1/2}$		Δ', $MPa^{1/2}$	
		Value	Rank	Value	Rank
Acetone	s	5.24	7	6.58	5
Chloroform	s	6.54	8	13.60	8
DMAC	+	3.44	4	5.47	3
DMF	+	0.74	1	4.22	1
Methanol	-	4.16	6	15.00	10
Nitroethane	-	2.84	3	6.16	4
NMP	+	2.44	2	4.29	2
Pyridine	+	3.64	5	8.10	6
TCE	s	6.74	9	13.68	9
THF	+	6.94	10	10.82	7

[a] + polymer was soluble in the solvent
s polymer was swollen in the solvent
- polymer was insoluble in the solvent

The solubility parameter approach; therefore, provides only a rough estimate of the polymer-solvent interactions and cannot be used for a precise quantitative analysis of these interactions. This is not surprizing because a considerable degree of uncertainty is associated with the estimation of solubility parameters of polymers by a group contribution method. In case of HSPPO, this problem is magnified because of lack of the data for the polar contribution of SO_2 group (Appendix B). Furthermore, comparison of the Hansen and the Hoy solubility parameters for solvents showed that, although the overall solubility parameters were close to each other for all solvents considered, their components varied considerably.

8.1.2 Intrinsic viscosity approach

The intrinsic viscosity approach has been commonly used to study polymer solvent-interactions. At very low concentrations (less than 1 g/dL) in good solvents, macromolecules are unfolded, obtaining the polymer configuration of the favorable polymer-solvent interactions to

the maximum extent. Consequently, the actual length of the macromolecule and hence the resistance to the shear force increases as the polymer-solvent interactions increase.

Table 8-2 shows the comparison of experimentally determined viscosities of solvents with those available in the literature [CRC Handbook of Chemistry and Physics, 1992-1993]. The average efflux time for each solvent was calculated from the three consecutive time readings. In all cases, the standard deviation was less than 0.2 % of the average value.

Table 8.2. Comparison of experimentally determined viscosities (η_1)[a] of solvents with the literature values (η_2) [CRC Handbook of Chemistry and Physics, 1992-1993].

Solvent	Avg. efflux time, s	ν cSt	ρ g/mL	η_1 cP	η_2 cP	Difference[c]
NMP[b]	194.89	1.563	1.033	1.615	1.67	-3.4%
NMP	424.28	1.542	1.033	1.593	1.67	-4.8%
DMAC	260.61	0.947	0.937	0.887	1.956	-121%
DMF	223.68	0.813	0.945	0.768	0.749	2.5%
Pyridine	234.27	0.852	0.979	0.834	0.879	-5.4%
THF	141.17	0.513	0.882	0.453	0.456	0.7%

[a] Capillary size 50, capillary constant at 25°C = 0.003635
[b] Measured in viscometer with capillary of size 75.
[c] Error = $(\eta_1 - \eta_2 / \eta_1)$ 100%

It can be noticed from Table 8-2 that there is more than 100% discrepancy between the experimental and literature viscosities of DMAC. The data in Table 8-2 is based on DMAC purchased from BDH Chemicals Canada Limited, Toronto, Ontario, Canada. Viscosity measurement was repeated using DMAC purchased from Fisher Scientific, Ottawa, Ontario, Canada. Its value was found to be 0.901 cP, which is similar to the experimental viscosity listed in Table 8-2. Viscosities of other solvents are close to the literature values. While the viscosity measurement was conducted with a viscometer of capillary size 50, the viscosity of NMP was also measured with a viscometer of size 75. The viscosities of NMP determined in both viscometers, as can be seen in Table 8-2, were close to each other.

Figures 8-1 – 8-5 show the relationship between reduced viscosity (η_{sp}/c) and concentration of polymer (c) in dilute solutions of HSPPO-1.37 in NMP, DMAC, DMF, Pyridine, and THF, respectively. As defined by Eq. (4.10), the intercept of the reduced viscosity at zero concentration is the intrinsic viscosity for a given polymer-solvent system. It can be noticed that the intercept can be easily obtained by the linear extrapolation for NMP and pyridine solutions. The intrinsic viscosities of HSPPO-1.37 in NMP and pyridine were found to be 1.13 and 1.08 dL/g, respectively. This indicates that NMP is a better solvent for HSPPO-1.37 than pyridine.

In the THF solution (Figure 8-5), the reduced viscosity decreases with a decrease of concentration of polymer; however, unlike the solutions in NMP (Figure 8-1) and pyridine (Figure 8-4), a linear relationship does not hold. The curve is concave upward. On the other hand, the DMAC (Figure 8-2) and DMF (Figure 8-3) solutions show curves, which are concave downward.

According to the solubility tests of HSPPO of different *IEC*s in THF and DMAC presented in Table 7-1, THF dissolved HSPPO of *IEC* equal to 1.37 meq/g and lower, whereas DMAC dissolved HSPPO of *IEC* equal to 1.37 meq/g and higher. Both THF and DMAC are; therefore, the limiting (weak) solvents for HSPPO-1.37. THF is a weak solvent because HSPPO-1.37 is too polar for THF, while DMAC is a weak solvent because HSPPO-1.37 is not sufficiently polar for DMAC.

Figure 8-6 shows the relationship between reduced viscosity and concentration for the system HSPPO-1.01 and THF. Unlike Figure 8-5, the reduced viscosity decreases linearly with decrease in concentration. Consequently, the intrinsic viscosity for HSPPO-1.01-THF system can be determined and is equal to 1.02 dL/g. Considering that THF is a stronger solvent for HSPPO-1.01 than for HSPPO-1.37, it seams that weak polymer-solvent interactions are responsible for non-linear relationships between reduced viscosity and concentration.

The summary of the intrinsic viscosity measurements along with the Hansen solubility parameters difference Δ' is given in Table 8-3. The intrinsic viscosity seems to be a better means for the evaluation of polymer-solvent interactions, since it is an experimental value. The comparison of Δ' values with intrinsic viscosity data further reinforces the earlier conclusion that

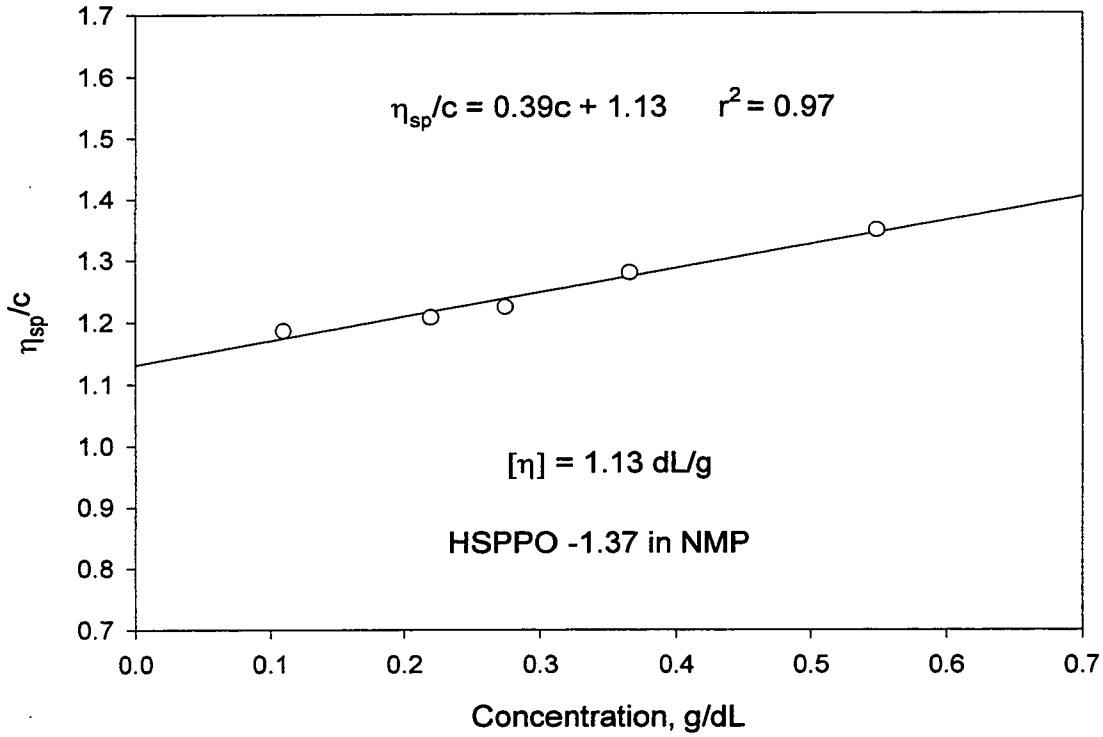

Figure 8-1. Determination of intrinsic viscosity of high molecular weight HSPPO-1.37 in NMP at 25°C.

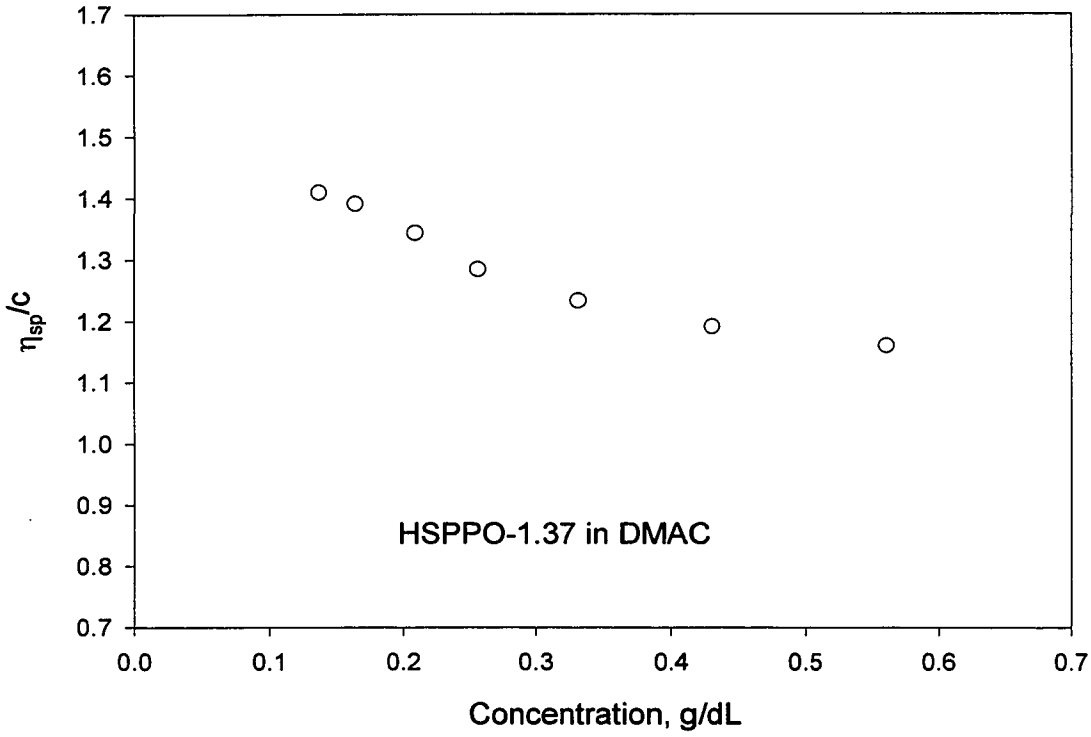

Figure 8-2. Determination of intrinsic viscosity of high molecular weight HSPPO-1.37 in DMAC at 25°C.

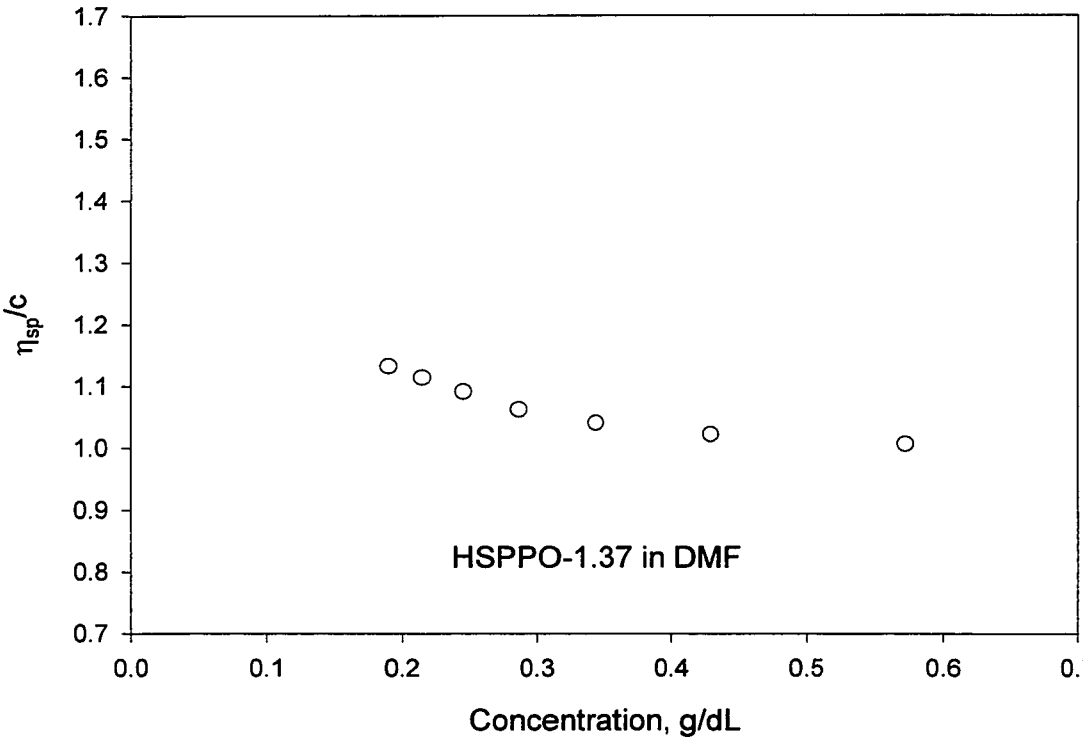

Figure 8-3. Determination of intrinsic viscosity of high molecular weight HSPPO-1.37 in DMF at 25°C.

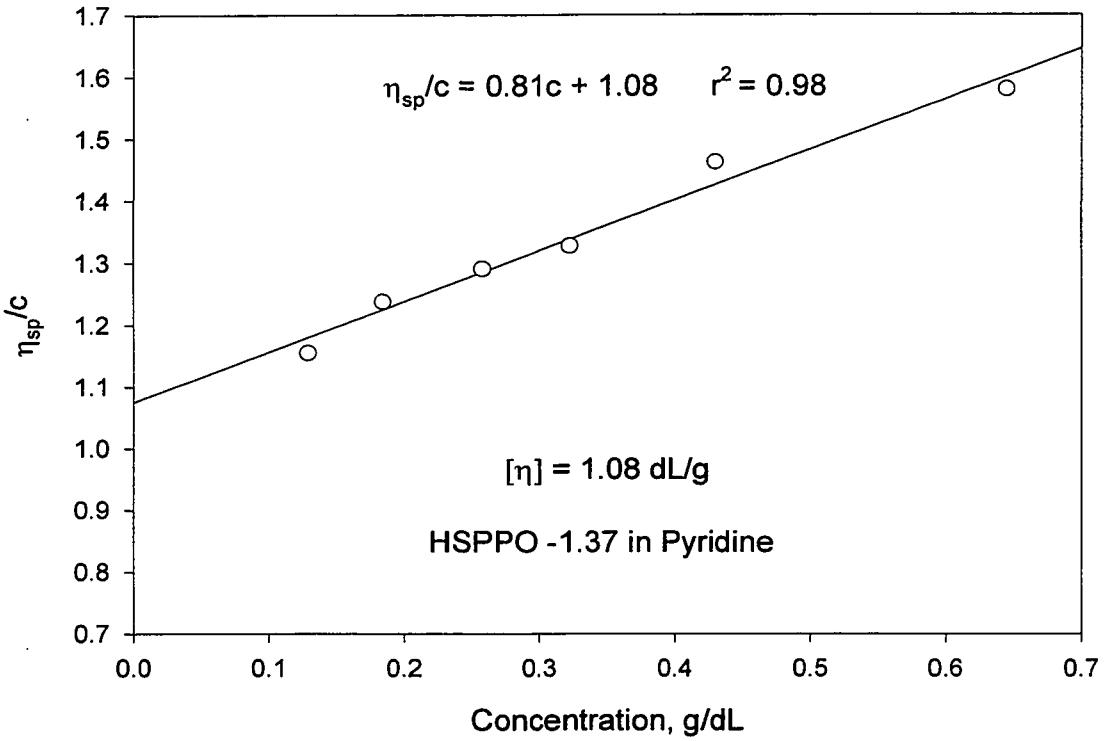

Figure 8-4. Determination of intrinsic viscosity of high molecular weight HSPPO-1.37 in pyridine at 25°C.

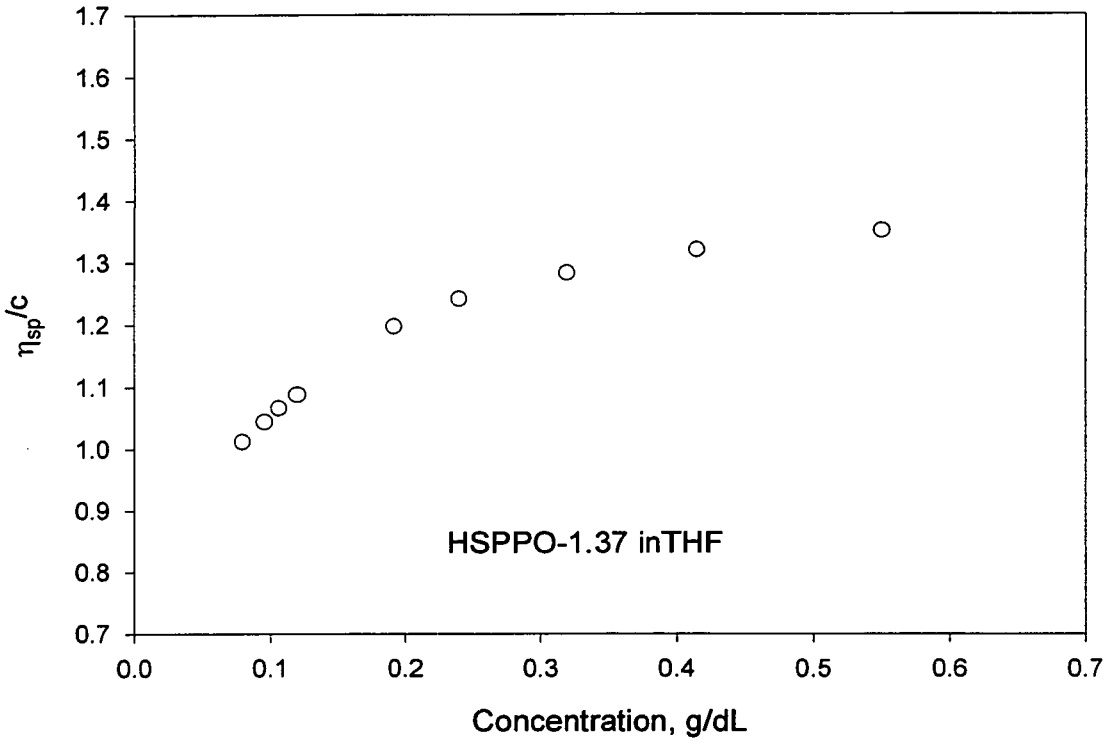

Figure 8-5. Determination of intrinsic viscosity of high molecular weight HSPPO-1.37 in THF at 25°C.

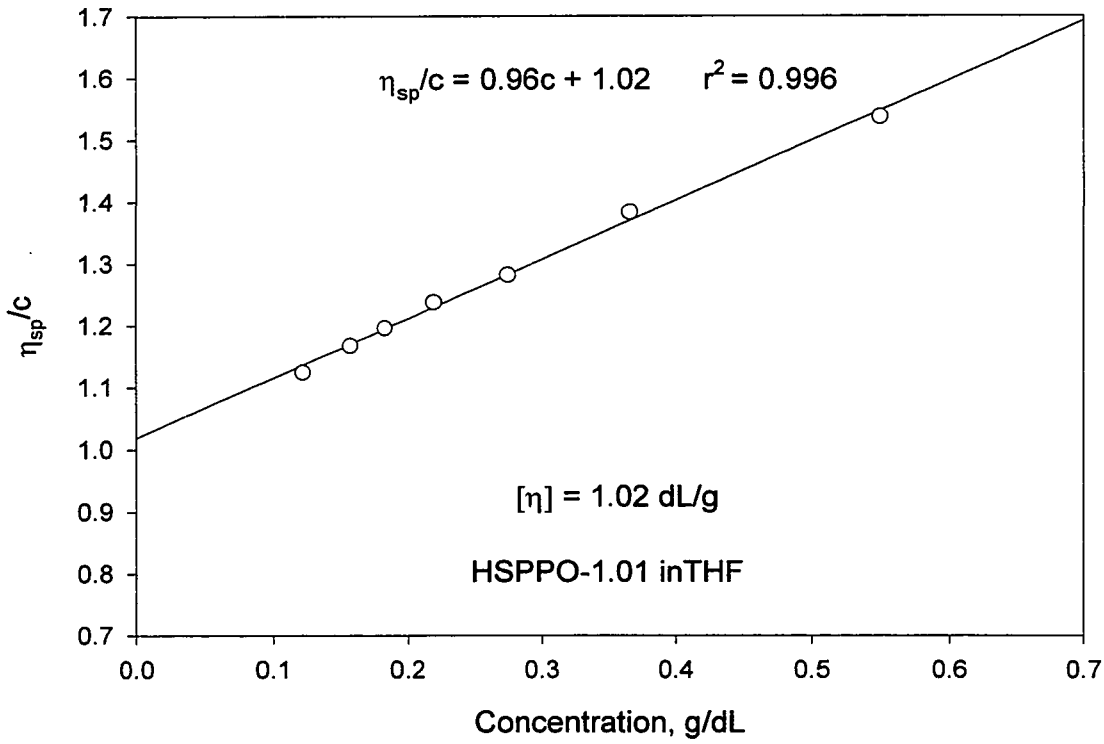

Figure 8-6. Determination of intrinsic viscosity of high molecular weight HSPPO-1.01 in THF at 25°C.

Table 8-3. Summary of intrinsic viscosity measurements of high molecular weight HSPPO-1.37 in organic solvents.

IEC, meq/g	Solvent	[η], dL/g[a]	Δ', $MPa^{1/2}$
1.37	NMP	1.13	4.29
1.37	DMAC	n/d	5.47
1.37	DMF	n/d	4.22
1.37	Pyridine	1.09	8.10
1.37	THF	n/d	10.82
1.01	THF	1.02	10.12

[a] n/d - [η] not determined due to a non-linear relationship between η_{sp}/c and c.

the solubility parameter approach provides only a very rough estimate of the polymer-solvent interactions. For example, Δ' values for HSPPO-1.37-DMF and HSPPO-1.37-DMAC are less than that for HSPPO-1.37-pyridine, indicating that DMF and DMAC exert stronger interactions on HSPPO-1.37 than pyridine. On the other hand, considering that a linear relationship between reduced viscosity and concentration is inherent to strong while a non-linear relationship is inherent to weak solvents; pyridine exerts stronger interactions on HSPPO-1.37 than DMF and DMAC. It should be noted that a stronger HSPPO-1.01-THF interaction than HSPPO-1.37-THF is also predictable by the solubility parameter approach.

Although the intrinsic viscosity approach may provide a more reliable estimation of polymer-solvent interactions than the solubility parameter approach, its applicability is limited. Based on this approach one can conclude that NMP is a stronger solvent for HSPPO-1.37 than pyridine, and that both NMP and pyridine are stronger than DMF, DMAC and THF, but no distinction can be made between DMF, DMAC and THF because of non-linear relationships.

8.1.3 Relative viscosity approach

In the relative viscosity approach, it is assumed that in concentrated polymer solutions, a decrease in relative viscosity of solution indicates an increase in polymer solvent-interactions. The major advantage of this approach over the intrinsic viscosity approach is that the viscosity measurement is done for the actual casting solution.

The efflux times of pure solvents required for calculation of relative viscosities of the corresponding polymer solutions were shown in Table 8-2. Despite some discrepancies between experimentally determined and literature viscosities, especially in case of DMAC, the former viscosities were used for calculation of relative viscosities of casting solutions.

The efflux times of casting solutions were measured at 25°C using a viscometer equipped with capillary of size 150. The concentration of HSPPO-1.37 in all solutions was 4.0 g/dL. For each polymer solution three consecutive efflux times were measured and averaged. The readings were repeated after one day using a new sample of polymer solution from the same polymer solution batch. Table 8-4 shows the comparison of the average efflux times obtained in two sets of runs along with the standard deviations from the readings in each set. The last column in Table 8-4 shows the flow times taken for calculation of the kinematic viscosity of polymer solutions.

Table 8-4. Efflux times of 4.0 g/dL solutions of high molecular weight HSPPO-1.37 in organic solvents at 25°C in a viscometer equipped with a capillary of size 150.

Solvent	Efflux time 1, s		Efflux time 2, s		Efflux time, s
	Avg.	St. Dev.	Avg.	St. Dev.	
NMP	430.78	1.08	432.50	0.95	431.64
DMAC	465.69	0.86	462.21	0.81	463.95
DMF	420.22	0.28	415.56	1.14	417.89
Pyridine	232.10	0.19	236.44	0.72	234.27
THF	306.01	0.48	315.12	3.17	306.01

It can be noticed from Table 8-4 that in general, the average efflux times obtained in two independent sets of runs were close to each other. The exception was the THF solution for which the average efflux time obtained in the second set of runs was 3% greater than that in the first set. Furthermore, it was observed that the efflux times in the second set were increasing in the consecutive runs. The second run for the THF solution was; therefore, ignored. In all other cases, the average of the average values obtained in the first and second runs was used for calculation of the kinematic viscosity.

The relative viscosity (η_{rel}) is the ratio of the absolute viscosities of solution and solvent (Eq. 4.13). Since the density of a 4.0 g/dL polymer solution was not significantly different from the density of pure solvent, η_{rel} was approximated by the ratio of kinematic viscosities of polymer solution and solvent. The summary of the relative viscosities of the HSPPO-1.37 solutions is presented in Table 8-5. The order of increasing relative viscosity is also given. As relative viscosity increases, the solvent strength decreases. The ranking in solvent strength was also made by intrinsic viscosity and Hansen solubility parameter difference.

Table 8-5. Summary of relative viscosities of 4.0 g/dL high molecular weight HSPPO-1.37 solutions in organic solvents at 25°C. Comparison of strength of solvents based on relative viscosity, intrinsic viscosity and Hansen solubility parameter approaches.

Solvent	ν, (cSt)	η_{rel}	Solvent strength rank		
			η_{rel}	[η], dL/g	Δ', $MPa^{1/2}$
NMP	15.84	10.27	2	1	2
DMAC	17.03	17.98	3	3-5	3
DMF	15.34	18.87	4	3-5	1
Pyridine	8.60	10.09	1	2	4
THF	11.23	21.89	5	3-5	5

According to the relative viscosity approach, the solvent strength decreases in the following order: pyridine > NMP > DMAC > DMF > THF. It can be noticed that the relative viscosities of the pyridine and NMP solutions are similar and they are significantly lower than those of DMAC, DMF, and THF solutions. Consequently, pyridine and NMP are considered to be significantly stronger solvents to HSPPO-1.37 than DMAC, DMF and THF. A similar order of solvent strength was also obtained by the intrinsic viscosity. Unlike the intrinsic viscosity, the relative viscosity approach allows to distinguish between the strength of DMAC, DMF and THF. It should be noted that according to the intrinsic viscosity approach, NMP was concluded to be a stronger solvent for HSPPO-1.37 than pyridine. The difference; however, between NMP and pyridine is small both in relative viscosity and intrinsic viscosity.

The comparison of solvent strength based on the relative viscosity and Hansen solubility parameter approaches reveals that NMP, DMAC and THF are ranked in the same positions. This

may seem surprising considering the earlier conclusion that the Hansen solubility parameter approach provides only a very rough estimate for the polymer-solvent interactions. On the other hand, the Hansen solubility parameter entirely mispredicts the strength of pyridine and DMF on HSPPO-1.37 polymer. The same rankings of NMP, DMAC and THF in the relative viscosity and Hansen solubility parameter approaches appear to be coincidental.

The relative viscosity approach is applicable for concentrated polymer solutions. The term concentrated polymer solution is; however, not well defined. For example, Okuno *et al.* (1993), who studied 4.0 g/dL solutions of polyvinyl chloride (PVC) in THF with different non-solvent additives, concluded that the relative viscosity increases with increase in the solvent strength. This is entirely opposite to what is being assumed in this study. The relation between viscosity and polymer-solvent interactions reported by Okuno *et al.* (1993) is characteristic for dilute polymer solutions in which macromolecules do not form agglomerates.

Although the concentration of polymer solutions studied by Okuno *et al.*(1993) was the same as the concentration of HSPPO-1.37 solutions under investigation, there are considerable differences between the polymers used in both studies. PVC considered by Okuno *et al.* (1993) had the molecular weight equal to 30,000, which is one order of magnitude less than the molecular weight of HSPPO. It is believed that for a given concentration of polymer solution, the chain entanglement and hence the tendency to form macromolecular aggregates increases with an increase in the molecular weight of polymer. The structure of the polymer solution is; therefore, governed not only by the concentration of polymer, but also by its molecular weight.

This assumption is justified when the maximum relative viscosity reported by Okuno *et al.* (1993) (η_{rel} equal to 4.6) is compared with those of HSPPO-1.37 solutions (η_{rel} equal to 10 - 21). More than 100% greater relative viscosities of HSPPO-1.37 than those of PVC solutions, at the same polymer concentration, indicate a greater degree of chain entanglement in the former solutions.

8.2 Other Properties of Solvents

The solvent size which affects free volume in the selective layer of a membrane, is conveniently represented by the molar volume of solvent [Kesting *et al.*, 1990]. The molar

volume of solvent is available in many references. The values presented in Table 8.6 were taken from the "Handbook of solubility parameters and other cohesion parameters" [Barton, 1983].

The solvent volatility influences desolvation and gelation kinetics and consequently the structure of the final membrane [Kesting and Fritzsche, 1993]. Solvent volatility can be expressed by the difference between the boiling point at atmospheric pressure of solvent and the casting temperature, or by the vapor pressure of solvent at the casting temperature. Both ways of expressing solvent volatility are included in Table 8-6. The boiling points of solvents at atmospheric pressure were taken from "CRC Handbook of Physics and Chemistry" [Linde, 1992-1993], while the vapor pressures of solvents at casting temperatures were obtained from the British Gas Database [Laverty, 1995].

The summary of properties of solvents used for dissolution of HSPPO-1.37 along with the casting temperatures is presented in Table 8-6. The vapor pressures of solvents shown in this table are the values at casting temperatures, while the relative viscosities of polymer solutions are given at 25 °C. This is because, the polymer solutions were kept at room temperature prior to casting. Except for the membranes made from a THF solution, all other films were cast at elevated temperatures.

Table 8.6 Summary of properties of solvents used for preparation of 4.0 g/dL solutions of high molecular weight HSPPO-1.37.

Solvent	M^a g/mol	V cm^3/mol	$T_{N.B.P.}$ °C	$T_{casting}$ °C	P_v kPa	η cP	η_{rel}
NMP	99.13	96.5	202	60	0.45	1.593	10.27
DMAC	87.62	92.5	164.5	60	2.01	0.887	17.98
DMF	73.10	77.0	153	60	3.71	0.768	18.87
Pyridine	79.10	80.9	115	40	5.94	0.834	10.09
THF	72.11	81.7	65	25	22.0	0.453	21.89

[a] Molecular weight of solvent

Table 8-6 shows that the variation in molar volumes is small. The difference between the smallest solvent - DMF and the largest solvent - NMP, is only 25%. On the other hand, there is a two-order of magnitude difference in vapor pressures between the least volatile solvent - NMP

and the most volatile solvent - THF. The variation in volatility of solvents is; therefore, more than the variation in other parameters.

8.3 Surface Morphology by TM AFM

Surface structure of membranes was characterized in terms of the mean roughness (R_a), the root mean square of the Z data (R_q), the mean difference between the five highest peaks and the five lowest valleys (R_z), the average peak height (h_{avg}), and the peak count. These parameters were defined in Section 5.5.5.1. Some characteristic features found on surface images were also measured and appropriate comparisons were made. For each membrane, at least two samples were prepared for the microscopic analysis, and at least two surface images in different sections of each sample were obtained. All images were obtained using the same AFM probe. The average roughness parameters along with the corresponding standard deviation values are summarized in Table 8-7 for membranes prepared using different solvents in casting solutions.

Figures 8-7 – 8-11 show the representative surface images of HSPPO-1.37 membranes prepared using different solvents. The images are presented in a 12 x 12 μm scanning area with a 1.0 μm Z range. These images are considered as representative, because their roughness parameters are closest to the average values listed in Table 8-7. The exception is the surface image of the membrane prepared from THF shown in Figure 8-11, which corresponds to the minimum roughness parameters. Since the surfaces of other THF membranes are rougher, their images would require Z range larger than 1.0 μm. The comparison with images of other solvents would then be difficult because of different Z ranges. Figures 8-12 and 8-13 show the surface images of the membranes prepared from NMP and pyridine, respectively, in a 0.75 x 0.75 μm scanning area with a 50 nm Z range. It should be emphasized that Z axis in all images shown in Figures 8-7 – 8-13 is expanded relative to XY plane; therefore, the surfaces are not as "bumpy" as they appear on the images.

8.3.1 Comparison of surfaces images

Before surface images are compared, it should be noted that membranes prepared from THF had different appearance than the other HSPPO-1.37 membranes. The surface of the THF

membranes looked "wavy", and was transparent with a light brown color. Other membranes looked smooth and were generally transparent and colorless.

Inspection of surface images shown in Figures 8-7 – 8-13 provides the basis for qualitative comparison of membranes prepared from different casting solvents. The surface images of the membranes prepared from NMP and pyridine shown in Figures 8-7 and 8-10, respectively, are not uniform. Large irregular features are found on a smooth background. Zooming into smooth sections of these images yields the images shown in Figures 8-12 and 8-13, respectively. Unlike the images in the large scanning area, those depicted in Figures 8-12 and 8-13 have rather uniform granular structures with diameters of grains ranging from 30 to 60 nm. Referring to four tiers of structure in polymeric membranes proposed by Kesting (1990), these grains represent the nodules, that is the macromolecular aggregates.

On the other hand, the surface images of the membranes prepared from DMAC, DMF, and THF shown in Figures 8-8, 8-9 and 8-11, respectively, show relatively uniform granular structures. The grains on these images are considerably larger than those found on the surface images of membranes prepared from NMP and pyridine. Their size range from 100 to 400 nm in diameter, depending on the solvent used. The size of the grains increases in the following order: DMAC < DMF < THF. Considering four tiers of structure in polymeric membranes proposed by Kesting (1990), these grains represent the aggregates of nodules sometimes referred to as the nodule aggregates.

Although the surface image of the membrane prepared from DMAC looks similar to the images of the membranes prepared from DMF and THF, the size of the nodular aggregates is considerably smaller than that on the membranes prepared from DMF and THF. Furthermore, one can also notice a small flat section located in the upper left corner of this image (Figure 8-8). This indicates some irregularity in the surface morphology of the membrane prepared from DMAC. The morphology of the membrane prepared from DMAC; therefore, represents a link between the morphologies of the membranes prepared from THF and DMF and those prepared from NMP and pyridine.

Attempts to obtain surface images in a 0.75 x 0.75 μm scanning area for the membranes prepared from DMF and THF were not successful. The resulting images had poor resolution

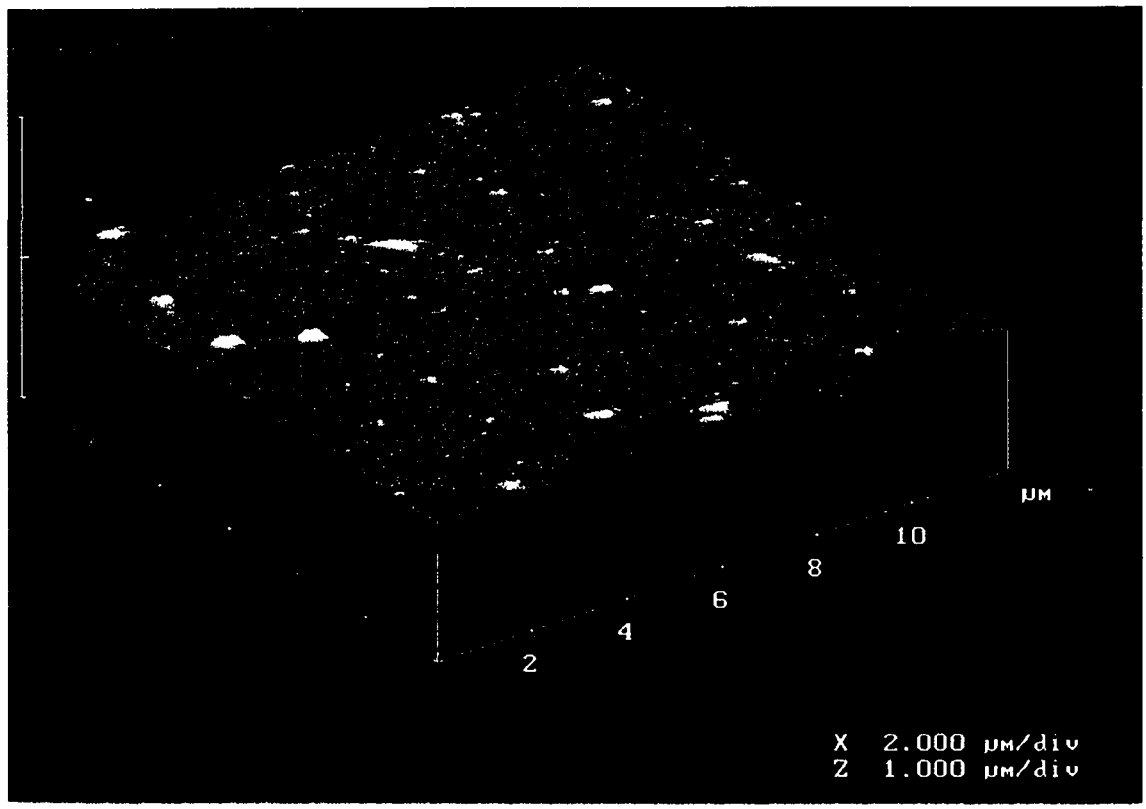

Figure 8-7. Surface image in 12 x 12 μm scan size by atomic force microscope in tapping mode of dense high molecular weight HSPPO-1.37 membrane prepared from NMP solution. Casting at 60°C, casting solution at room temperature.

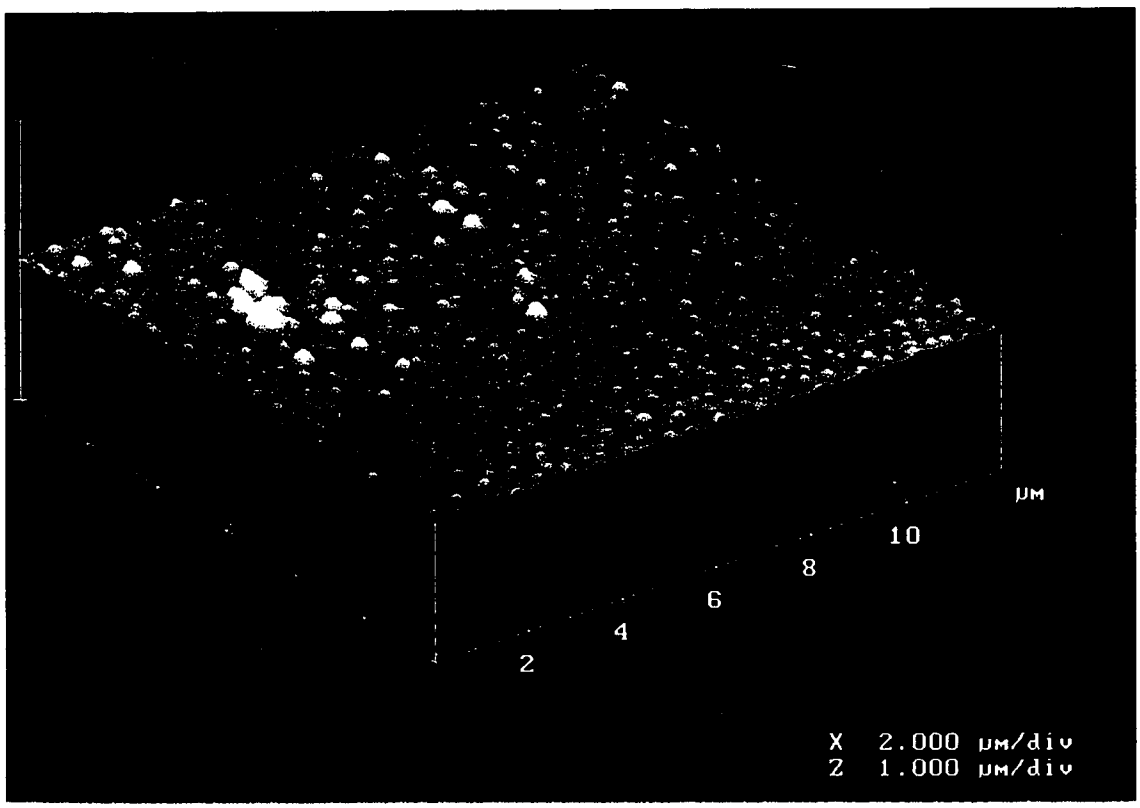

Figure. 8.8 Surface image in 12 x 12 μm scan size by atomic force microscope in tapping mode of dense high molecular weight HSPPO-1.37 membranes prepared from DMAC solution. Casting at 60°C, casting solution at room temperature.

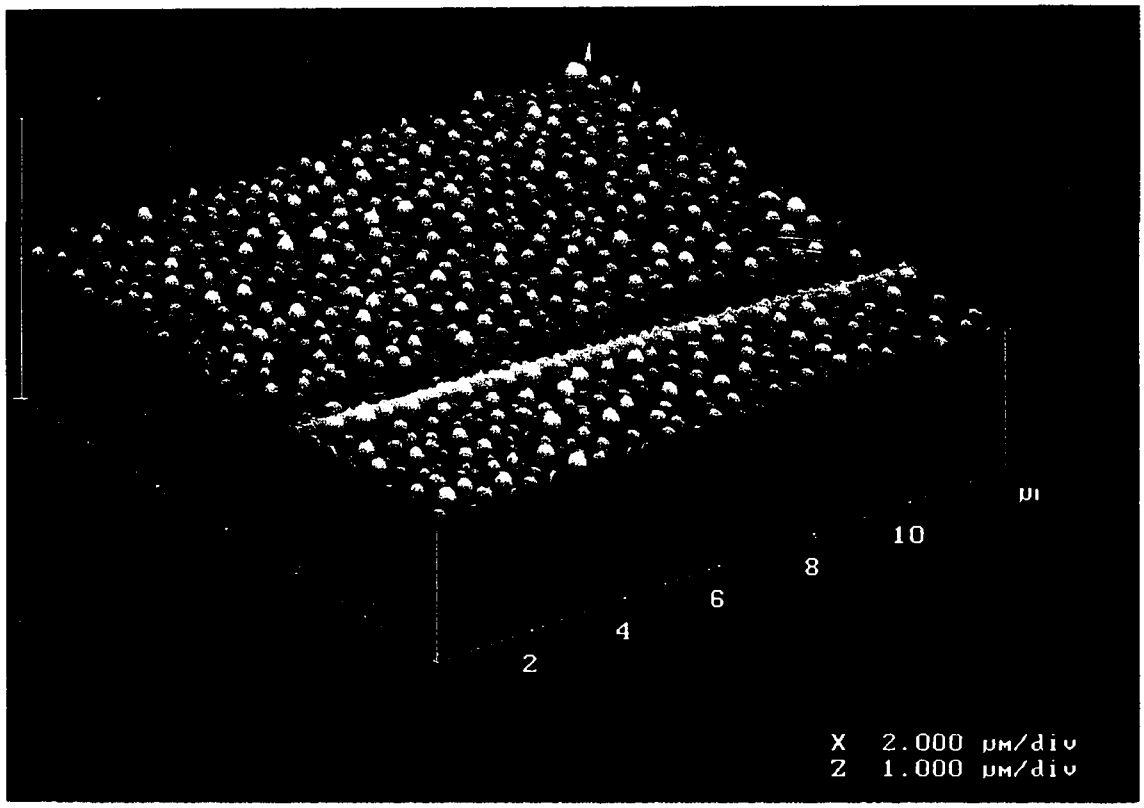

Figure. 8.9 Surface image in 12 x 12 μm scan size by atomic force microscope in tapping mode of dense high molecular weight HSPPO-1.37 membrane prepared from DMF solution. Casting at 60°C, casting solution at room temperature.

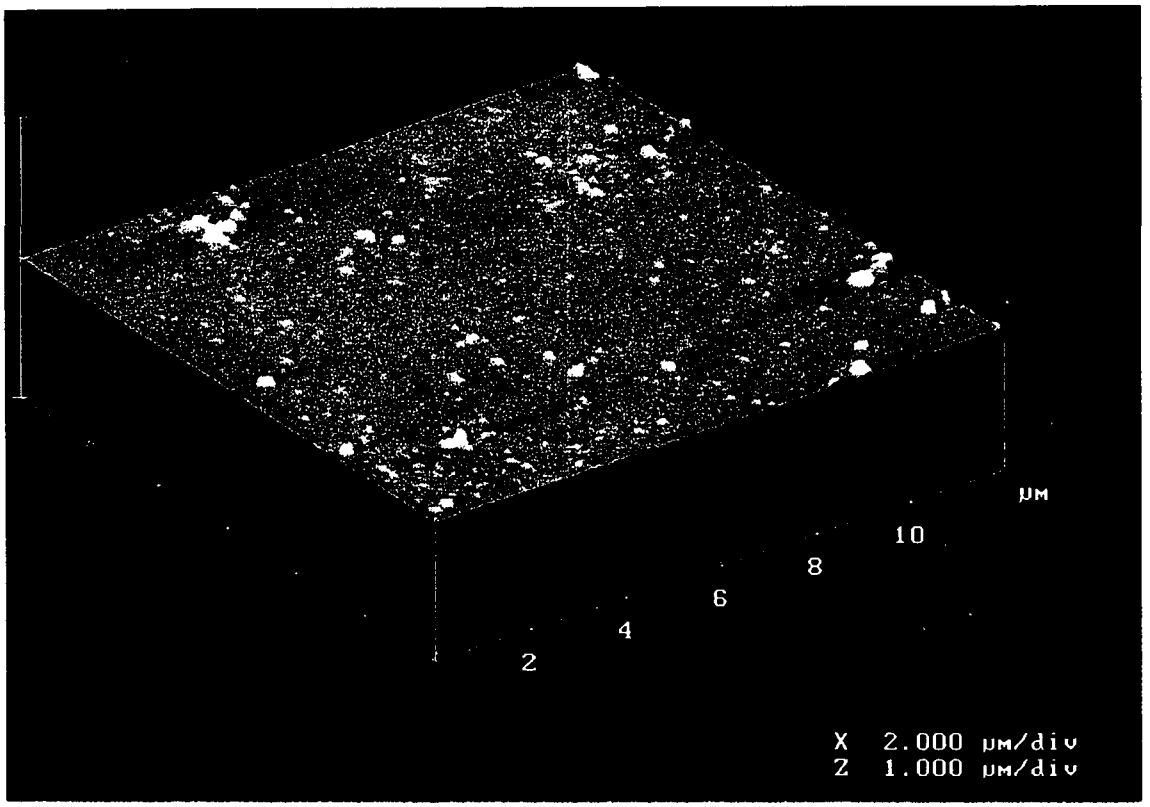

Figure. 8.10 Surface image in 12 x 12 μm scan size mode atomic force microscope in by tapping of dense high molecular weight HSPPO-1.37 membrane prepared from pyridine solution. Casting at 40°C, casting solution at room temperature.

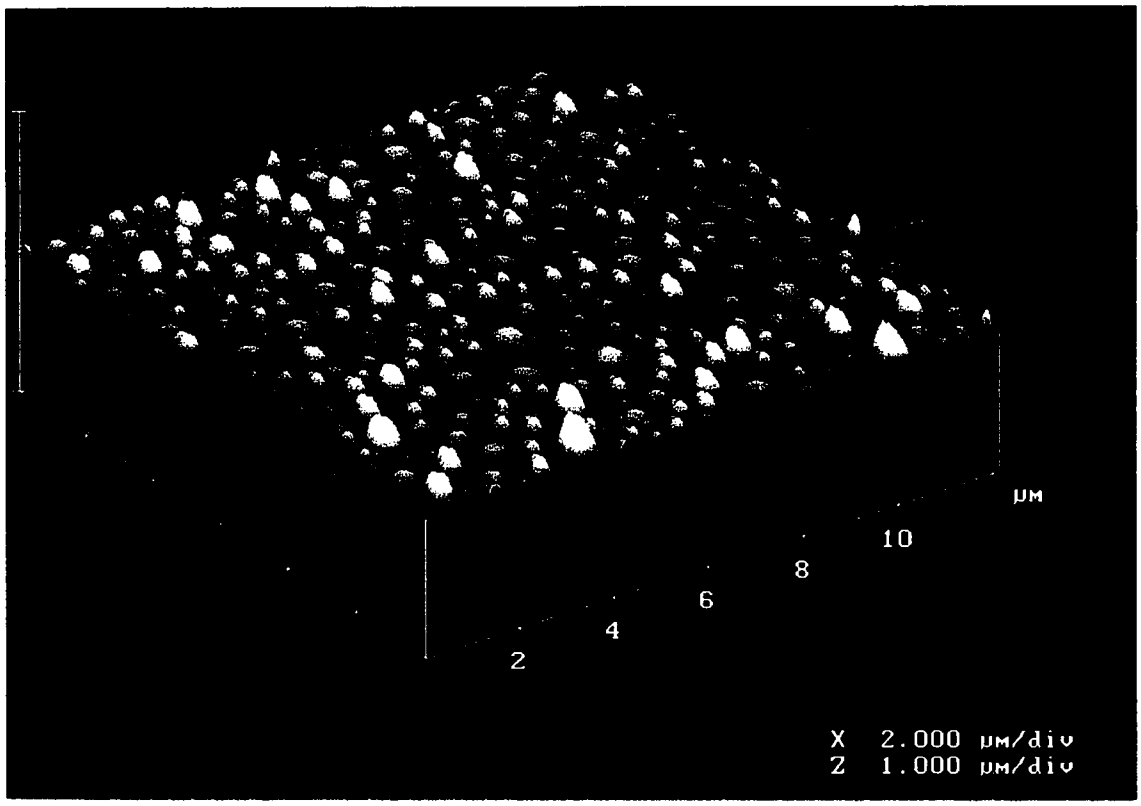

Figure. 8.11 Surface image in 12 x 12 μm scan size by atomic force microscope in tapping mode of dense high molecular weight HSPPO-1.37 membrane prepared from THF solution. Casting and casting solution at room temperature.

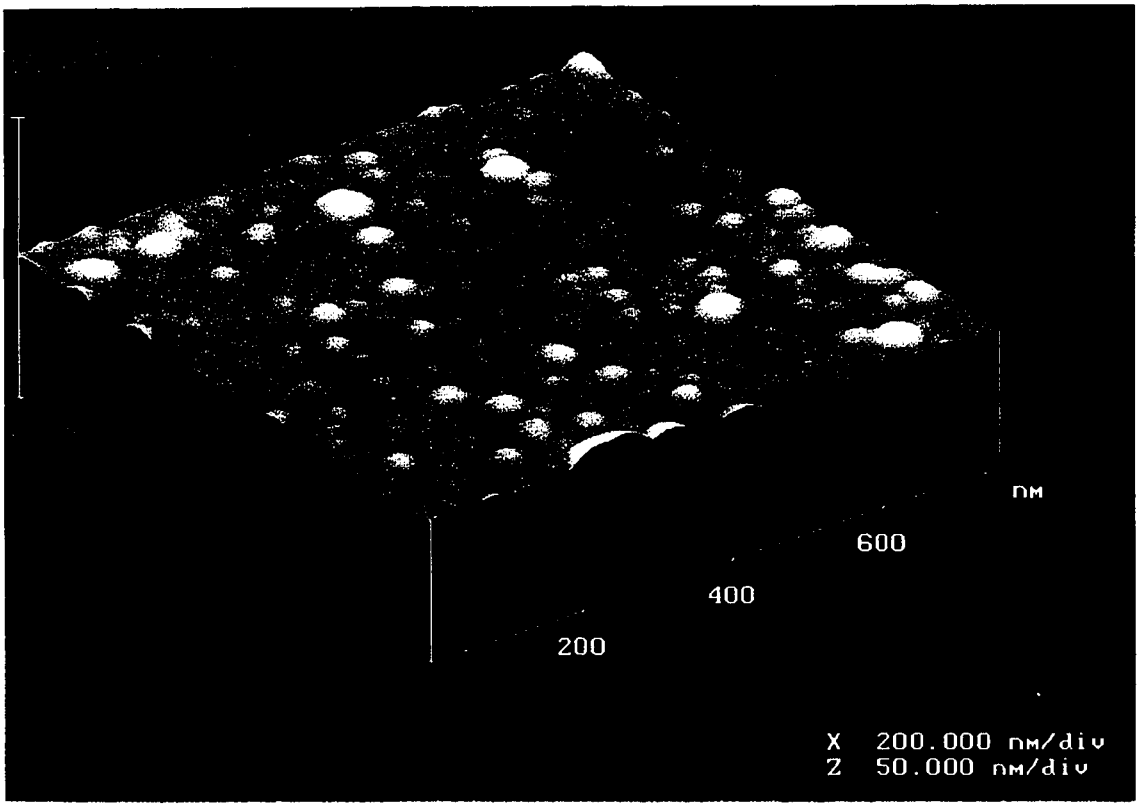

Figure. 8.12 Surface image in 0.75 x 0.75 μm scan size by atomic force microscope in tapping mode of dense high molecular weight HSPPO-1.37 membranes prepared from NMP solution. Casting at 60°C, casting solution at room temperature.

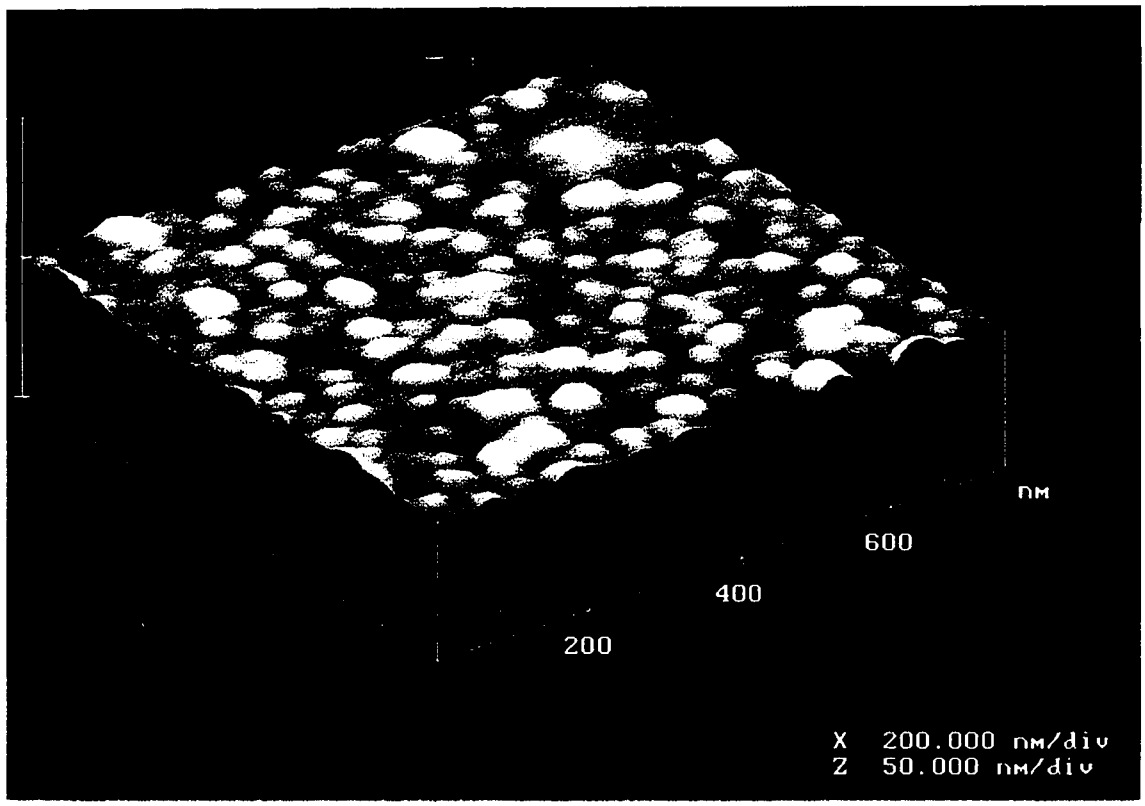

Figure. 8.13 Surface image in 0.75x 0.75 μm scan size by atomic force microscope in tapping mode of dense high molecular weight HSPPO-1.37 membrane prepared from pyridine solution. Casting at 40°C, casting solution at room temperature.

because of the influence of large nodule aggregates. When a square with an area equal to 0.75 x 0.75 μm is placed anywhere on the images shown in Figures 8-9 and 8-11, it will always contain at least one nodule aggregate. Because of height of nodule aggregates, the *Z* range of a scan cannot be decreased significantly, which prevents observation of small, flat features on the surface. Furthermore, because of the presence of nodule aggregates, scanning has to be performed over an inclined surface of changing slope, which further diminishes resolution of such image. The problem of obtaining high-resolution images on rough surfaces was also indicated by Bowen *et al.* (1996a).

The ultimate goal of microscopic analysis of membrane surface is to investigate the structure that is responsible for selective properties of the membrane. Kesting (1990) proposed that separation of gases in polymeric membranes occurs in 2-5 Å pores formed by intra-molecular chain segment displacements in nodule interior and in 3-10 Å holes in low-density regions between nodules. It is clear that this level of membrane structure is beyond the current resolution of TM AFM. A question then arises, if there is any relationship between the structure that governs gas transport properties of the membrane and the surface structure that can be observed under AFM. To answer the question, one needs to correlate gas transport properties of the membranes to some quantities that characterize the surface structure.

8.3.2 Comparison and interpretation of roughness parameters

Roughness parameters represent quantification of surface images. The definitions of roughness parameters used in this study were provided in Chapter 5. Considering the data presented in Table 8-7, it can be noticed that roughness parameters vary considerably for a given type of membrane. In extreme cases, the standard deviations are up to 50% of the corresponding average values. Despite this, the change in the roughness parameters resulting from the change in solvent is very clear. Considering the values of R_a, R_q, R_z, and h_{avg}, one can notice that they all increase in the following order: NMP < pyridine < DMAC < DMF < THF. This order of surface roughness is consistent with what was concluded based on the visual inspection of Figures 8-7 – 8-13.

It can be noticed that R_q for NMP and pyridine membranes are about 100% larger than the corresponding R_a values. On the other hand, for other membranes R_q differs from R_a not more than 40%. Considering that R_a indicates the average Z value, while R_q the standard deviation from Z values within a given scanning area, it is clear that the R_q /R_a ratio should increase when the surface morphology becomes more irregular. It is the case when some nodules form large nodular aggregates while the majority of nodules exist as separate entities. Comparison of the values of R_z and h_{avg} can provide a similar analysis. The value of R_z, which indicates the average difference between the five highest peaks and the five lowest valleys within the scanning area, is 8-10 times greater than the average peak height (h_{avg}) in the surface of membranes prepared from NMP and pyridine. On the other, the ratio is less than 4 for other membranes. It is obvious that when the surface contains some isolated large features, the ratio R_z/h_{avg} should be greater than that for the surface that contains uniformly sized features.

It can also be noticed that the increasing order of peak count does not agree with the increasing order of other roughness parameters. In fact, the lowest peak count is reported for the membrane prepared from THF, which showed the largest roughness parameters. This is not

Table 8-7. Summary of surface roughness parameters in 12 x 12 μm scan size of dense high molecular weight HSPPO-1.37 membranes prepared from different casting solutions.

Solvent	n		R_a (nm)	R_q (nm)	R_z (nm)	h_{avg} (nm)	peak count
NMP	4	Avg.	1.53	3.13	57.7	6.62	594
		StDev.	0.75	1.30	9.70	2.66	227
DMAC	6	Avg.	12.5	16.8	134	31.2	573
		StDev.	4.43	5.10	24.1	7.53	80
DMF	4	Avg.	22.3	28.9	184	59.1	660
		StDev.	8.94	9.99	41.1	20.6	82
Pyridine	4	Avg.	2.30	4.56	100	9.72	606
		StDev.	0.51	0.66	12.8	1.28	142
THF	4	Avg.	34.8	44.9	304	94.4	347
		StDev.	8.12	9.12	36.4	28.4	110
NMP[a]	1	-	0.69	0.98	7.11	1.88	306
Pyridine[a]	1	-	1.06	1.37	9.81	2.41	127

[a] Roughness parameters obtained in small scan size, 0.75x0.75 μm.

surprising considering that the size of nodular aggregates on THF membrane is larger than on any other membrane and, consequently less nodular aggregates can be fitted within the scanning area. On the other hand, the highest peak count is reported for DMF membrane whose roughness parameter is the second largest.

The roughness parameters in the small scanning area (0.75 x 0.75μm) are considerably smaller than the roughness parameters in the large scanning area (12 x 12 μm). Furthermore, the ratios R_q/R_a and R_z/h_{avg} decrease with a decrease in the scanning area. This indicates that images obtained in the smaller scanning area are smoother and more uniform than those in the larger scanning area. This is not surprising, because the images shown in Figures 8-12 and 8-13 were purposely taken from the flat and uniform section of Figures 8-7 and 8-10, respectively.

The comparison of roughness parameters obtained for different scan sizes indicates subjectivity of roughness parameters. Even though the images in the smaller scanning area may reveal more features of the surface structure, these images can not be considered as representative for a given membrane. It would be interesting to compare the images on the smaller scanning area of THF, DMF and DMAC membranes, if they were obtainable, with those observed in Figures. 8-12 and 8-13. Because of the difficulty in obtaining high-resolution images for THF, DMF and DMAC membranes; however, such comparison is impossible. The comparison of roughness parameters obtained from the larger scan images appears to be the only possible way.

8.3.3 Correlation of the surface morphology to the properties of casting solvent

Figure 8-14 presents the plots of surface roughness of HSPPO-1.37 membranes versus the properties of solvents. Surface roughness in Figure 8-14 is expressed by the R_a parameter. The solvent properties considered include solvent size expressed by the molar volume (Figure 8-14a), solvent volatility expressed by the vapor pressure at casting temperature (Figure 8-14b), and solvent strength expressed by the reciprocal of the relative viscosity of casting solution (Figure 8-14c). The properties of solvents along with the values of R_a used for construction of Figure 8-14 are shown in Table 8.8.

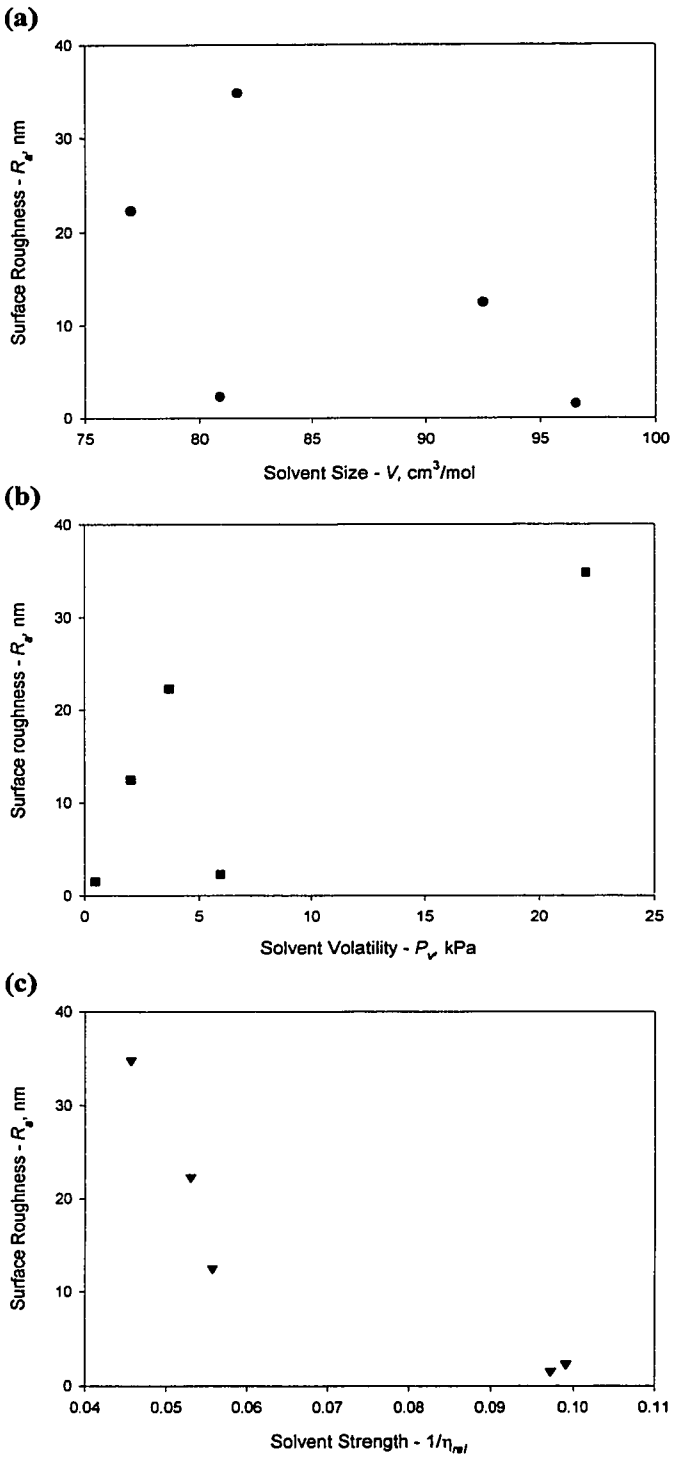

Figure 8-14. Effect of properties of solvent in casting solution on surface roughness of dense high molecular weight HSPPO-1.37 membranes; (a) effect of solvent size; (b) effect of solvent volatility; (c) effect of solvent strength.

The following trends are found in Figures 8-14a-c; decrease of surface roughness with increase in solvent size, increase in surface roughness with increase in solvent volatility, and decrease in surface roughness with increase in solvent strength. These trends are discussed in the following sections.

8.3.3.1 Effect of solvent size

Assuming that solvent molecules in a polymer solution act as transient templates, the membrane prepared from the polymer solution in a "large" solvent should have more free volume than that prepared from the polymer solution in a "small" solvent [Kesting, 1990]. If the surface structure of homogeneous membrane is indicative of the structure of the membrane interior, rougher surface should correspond to greater free volume. Consequently, an increase in the solvent size should result in an increase in the surface roughness of the membrane. According to Figure 8-14a, there is no clear relationship between solvent size and surface roughness. Excluding the membrane prepared from pyridine solution, it appears that surface roughness decreases with an increase of solvent size, which is opposite to the anticipated effect of the solvent size.

There could be several reasons for this inconsistency. Firstly, for a solvent to act as a transient template, the solvent must be removed rapidly following the gelation of polymer solution, which is not necessarily a case during formation of homogeneous membranes. Secondly, as indicated in Table 8-8 the variation in molar volumes of solvents is rather small. Even if the effect of solvent size is expected, the effect might be insignificant because of small difference in molar volumes. It is; therefore, safe to conclude that any trend between solvent size and surface roughness observed in Figure 8-14a is purely coincidental.

8.3.3.2 Effect of solvent volatility

The effect of solvent volatility was studied by Khulbe *et al.* (1996a) for dense PPO membranes prepared from chloroform and trichloroethylene (TCE) solutions. Since chloroform and TCE have similar solubility parameters, they attributed any difference in membrane morphologies to the difference in solvent volatility. They reported the average diameter of

nodules found on the top surface of the membrane prepared from more volatile chloroform solution to be twice as large as that found on the top surface of the membrane prepared from less volatile TCE solution [Khulbe *et al.*, 1996a].

Due to rapid evaporation of solvent, the nodules produced from the polymer dissolved in more volatile solvents can contain larger free volume entrapped inside the nodules, which results

Table 8-8. Effect of solvent properties on surface roughness of dense high molecular weight HSPPO-1.37 membranes.

Solvent	Properties of solvents			Roughness
	V (cm^3/mol)	P_v (kPa)	$1/\eta_{rel}$	R_a (nm)
NMP	96.5	0.45	0.0973	1.53
DMAC	92.5	2.01	0.0556	12.5
DMF	77.0	3.71	0.0530	22.3
Pyridine	80.9	5.94	0.0991	2.30
THF	81.7	22.0	0.0457	34.8

in larger dimensions of nodules [Khulbe *et al.*, 1996a]. This phenomenon is similar to the one discussed by Kesting and Fritzsche (1993) in preparation of asymmetric membranes by phase inversion. It is; therefore, anticipated that homogeneous membranes prepared from more volatile solvents should have larger features (nodules or nodule aggregates), greater surface roughness and consequently larger free volume than those prepared from less volatile solvents.

Considering Figure 8-14b, it can be noticed that surface roughness increases with volatility of casting solvent, as expected. The exception is the membrane prepared from the pyridine solution. Although pyridine is the second most volatile solvent, the roughness parameters of the pyridine membrane are considerably lower than those for the membranes prepared from less volatile DMAC and DMF. This indicates that some parameter or parameters other than solvent volatility also influence surface roughness. The influence of solvent size was ruled out in the previous section. Another parameter influencing surface morphology is the solvent strength.

8.3.3.3 Effect of solvent strength

It was indicated in Chapter 4 that the relative viscosity of a polymer solution is a measure of the polymer chain entanglement. The chain entanglement is enhanced when polymer-solvent interactions are weak since macromolecules tend to form macromolecular aggregates in the polymer solution. Upon evaporation of solvent, polymer starts to precipitate around some precipitation centers, that is, around the regions of high local concentration of polymer. Macromolecular aggregates existing in the polymer solution at the beginning of solvent evaporation can be considered as such precipitation centers. Formation and growth of nodules and further aggregation of nodules will; therefore, be enhanced when polymer-solvent interactions are weak. On the other hand, when strong interactions between polymer and solvent exist, formation of nodules will be delayed and consequently their size is expected to be smaller. In some cases formation of nodular aggregates is totally prevented.

It is anticipated; therefore, that surface roughness of polymeric membranes should decrease with an increase in the solvent strength. This anticipated effect is confirmed by the experimental results presented in Figure 8-14c.

8.3.3.4 Combined effect of solvent strength and solvent volatility

An increase in solvent strength (a decrease in relative viscosity of casting solution) and a decrease in solvent volatility appear to have a similar effect on surface roughness of the dense membranes. In both cases, the surface roughness decreases.

Comparing pyridine and DMAC, the vapor pressure of DMAC at casting temperature is one third that of pyridine, while the relative viscosity of DMAC solution is almost twice as large as that of the pyridine solution. The roughness parameter of the DMAC membrane is more than five-fold greater than the roughness parameter of the pyridine membrane. Comparing NMP and pyridine, the relative viscosities of NMP and pyridine solutions are comparable, while the vapor pressure of NMP at casting temperature is more than one order of magnitude smaller than that of pyridine. Yet the roughness parameters of the pyridine membranes are only 30-60% greater than the roughness parameters of the NMP membranes. These two examples suggest that the relative

viscosity of casting solution has a stronger influence on the surface roughness than the volatility of solvent.

Considering that relative viscosity is a measure of the polymer-solvent interactions, it appears that solvent strength is a dominating factor in determining the surface morphology of the HSPPO-1.37 membranes. The effect of solvent strength and solvent volatility on surface morphology will be discussed further in Chapter 9 when the effects of casting temperature and temperature of casting solution are considered.

8.4 Gas Transport Properties

The summary of permeabilities and permselectivities of homogeneous HSPPO-1.37 membranes prepared from different solvents is presented in Table 8-9. All data were obtained in the CV testing system. The data for the membranes prepared from the DMAC solution was already presented in Table 6-4. The membranes prepared from THF were laminated with a silicone film prior to gas permeation experiments. Pre-tests in the CP system showed that THF membranes had high flux and no selectivity. Permeabilities of laminated membranes were calculated using Eq. 7-1.

Figures 8-15a &b show a graphical representation of the data presented in Table 8-9. The points in the figures represent the average permeabilities and permeability ratios for a given type of membrane. Figure 8-15a presents a relationship between O_2 permeability and O_2/N_2 permeability ratio for HSPPO-1.37 membranes along with the upper-bound line for this pair of gases. A similar relationship for CO_2/CH_4 gas pair is shown in Figure 8-15b. The relationships in both figures are presented in a log-log domain.

It is evident that permeability of HSPPO-1.37 membranes change with the solvent. For example changing the solvent from NMP to pyridine results in more than two-fold increase in O_2 and CO_2 permeabilities. This increase in membrane permeability is associated with a 10-15% decrease in O_2/N_2 and CO_2/CH_4 permeability ratios. Permeability of membranes increases in the following order of casting solvents: NMP < DMF < DMAC < THF < Pyridine. An increase in permeability of the HSPPO-1.37 membranes is generally associated with a decrease in

Table 8-9. Summary of gas permeation properties of dense high molecular weight HSPPO-1.37 membranes prepared from different casting solutions.

Solvent	Permeability, Barrer				Permselectivity	
	N_2	O_2	CH_4	CO_2	O_2/N_2	CO_2/CH_4
NMP	0.25	1.74	0.20	7.54	6.95	38.39
	0.27	1.86	0.22	8.63	6.88	39.22
DMAC	0.45	2.85	0.34	13.15	6.29	37.10
	0.54	3.38	0.45	16.29	6.30	36.28
	0.51	3.24	0.46	16.04	6.40	34.81
DMF	0.44	2.74	0.36	13.10	6.24	36.72
	0.51	3.25	0.42	15.09	6.38	35.94
Pyridine	0.77	4.69	0.68	23.51	6.09	34.65
	0.83	5.03	0.77	26.27	6.06	34.12
THF[a]	0.56	3.59	0.53	17.37	6.36	32.97
	0.66	4.07	0.62	21.02	6.16	33.91
	0.62	3.86	0.54	17.68	6.26	32.96

[a] Membranes laminated with SR film

permselectivity. This represents a typical trade-off behavior between permeability and permselectivity for polymeric membranes.

It can be noticed that combination of O_2 permeability and O_2/N_2 permselectivity places the HSPPO-1.37 membranes below the upper-bound line. Although replacing solvent results in changes in both permeability and permselectivity of films, there is no clear advantage for the replacement of solvent, since the distance between the upper-bound line and the experimental point is similar for all solvents. On the other hand, considering the combination of CO_2 permeability and CO_2/CH_4 permeability ratio, it appears that an increase in permeability ratio associated with the replacement of pyridine in casting solution by NMP does not compensate the loss in membrane permeability. Consequently, the membrane prepared from pyridine solution falls closer to the upper bound line than the membrane prepared form the NMP solution.

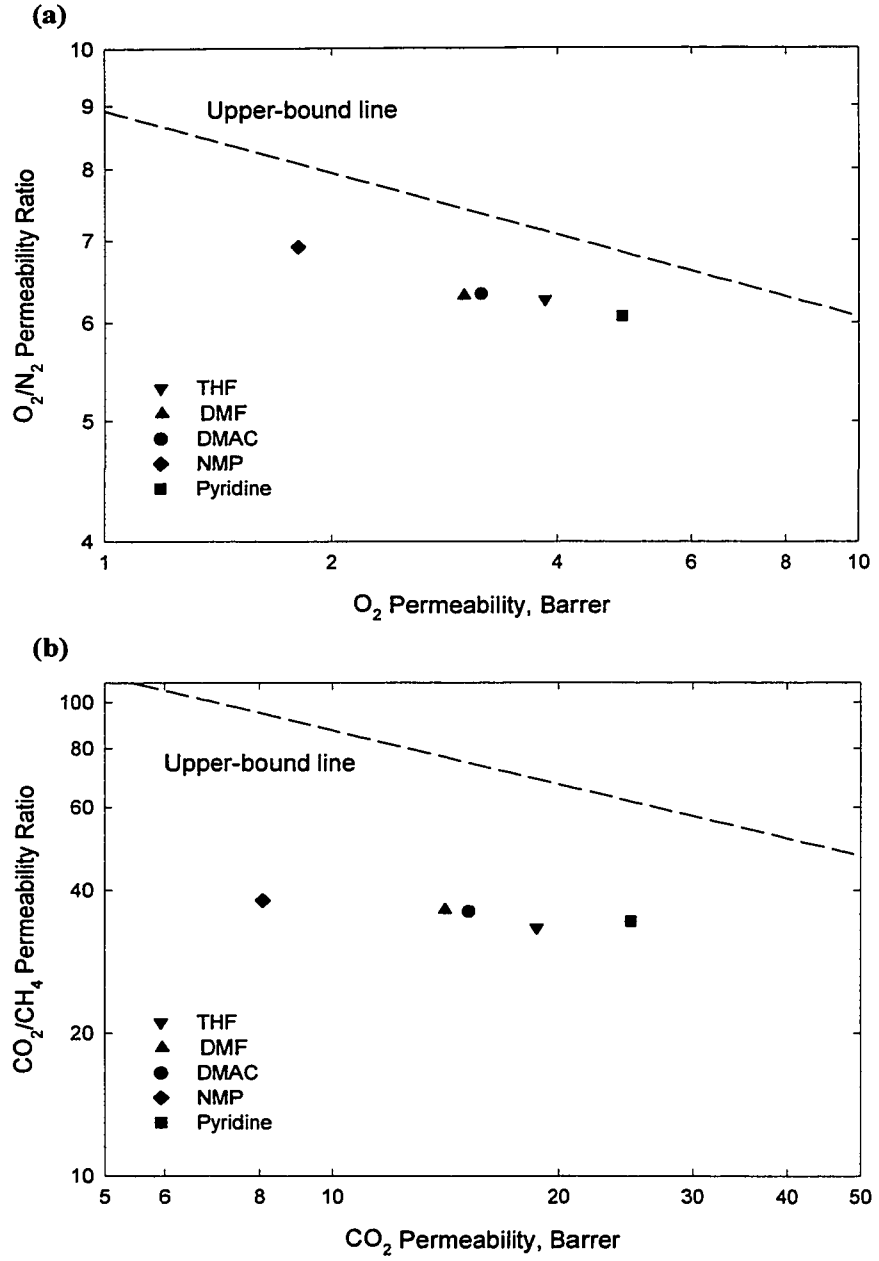

Figure 8.15 Effect of solvent in casting solution on combination of **(a)** O_2 permeability and O_2/N_2 permeability ratio and **(b)** CO_2 permeability versus CO_2/CH_4 permeability ratio of dense high molecular weight HSPPO-1.37 membranes.

8.4.1 Effect of surface roughness on gas transport properties

Surface roughness and gas permeation properties of dense HSPPO-1.37 membranes are both affected by the solvent. As discussed earlier, an increase in surface roughness means an increase in the free volume of the membrane. The greater free volume, in turn, should result in the greater permeability. Consequently, an increase in surface roughness should result in an increase in membrane permeability.

Figure 8-16 presents the plots of surface roughness versus gas transport properties of dense HSPPO-1.37 membranes. The surface roughness of membranes is represented by the average R_a parameter for a given surface. O_2 permeability (Figure 8-16a) and O_2/N_2 permeability ratio (Figure 8-16b) represent the gas transport properties of HSPPO-1.37 membranes.

It is evident from Figure 8-16 that there is no correlation between roughness parameter and permeability or permeability ratio of membranes. On one hand, the NMP membrane has the smallest roughness parameters and it is the least permeable and most selective. On the other hand, the pyridine membrane, which has the second smallest roughness parameters, is the most permeable and the least selective. It should be noted that roughness parameters of NMP and pyridine membranes are close to each other, while they are far apart from those of other membranes. The pyridine membrane is considerably more permeable than THF and DMF membranes, which have one order of magnitude greater surface roughness parameters than the pyridine membranes. The anticipated relationship between surface roughness and gas transport properties of membranes was not observed, at least for the given resolution of the AFM equipment.

The relationship between surface roughness and the permeation properties was expected based on the assumption that surface morphology of a homogeneous membrane is an indication of its internal structure. This assumption is valid only when the membrane is uniform in its structure across the cross-section. A membrane is called "homogeneous" when it is prepared by complete evaporation of solvent. The films under study are therefore homogeneous, implying that their structure is isotropic.

Khulbe *et al.* (1996b), who studied morphology of the top and the bottom surfaces of PPO membranes prepared by complete evaporation of chloroform solvent, observed different

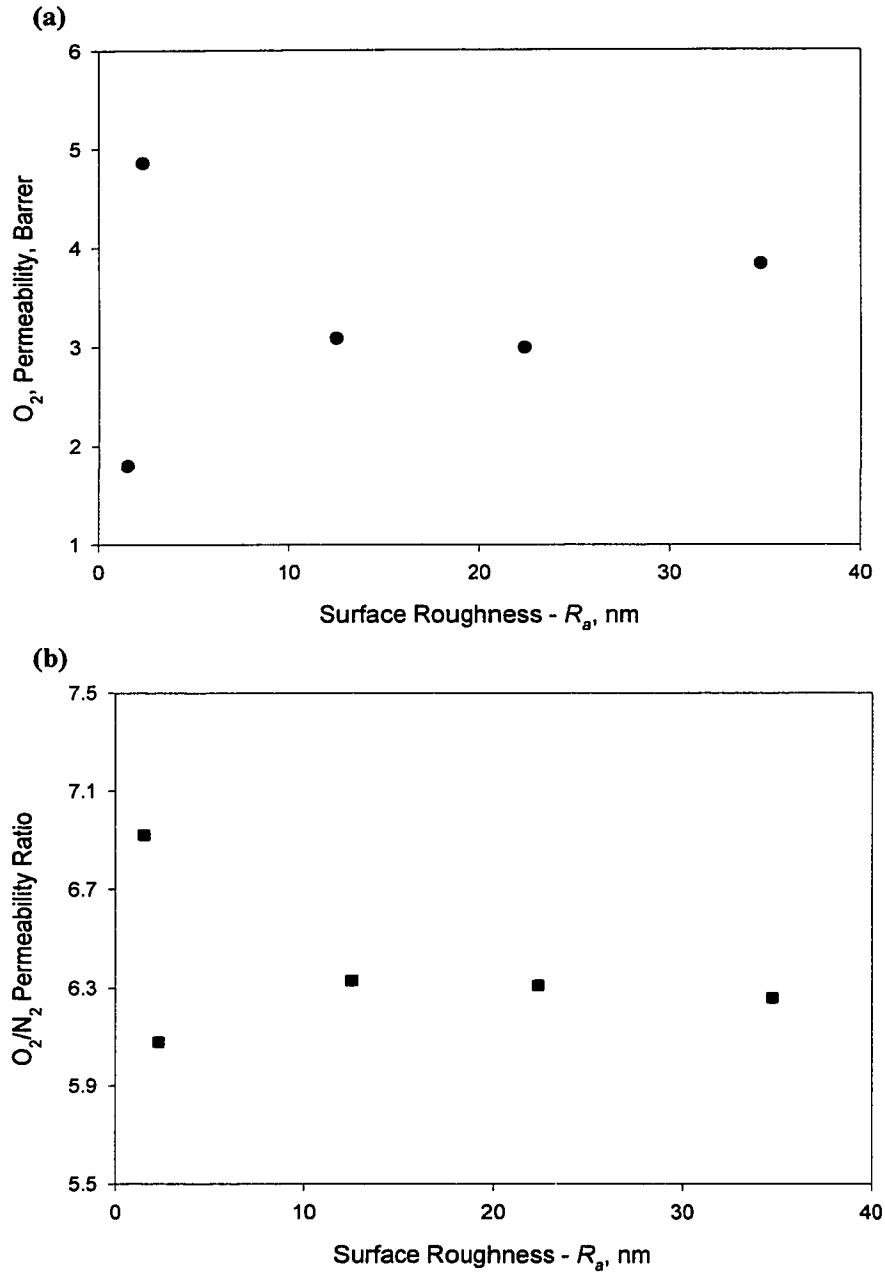

Figure 8.16 Effect of surface roughness on **(a)** O_2 permeability and **(b)** O_2/N_2 permeability ratio of dense high molecular weight HSPPO-1.37 membranes prepared using different casting solutions.

morphologies on the top and the bottom surfaces of the membranes. Nodules at the bottom surface were twice as large as the nodules on the top surface of the membrane [Khulbe *et al.*, 1996b]. The difference between the top and the bottom surfaces of a homogeneous membranes was also reported for a PPO membrane prepared from TCE solution [Khulbe *et al.*, 1996a] and for PPO membranes prepared from chloroform solution at different temperatures [Khulbe *et al.*, 1997]. These observations deny the isotropic structure of homogeneous membranes.

According to Kesting (1990), separation of gases by polymeric membranes occurs both in the nodule interior and in the interstitial regions between nodules. The former level of structure is beyond observation by current resolutions achievable under AFM. The latter level of structure; however, which depends on the size and distribution of nodules, can be observed under AFM. In fact, nodules of diameter ranging from 30 to 60 nm were observed on surface images of membranes prepared from NMP and pyridine (Figures 8-12 and 8-13). In case of other membranes, nodule resolutions were not achieved because of interference from large nodular aggregates, which was discussed in Section 8.3.

Considering that evaporation rate of solvent is faster at the top surface than in the membrane interior, it is possible that formation of nodular aggregates is enhanced on the top surface, especially in case of weak polymer-solvent interactions. Furthermore, agglomeration of nodules on the top surface is enhanced by the surface tension working at the casting solution-air interface [Kesting and Fritzsche, 1993]. In such a case, large roughness parameters due to the presence of nodular aggregates in the membrane surface would not indicate the actual porosity of the membrane interior.

8.4.2 Effect of solvent properties

Figure 8-17 presents the effect of solvent properties on O_2 permeability of HSPPO-1.37 membranes. The O_2 permeability represents gas transport properties of the membranes. The properties of solvents under consideration include solvent size expressed by the molar volume (Figure 8-17a), solvent volatility expressed by the vapor pressure at casting temperature (Figure 8-17b), and solvent strength expressed by the reciprocal of the relative viscosity of casting solution (Figure 8-17c). The properties of solvents along with the O_2 permeability data used for

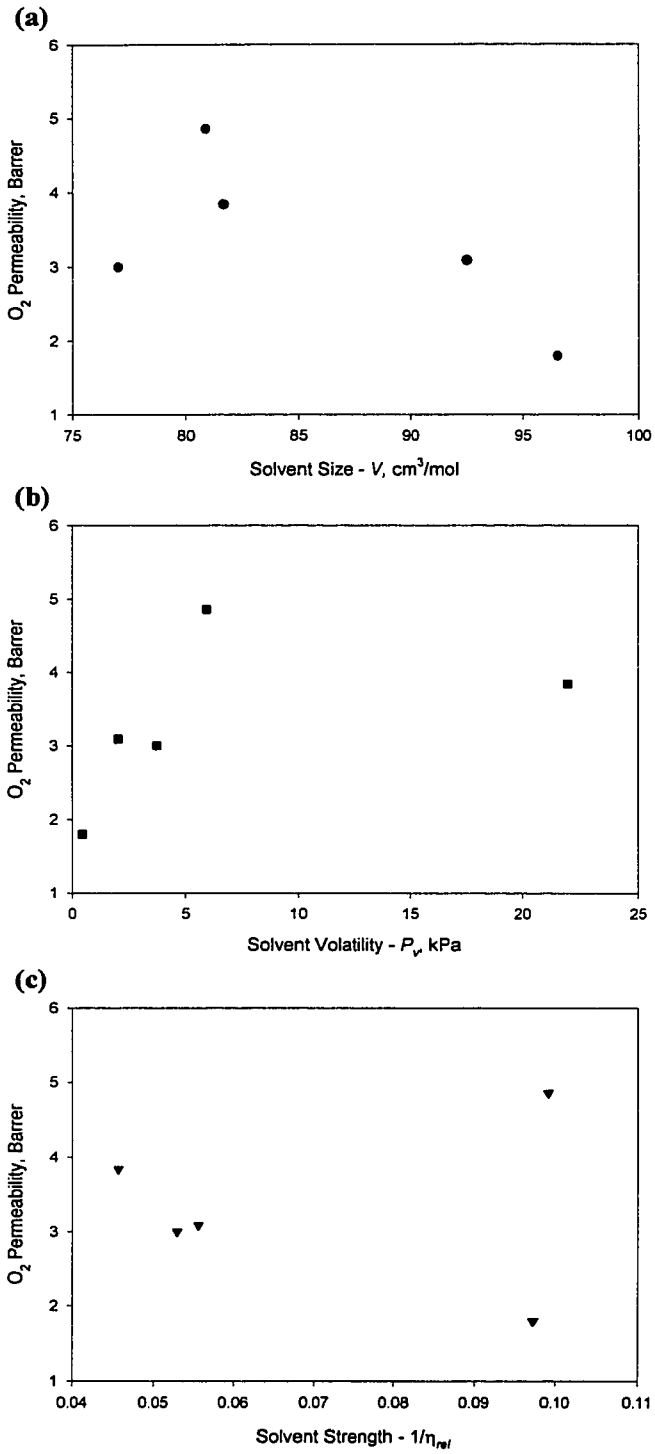

Figure 8-17. Effect of properties of solvent in casting solution on O_2 permeability of dense high molecular weight HSPPO-1.37 membranes; (a) effect of solvent size; (b) effect of solvent volatility; (c) effect of solvent strength.

construction of Figure 8-17 are shown in Table 8-10. The trends observed in Figure 8-17 are discussed in the following subsections.

8.4.2.1 Effect of solvent size

According to Figure 8-17a, O_2 permeability decreases with an increase in solvent molar size. This trend is exactly opposite to what was expected assuming that solvent molecules act as

Table 8-10. Effect of solvent properties on O_2 permeability of dense high molecular weight HSPPO-1.37 membranes.

Solvent	Solvent properties			$P(O_2)$ Barrer
	V, cm^3/mol	P_v, kPa	$1/\eta_{rel}$	
NMP	96.5	0.45	0.0973	1.80
DMAC	92.5	2.01	0.0556	3.09
DMF	77.0	3.71	0.0530	3.00
Pyridine	80.9	5.94	0.0991	4.86
THF	81.7	22.0	0.0457	3.84

transient templates in polymer solution [Kesting 1990]. As indicated in Section 8.3.3.1, the differences between molar volumes of solvents under consideration were; however, small. Moreover, an increase in membrane permeability with an increase in molar volume of solvent would be observed only above a certain value of molar volume. In case of asymmetric hollow fibers made from polysulfone, this critical molar volume was about 150 mL/mol [Kesting, 1990]. It is; therefore, not surprising that the anticipated effect of solvent size was not observed, considering the fact that all solvents used for dissolution of HSPPO-1.37 had molar volumes less than 100 mL/mol.

8.4.2.2 Effect of solvent volatility

The comparison of the NMP and pyridine membranes represents a good example for investigation of the effect of solvent volatility. The strength of NMP and pyridine in the solution with HSPPO-1.37 is comparable, as indicated by the similar intrinsic and relative viscosities (Table 8-10). The difference in gas transport properties of these membranes can; therefore, be

attributed to the difference in volatility of NMP and pyridine. The surface images of these two membranes are similar as shown in Figures 8-12 and 8-13, although the size of nodules and roughness parameters on the surface of the pyridine membranes are larger than those on the surface of the NMP membranes. On the other hand, NMP and pyridine membranes represent the two extreme cases of the gas transport properties; the pyridine membranes being the most permeable and the least selective, while the NMP membranes being the least permeable and the most selective (Table 8-8).

According to Khulbe et al. (1996a), an increase in solvent volatility results in preserving more of the polymer structure present in the polymer solution. Accordingly, the nodules produced from the solution in more volatile solvents should contain more free volume entrapped inside nodules, compared to those produced from less volatile solvents. Consequently, the greater the free volume the greater the membrane permeability. Hence, an increase in membrane permeability is anticipated as a result of an increase in solvent volatility.

Figure 8-17b shows the plot of vapor pressure of solvents versus O_2 permeability of HSPPO-1.37 membranes. It can be noticed that, in general, the anticipated trend between solvent volatility and membrane permeability is present in this figure. The membrane prepared from THF solution represents the outstanding point in Figure 8-17b. Even though THF has vapor pressure four times greater than pyridine, the THF membrane is less permeable than the pyridine membranes. Also, the differences between permeability of THF membrane and that of membranes prepared from DMAC and DMF are not very significant, despite a one-order of magnitude difference between vapor pressures of THF and the latter solvents. It should be emphasized; however, that gas transport properties of the THF membranes were calculated from the permeation data obtained from the membranes laminated with a silicone rubber film.

8.4.2.3 Effect of solvent strength

It was suggested in Section 8.3.3.3 that weak polymer-solvent interactions enhance aggregation of macromolecules in the casting solution. In turn, these aggregates will form the nodules, and possibly nodule aggregates, which can be observed on the surface of dry membranes. In a simplified view, polymeric membrane consists of nodules, nodule aggregates

and interstitial regions, which are the regions between nodules and between nodule aggregates. If the interstitial regions were free of matter, then the size of nodules and nodular aggregates would determine the size of pores available for gas permeation. In such a case, solvent strength which appears to influence the formation of nodules, nodular aggregates and their sizes, would be a parameter affecting directly the gas permeation properties of polymeric membranes prepared by complete evaporation of the solvent.

Nevertheless, the interstitial regions are not free of matter, but are the regions of lower polymer density than the interior of nodules. Consequently, gas permeates more readily through interstitial regions than through nodules. Hence, it is difficult to predict gas permeation properties of a membrane based only on the size of nodules or nodule aggregates, because the macromolecular packing densities in the interstitial regions vary from membrane to membrane.

Figure 8-17c shows that there is no clear correlation between O_2 permeability of HSPPO-1.37 membranes and solvent strength expressed by the reciprocal of the relative viscosity of casting solution. However, when the membrane prepared from pyridine solution is excluded, it appears that O_2 permeability decreases with an increase in the strength of solvent. As already stated, the strength of pyridine and NMP in the solution with HSPPO-1.37 is comparable, but the pyridine membrane is the most permeable while the NMP membranes is the least permeable among the membranes under consideration.

8.4.2.4 Combined effect of solvent strength and solvent volatility

A lack of clear correlation between solvent strength and permeability of membranes results from the influence of solvent volatility and the fact that large roughness parameters are not necessarily indicative of high permeabilities of dense membranes. On the contrary, the DMAC, DMF, and THF membranes, which show high surface roughness, are less permeable than the pyridine membrane, which has a relatively smooth surface.

One could argue, why the THF membranes are considered less permeable than the pyridine membranes. In fact, the non-laminated THF membranes showed more than two-orders of magnitude greater permeability for O_2 than the laminated membranes. But the former membranes showed practically no selectivity. A decrease in permeability associated with an

increase in permselectivity after lamination with silicone rubber indicates that high permeability of the non-laminated membranes was a result of some defects existing in the membrane structure rather than a generally open structure [Henis and Tripodi, 1981]. A question that arises is, why these defects occurred only in case of the membranes prepared from THF?

According to the characterization of solvents in terms of their strength and volatility, THF is the weakest and the most volatile among solvents used for preparation of the HSPPO-1.37 membranes. Because of weak polymer-solvent interactions, macromolecules tend to agglomerate already in the polymer solution. After casting, the agglomeration and growth of nodular aggregates is enhanced by a rapid evaporation of the solvent. It is expected that when the size of nodular aggregates increase, it is more difficult to fill the increasing gaps between the aggregates. This may consequently lead to incomplete coalescence of nodular aggregates and eventually to defects in the membrane structure.

Considering combined effect of solvent strength and solvent volatility as described above, the defects in the structure of the THF membranes can be explained. Furthermore, this mechanism can be applied for explanation of gas permeation performance of membranes prepared from other solvents. For example, the DMF membranes represent the case of membranes prepared from a solvent which is weak but not very volatile. Because of lower volatility of DMF compared with THF, the large nodular aggregates, which were formed because of the weak polymer-solvent interactions, had a chance to coalesce during evaporation of solvent. Consequently, these membranes did not show any defects in their structure.

8.5 Thermogravimetric Analysis

The discussion on the effect of solvent strength and solvent volatility on the gas transport properties of HSPPO-1.37 was based on the assumption that there is no residual solvent in the membrane. On the other hand, the residual solvent has a profound effect on gas transport properties of polymeric membranes as already discussed in Chapter 4. Thermogravimetric analysis (TGA) discussed so far pertained to the effect of *IEC* (Figure 6-3) and to the effect of metal cation (Figure 7-1). The membranes had shown in Figures. 6-3 and 7-1 were prepared

using DMAC. In this section, the TGA spectra of HSPPO-1.37 membranes prepared from different solvents are compared.

Figure 8-18 shows the TGA spectra of HSPPO-1.37 membranes prepared from THF, DMF and NMP, respectively. The spectra of membranes prepared from DMAC and pyridine are not shown in Figure 8-18 for clearer presentation of the figure. The spectrum of the HSPPO-1.37 membrane prepared from DMAC was already shown in Figure 6-3. The data pertaining to the spectra of all HSPPO-1.37 membranes are summarized in Table 8-11.

Figure 8-18 shows that there are three weight loss stages followed by the final decomposition of polymer, which is similar to the spectra of Figures 6-3 and 7-1. The major weight loss occurs in the second stage. The weight loss in this stage was attributed to the decomposition of sulfonic groups. This assumption is confirmed by the data shown in Figure 8-18, which indicates that the second weight loss stage occurs in a similar temperature interval, regardless of the solvent. The membranes in Figure 8.18 were prepared using solvents of different normal boiling points (T_{NBP}), that is the boiling points at the pressure of 101.3 kPa. For example, T_{NBP} of THF equals to 65°C while T_{NBP} of NMP equals to 202°C.

If the weight loss in the second stage were entirely due to decomposition of sulfonic groups, it should have been the same for all HSPPO-1.37 membranes regardless of the solvent. Nevertheless, it can be noticed from Table 8-11 that there is some difference in the weight loss in the second stage when the solvent is changed. The difference in the weight loss in the second stage could indicate different levels of residual solvent in membranes. The maximum weight loss of 11.8% occurred for the DMF membrane, while the minimum weight loss of 10.8% occurred for the THF membrane. Thus, if the weight loss in the second stage were any indication of the residual solvent content, it would have increased in the following order: THF < DMAC = NMP < pyridine < DMF.

As discussed in Chapter 4, when a residual solvent is present in small quantities, it acts as an antiplasticizer, that is, it occupies the Langmuir sorption sites, decreasing free volume and permeability of membrane [Kesting and Fritzsche, 1993]. Hence, the increasing order of the content of residual solvent should agree with the decreasing order in membrane permeability. Recalling permeability data presented in the previous section, it is clearly not the case. It can;

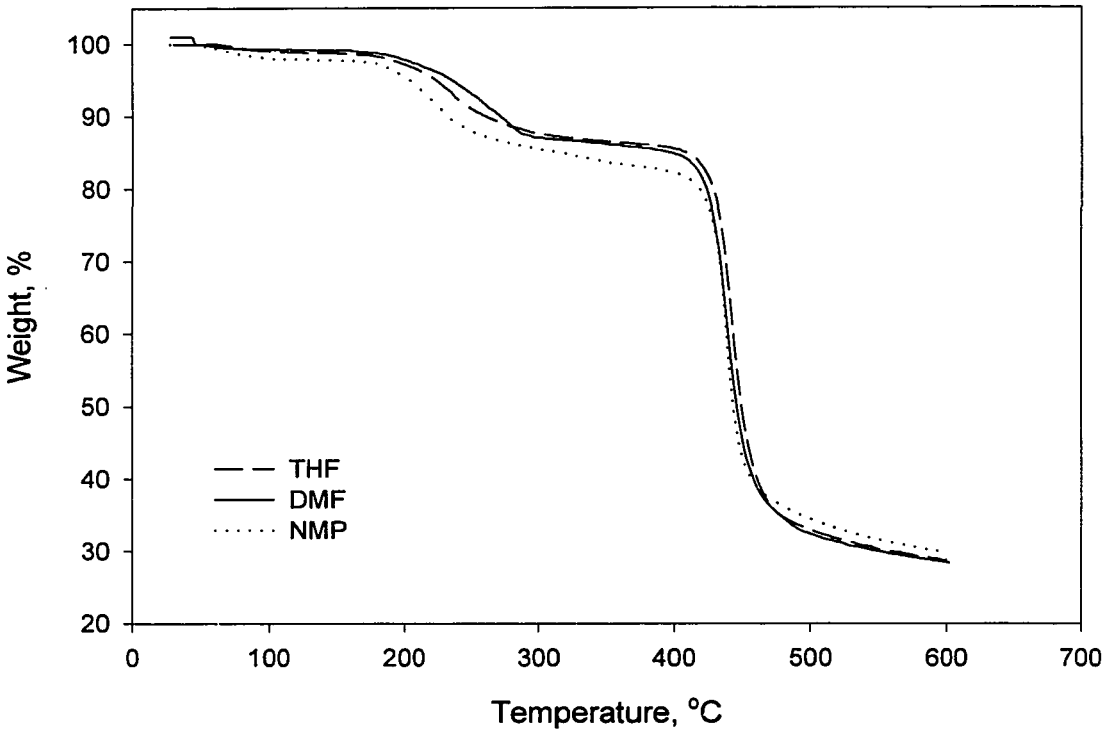

Figure 8.18 Thermal stability of dense high molecular weight HSPPO-1.37 membranes prepared from different casting solutions.

Table 8-11. Summary of TGA analysis of dense high molecular weight HSPPO-1.37 membranes prepared from different casting solutions.

Solvent	Stages of weight loss					
	First Stage		Second Stage		Third Stage	
	Range, °C	Loss, wt%	Range, °C	Loss, wt%	Range, °C	Loss, wt%
NMP	< 100	2.5	175 - 275	11.0	275 - 412	4.8
DMAC	< 100	2.0	175 - 297	11.0	297 - 409	3.0
DMF	< 100	1.0	175 - 295	11.8	295 - 407	2.9
Pyridine	< 100	1.5	175 - 285	11.5	285 - 415	4.0
THF	< 100	2.0	175 - 300	10.8	300 - 425	3.6

therefore, be concluded that the weight loss in the second stage has nothing to do with the amount of the residual solvent in the membrane.

Following the second stage, the weight of membranes continues to decrease. As discussed in Chapter 6, the weight loss following the second stage is attributed to the beginning of the final decomposition of polymer. It appears that the effect of residual solvent on the membrane gas transport can be neglected, either because it does not exit in the membrane after the drying procedure described in Chapter 5, or its quantity is too small to influence gas transport properties of the membrane.

8.6 Chapter Summary

Solutions of high molecular weight HSPPO-1.37 in organic solvents of a concentration 4.0 g/dL behave like concentrated polymer solutions, *i.e.*, an increase in the polymer-solvent interactions results in a decrease in the relative viscosity of the polymer solution. This relationship between polymer-solvent interactions and the relative viscosity of polymer solution indicates the existence of some form of macromolecular aggregates in the polymer solution. The tendency for macromolecules to aggregate in the polymer solution is enhanced by weak polymer-solvent and strong polymer-polymer interactions.

AFM analysis reveals the existence of nodules and nodule aggregates in the surface of dense polymeric membranes. Weak polymer-solvent interactions and high volatility of polymer

solution enhance aggregation of nodules into nodule aggregates. Formation of large nodule aggregates in turn increases the surface roughness. For a given polymer (HSPPO-1.37), the change of solvent from NMP (strong polymer-solvent interactions and low volatility) to THF (weak polymer solvent interactions and high volatility) results in more than two orders of magnitude increase in surface roughness.

For a given polymer (HSPPO-1.37), the change of solvent from NMP (strong polymer-solvent interactions and low volatility) to pyridine (strong polymer-solvent interactions and high volatility) results in a more than two-fold increase permeability and a 12% decrease in ideal selectivity of the membrane.

CHAPTER 9

Effect of Casting Temperature and Temperature of Casting Solution

It was concluded in Chapter 8 that changes in surface morphology and gas transport properties of dense high molecular weight HSPPO-1.37 membranes were due to a combined effects of polymer-solvent interactions and volatility of casting solution. It is difficult; however, to decouple these effects since the change of solvent in casting solution results in simultaneous changes in polymer-solvent interactions and volatility of casting solution.

The volatility of solution can also be changed by changing the temperature instead of the solvent. Hence two series of dense membranes were prepared in which solution temperature and the film casting temperature were controlled separately. In the first series, polymer solutions, which had been kept at room temperature, were cast in an oven at elevated temperatures. The second set of membranes was prepared from the same polymer solutions, but the temperature of polymer solution was the same as the casting temperature in the oven. Before discussing the effect of casting temperature of the temperature of casting solution, the properties of polymer solutions at different temperatures are examined.

9.1 Effect of Temperature on Properties of Polymer Solutions

An increase in temperature of polymer solution increases its volatility. The change in polymer-solvent interactions due to an increase in the temperature of polymer solution is, as indicated in Section 4.4.3 theoretically unpredictable.

9.1.1 Volatilities of pure solvents

Volatilities of polymer solutions can be approximated by volatilities of pure solvents. Table 9-1 presents vapor pressures of NMP and DMAC at different temperatures. The values for vapor pressures of solvents at elevated temperatures were obtained from the British Gas Database [Laverty, 1995]. It can be noticed that for both solvents a 20°C increase in temperature results in more than a two-fold increase in the vapor pressure. For any temperature, the vapor pressure of DMAC is greater than the vapor pressure of NMP. The ratio of the vapor pressure of DMAC to the vapor pressure of NMP decreases from 5.8 at 25°C to 3.6 at 100°C.

Table 9-1. Vapor pressures of pure DMAC and NMP at different temperatures.

Solvent	Vapor Pressure, kPa				
	25°C	40°C	60°C	80°C	100°C
DMAC	0.267	0.675	2.013	5.207	11.99
NMP	0.046	0.131	0.447	1.303	3.327

9.1.2 Relative viscosity

The relative viscosity of polymer solution approximates polymer-solvent interactions in the polymer solution. The relative viscosity, which is the ratio of absolute viscosities of polymer solution and solvent, was calculated by the ratio of kinematic viscosities of polymer solution and solvent. Similar densities of a 4.0 g/dL polymer solution and pure solvent at room temperature justify this simplification. The effect of temperature on the relative viscosity of polymer solution was evaluated using solutions of HSPPO-1.37 in NMP and DMAC, respectively. The concentration of polymer was 4.0 g/dL. In addition to the efflux times at 25°C, the readings were taken at 40, 60 and 80°C. The efflux times of solvents and solutions used for calculation of the relative viscosities were the average values from two independent series of measurements for each solvent and solution.

Figure 9-1 shows the effect of temperature on the relative viscosity of the solutions of HSPPO-1.37 in DMAC and NMP, respectively. The numerical values of kinematic and relative viscosities of DMAC and NMP as well as those of the corresponding polymer solutions can be

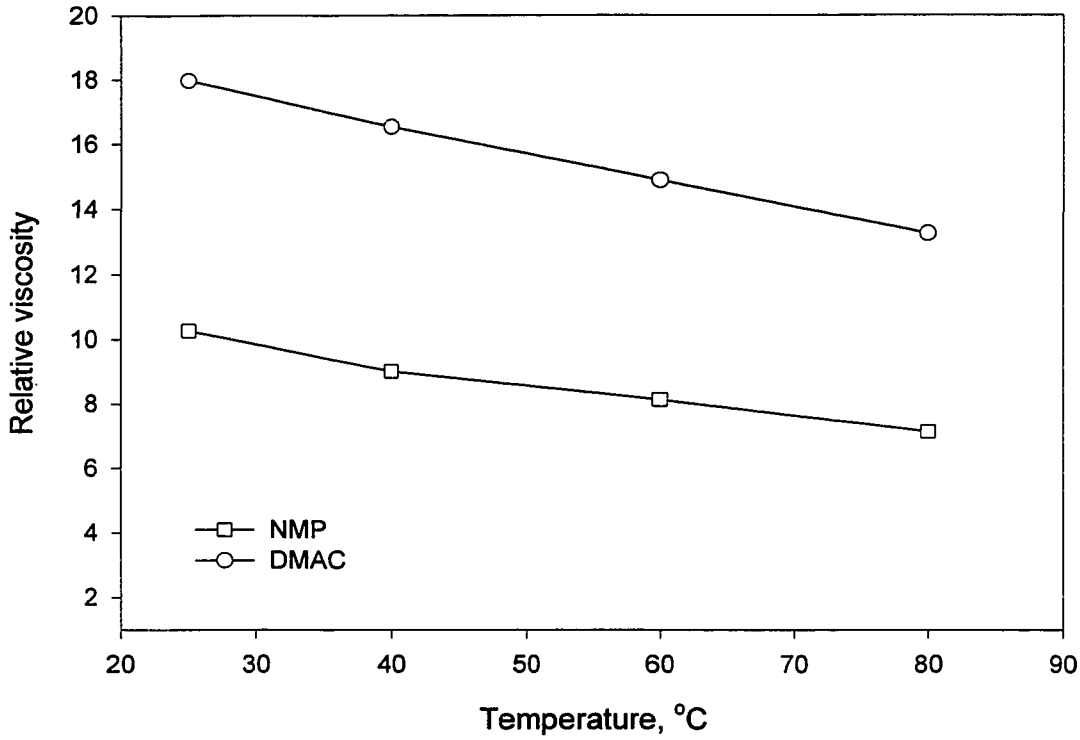

Figure 9-1. Effect of temperature on relative viscosity of high molecular weight HSPPO-1.37 solutions in DMAC and NMP. Concentration of polymer solutions, 4.0 g/dL.

found in Table 9-2. As the temperature of polymer solution increases the viscosities of both solvent and polymer solution decrease. The rate of decrease with temperature is; however, greater for the polymer solution than for the solvent. The net effect is; therefore, a decrease in the relative viscosity of polymer solution with an increase in temperature. Figure 9-1 shows that the decrease is linear for both DMAC and NMP solutions.

The decrease in the relative viscosity with an increase in temperature of polymer solution can be interpreted considering Kesting's notion that nodules, that is macromolecular aggregates, exist in all but very dilute polymer solutions. As the temperature of polymer solution increases, the kinetic energies of both polymer and solvent molecules increase. This must inevitably lead to the break-up of nodules, because the inter- and intra-molecular forces can no longer hold macromolecules together when kinetic energies are high. Moreover, solvent molecules having greater kinetic energies have better access to the macromolecules. Consequently, the viscosity of polymer solution decreases with temperature.

A decrease in the viscosity of liquids with an increase in temperature can be predicted theoretically (Bird *et al.*, 1960). The faster rate of decrease in the viscosity of polymer solution compared to the viscosity of solvent is probably due to the break-up of nodules. If the polymer solution consisted of uniformly distributed macromolecules, a decrease in the viscosity of such solution would be comparable to the decrease in the viscosity of solvent. A decrease in the relative viscosity of polymer solution with temperature indicates not only an increase in polymer-solvent interactions, but also provides indication of the existence of macromolecular aggregates in relatively dilute polymer solutions.

9.2.1.1 Effect of IEC of HSPPO

Figure 9-2 shows the effect of temperature on the relative viscosity of DMAC solutions of HSPPO-1.37 and HSPPO-1.80, respectively. The numerical values of the kinematic viscosities and the relative viscosities of these solutions are summarized in Table 9-2. It can be noticed in Figure 9-2 that relative viscosities of both solutions decrease linearly with temperature. Furthermore, the relative viscosity of HSPPO-1.80 is always lower than that of HSPPO-1.37. As the *IEC* of HSPPO increases, it is anticipated that the inter- and intra-molecular interactions

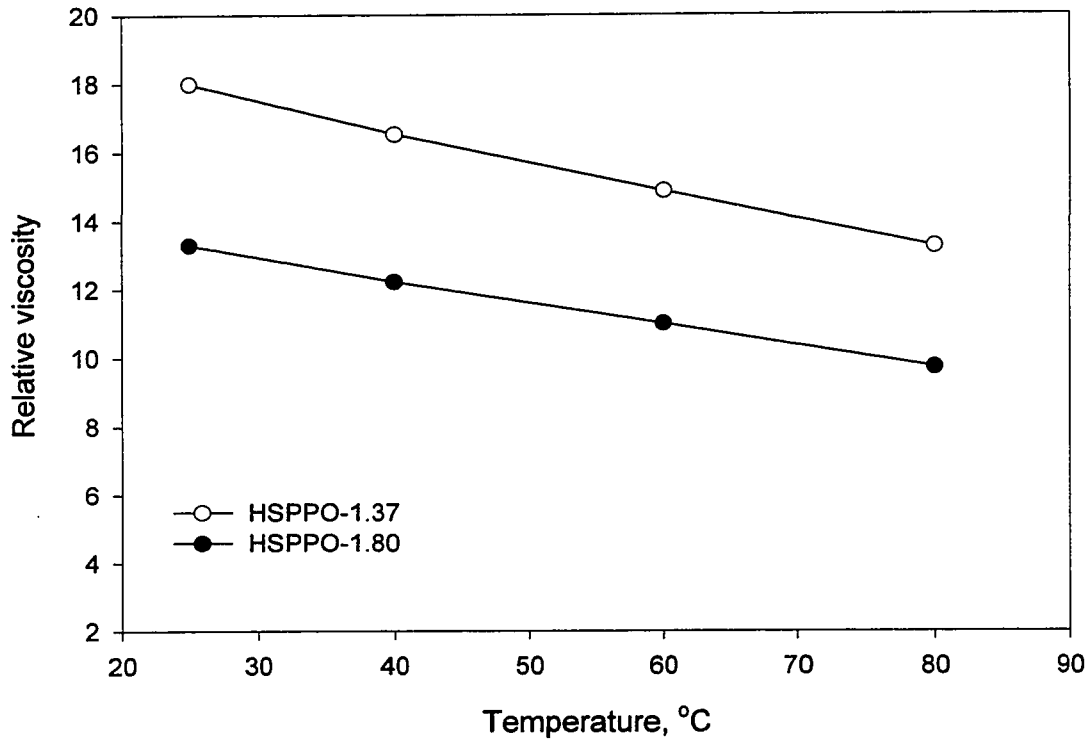

Figure 9-2. Effect of temperature on relative viscosity of DMAC solutions of high molecular weight HSPPO-1.37 and HSPPO-1.80. Concentration of polymer solutions, 4.0 g/dL.

between polymeric chains would increase as a result of an increased number of sulfonic groups in the polymer backbone. Sulfonic groups are also interacting with DMAC molecules. Since the relative viscosity of HSPPO solution in DMAC decreases with an increase in the *IEC* value of the polymer (polymer-solvent interactions increase), the interactions between sulfonic groups and DMAC molecules must overbalance those between sulfonic groups on the same and neighboring chains.

The observed increase in the HSPPO-DMAC interactions with an increase in the *IEC* of the polymer is consistent with the results of solubility tests of HSPPO summarized in Table 7-1. According to these results, DMAC was a poor solvent for HSPPO-1.37 because the polymer was not sufficiently polar for this solvent. An increase in *IEC* from 1.37 to 1.80 meq/g increases the polarity of HSPPO.

9.2.1.2 Effect of sodium cation

Figure 9-3 shows the effects of temperature on the relative viscosities of DMAC solutions of NaSPPO-1.37 and NaSPPO-1.80 along with those for the DMAC solutions of HSPPO-1.37 and HSPPO-1.80. The comparison of relative viscosities of the DMAC solutions of HSPPO and NaSPPO of the same *IEC* value allows for the evaluation of the effect of substitution of the proton in sulfonic groups by sodium cation on the relative viscosity and hence on the polymer-solvent interactions. The numerical values of the kinematic viscosities and the relative viscosities for the DMAC solutions of NaSPPO-1.37 and NaSPPO-1.80 are found in Table 9-2.

It can be noticed in Figure 9-3 that the relative viscosities of polymer solutions decrease considerably after substitution of the proton in sulfonic groups with sodium cations. The effect of such substitution appears to be more significant for the polymer of the higher *IEC* value. HSPPO-1.37 has sulfonic groups on approximately every fifth repeat unit while HSPPO-1.80 has sulfonic groups on approximately every fourth unit. Consequently, more sodium cations are introduced to the polymer of the higher *IEC* value, which explains the greater change in the relative viscosity of the corresponding polymer solution.

The results of solubility tests of HSPPO and NaSPPO in THF and DMAC presented in Table 7-1 indicate that substitution of the proton in sulfonic groups by sodium cations increases

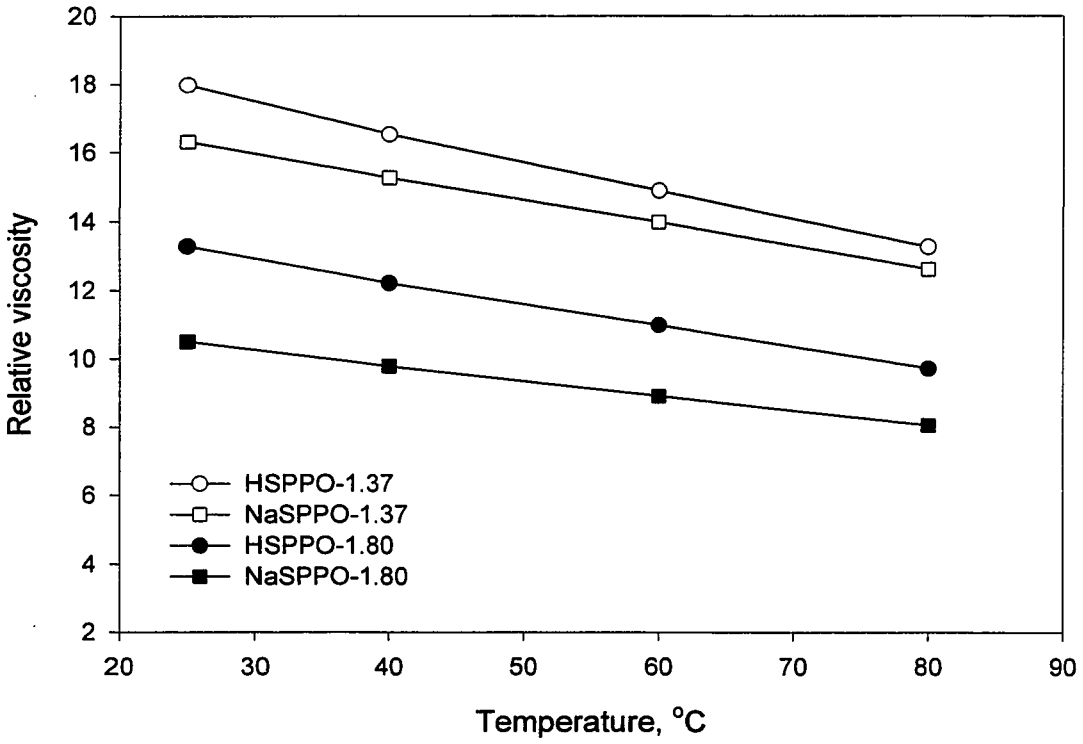

Figure 9-3. Effect of temperature on relative viscosity of DMAC solutions of high molecular weight HSPPO and NaSPPO. Concentration of polymer solutions, 4.0 g/dL.

polarity of the polymer. An effect on the relative viscosity similar to that of an increase in *IEC* is thus expected. The results shown in Fig. 9-3 confirm this anticipated effect.

Table 9-2. Effect of temperature on kinematic and relative viscosities SPPO solutions in NMP and DMAC[a].

Solvent	Polymer		Viscosity			
			25°C	40°C	60°C	80°C
DMAC	HSPPO-1.37	ν, cSt	17.03	13.11	9.67	7.26
		η_{rel}	17.98	16.53	14.88	13.26
NMP	HSPPO-1.37	ν, cSt	15.84	11.15	8.30	5.66
		η_{rel}	10.27	9.01	8.14	7.13
DMAC	HSPPO-1.80	ν, cSt	12.59	9.69	7.14	5.32
		η_{rel}	13.29	12.22	10.99	9.72
DMAC	NaSPPO-1.37	ν, cSt	15.45	12.10	9.09	6.41
		η_{rel}	16.31	15.26	13.98	12.62
DMAC	NaSPPO-1.80	ν, cSt	9.95	7.76	5.79	4.41
		η_{rel}	10.51	9.79	8.91	8.05
DMAC	-	ν, cSt	0.947	0.793	0.650	0.548
NMP	-	ν, cSt	1.542	1.238	1.019	0.794

[a] All polymer solutions of concentration equal to 4.0g/dL

It should be noted that the discussion presented in this and in the previous section is restricted to the polymer solutions in DMAC and cannot be generalized to other solvents. But the above discussion is believed to offer a further justification for the use of the relative viscosity approach to express the strength of polymer-solvent interactions in polymer solutions.

9.2 Effect of Casting Temperature on Film Properties

The effect of casting temperature was studied using dense high molecular weight HSPPO-1.80 and NaSPPO-1.80 films. The films were prepared from polymer solutions in DMAC of a concentration equal to 4.0 g/dL. Prior to casting, the polymer solutions were kept at room temperature. The membranes were cast in a forced air convection oven. For each polymer

solution four casting temperatures were examined. The HSPPO-1.80 membranes were cast at 60, 80, 100, and 120°C, while the NaSPPO-1.80 membranes were cast at 40, 60, 80, and 100°C.

9.2.1 TM AFM observations in large scan size

Figures 9-4 – 9-9 show the TM AFM images in the large scan size (scanning area equal to 12 x 12 μm) of HSPPO-1.80 and NaSPPO-1.80 membranes cast at different casting temperatures from polymer solutions at ambient temperature. Table 9-3 summarizes the surface analysis of the membranes. The surfaces were characterized in terms of two roughness parameters, R_a and R_q. The roughness parameters were defined in Chapter 5. In addition to the roughness parameters, the dimensions of grains in the X-Y plane were measured and the average value is reported as a diameter of nodule aggregate (d_N). The data shown in Table 9-3 represent

Table 9-3. Summary of image analysis in a 12 x 12 μm scan area by TM AFM of dense high molecular weight SPPO-1.80 membranes prepared at different casting temperatures [a].

Cation	Casting Temp., °C	n		R_a, nm	R_q, nm	d_N, nm
H	60	3	Avg.	0.92	1.19	-
			St.Dev.	0.15	0.14	-
H	80	4	Avg.	10.8	17.6	334
			St.Dev.	2.5	2.1	132
H	100	4	Avg.	25.4	38.5	555
			St.Dev.	3.7	4.6	77
H	120	3	Avg.	22.1	40.3	769
			St.Dev.	5.0	7.2	48
Na	40	3	Avg.	2.57	3.32	735
			St.Dev.	0.43	0.64	172
Na	60	4	Avg.	1.64	2.29	828
			St.Dev.	0.41	0.49	166
Na	80	4	Avg.	4.38	6.19	1022
			St.Dev.	0.40	0.56	262
Na	100	3	Avg.	4.68	6.53	1213
			St.Dev.	0.92	1.04	225

[a] Casting solution temperature, ambient

the average and standard deviation values from at least three images of the same type. The number of images (n) examined for a given type of surface is provided in column 3 within the Table 9-3. All the images were obtained using the same TM AFM scanning probe.

The changes in surface morphology of HSPPO-1.80 membranes as the casting temperature increases from 60 to 120°C are illustrated on Figures 9-4 – 9-7. The membrane cast at 60°C (Figure 9-4) is flat and uniform. There are no grains on the surface. As the casting temperature increases to 80°C, there is a dramatic change in the surface morphology of the membrane. It can be noticed in Figure 9-5 that there are a number of small grains that are uniformly distributed on the surface. Apart from grains of diameter ranging between 300 and 400 nm, which represent nodule aggregates, there are smaller grains of diameter less than 100 nm. The smaller grains are considered to be nodules. When the casting temperature increases to 100°C, the average diameter of nodule aggregates increases to 555 nm (Figure 9-6). The smaller grains, which were visible on the image in Figure 9-5, disappear. It seems that the smaller grains were incorporated into large nodule aggregates. A further increase in casting temperature results in a further increase in the size of the nodule aggregates. The average diameter of nodule aggregates in Figure 9-7 is 769 nm. While the size of nodule aggregates increases, their number on the surface decreases. This is illustrated by the comparison of the images in Figures 9-6 and 9-7. Despite the increase in the average diameter of nodule aggregates from 555 to 769 nm, the value of R_a decreases from 25.4 to 22.1 nm. At the same time, the value of R_q increases from 38.5 to 40.3 nm. This indicates an increasing irregularity of the membrane surface with an increase in casting temperature.

Figures 9-8 and 9-9 show the surface images in the large scan size observed by TM AFM of NaSPPO-1.80 membranes cast at 60°C and 80°C, respectively. In comparison to the images of HSPPO-1.80 membranes cast at the same temperatures (Figures. 9-4 and 9-5), the images of NaSPPO-1.80 membranes are considerably different. The change in the surface morphology resulting from an increase in casting temperature is also less significant for NaSPPO-1.80 membranes. Figure 9-8, which presents the surface image of the NaSPPO-1.80 membrane prepared at 60°C, reveals that there are several grains in the surface of this membrane. The grains, which represent nodular aggregates, are rather flat but they have large dimensions in the

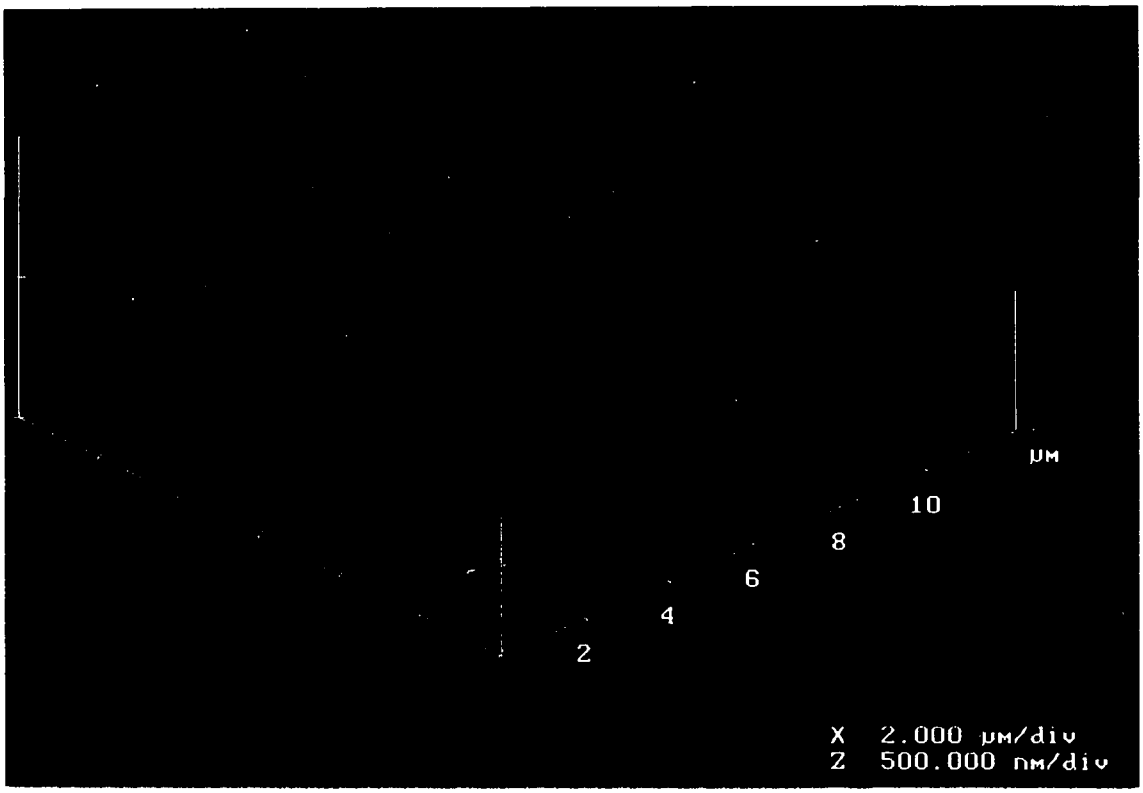

Figure 9-4. Surface image in 12 x 12 µm scan size by atomic force microscope in tapping mode of dense high molecular weight HSPPO-1.80 membrane cast at 60°C from DMAC solution. Casting solution at room temperature.

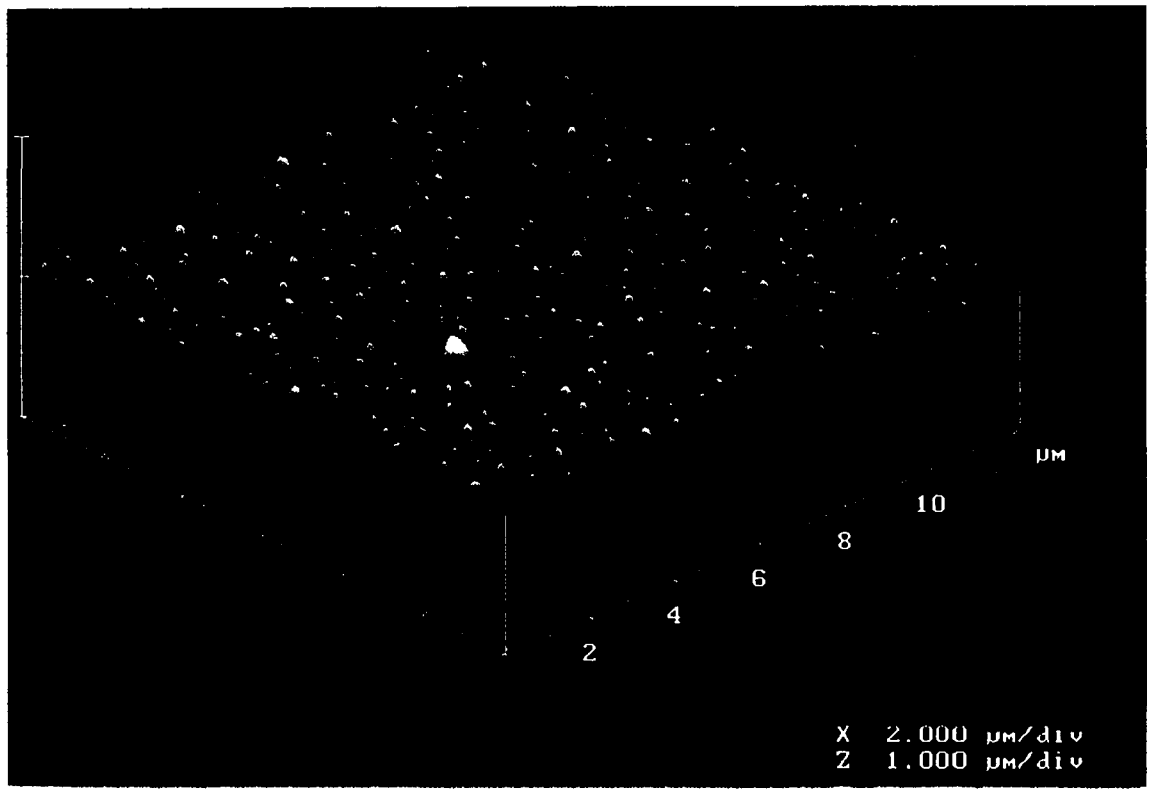

Figure 9-5. Surface image in 12 x 12 μm scan size by atomic force microscope in tapping mode of dense high molecular weight HSPPO-1.80 membrane cast at 80°C from DMAC solution. Casting solution at room temperature.

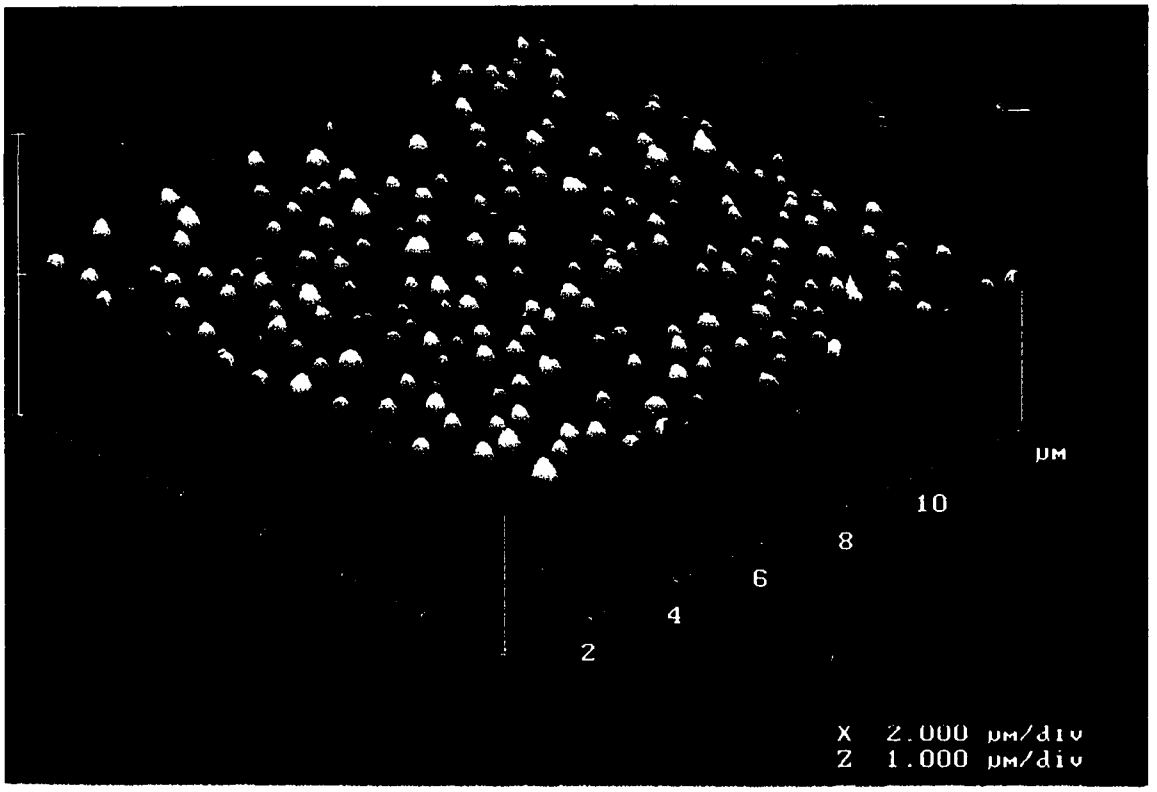

Figure 9-6. Surface image in 12 x 12 µm scan size by atomic force microscope in tapping mode of dense high molecular weight HSPPO-1.80 membrane cast at 100°C from DMAC solution. Casting solution at room temperature.

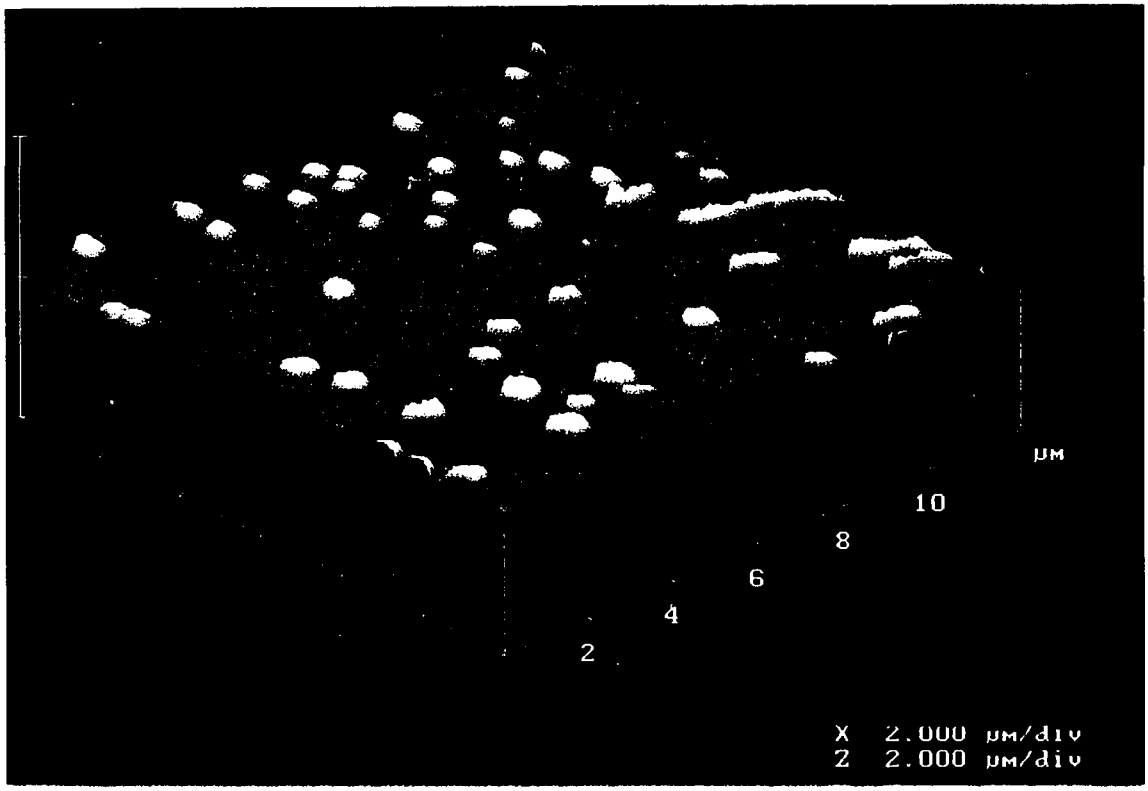

Figure 9-7. Surface image in 12 x 12 µm scan size by atomic force microscope in tapping mode of dense high molecular weight HSPPO-1.80 membrane cast at 120°C from DMAC solution. Casting solution at room temperature.

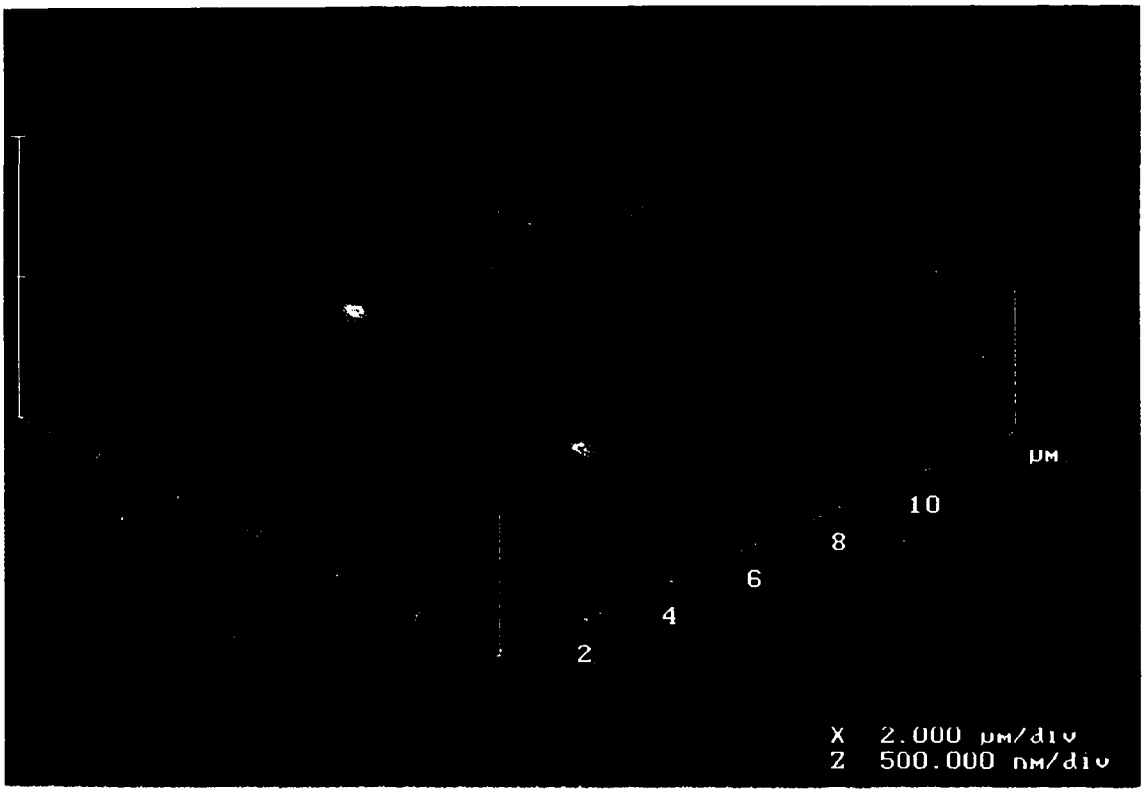

Figure 9-8. Surface image in 12 x 12 µm scan size by atomic force microscope in tapping mode of dense high molecular weight NaSPPO-1.80 membrane cast at 60°C from DMAC solution. Casting solution at room temperature.

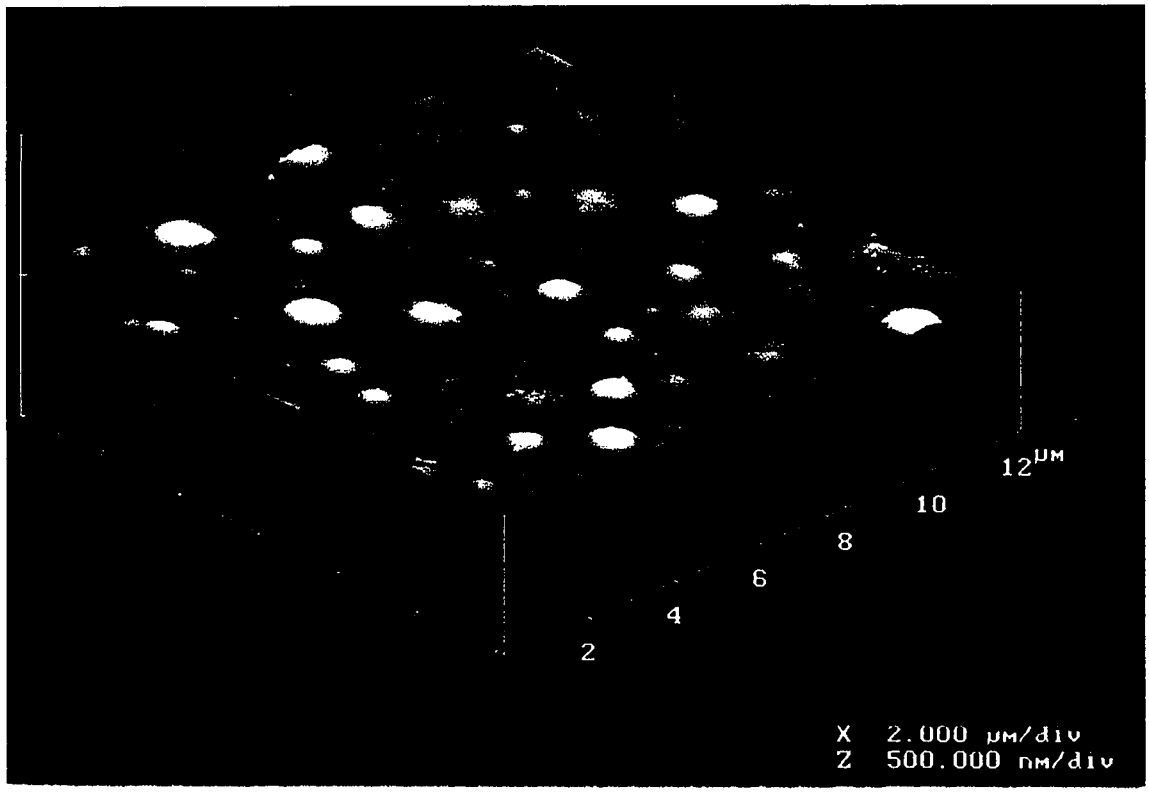

Figure 9-9. Surface image in 12 x 12 μm scan size by atomic force microscope in tapping mode of dense high molecular weight NaSPPO-1.80 membrane cast at 80°C from DMAC solution. Casting solution at room temperature.

X-Y plane. The average diameter of nodule aggregates in Figure 9-8 of 828 nm is greater than the diameter of the largest nodule aggregates found on the surface of HSPPO-1.80 membranes (membranes cast at 120°C). At the same time, R_a of NaSPPO-1.80 cast at 60°C (1.64 nm) is one order of magnitude lower than R_a of HSPPO-1.80 cast at 120°C (22.1 nm). The nodule aggregates in Figure 9-8 appear to grow to the periphery of the circular depressions that exist in the membrane surface. As the casting temperature increases, the number of nodule aggregates and their diameters increase (Figure 9-9). Consequently, the depressions disappear. The images of NaSPPO-1.80 cast at 40 and 80°C are not shown. These images were similar to those presented in Figures. 9-8 and 9-9 as indicated by similar roughness parameters of all NaSPPO-1.80 membranes regardless of the casting temperature.

Figure 9-10 summarizes the effect of casting temperature on surface morphology of HSPPO-1.80 and NaSPPO-1.80 membranes. It is evident that for both HSPPO-1.80 and NaSPPO-1.80 agglomeration of nodules into nodule aggregates is enhanced by an increase in casting temperature. This is indicated by a linear increase in the average diameter of nodule aggregate in Figure 9-10a. While the nodule aggregates in HSPPO-1.80 grow both horizontally and vertically, the nodule aggregates in NaSPPO-1.80 grow only horizontally (increase in diameter). Consequently, a significant increase in the surface roughness associated with the growth of nodular aggregates in HSPPO-1.80 is not observed for NaSPPO-1.80 (Figure 9-10b).

The observed effect of casting temperature on the surface roughness and the average diameter of nodule aggregates of HSPPO-1.80 membranes indicates the importance of solvent volatility as a parameter governing surface morphology of the membranes prepared by complete evaporation of solvent. On the other hand, despite an increase in the average diameter of nodule aggregates, the surface roughness of NaSPPO-1.80 membranes does not change significantly as the casting temperature increases from 40 to 100°C.

The lack of significant changes in surface roughness of NaSPPO-1.80 membranes despite a more than one order of magnitude difference in the vapor pressure of DMAC at 40°C and 100°C can be related to the polymer-solvent interactions between NaSPPO-1.80 and DMAC. Figure 9-3 shows that at any temperature the relative viscosity of NaSPPO-1.80 in DMAC was lower than the relative viscosity of HSPPO-1.80 in that solvent. This indicates stronger polymer

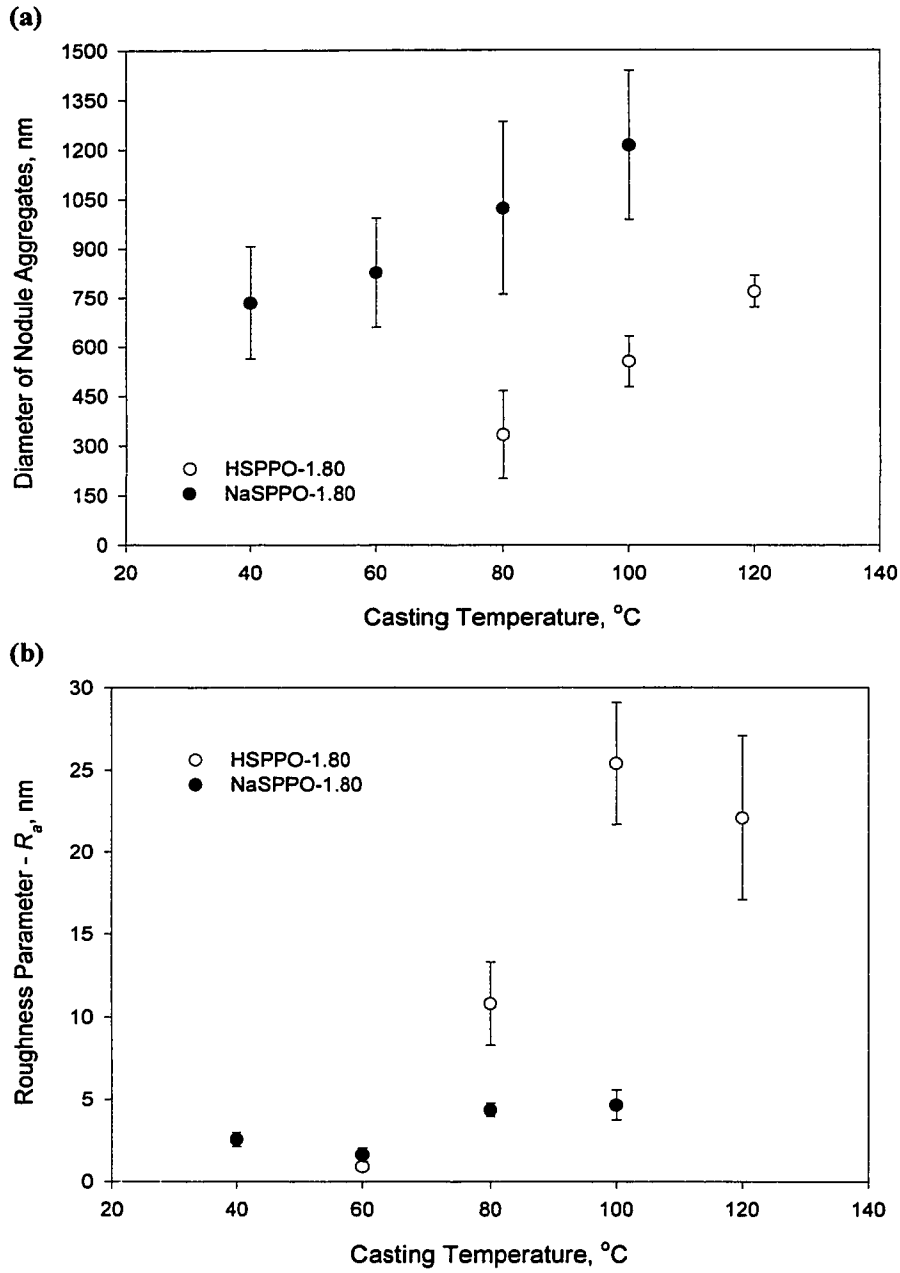

Figure 9-10. Effect of casting temperature on **(a)** average diameter of nodule aggregates and **(b)** surface roughness of dense high molecular weight HSPPO-1.80 and NaSPPO-1.80 membranes observed by atomic force microscope in tapping mode in the large scan size. Casting solutions at room temperature.

solvent interactions in the former solution. Recalling HSPPO-1.37 membranes prepared from NMP and pyridine solutions, respectively; they had similar surface roughness despite a more than one order of magnitude difference in the vapor pressures of NMP and pyridine. At the same time, the relative viscosities of both solutions were low and similar to the relative viscosity of NaSPPO-1.80 in DMAC at room temperature. It appears that strong polymer-solvent interactions can diminish the influence of solvent volatility on surface morphology when the scan size of the TM AFM image is as large as 12 x 12 μm.

9.2.2 TM AFM observations in small scan size

It is interesting to note that nodule aggregates in HSPPO-1.80 and NaSPPO-1.80 membranes appear on a broad background of a uniform and flat surface. This allowed to obtain high-resolution images in a small scan size (scanning area equal to 0.65 x 0.65 μm) by zooming into "smooth" sections of the larger images.

Figures 9-11 and 9-12 present the surface images in the small scan size of HSPPO-1.80 membranes cast at 60°C and 100°C, respectively, from polymer solution at ambient temperature. The images reveal a very uniform, granular structure of both surfaces with the diameter of grains ranging from 20 to 45 nm. Referring to four tiers of structure in polymeric membranes proposed by Kesting (1990), these grains represent the nodules. It can be noticed that the nodules in Figure 9-11 are larger than the nodules in Figure 9-12. This indicates that for HSPPO-1.80 membranes the size of the nodules decreases with an increase in casting temperature.

Figures 9-13 and 9-14 present the surface images in the small scan size of NaSPPO-1.80 membranes cast at 60°C and 100°C, respectively, from polymer solutions at ambient temperature. Similar to HSPPO-1.80, the surface of NaSPPO-1.80 membranes has a nodular structure. The size of nodules also decreases with an increase in casting temperature. For a given casting temperature, the nodules on the surface of NaSPPO-1.80 membranes appear to be slightly larger than the nodules on the surface of HSPPO-1.80 membranes.

Table 9-4 summarizes the surface analysis in the small scan size of HSPPO-1.80 and NaSPPO-1.80 membranes. For each type of surface at least three images were obtained and

Table 9-4. Summary of image analysis in a 0.65 x 0.65 μm scan area by TM AFM of dense high molecular weight SPPO-1.80 membranes prepared at different casting temperatures[a].

Cation	Casting. Temp,°C	n		R_a, nm	R_q, nm	d_n, nm
H	60	3	Avg.	0.25	0.32	38.1
			St.Dev.	0.04	0.05	6.6
H	80	3	Avg.	3.83	5.48	67.7
			St.Dev.	0.67	1.45	11.1
H	100	4	Avg.	0.24	0.31	33.2
			St.Dev.	0.05	0.03	5.7
H	120	4	Avg.	0.21	0.26	31.3
			St.Dev.	0.04	0.02	4.6
Na	40	3	Avg.	0.28	0.37	40.2
			St.Dev.	0.06	0.06	1.7
Na	60	3	Avg.	0.27	0.34	38.6
			St.Dev.	0.04	0.05	5.9
Na	80	3	Avg.	0.59	0.78	33.1
			St.Dev.	0.13	0.16	7.3
Na	100	3	Avg.	0.43	0.58	33.9
			St.Dev.	0.07	0.10	8.5

[a] Casting solution temperature, ambient

analyzed. The surfaces were characterized in terms of two roughness parameters, R_a and R_q, and the average diameter of nodules (d_n).

The analysis of surface images confirms that except for the membranes cast at 80°C, the average diameter of nodules in NaSPPO-1.80 is larger than the average diameter of nodules in HSPPO-1.80. The differences; however, are very small. Also, except for the membrane cast at 80°C, the roughness parameters are larger for NaSPPO-1.80 than for HSPPO-1.80 membranes. The exceptionally high roughness parameter of the HSPPO-1.80 membrane prepared at 80°C in the small scan size is a result of the existence of intermediately sized grains. These grains, which can be considered as large nodules or small nodule aggregates, were visible in the large scan size image of the surface of HSPPO-1.80 membrane (Figure 9-5). They were not observed on any other surface. The average diameter of nodule observed in the other images ranged between 30 and 40 nm.

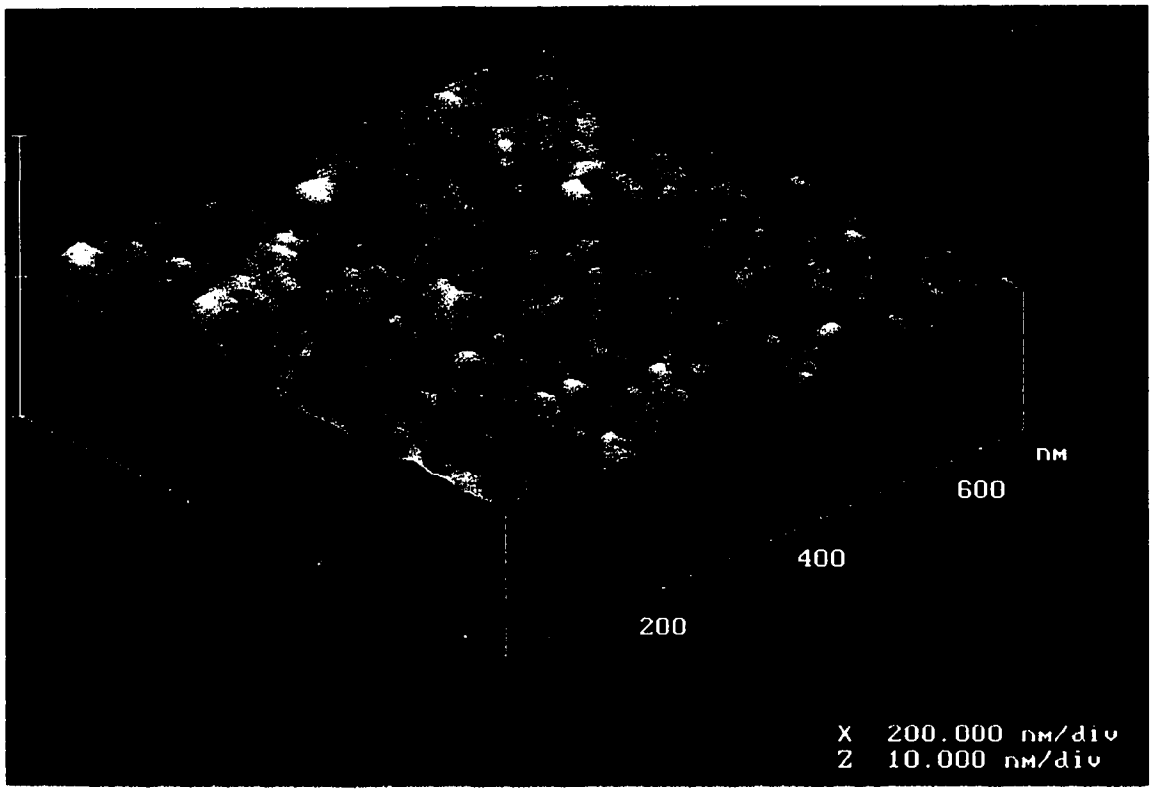

Figure 9-11. Surface image in 0.65 x 0.65 μm scan size by atomic force microscope in tapping mode of dense high molecular weight HSPPO-1.80 membrane cast at 60°C from DMAC solution. Casting solution at room temperature.

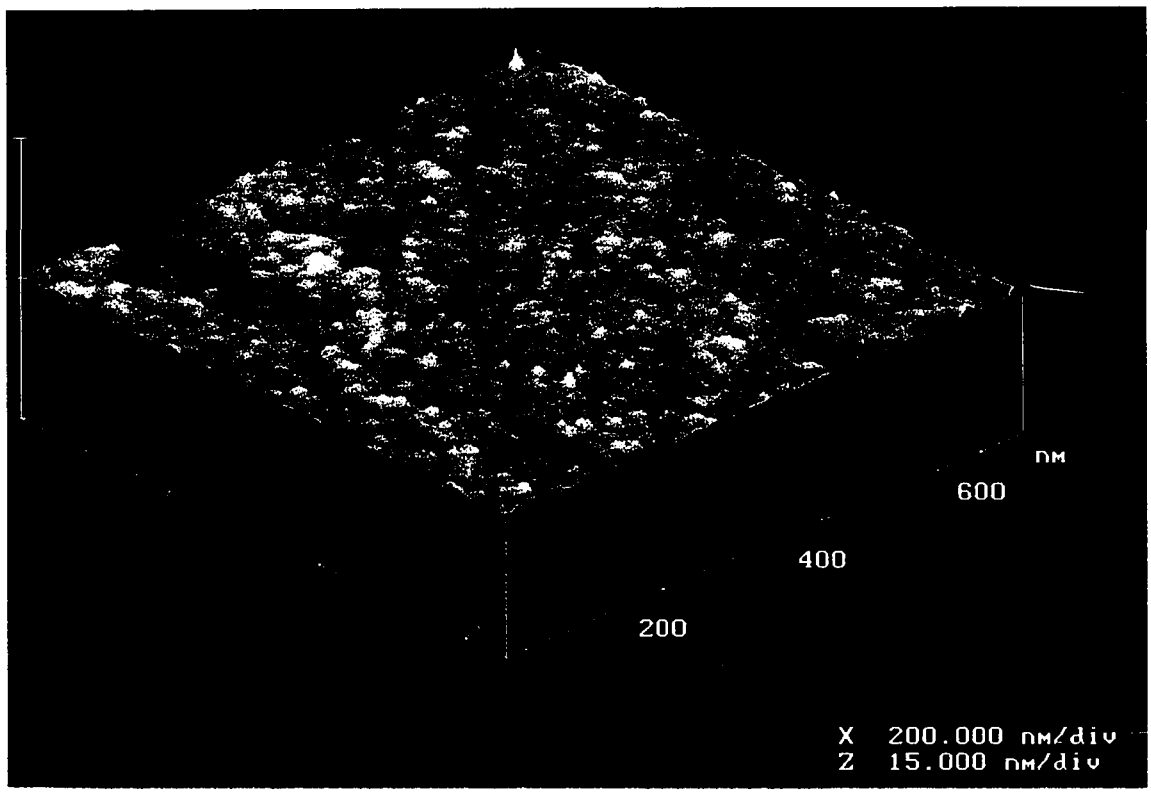

Figure 9-12. Surface image in 0.65 x 0.65 μm scan size by atomic force microscope in tapping mode of dense high molecular weight HSPPO-1.80 membrane cast at 100°C from DMAC solution. Casting solution at room temperature.

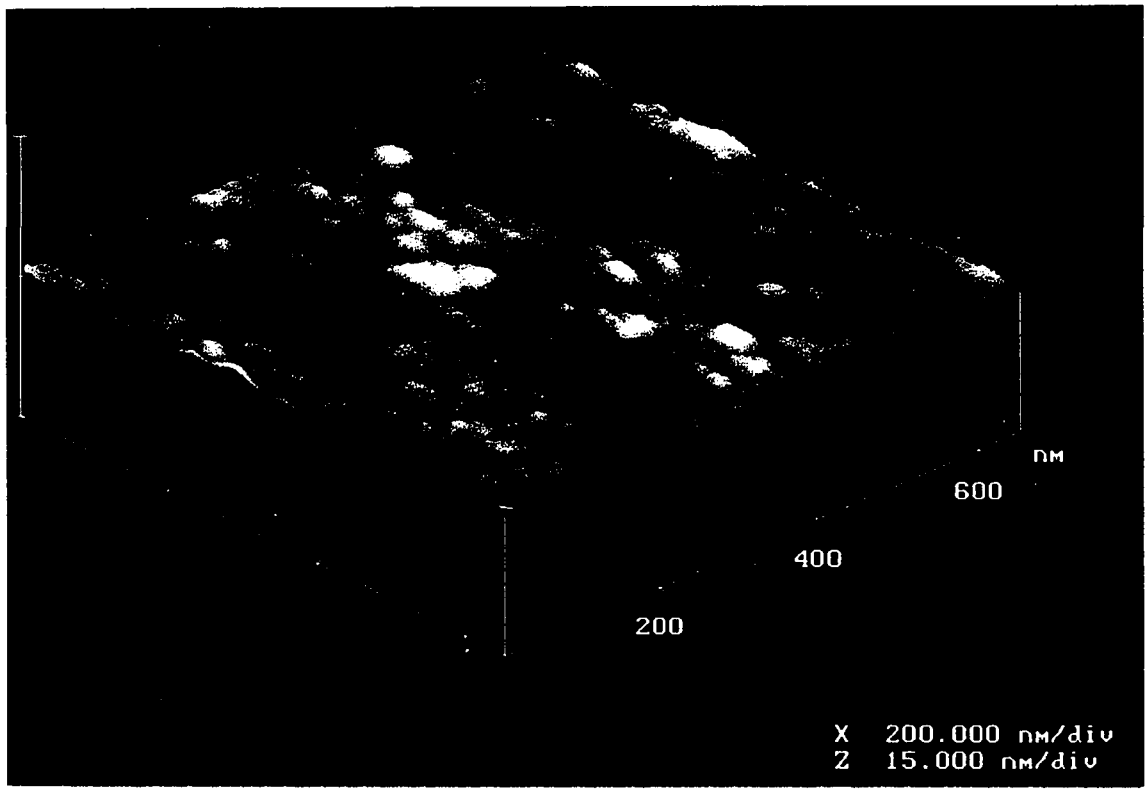

Figure 9-13. Surface image in 0.65 x 0.65 μm scan size by atomic force microscope in tapping mode of dense high molecular weight NaSPPO-1.80 membrane cast at 60°C from DMAC solution. Casting solution at room temperature.

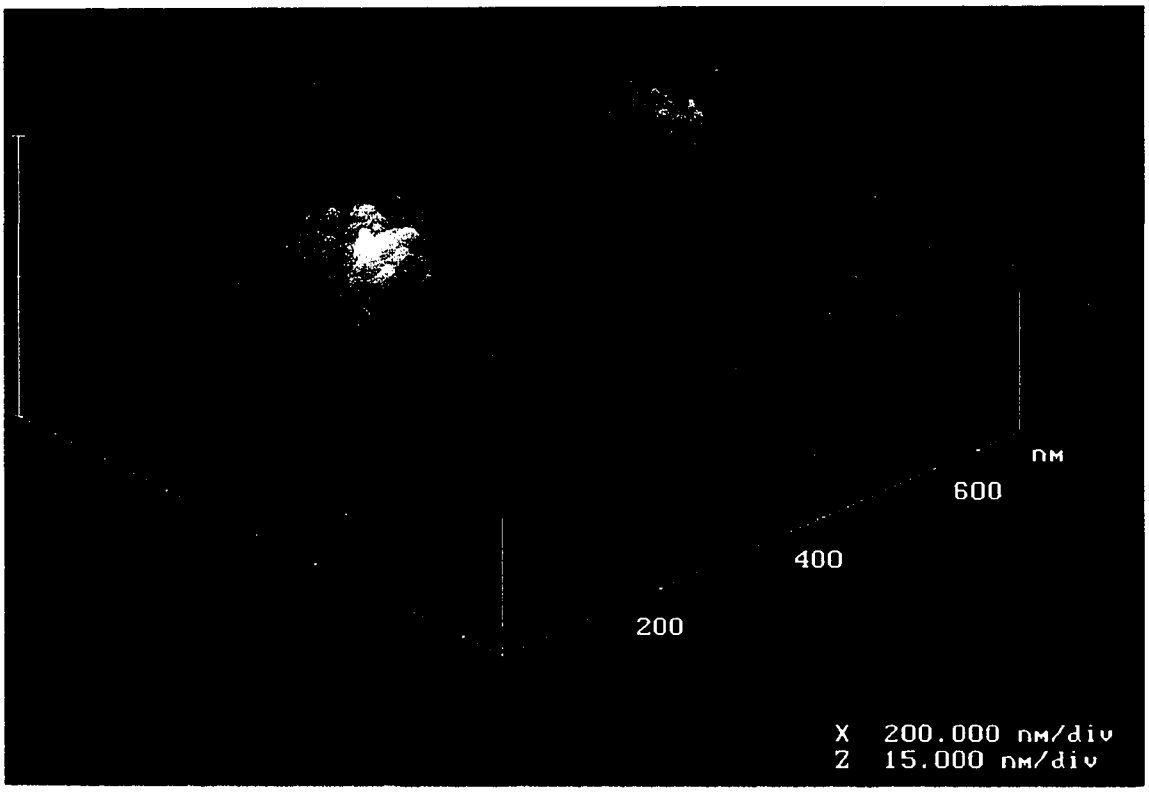

Figure 9-14. Surface image in 0.65 x 0.65 μm scan size by atomic force microscope in tapping mode of dense high molecular weight NaSPPO-1.80 membrane cast at 100°C from DMAC solution. Casting solution at room temperature.

Figure 9-15 summarizes graphically the effect of casting temperature on surface morphology of HSPPO-1.80 and NaSPPO-1.80 membranes based on a small scan. It can be noticed that in general the average diameter of nodules in both HSPPO-1.80 and NaSPPO-1.80 membranes decreases with an increase in casting temperature (Figure 9-15a). On the other hand, surface roughness increases slightly with an increase in casting temperature (Figure 9-15b). The data for HSPPO-1.80 cast at 80°C is an exception. The effect of casting temperature on the average diameter of nodules (Figure 9-15a) is exactly opposite to the effect of casting temperature on the average diameter of nodule aggregates shown in Fig 9-10a.

When the solvent begins to evaporate from the cast film, polymer-polymer interactions increase and the polymer starts to precipitate in regions of high local polymer concentration. The regions of high local polymer concentration exist in the polymer solution even before casting due to because of agglomeration of macromolecules. The existence of macromolecular aggregates in the polymer solutions was indicated by the relationship between relative viscosity and temperature, as discussed in Section 9.1.2. As the evaporation of solvent progresses, macromolecules from the regions of lower polymer concentration are incorporated into existing macromolecular aggregates (nodules). This leads to the growth of nodules. When the evaporation of solvent from the cast film is fast, a sudden increase in polymer-polymer interactions may bring together the entire macromolecular aggregates (nodules), which leads to the formation of nodule aggregates. At the same time, the individual nodules should be smaller because of a shorter time available for their growth.

Considering the above mechanism of surface formation of solution cast films, one can explain the observed correlations between casting temperature and the size of nodule and the size of nodule aggregates. The above mechanism; however, ignores the effect of polymer-solvent interactions. It is believed that weak polymer-solvent interactions lead to a more extensive aggregation of macromolecules in polymer solution. Consequently, it was anticipated that for the membranes prepared from a given solvent (DMAC) at a given casting temperature the size of nodules in HSPPO-1.80 (weak polymer-solvent interactions) should be larger than the size of nodules in NaSPPO-1.80 membranes (strong polymer-solvent interactions). This anticipated

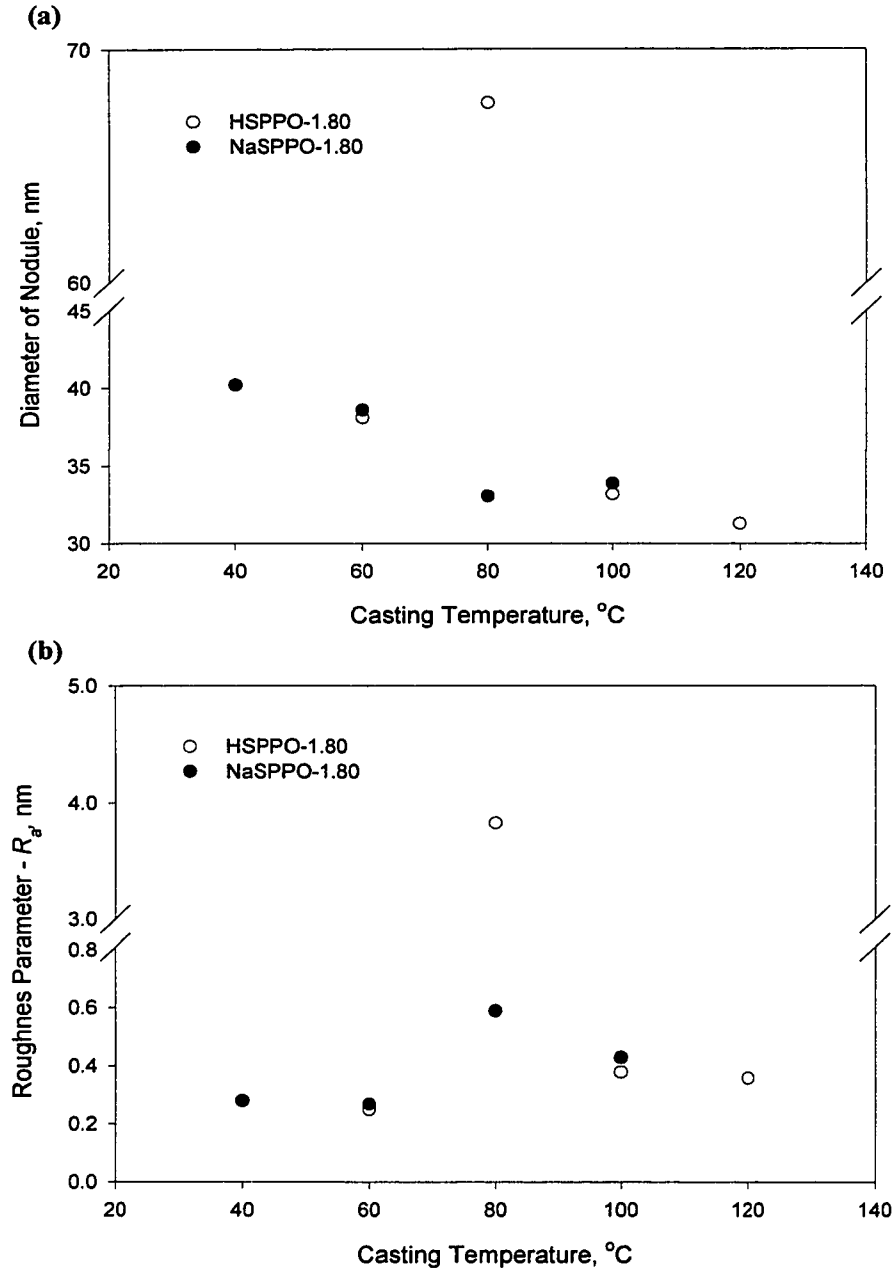

Figure 9-15. Effect of casting temperature on **(a)** average diameter of nodules and **(b)** surface roughness of dense high molecular weight HSPPO-1.80 and NaSPPO-1.80 membranes observed by atomic force microscope in tapping mode in the small scan size. Casting solutions at room temperature.

effect of polymer solvent-interactions was not confirmed by the experimental data shown in Table 9-4 and Figure 9-15a.

9.2.3 Gas permeation performance

Table 9-5 presents the summary of gas transport properties of dense high molecular weight HSPPO-1.80 and NaSPPO-1.80 membranes prepared at different casting temperatures when casting solution temperature were ambient. All membranes were tested for gas permeation in the CP testing system. The HSPPO-1.80 membranes were tested in October and November 1996. During this period the temperature in the laboratory oscillated between 21.5 and 23°C, while the relative humidity ranged from 25 to 40%. The NaSPPO-1.80 membranes were tested in June and July 1997. During this period the temperature in the laboratory oscillated between 22.0

Table 9-5. Summary of gas transport properties of dense high molecular weight SPPO-1.80 membranes prepared at different casting temperatures[a].

Cation	Casting Temp,°C	*n*		Permeability, Barrer O_2	Permeability, Barrer CO_2	Permeability Ratio O_2/N_2	Permeability Ratio CO_2/CH_4
H	60	5	Avg.	1.74	11.86	5.89	49.04
			St.Dev.	0.07	0.69	0.25	1.35
H	80	3	Avg.	1.48	9.26	5.85	44.26
			St.Dev.	0.09	0.99	0.07	1.39
H	100	4	Avg.	1.61	9.82	5.78	41.81
			St.Dev.	0.10	0.84	0.10	3.22
H	120	2	Avg.	4.49	31.04	4.67	27.56
			St.Dev.	0.11	1.14	0.32	5.94
Na	40	3	Avg.	2.60	28.56	4.56	59.58
			St.Dev.	0.15	2.62	0.03	6.43
Na	60	2	Avg.	2.59	25.64	4.82	54.82
			St.Dev.	0	2.05	0.13	5.97
Na	80	2	Avg.	2.60	26.92	4.71	58.38
			St.Dev.	0.32	0.45	0.12	3.09
Na	100	2	Avg.	2.55	25.13	4.90	55.46
			St.Dev.	0.15	0.14	0.13	0.66

[a] Casting solution temperature, ambient

and 23.5°C, while the relative humidity ranged from 38 to 55%.

Table 9-6 presents of gas permeation properties of HSPPO-1.80 and NaSPPO-1.80 membranes cast at 60°C from DMAC solutions at ambient temperature. Data from CP and CV systems were compared. The gas permeation properties of HSPPO-1.80 membranes measured by the CV system have already been presented in Table 6-6 and the gas permeation properties of NaSPPO-1.80 membranes measured by the CV system have already been presented in Table 7-4. As indicated in Section 6.5.3, since the permeate side of the CP system is open to atmosphere, the gas permeation properties measured in this system may be influenced the atmospheric conditions, particularly by the vapor pressure in the atmosphere, which is expressed by the relative humidity. On the other hand, the vapor pressure in the permeate side of the CV system was zero because all water had been removed completely from the system prior to gas permeation tests.

Table 9-6. Effect of relative humidity in the atmosphere on permeability of dense high molecular weight SPPO-1.80 membranes prepared from DMAC solutions[a].

Cation	RH[b]	Permeability, Barrer		Permeability Ratio	
	%	O_2	CO_2	O_2/N_2	CO_2/CH_4
H	25-40[c]	1.74	11.86	5.89	49.04
	0[d]	2.11	10.78	6.69	43.38
Na	38-55[c]	2.59	25.64	4.82	54.82
	0[d]	3.47	17.41	7.06	42.85

[a] Membranes cast at 60°C, casting solution at room temperature
[b] Relative humidity
[c] Test done by CP system
[d] Test done by CV system

It can be noticed in Table 9-6 that CO_2 permeability and CO_2/CH_4 permeability ratio measured by the CP system were greater than those measured by the CV system. On the other hand, O_2 permeability and O_2/N_2 permeability ratio measured by the CP system were lower than those measured by the CV system. The above effect of testing system or more specifically the effect of relative humidity in the atmosphere on the observed permeation properties of HSPPO-

1.80 and NaSPPO-1.80 membranes is consistent with that for HSPPO-1.37 membranes reported in Section 6.5.3.

The effect of casting temperature on permeability and permselectivity of HSPPO-1.80 and NaSPPO-1.80 membranes is shown graphically in Figures 9-16 and 9-17, respectively. It can be noticed that permeability of the HSPPO-1.80 membranes cast at 80 and 100°C is slightly lower than the permeability of the HSPPO-1.80 membranes cast at 60°C. When the casting temperature was 120°C, the permeability increased more than two folds (Figure 9-16). It should be mentioned that membranes cast at 120°C appeared different from other membranes. They were dark, wavy and non-uniform. ^{1}H NMR analysis of these membranes revealed a decrease in *IEC* from 1.80 meq/g (original polymer) to 0.55 meq/g. On the other hand, *IEC* of the membranes cast at 100°C was 1.70 meq/g, which represents a small decrease from the original *IEC* of the polymer. An increase in casting temperature results in a decrease in permselectivity of HSPPO-1.80 membranes. The decrease in permselectivity of HSPPO-1.80 membranes is more evident for CO_2/CH_4 (Figure 9-17b) than for O_2/N_2 (Figure 9-17a). Regarding NaSPPO-1.80 membranes, the change in casting temperature affects their permeability and permselectivity only slightly and no clear trends are observed in Figures 9-16 and 9-17.

9.2.4 Effect of surface morphology on gas transport properties

In section 8.4.1 it was concluded that there is no correlation between surface roughness observed by TM AFM in the large scan size and gas transport properties of HSPPO-1.37 membranes prepared from different casting solutions. It was anticipated; however, that systematic analysis of surface morphology at higher resolutions could reveal some correlations between surface structure and gas transport properties. In case of HSPPO-1.37 membranes a systematic study at higher resolutions was not possible. On the other hand, in case of HSPPO-1.80 and NaSPPO-1.80, it was possible to obtain "nodular resolutions" for all studied membranes.

It was observed that an increase in casting temperature resulted in a decrease in the average diameter of nodule (Figure 9-15a). This effect was the same for both HSPPO-1.80 and NaSPPO-1.80 membranes. On the other hand, an increase in casting temperature did not affect

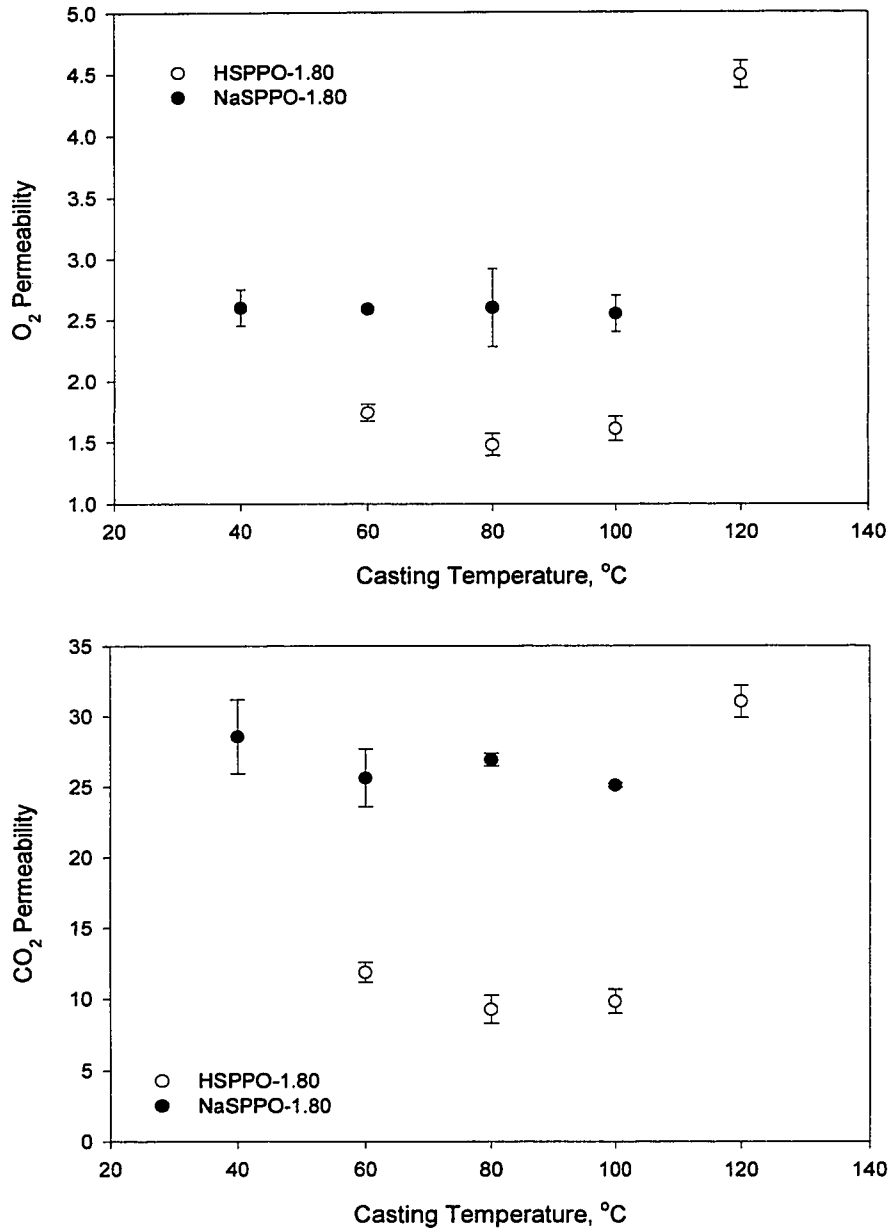

Figure 9-16. Effect of casting temperature on **(a)** O_2 and **(b)** CO_2 permeability of dense high molecular weight HSPPO-1.80 and NaSPPO-1.80 membranes. Casting solutions at room temperature.

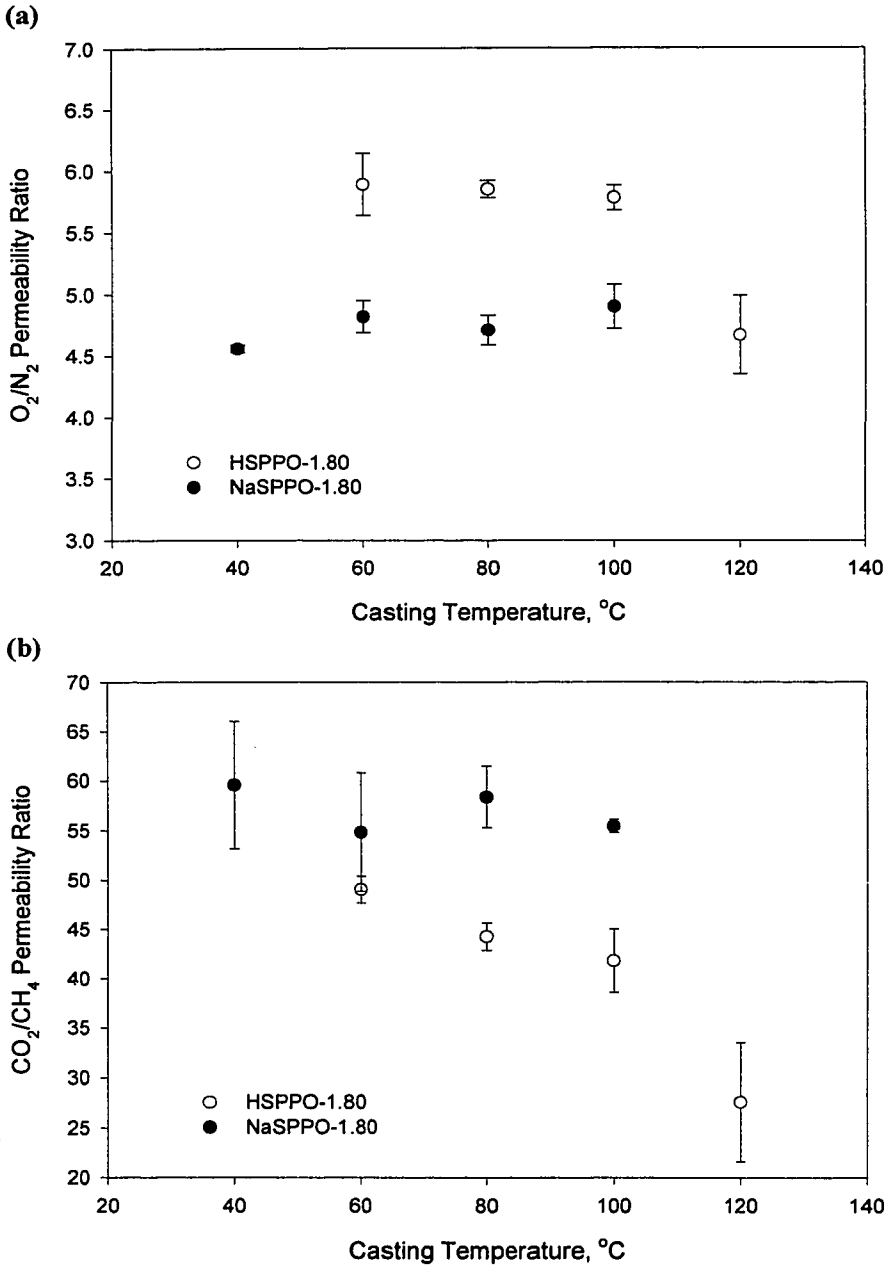

Figure 9-17. Effect of casting temperature on **(a)** O_2/N_2 and **(b)** CO_2/CH_4 permeability ratio of dense high molecular weight HSPPO-1.80 and NaSPPO-1.80 membranes. Casting solutions at room temperature.

gas transport properties of NaSPPO-1.80 membranes, while it had some effect on gas transport properties of HSPPO-1.80 membranes. Except for CO_2/CH_4 permeability ratio of HSPPO-1.80 membranes, the effect of casting temperature on gas transport properties of HSPPO-1.80 membranes was not very significant. The experimental data obtained in this study does not allow to correlate gas transport properties with surface morphology observed by TM AFM in the small scan size, in which the nodular structure of the membrane surface is clearly revealed. This does not mean; however, that such correlation does not exist.

As already discussed, gas permeation properties measured by the CP system are influenced by relative humidity in the atmosphere. It is possible that even if some clear trend between casting temperature and gas transport properties exited, it could have been obscured by the effect of relative humidity in the atmosphere. It should also be pointed out that, the fact that some changes in gas permeation properties were observed for HSPPO-1.80 while they were not observed for NaSPPO membranes, could have been due to higher relative humidities in the atmosphere under which the latter membranes were tested.

The current experimental results do not allow for correlating gas transport properties with surface morphology observed in the small scan size. On the other hand, a decrease in CO_2/CH_4 permeability ratio accompanied with a small decrease in CO_2 permeability of HSPPO-1.80 membranes, when the temperature was increased from 60 to 100°C, can be explained considering surface the morphology observed in the large scan size. The agglomeration of nodules on the membrane surface was enhanced by an increase in casting temperature. It is considered that the packing density of the polymer is higher in the nodule aggregate. Hence, the permeability of gases through dense nodule aggregates is lower than that through less dense smooth section of the membrane surface. The growth of nodule aggregates occurs at the expense of macromolecules surrounding the nodule aggregates. Consequently, the growth of nodule aggregates may lead to formation of some microdefects in the region surrounding large nodule aggregates. The microdefects would deteriorate separation properties of the membrane. At the same time, permeability of such membrane could also be low, because of the presence of low permeability nodule aggregates on the membrane surface.

The above mechanism for a simultaneous decrease in permeability and permselectivity of HSPPO-1.80 membranes with an increase in casting temperature is consistent with the combined effect of solvent strength and solvent volatility proposed in Section 8.4.2.3. The latter effect could explain formation of defects in HSPPO-1.37 membranes prepared from THF and also the experimental results that membranes with high surface roughness (HSPPO-1.37 membranes prepared from THF, DMF and DMAC, respectively) had lower permeability than the membrane with low surface roughness (prepared from pyridine).

9.3 Effect of Temperature of Casting Solution

The effect of temperature of casting solution on the properties of dense high molecular weight membranes was studied using solutions of HSPPO-1.80 and NaSPPO-1.80 in DMAC. The concentration of these polymer solutions at room temperature was 4.0 g/dL. The same polymer solutions were also used to study the effect of casting temperature discussed in the previous section. Membranes were prepared in the same way as explained previously except for that the polymer solutions were kept at casting temperature prior to casting. Two different temperatures, *i.e.* 60 and 80°C, were considered for each polymer solution.

9.3.1 TM AFM analysis

The summaries of TM AFM analysis in both large and small scan sizes of dense HSPPO-1.80 and NaSPPO-1.80 membranes are presented in Table 9-7. As previously, the surfaces were characterized by two roughness parameters, R_a and R_q, and the average diameter of nodule (small scan size) as well as the average diameter of nodule aggregates (large scan size). All images were obtained using the same TM AFM scanning probe.

It can be noticed that roughness parameters for HSPPO-1.80 membranes determined in the large scan size are slightly lower than the roughness parameters for NaSPPO-1.80 membranes prepared at the same casting conditions. For both HSPPO-1.80 and NaSPPO-1.80 membranes the roughness parameters, *i.e.*, R_a and R_q, increase slightly with an increase in casting solution temperatures. In case of NaSPPO-1.80 membranes, it is also observed that the average diameter of nodule aggregates increases with an increase in temperature. The nodule aggregates

Table 9-7. Summary of surface analysis by TM AFM of dense high molecular weight SPPO-1.80 membranes prepared from casting solutions of different temperatures[a].

Cation	Sol.Temp. °C	Scan Size μm	*n*		R_a, nm	R_q, nm	d_N or d_n nm
H	60	12x12	3	Avg.	1.32	1.51	-
				St.Dev.	0.28	0.27	-
		0.65x0.65	3	Avg.	0.27	0.35	38.3
				St.Dev.	0.05	0.06	4.9
H	80	12x12	3	Avg.	2.11	2.64	-
				St.Dev.	0.38	0.49	-
		0.65x0.65	4	Avg.	0.31	0.40	36.1
				St.Dev.	0.05	0.09	6.1
Na	60	12x12	4	Avg.	1.92	2.67	754
				St.Dev.	0.32	0.51	110
		0.65x0.65	4	Avg.	0.46	0.56	38.1
				St.Dev.	0.07	0.10	4.2
Na	80	12x12	3	Avg.	2.13	2.82	894
				St.Dev.	0.45	0.48	117
		0.65x0.65	3	Avg.	0.35	0.41	35.4
				St.Dev.	0.07	0.10	5.5

[a] Casting temperature equal to the temperature of casting solution
[b] Average diameter of nodule aggregates in 12 x 12 μm size or average diameter of nodules in 0.65 x 0.65 μm scan size

observed on the surface of these membranes are similar to nodule aggregates observed on the surface of membranes prepared form casting solution at room temperature (Figures 9-8 and 9-9). On the other hand, nodule aggregates were not observed on the surface of HSPPO-1.80 membranes. From the analysis using the small scan size, it can be noticed that the roughness parameters for both HSPPO-1.80 and NaSPPO-1.80 membranes are similar. The average diameter of nodules decreases slightly with an increase in temperature for both HSPPO-1.80 and NaSPPO-1.80 membranes. The nodules observed on the surface of HSPPO-1.80 membranes are slightly larger than the nodules observed on the surface of NaSPPO-1.80 membranes prepared under the same conditions.

Table 9-8 shows the effect of casting solution temperature on surface morphology of dense HSPPO-1.80 and NaSPPO-1.80 membranes. The membranes are compared in terms of the

Table 9-8. Effect of casting temperature and temperature of casting solution on surface morphology of dense high molecular weight SPPO-1.80 membranes observed in small scan size by TM AFM.

Cation	Casting Temp., °C	Solution Temp, °C	Roughness R_a, nm	Roughness R_q, nm	Nodule d_n, nm
H	60	60	0.27	0.35	38.3
		22	0.25	0.32	38.1
	80	80	0.31	0.40	36.1
		22	3.83	5.48	67.7
Na	60	60	0.46	0.56	38.1
		22	0.28	0.37	38.6
	80	80	0.35	0.41	35.4
		22	0.59	0.78	33.1

roughness parameters and the average diameter of nodule observed in the small scan size. The most significant effect of the temperature of casting solution is observed for HSPPO-1.80 membranes cast at 80°C. It can be noticed that an increase in temperature of casting solution from 22°C (room temperature) to 80°C results in more than one order of magnitude decrease in roughness parameters. The surface morphologies of the HSPPO-1.80 membranes cast at 80°C from casting solutions of 22°C and 80°C are presented in Figures 9-18a and 9-18b, respectively. Both images are shown in the same scan size (scanning area equal to 3 x 3 μm). It can be noticed that an increase in temperature of casting solution from 22 to 80°C results in disappearance of nodule aggregates from the surface of HSPPO-1.80 membranes. The disappearance of nodule aggregates from the surface of the membrane is responsible for the decrease in roughness parameters. In case of other membranes, the effect of change in casting temperature on surface morphology is not significant. There is no clear trend observed between the temperature of casting solution and the roughness parameters and the average diameter of nodules.

The observed disappearance of nodule aggregates from the surface of HSPPO-1.80 membranes resulting from an increase in the temperature of casting solution is consistent with the effect of solvent strength on surface morphology suggested in Section 8.3.3.1. It was proposed that strong polymer-solvent interactions might prevent formation of large nodule

(a)

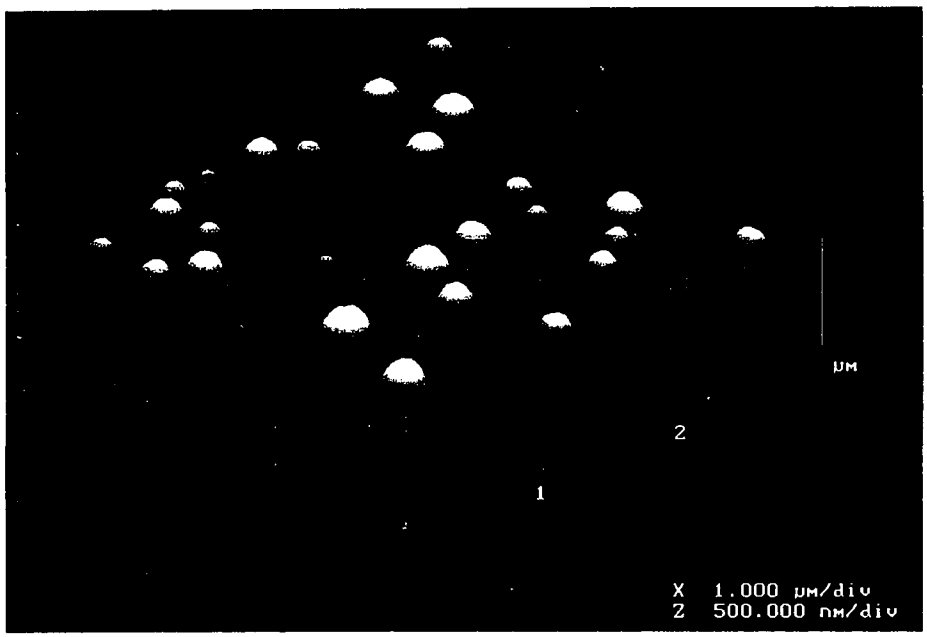

(b)

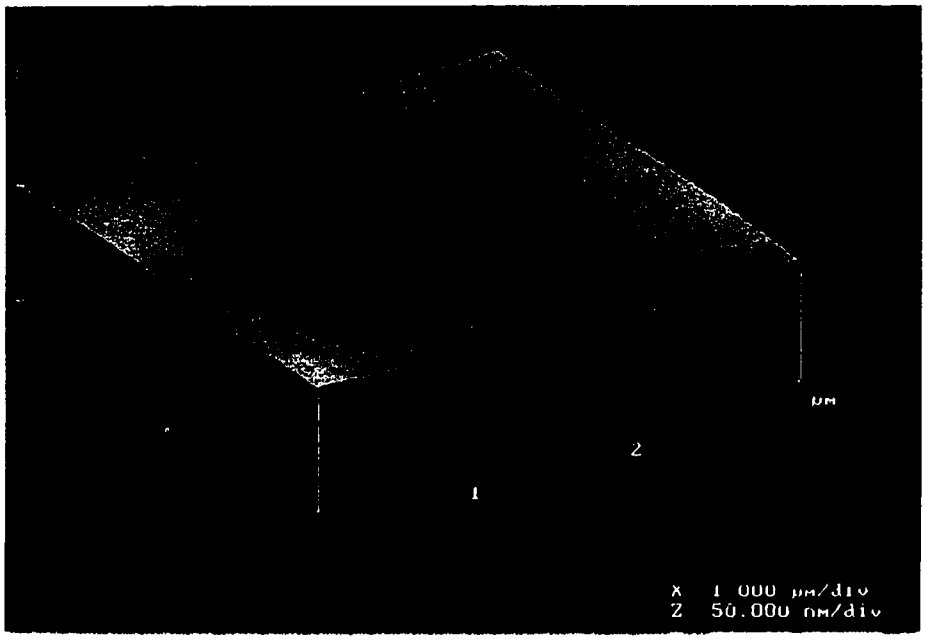

Figure 9-18. Effect of temperature of casting solution on surface morphology of dense high molecular weight HSPPO-1.80 membranes cast at 80°C; **(a)** casting solution at room temperature (22°C); **(b)** casting solution at 80°C.

aggregates on the surface of dense polymeric membranes. As shown in Figure 9-2 an increase in temperature results in a decrease in the relative viscosity of the solution of HSPPO-1.80 in DMAC and hence to an increase in the strength of interactions between HSPPO-1.80 and DMAC.

It should be pointed out that an increase in the temperature of polymer solution did not result in the disappearance of nodule aggregates from the surface of NaSPPO-1.80 membranes. The nodule aggregates are present on the surface of NaSPPO-1.80 membrane despite strong polymer solvent interactions between NaSPPO-1.80 and DMAC. As shown in Figure 9-3, for a given temperature, the relative viscosity of NaSPPO-1.80 in DMAC is lower than the relative viscosity of HSPPO-1.80 in DMAC. Unlike the nodule aggregates present on the surface of HSPPO-1.80 membranes, the nodule aggregates observed on the surface of NaSPPO-1.80 membranes are flat and their presence does not result in high roughness of the membrane surface. Even though the grains observed in the large scan size of HSPPO-1.80 membranes (Figures 9-5 – 9-7) and the grains observed in the large scan size of NaSPPO-1.80 membranes (Figures 9-8 and 9-9) are both referred to as nodule aggregates, they clearly represent different polymeric structures.

9.3.2 Gas transport properties

The summary of gas transport properties of dense high molecular weight HSPPO-1.80 and NaSPPO-1.80 membranes cast from polymer solutions at a temperature equal to the casting temperature is presented in Table 9-9. The membranes were tested for gas permeation in the CP testing system. The HSPPO-1.80 membranes were tested in October and November 1996. During this period the temperature in the laboratory oscillated between 21.5 and 23°C, while the relative humidity ranged from 25 to 40%. The NaSPPO-1.80 membranes were tested in June and July 1997. During this period the temperature in the laboratory oscillated between 22.0 and 23.5°C, while the relative humidity ranged from 38 to 55%.

It can be noticed in Table 9-9 that a simultaneous increase in casting temperature and the temperature of casting solution from 60 to 80°C, results in a slight increase in permeability and a slight decrease in permselectivity for both HSPPO-1.80 and NaSPPO-1.80 membranes. This is

different from the effect of casting temperature when the casting solution was kept at room temperature.

Table 9-9. Summary of gas permeation properties of dense high molecular weight SPPO-1.80 membranes prepared from polymer solutions of different temperatures [a].

Cation	Solution Temp.,°C	*n*		Permeability, Barrer O_2	Permeability, Barrer CO_2	Permeability Ratio O_2/N_2	Permeability Ratio CO_2/CH_4
H	60	3	Avg.	2.02	13.88	5.80	46.67
			St.Dev.	0.20	1.15	0.09	1.19
H	80	3	Avg.	2.28	14.63	5.73	44.77
			St.Dev.	0.18	0.73	0.14	2.16
Na	60	3	Avg.	2.95	29.31	4.77	55.97
			St.Dev.	0.06	0.85	0.04	4.43
Na	80	3	Avg.	3.04	29.98	4.67	55.00
			St.Dev.	0.15	2.31	0.11	3.54

[a] Casting temperature equal to the temperature of casting solution

Table 9-10 compares the performance of membranes cast at 60°C and 80°C. For each casting temperature, the casting solution temperature was either ambient (22°C) or the same as the casting temperature. This comparison is valid because the membranes from a given polymer were tested in the same testing system at the same time.

It can be noticed from Table 9-10 that the casting temperature and the temperature of casting solution have a strong influence on the permeability of HSPPO-1.80 membranes. This can be illustrated by the example of the average O_2 permeabilities of HSPPO-1.80 membranes. An increase in casting temperature from 60 to 80°C while maintaining the casting solution temperature at 22°C results in a decrease in O_2 permeability from 1.74 to 1.49 Barrer. When both casting and casting solution temperatures were changed from 60 to 80°C, O_2 permeability changed from 2.02 to 2.28 Barrer. An increase of polymer solution temperature from 22 to 80°C, while maintaining the casting temperature at 80°C, increases O_2 permeability from 1.49 to 2.28 Barrer. This is a more than 50% increase in permeability, which is associated with only a 2%

Table 9-10. Effect of casting temperature and temperature of casting solution on gas transport properties of dense high molecular weight SPPO-1.80 membranes.

Cation	Casting Temp., °C	Solution Temp., °C	Permeability O_2	Permeability CO_2	Permselectivity O_2/N_2	Permselectivity CO_2/CH_4
H	60	22	1.74	11.86	5.87	49.04
		60	2.02	13.88	5.80	46.67
	80	22	1.49	9.26	5.85	44.26
		80	2.28	14.63	5.73	44.78
Na	60	22	2.59	25.64	4.82	54.82
		60	2.94	29.31	4.77	55.92
	80	22	2.60	26.92	4.71	58.38
		80	3.04	29.98	4.67	55.00

decrease in O_2/N_2 permeability ratio. The above example represents a method to improve gas transport properties of HSPPO-1.80 membranes.

9.3.3 Effect of surface morphology on gas transport properties

A simultaneous increase in casting and casting solution temperatures from 60 to 80°C results in a decrease in the average diameter of nodules for both HSPPO-1.80 and NaSPPO-1.80 membranes. At the same time, permeabilities of both membranes increase. This might suggest that there is a correlation between the size of nodules and the membrane permeability. In Section 9.2; however, it was reported that a similar change in the average diameter of nodules was associated with no change or a small decrease in membrane permeability. These inconsistent effects of the average diameter of nodules on membrane permeability indicates that at a given resolution of TM AFM, there is no clear correlation between surface morphology and gas transport properties.

Although there is no direct relationship between surface images both in μm and sub-μm scan range and gas transport properties, the analysis of the surface of dense polymeric membranes by TM AFM has allowed the identification of an undesirable surface morphology. The undesirable surface morphology is represented by a surface with high roughness parameters arising from the presence of large nodule aggregates. Such undesirable surface morphology

originates from casting solutions possessing the following properties; 1) weak polymer-solvent interactions (expressed by the relative viscosity of casting solution), 2) high volatility of solvent in casting solution which enhances aggregation of nodule and high surface roughness. It was; however, observed that, when polymer-solvent interactions are relatively strong, volatility of solvent in casting solution has little effect on surface morphology of the membrane.

9.4 Chapter Summary

An increase in temperature of the polymer solution results in a linear decrease in the relative viscosity, which indicates an increase in polymer-solvent interactions. The reported effect of the temperature of polymer solution on the relative viscosity supports the Kesting's notion that macromolecular aggregates exist even in dilute polymer solutions.

The influence of the casting temperature (volatility of casting solution) on the surface morphology depends on the polymer-solvent interactions. In case of HSPPO-1.80 in DMAC (weak polymer-solvent interactions) an increase in casting temperature from 60 to 100°C, while the initial temperature of casting solution is constant and equal to room temperature, results in more than two orders of magnitude increase in surface roughness. In case of NaSPPO-1.80 in DMAC (strong polymer-solvent interactions) the same change in temperature results only in a small change in surface roughness. The changes in surface morphology of HSPPO-1.80 resulting from increased casting temperature can be minimized by an increase in the initial temperature of casting solution, which increases polymer-solvent interactions.

For a given polymer solution (HSPPO-1.80 in DMAC, NaSPPO-1.80 in DMAC) an increase in casting temperature, while the initial temperature of casting solution is constant and equal to room temperature, does not change, with the exception of HSPPO-1.80 cast at 120°C, the permeability of the membrane significantly. A simultaneous increase in the casting temperature and the temperature of polymer solution results in a slight increase in membrane permeability and generally no changes the membrane permselectivity.

There is no direct relationship between surface morphology observed in μm and sub-μm scan size and gas transport properties; however, very high surface roughness due to large nodule aggregates is not desirable. Permeability of membranes with such surfaces is not higher and

usually lower than permeability of membranes with smoother surfaces. On the other hand, presence of large nodular aggregates and high surface roughness is always associated with lower ideal selectivity of membrane. Eventually, an increase in surface roughness may lead to the formation of defects in the membrane structure (HSPPO-1.80 in DMAC cast at 120°C, HSPPO-1.37 in THF).

PART IV

Conclusions, Recommendations And Contributions

CHAPTER 10

Conclusions

The following is the list of conclusions that were reached in this thesis concerning the improvement of gas transport properties of PPO by chemical and physical modification of the polymer. The conclusions are presented in three parts. The first part pertains to the material development aspect of this project. The second part pertains to the effect of casting conditions. The last part summarizes the findings related to effect of testing conditions.

10.1 Material Development

10.1.1 HSPPO

- The use of high molecular weight PPO for the sulfonation studies limits the sulfonation capacity of the polymer due to the reduced solubility of the high molecular weight PPO in the solvent.
- Sulfonation of PPO with chlorosulfonic acid may lead to a sulfonated-chlorinated product.
- Sulfonated PPO in a protonated form (HSPPO) is not thermally stable because of the decomposition of sulfonic groups at above 175°C. The final decomposition of the polymer begins at above 400°C.
- Sulfonation of PPO results in an increase in density linearly with respect to the *IEC* value while the average d-spacing in polymer remains constant.
- The modified fractional free volume model proposed recently by Park and Paul (1997) fails to predict permeability of HSPPO.

- An increase in *IEC* results in a decrease in permeability and an increase in ideal selectivity of HSPPO.

- The combination of permeability and ideal selectivity for both O_2/N_2 and CO_2/CH_4 places the HSPPO above the respective tradeoff lines for standard commercial polymers but below the respective upper-bound lines. An increase in *IEC* brings the permeability versus ideal selectivity relationship closer to the upper-bound line. This improvement in gas transport is more apparent for the O_2/N_2 gas pair than for the CO_2/CH_4 gas pair.

10.1.2 MeSPPO

- Substitution of the proton in sulfonic groups by a metal cation increases polarity of the polymer.

- Sulfonated PPO in a metal form (MeSPPO) is more thermally stable than HSPPO.

- Despite a greater density, MeSPPO is more permeable to gases than HSPPO. The increase in permeability resulting from the exchange of proton with a metal cation depends on the *IEC* of the polymer. The maximum increase is observed for the polymer of *IEC* equal to 1.37 meq/g.

- High molecular weight NaSPPO shows a unique relationship between permeability and the *IEC* of the polymer, *i.e.*, the plot of permeability versus *IEC* of NaSPPO shows a maximum permeability, which occurs for the polymer of *IEC*, equal to 1.37 meq/g.

- MeSPPO, which show an increase in peak intensity on the X-ray diffraction spectrum and an increase in d-spacing compared to the corresponding HSPPO, show no change or an increase in ideal selectivity.

- Substitution of the proton in sulfonic groups by a metal cation improves the gas transport properties of the polymer. In particular, the combination of O_2 permeability and O_2/N_2 ideal selectivity of MgSPPO-1.37 and MgSPPO-1.80 places these polymers above the upper-bound line.

- The actual separation factors for O_2/N_2 and CO_2/CH_4 measured in a constant volume testing system (permeate side at vacuum) are lower than the ideal values; however, the maximum difference does not exceed 13%.

10.2 Effect of Casting Conditions

10.2.1 Polymer solution

- Solutions of high molecular weight HSPPO-1.37 in organic solvents of a concentration 4.0 g/dL behave like concentrated polymer solutions, *i.e.*, an increase in polymer-solvent interactions results in a decrease in the relative viscosity of the polymer solution.
- The observed relationship between polymer-solvent interactions and the relative viscosity of polymer solution indicates the existence of some form of macromolecular aggregates in the polymer solution.
- An increase in the temperature of polymer solution results in an increase in polymer-solvent interactions.

10.2.2 Surface morphology

- AFM analysis reveals the existence of nodules and nodule aggregates in the surface of dense polymeric membranes. Weak polymer-solvent interactions and high volatility of polymer solution enhance formation of large nodule aggregates, which is associated with a high surface roughness.
- In the absence of strong polymer-solvent interactions, an increase in casting temperature (an increase in volatility of casting solution) results in a significant increase in the surface roughness of the membrane.
- An increase in the surface roughness resulting from an increase in the casting temperature can be minimized by an increase in the temperature of casting solution.

10.2.3 Gas transport properties

- For a given polymer (HSPPO-1.37), the change of solvent from NMP (strong polymer-solvent interactions and low volatility) to pyridine (strong polymer-solvent interactions and high volatility) results in a more than two-fold increase permeability and a 12% decrease in ideal selectivity of the membrane.

- For given polymer solutions (HSPPO-1.80 in DMAC, NaSPPO-1.80 in DMAC) an increase in casting temperature, while the initial temperature of casting solution is constant and equal to ambient temperature, does not change the permeability of the membrane significantly. At the same time, permselectivity of the membrane may slightly decrease.

- Adjusting the casting temperature and the temperature of polymer solution simultaneously may lead to an improvement in gas transport properties of the membranes, as for example in the case of HSPPO-1.80 prepared from DMAC solution.

- There is no direct relationship between surface morphology observed in μm and sub-μm scan sizes and gas transport properties; however, very high surface roughness due to large nodule aggregates is not desirable. Permeability and permselectivity of the membranes with such surfaces is usually lower than for the membranes with smoother surfaces. Furthermore, the presence of large nodule aggregates and high surface roughness may lead to the formation of defects in the membrane structure (HSPPO-1.37 in THF, HSPPO-1.80 in DMAC cast at 120°C).

10.3 Effect of Testing Conditions

- Gas transport properties of membranes tested in a constant pressure testing system, in which permeate side is open to atmosphere, are influenced by relative humidity in the atmosphere.

- An increase in relative humidity in the atmosphere increases the apparent CO_2 permeability and CO_2/CH_4 permeability ratio and decreases the apparent O_2 permeability and O_2/N_2 permeability ratio measured in a constant pressure system. The change in gas transport properties may be as high as 25% when the relative humidity is changed form 10 to 50%.

CHAPTER 11

Recommendations

The following are the recommendations formulated based on the results of the present work:

- Development of thin film composite or asymmetric integrally skinned asymmetric membranes from the most promising polymers, *i.e.*, MgSPPO-1.37 and MgSPPO-1.80.
- Investigation of simultaneous sulfonation and chlorination of PPO by chlorosulfonic acid. Sulfonated-brominated PPO is known to have promising gas transport properties. The same can be expected for sulfonated-chlorinated PPO.
- Implementation of computer molecular simulation for SPPO macromolecules of different *IEC*, molecular weight and cations in the sulfonic groups in order to investigate the conditions at which fixed micropores are formed in the polymer.
- Study of sorption isotherms of different gases in HSPPO and MeSPPO to determine differences in affinity of different gases to different membrane materials. This may facilitate the development of a model for gas transport in polymers based on the assumption of the existence of continuous passages (fixed micropores) in the membrane.
- Formation of polymer-zeolite complexes. Incorporation of metal cations into sulfonic groups improves the gas transport properties of SPPO. Introduction of zeolites into the backbone of SPPO would allow incorporating of larger quantities of metals without increasing the *IEC* of the polymer.

- Study of the combined effects of polymer-solvent interactions and volatility of polymer solution considering polymers of different polarities and wider ranges of casting and polymer solution temperatures.

- Design of a gas testing system with controllable permeate side humidity. This could be accomplished by flowing a sweep gas at the permeate side of the membrane. Sweep gas of known flow rate could be loaded with a desired level of humidity. Permeation rates would be measured by using a gas chromatograph. This would allow investigating if the actual CO_2/CH_4 separation factor can be increased at higher permeate side humidity levels. The membranes from a wide range of polarities should be incorporated in this study.

CHAPTER 12

Contributions

The following is the list of contributions in the fields of membrane science and technology, polymer science, and chemical engineering, which have been made as a result of this work. The order in which the contributions appear follows the order in which the results of this work were presented:

- Gas transport properties of high molecular weight sulfonated PPO in protonated and metal forms have been reported for the first time.
- The reported gas transport properties of high molecular weight sulfonated PPO in metal forms confirm possibility of simultaneous increase in gas permeability and gas selectivity by tailoring the chemical structure of polymers.
- Polymeric materials (MgSPPO-1.37 and MgSPPO-1.80) with excellent potential for O_2/N_2 separation have been developed.
- The observation that the modified fractional free volume model of Park and Paul fails to predict permeability of sulfonated PPO should provide another driver in the development of free volume models for gas transport.
- The reported relationship between *IEC* and gas permeability for high molecular weight sulfonated PPO in sodium form is unique. The interpretation of the observed relationship considering a combined effect of high polarity of substituent groups, high molecular weight of polymer and high free volume of the base polymer, is novel.
- The influence of the atmospheric humidity on the gas transport properties of membranes measured in a system with permeate side open to atmosphere (constant pressure system) has been reported for the first time.

- The polymer solution on polymer solvent interaction and relative viscosity supports the notion that macromolecular aggregates exist in relatively dilute polymer solutions.

- The conclusion from the study on the effect of casting parameters on the properties of dense polymeric membranes challenges a widely accepted belief in the membrane community that the properties of dense polymeric membranes are governed entirely by the chemistry of polymer.

- The proposed phenomenological relationships for dense polymeric membranes between the casting conditions and the surface morphology and between the casting conditions and the gas transport properties are novel. The proposed relationships can be utilized in the development of industrially useful thin film composite membranes.

Bibliography

Aguilar-Vega, M. and Paul, D. R., "Gas Transport Properties of Polyphenylene Ethers", J. Polym. Sci., Part B, Polym. Phys. Ed., **31**, 1577(1993).

Aycock, D., "Polyphenylene Ether", in Encyclopedia of Polymer Science and Technology, vol. 13, Wiley Interscience Publishers, New York, NY, 1974.

Barton, A. F. M., "CRC Handbook of Solubility Parameters and Other Cohesion Parameters", CRC Press, Inc., Boca Raton, Fl, 1983, Chapter 15.

Bikson, B., Nelson, J. K., Goetz, G. and Ozcayir, Y., "Semipermeable Membranes Based on Certain Sulfonated Substituted Polysulfone Polymers", US Pat. 5,071,488 (1991).

Bikson, B. and Nelson, J. K., "Production and Use of Improved Composite Fluid Separation Membranes", US Patent 5,356,459, 1994.

Binning, G, Quate, C. F. and Gerber, C., "Atomic Force Microscope", Phys. Rev. Lett., **56**, 930 (1986).

Bird, R. B., Steward, W. E. and Lightfoot, E. N., "Transport Phenomena", John Wiley & Sons, New York (1960) p. 15.

Blanks, R. F. and Prausnitz, J. M., "Thermodynamics of Polymer Solubility in Polar and Nonpolar Systems", Ind. Eng. Chem. Fund., **3**(1), 1 (1964).

Bowen, W. R, Hilal, N., Lovitt, R. W. and Williams, P. M., "Visualization of an Ultrafiltration Membrane by Non-Contact Atomic Force Microscopy at a Single Pore Resolution", J. Membrane Sci., **110**, 229 (1996a).

Bowen, W. R, Hilal, N., Lovitt, R. W. and Williams, P. M., "Atomic Force Microscope Studies of Membranes: Surface Pore Structure of Cyclopore and Anopore Membranes", J. Membrane Sci., **110**, 233 (1996b).

Bristow, G. M. and Watson, W. F., "Cohesive Energy Densities of Polymers", Trans. Faraday Soc., **54**, 1731 (1958).

Burrell, H., "Solubility Parameters", Interchem. Rev., **14**, 3 (1955).

Chen, W. J. and Martin, C. R., "Gas Transport Properties of Sulfonated Polystyrenes", J. Membrane Sci., **95**, 51 (1994).

Chern, R. T., Koros, W. J., Hopfenberg, H. B. and Stannet, V. T., Chapter 2 in Materials Science of Synthetic Membranes, ACS Symposium Series 269, American Chemical Society, Washington, DC, 1985

Chern, R. T., Sheu, F. R., Jia, L., Stannet, V. T. and Hopfenberg, H. B., "Transport of Gases in Unmodified and Aryl-Brominated 2,6-dimethyl-1,4-poly(phenylene oxide)", J. Membrane Sci., **35**, 103 (1987).

Chiou, J. S. and Paul, D. R., "Gas Permeation of in a Dry Nafion Membrane", Ind. Eng. Chem. Res., **27**, 2161 (1988).

Danner, R. P. and High, M. S., "Handbook of Polymer Solution Thermodynamics", Design Institute for Physical Properties Data, American Institute of Chemical Engineers, New York, NY, 1993.

Dietz, P., Hansma, P. K., Inacker, O., Lehmann, H. D. and Herrmann, K. H., "Surface Pore Structure of Micro- and Ultrafiltration Membranes Imaged with the Atomic Force Microscope", J. Membrane Sci., **65**, 101 (1992).

Digital Instruments Inc., "NanoScope III, Control System Manual", Santa Barbara, CA, Dec., 1993.

Doolitle, A. K., "The Technology of Solvents and Plasticizers", John Wiley, New York, NY, 1954.

Ferry, J. D., Foster, E. L., Browning, G. V. and Sawyer, W. M., "Viscosities of Concentrated Polyvinyl Acetate Solutions in Various Solvents", J. Colloid. Sci., **6**, 377 (1951).

Flory, P. J., "Principles of Polymer Chemistry", Cornell University Press, Ithaca, NY, 1953.

Fritzsche, A. K., Arevalo, A. R., Moore, M.D., Elings, V. B., Kjoller, K. and Wu, C. M., "The Surface Structure and Morphology of Polyvinylidene Fluoride Microfiltration Membranes by Atomic Force Microscopy", J. Membrane Sci., **68**, 65 (1992a).

Fritzsche, A. K., Arevalo, A. R., Moore, M. D., Weber, C. J., Elings, V. B., Kjoller, K. and Wu, C. M., "Image Enhancement of Polyethersulfone Ultrafiltration Membrane Surface for Atomic Force Microscopy", J. Appl. Polym. Sci., **46**, 167 (1992b).

Fritzsche, A. K., Arevalo, A. R., Connoly, A. F., Moore, M. D., Elings, V. B. and Wu, C. M., "The Structure and Morphology of the Skin of Polyethersulfone Ultrafiltration Membranes: a Comparative Atomic Force Microscope and Scanning Electron Microscope Study", J. Appl. Polym. Sci., **45**, 1945 (1992c).

Fu, H., Jia, L. and Xu, J., "Studies on the Sulfonation of Polyphenylene oxide (PPO) and Permeation Behavior of Gases and Water Vapor Through Sulfonated PPO Membranes. I. Sulfonation of PPO and Characterization of the Products", J. Appl. Polym. Sci., **51**, 1399 (1994a).

Fu, H., Jia, L. and Xu, J., "Studies on the Sulfonation of Polyphenylene oxide (PPO) and Permeation Behavior of Gases and Water Vapor through Sulfonated PPO Membranes. II. Permeation Behavior of Gases and Water Vapor through Sulfonated PPO membranes", J. Appl. Polym. Sci., **51**, 1405 (1994b).

Gandhi, K. S. and Williams, M. C. "Solvent Effects on the Viscosity of Moderately Concentrated Polymer Solutions", J. Polym. Sci. C., **35**, 211 (1971).

Grulke, E.A., "Solubility Parameter Values" in Polymer Handbook, eds. J. Braandrup and E.H. Immergut, Wiley, New York, 1989.

Hamza, A., Chowdhury, G., Matsuura, T., and Sourirajan, S., "Study on Reverse Osmosis Separation and Permeation Rate for Sulfonated Polyphenylene oxide Membranes of Different Ion Exchange Capacities", J. Appl. Polym. Sci., **58**, 613 (1995).

Hansen, C. M., "The Universality of Solubility Parameter", Ind. Eng. Chem. Prod. Res. Dev., **8**, 2 (1969).

Hansen, C. M. and Beerbower, A., "Solubility Parameters" in Kirk-Othmer Encyclopedia of Chemical Technology 2nd edition, Suppl. Vol., 889, ed. Standen, A., Interscience, New York, NY, 1971.

Hass, H., Farney, L. and Valle Jr., C., "Some Properties of Ethyl Cellulose Films", J. Colloid Sci., **7**, 584 (1952).

Hay, A. S., "High Performance Polymers: their Origin and Development", in Proceedings of the Symposium on the History of High Performance Polymers at the American Chemical Society Meeting, p. 209-213, Elsevier Publishing Co., New York, NY, 1986.

Hildebrand, J. H. and Scott, R. L., "The Solubility of Nonelectrolites", Reinhold, New York, NY, 1950.

Henis, J. M. S. and Tripodi, M. K., "Composite Hollow Fiber Membranes for Gas Separations: The Resistance Model Approach", J. Membrane Sci., **8**, 233 (1981).

Hoernschemeyer, D. H., "The Influence of Solvent Type on the Viscosity of Concentrated Polymer Solutions", J. Appl. Polym. Sci., **18**, 61 (1974).

Hoy, K. L., "New Values of the Solubility Parameter" J. Paint Technol. **42**, 76 (1970).

Hoy, K. L., " The Hoy Tables of Solubility Parameters", Union Carbide Corporation, Solvents and Coatings Material Division, South Charleston, WV, 1985.

Huang, R. Y. M. and Kim, J. J., "Synthesis and Transport Properties of Thin Composite Membranes I. Synthesis of PPO Polymer and its Sulfonation", J. Appl. Polym. Sci, **29**, 4017 (1984a).

Huang, R. Y. M. and Kim, J. J., "Synthesis and Transport Properties of Thin Composite Membranes. II. Preparation of Sulfonated Polyphenylene oxide Thin Composite Membranes for the Purification of Alberta Tar Sands Waste Waters", J. Appl. Polym. Sci, **29**, 4029 (1984b).

Industrial Membrane Research Institute, "Annual Progress Report for British Gas", Department of Chemical Engineering, University of Ottawa, Ottawa 1995.

Joly, C., Le Cerf, D., Sauvage, J. P., Chappey, C., Langevin, D. and Muller, G., "Solution Properties of a Fluorinated Polyimide and Film Characteristics, STEPI **4**, 379 (1996).

Jones, G. and Miles, J., "The Tensile Strength of Nitrocellulose Films, J. Soc Chem. Ind., **52**, T251 (1933).

Jordan, S. M., Henson, M. A. and Koros, W. J., "The Effect of Carbon Dioxide Conditioning on the Permeation Behavior of Hollow Fiber Asymmetric Membranes", J. Membrane Sci., **54**, 103 (1990).

Kamide, K. and Manabe, S., "Role of Micropore Separation Phenomena in the Formation of Porous Polymeric Membranes", in Materials Science of Synthetic Membranes, ACS Symposium Series 269, American Chemical Society, Washington, DC, 1985.

Katz, R. and Munk, B., "The Influence of the Solvent and Substrate on the Water Vapor Permeability of Films", J. Oil Colour Chemists' Assoc., **52**(5), 418 (1969).

Kesting, R. E. and Fritzsche, A. K., "Polymeric Gas Separation Membranes", John Wiley & Sons Inc., New York, NY, 1993.

Kesting, R. E., Fritzsche, A. K., Handermann, A. C., Murphy, M. K., Cruse, C. A., Malon, R. F. and Moore, M. D., "The Second-Generation Polysulfone Gas Separation Membranes. I. The Use of Lewis Acid : Base Complexes as Transient Templates to Increase Free Volume, J. Appl. Polym. Sci., **40**, 1557 (1990a).

Kesting R. E., Fritzsche, A. K., Cruse, C. A. and Moore, M. D., "The Second-Generation Polysulfone Gas Separation Membranes. II. The Relationship Between Sol Properties, Gel Microvoids, and Fiber Selectivity", J. Appl. Polym. Sci., **40**, 1575 (1990a).

Kesting, R. E., "The Four Tires of Structure in Integrally Skinned Phase Inversion Membranes and their Relevance to Various Separation Regimes", J. Appl. Polym. Sci., **41**, 2739 (1990).

Kesting, R. E., "Synthetic Polymeric Membranes: a Structural Perspective", 2nd. edition Wiley-Interscience, New York, NY, 1985.

Khulbe, K. C., Kruczek, B., Chowdhury, G., Gagne, S. and Matsuura, T., "Surface Morphology of Homogeneous and Asymmetric Membranes Made from Polyphenylene Oxide by Tapping Mode Atomic Force Microscope", J. Appl. Polym. Sci., **59**, 1151 (1996a).

Khulbe, K. C., Kruczek, B. Chowdhury, G., Gagne, S., Matsuura, T. and Verma, S. P., "Characterization of Membranes Prepared from Polyphenylene Oxide by Raman Scattering and Atomic Force Microscopy", J. Membrane Sci., **111**, 57 (1996b).

Khulbe, K. C., Chowdhury, G., Kruczek, B. Vujosevic, R., Matsuura, T. and Lamarche, G., "Characterization of PPO Dense Membrane Prepared at Different Temperature by ESR, Atomic Force Microscope and Gas Permeation", J. Membrane Sci., **126**, 115 (1997).

Kolonis, V., "Das untersuchen der Trocknung dunner Kunststoffschichten", Kolloid Z. Z. Polym., **226**(1), 40 (1968).

Koningsveld, R., "Phase Equilibria in Polymer System", Brit. Polym. J., **7**, 435 (1975).

Koros, W. J. and Fleming G. K., "Membrane-Based Gas Separation", J. Membrane Sci., **83**, 1 (1993).

Koros, W. J. and Hellums, M. W., "Transport Properties, Encyclopedia of Polymer Science", 2nd edition, Wiley-Interscience Publishers, New York, NY, Supplement Volume, 724, 1989.

Kruczek, B. and Matsuura, T., "Development and Characterization of Homogeneous Membranes Made from High Molecular Weight Sulfonated Polyphenylene Oxide", J. Membrane Sci., **146**, 249 (1998).

Kruczek, B., Khulbe, K. C., Chowdhury, G., Gagne S., and Matsuura, T., "A study on the Surface Morphology of Asymmetric and Dense Membranes by Atomic Force Microscopy", presented at 45th CSChE conference, Quebec City, October 16, 1995.

Laverty, B., British Gas, Private Communication, 1995.

Lee, M. W., "Selection of Barrier Materials from Molecular Structure", Polym. Eng. Sci., **20**, 65 (1980).

Linde, D. R. ed. "CRC Handbook of Chemistry and Physics, 73rd edition", CRC, London, 1992-1993.

Liu, C. and Martin, C. R., "Composite Membranes from Photochemical Synthesis of Ultrathin Polymer Films", Nature, **352**, 50 (1991).

Liu, C., Chen, W. J., and Martin, C. R., "Electrochemical Synthesis of Ultrathin-Film Composite Membranes", J. Membrane Sci., **65**, 113 (1992).

Maeda, Y., and Paul, D. R., "Effect of Antiplasticization on Selectivity and Productivity of Gas Separation Membranes", J. Membrane Sci., **30**, 1 (1987).

Mahajan, S. S., "Structural Modification of Poly(2,6-dimethyl-1,4-phenylene oxide)", Polym.-Plast. Tech. Eng., **30**(1), 27 (1991).

Matsuura, T., "Synthetic Membranes and Membrane Separation Processes", CRC Press, Boca Raton, FL, 1994.

Mattera, Jr., V. D. and Risen Jr., W. M. "Composition Dependence of Glass Transition Temperature of Sulfonated-Polystyrene Ionomers", J. Polym. Sci., Part B. Polym. Phys., **24**, 753 (1986).

Meares, P., "Polymer Structure and Bulk Properties", Van Nostrand, New York, NY, 1965.

Michaels, A. S., Vieth, W. R. and Barrie, J. A., "Solution of Gases in Polyethylene Terephthalale", J. Appl. Phys., **34**, 1 (1963).

Moe, M., Koros, W. J., Hoehn, H. H., and Husk, G. R., "Effects of Film History on Gas Transport in a Fluorinated Aromatic Polyimide", J. Appl. Polym. Sci., **36**, 1833 (1988).

Mohr, J. M. and Paul, D. R., "Effect of Casting Solvent on the Permeability of Poly(4-methyl-1-pentene), Polymer, **32**, 1236 (1991).

O'Brien, K. C., Koros, W. J. and Husk, G. R., "Influence of Casting and Curing Conditions on Gas Sorption and Transport in Polyimide Films", Polym. Eng. Sci., **27**(3), 211 (1987).

Okuno, H., Renzo, K. and Uragami, T., "Influence of Casting Solution Additive, Degree of Polymerization, and Polymer Concentration on Poly(vinyl chloride) Membrane Properties and Performance", J. Membrane. Sci., **83**, 199 (1993).

Pacter, A. and Nerurkar, M., "Crystallization in Films of Polar Vinyl Polymers I. Crystallinity of Polyvinyl Alcohol Films Prepared by Evaporation of Aqueous Solutions", Eur. Polymer J., **4**(6), 685 (1968).

Park, J. Y. and Paul, D. R., "Correlation and Prediction of Gas Permeability in Glassy Polymer Membrane Materials via Modified Free Volume based Group Contribution Method", J. Membrane Sci., **125**, 23 (1997).

Paul, D. R. and Koros, W. J., "Effect of Partially Immobilizing Sorption on Permeability and the Diffusivity Time-Lag", J. Polym. Sci., Polym. Phys. Ed., **14**, 675 (1976).

Pedretti, U., Gandini, A., Roggero, A., Sisto, C., Valentini, C., Assogna, A. and Stopponi, A., "Process for Preparing Modified Poly(2,6-dimethyl-P-oxyphenylene)", US Patent 5,169,416, Dec, 1992.

Percec, S., and Li, G., "Chemical Modification of Poly(2,6-dimethyl-1,4-phenylene oxide) and Properties of Resulting Polymers", ACS Symp. Ser. 364, American Chemical Society, Washington, DC, 16, 1988.

Percec, S., "Chemical Modification of Poly(2,6-dimethyl-1,4-phenylene oxide) by Friedel-Crafts Reactions", J. Appl. Polym. Sci., **33**, 191 (1987).

Pesek, S. C. and Koros, W. J., "Aqueous quenched asymmetric polysulfone membranes prepared by dry/wet phase separation", J. Membrane Sci., **81**, 71 (1993).

Petropoulos, J. H., "Quantitative Analysis of Gaseous Diffusion in Glassy Polymers", J. Polym. Sci., Part A-2, **8**, 1797 (1970).

Plate, N. A. and Yampol'skii, Yu., "High Free Volume Polymers", in Polymer Gas Separation Membranes, eds. Paul, D. R. and. Yampol'skii, Yu., CRC Press, London 1994, p. 156.

Polotskaya, G. A., Agranova, S. A., Gazdina, Yu., Kuznetsov P. and Nesterov, V. V., "Effect of Molecular Weight Parameters on Gas Transport Properties of Poly(2,6-dimethyl-1,4-phenylene oxide)", J. Appl. Polym. Sci., **62**, 2215 (1996).

Plummer, C. W., Kimura, G., and LaConti, A. B., "Development of SPPO Membranes for Reverse Osmosis", Office of Saline Water Research and Development Progress Report No. 551, General Electric Co., Lynn, Mass., 1970.

Prasad, R., "Comparison of Gas Separation Technologies" in Polymer Gas Separation Membranes, eds. Paul, D. R. and. Yampol'skii, Yu, CRC Press, London 1994.

Puleo, A. and Paul, D. R., "Selective Gas Transport in Miscible PPO-PS Blends, Polymer, **26**, 2055 (1989).

Rao, C. N. R., "Chemical Applications of Infrared Spectroscopy", Academic Press, New York, NY 1963, p. 617.

Robertson, R. E., "Polymer Order and Polymer Density", J. Phys. Chem., **69**, 1575 (1965).

Robeson, L. M., "Correlation of Separation Factor versus Permeability for Polymeric Membranes", J. Membrane Sci., **62**, 165 (1991).

Rodriguez, F., "Principles of Polymer Systems", Hemisphere Publishing Corporation, New York, NY 1989.

Salame, M., "Prediction of Gas Barrier Properties of High Polymers", Polym. Eng. Sci., **26**, 1543 (1986).

Schultz, R. and Asunmaa, S., "Ordered Water and the Ultrastructure of Cellular Plasma Membrane", Recent Progr. Surface Sci., **3**, 291 (1970).

Smid, C. P., Albers, J. H. M., and Kusters, A. P. M., "The Formation of Asymmetric Hollow Fiber Membranes for Gas Separation Using PPO of Different Intrinsic Viscosities", J. Membrane Sci., **64**, 121 (1991).

Sourirajan, S. and Matsuura, T., "Reverse Osmosis and Ultrafiltration: Science and Principles" NRCC Publ. 24188, 1985.

Sourirajan, S., "Reverse Osmosis and Synthetic Membranes", NRCC Publ. 15627, 1977.

Sourirajan, S., "The Interface-Morphology-Transport Approach to Membrane Separations and Cellulosic Membranes", J. Institution Eng. Singapore, **32**(3), 49 (1992).

Stern, S. .A., "Polymer for Gas Separations: the Next Decade", J. Membrane Sci., **94**, 1 (1994).

Story, B. J., and Koros, W. J., "Sorption and Transport of CO_2 and CH_4 in Chemically Modified Polyphenylene Oxide", J. Membrane Sci., **67**, 191 (1992).

Tabe Mohammadi, A., Matsuura, T. and Sourirajan, S., "Design and Construction of Gas Permeation System for Measurement of Low Permeation Rates and Permeate Compositions", J. Membrane Sci., **98**, 281 (1995).

Teplyakov, V. and Meares, P., "Correlation Aspects of the Selective Gas Permeabilities of Polymeric Materials and Membranes", Gas Sep. Puriff., **4**, 66 (1990).

Toi, K., Morel, G. and Paul, D. R., "Gas Sorption and Transport in Polyphenylene Oxide and Comparison with other Glassy Polymers", J. Appl. Polym. Sci., **27**, 2997(1982).

Uhlhorn, R. J. R., Keizer, K. and Burggaaf, A.J., "Gas and Surface Diffusion in Modified Gamma Alumina Systems", J. Membrane Sci., **46**, 225 (1989).

Van Dyk, J. W., Frisch, H. L. and Wu, D. T., "Solubility, Solvency, and Solubility Parameters", Ind. Eng. Chem. Prod. Res. Dev., **24**(3), 473 (1985).

Van Krevelen, D.W., "Properties of Polymers: Their Estimation and Correlation with Chemical Structure", Elsevier, Amsterdam, 1976.

Vieth, W. R. and Sladek, K. J., "A Model for Diffusion in Glassy Polymers", J. Colloid Sci., **20**, 1014 (1965).

Volkov, V. V., Khotimsky, V. S., Gokzshaev, M. B., Litvinova, E. G., Fadeev A. G. and Kelley, S. S., "Density and Free Volume of Poly[1-(trimethylsilyl)-1-propyne] Dense Films for Bioethanol Concentration by Organophilic Pervaporation Method", Rus. J. Phys. Chem., **71**, N9 (1997).

White, L. S., Blinka, T. A., Kloczewski, J. and Wang, I., "Properties of a Polyimide Gas Separation Membrane in Natural Gas Streams", J. Membrane Sci., **103**, 73 (1995).

Zolandz, R. and Fleming, G. K., "Gas Permeation" in Membrane Handbook, eds. Ho, W. S. W. and Sirkar, K. K., Van Nostrand Reinhold, New York, NY, 1992.

Zubov, P., Voronkov, V. and Sukhareva, L., "Effect of the Solvent and Polymer-Solid Interactions on the Structure and Properties of Polystyrene", in Chem. Abstr., **68**, 96306g, (1968).

Appendix A

NMR Spectroscopy

The analysis of the ^{1}H NMR spectrum of SPPO allows for determination of the degree of sulfonation (*DS*) and hence the ion exchange capacity (*IEC*) of the polymer. The following is the example of such analysis.

Figure A-1 presents the ^{1}H NMR spectrum of Batch No. 2 of HSPPO. One can notice a number of peaks in Figure A-1. Table A-1 summarizes the locations and intensities of the peaks observed in Figure A-1.

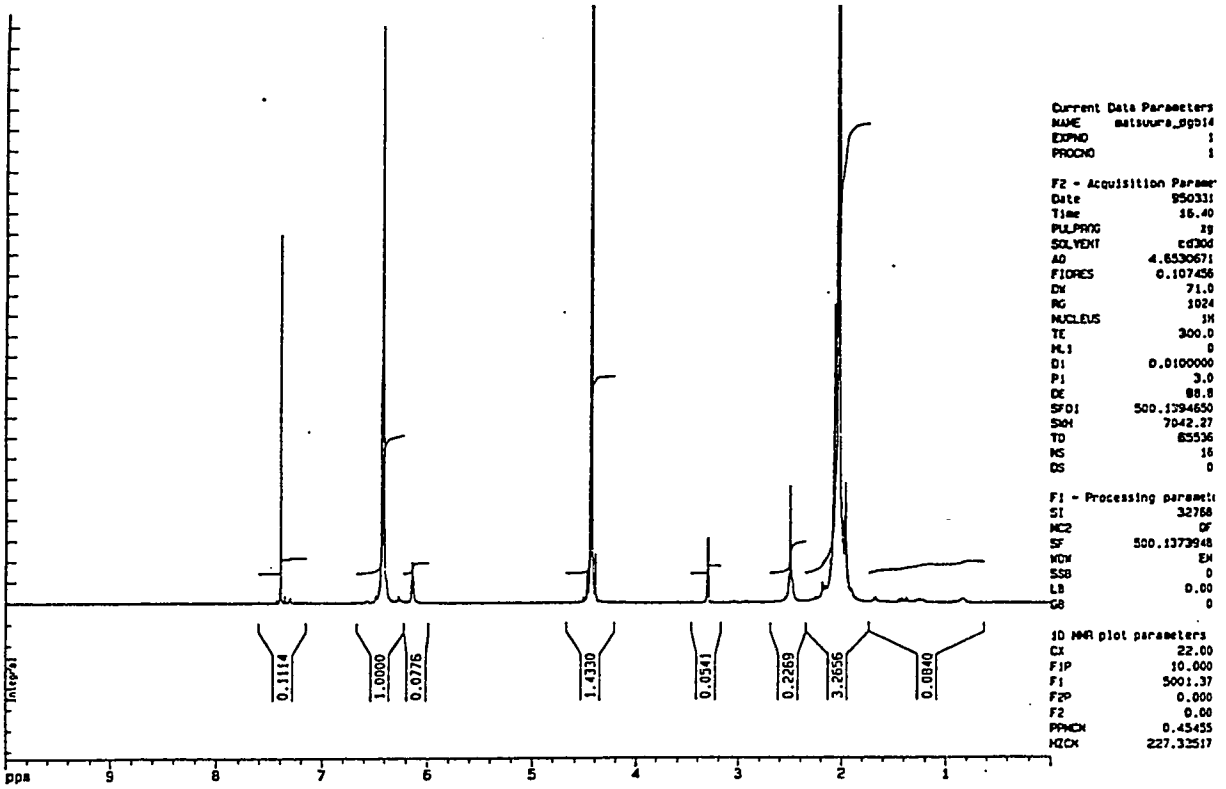

Figure A-1 ^{1}H NMR spectrum of Batch No.2 of HSPPO.

Table A-1 Summary of the ^{1}H NMR spectrum of Batch No. 2 of HSPPO.

Peak No.	Position, ppm	Intensity	Source
1	7.40	0.1114	$CDCl_3$
2[a]	6.42	1.0000	Ar-H
3[b]	6.14	0.0776	Ar-H
4	4.44	1.4330	OH/OD
5	3.30	0.0541	CD_3OD
6[b]	2.50	0.2269	Ar-CH_3
7[a]	2.03	3.2356	Ar-CH_3

[a] Unsubstituted PPO unit
[b] Substituted PPO unit

Peaks 1 and 5 come from the deuteron in chloroform-*d* and the deuterons in methyl-d_3 alcohol-*d*, respectively. The mixture of chloroform-*d* and methyl-d_3 alcohol-*d* was used for dissolving the polymer sample. Peak 4 comes from the protons in water and sulfonic groups. Peaks 1, 4, and 5 are not considered in the further analysis.

Peaks 2 and 3 come from the protons attached to the unsubstituted and substituted PPO units, respectively. If there are two units, one substituted and one unsubstituted, the intensity of peak 2 (I_2) will be twice the intensity of peak 3 (I_3). This is due to the fact that the sulfonic group replaces one of the aromatic protons on the substituted unit. The degree of sulfonation (*DS*) of SPPO can be calculated from the following equation

(A.1)

Using the peak intensities listed in Table A-1, the *DS* of Batch No.2, calculated by Eq. (A.1), is equal to 0.134. The *IEC* and The *DS* are related by the following equation

(A.2)

where 200 and 120 are the molecular weights of the substituted and unsubstituted PPO repeat units, respectively. The *IEC* of Batch No.2, calculated by Eq. (A.2), is equal to 1.03 meq/g.

Alternatively, the *DS* can be determined based on the intensity of peak 6 (I_6) and the intensity of peak 7 (I_7). Peak 6 comes from the protons attached to the methyl group in the *ortho* position relative to the sulfonic group. Peak 7 comes from the protons attached to the methyl group in the *para* position relative to the sulfonic group and from the protons attached to the methyl groups of the unsubstituted PPO units. Based on I_6 and I_7, the *DS* can by calculated by

(A.3)

Using the peak intensities listed in Table A-1, the *DS* of Batch No.2, calculated by Eq. (A.3), is equal to 0.130. Considering Eq. (A-2), the *DS* of 0.130 corresponds to the *IEC* equal to 1.00 meq/g.

The *DS* calculated by Eqs. (A.1) and (A.3) are slightly different. The value calculated by Eq. (A.1) is considered more reliable and is used to represent the *DS* and hence the *IEC* of polymer determined by ^{1}H NMR in Table 6-1.

Appendix B

Evaluation of Solubility Parameters

Solubility parameter data is available for a wide variety of solvents and some polymers. It can also be generated using a group contribution method. The comparison of the solubility parameters of polymer and solvent provides the basis for the evaluation of the polymer-solvent interactions.

B.1 Solvents

The Hansen and Hildebrand solubility parameters of solvents considered for dissolution of SPPO are presented in Table B-1. These solvents include, acetone, chloroform, N,N-dimethylacetamide (DMAC), N,N-dimethylformamide (DMF), methanol, nitroethane, N-methyl-2-pyrrolidone (NMP), pyridine, trichloroethylene (TCE), and tetrahydrofuran (THF). The total solubility parameter (δ_t) is calculated from Eq. (B.1) using the Hansen solubility parameters, and its value is compared with the Hildebrand parameter (δ).

$$\delta^2 = \delta_d^2 + \delta_p^2 + \delta_h^2 \qquad \text{(B.1)}$$

where δ_d is the dispersive term, δ_p is the polar term, and δ_h is the hydrogen bond term. It can be noticed that in general δ_t and δ are close to each other for all solvents. The only exception is the nitroethane for which δ is 9% greater than δ_t.

Another comprehensive list of three-component solubility parameters was compiled by Hoy (1970). Similarly to Hansen, the Hoy parameters represent the dispersive, polar, and hydrogen bond components of the solubility parameter. Table B-2 shows the summary of Hoy solubility parameters along with the total and Hildebrand solubility parameters for the solvents listed in Table B-1. The total solubility parameter (δ_t) in Table B-2 was calculated from Eq. (B.1) using the Hoy solubility parameters, and its value can be compared with the Hildebrand parameter (δ).

Table B-1. Hansen and Hildebrand solubility parameters for selected organic solvents [Hansen and Beerbower, 1971].

	δ_d $MPa^{1/2}$	δ_p $MPa^{1/2}$	δ_h $MPa^{1/2}$	δ_t $MPa^{1/2}$	δ $MPa^{1/2}$
Acetone	15.5	10.4	7.0	19.9	20.3
Chloroform	17.8	3.1	5.7	19.0	19.0
DMAC	16.8	11.5	10.2	22.8	22.1
DMF	17.4	13.7	11.3	24.8	24.8
Methanol	15.1	12.3	22.3	29.6	29.7
Nitroethane	16.2	12.1	4.1	20.6	22.7
NMP	18.0	12.3	7.2	23.0	23.1
Pyridine	19.0	8.8	5.9	21.7	21.9
TCE	18.0	3.1	5.3	19.0	18.8
THF	16.8	5.7	8.0	19.5	18.6

Table B-2. Hoy and Hildebrand solubility parameters for selected organic solvents [Hoy, 1985].

	δ_d $MPa^{1/2}$	δ_p $MPa^{1/2}$	δ_h $MPa^{1/2}$	δ_t $MPa^{1/2}$	δ $MPa^{1/2}$
Acetone	13.0	9.8	11.0	19.7	20.3
Chloroform	11.0	13.7	6.3	18.7	19.0
DMAC	-	-	-	-	22.1
DMF	-	-	-	-	24.8
Methanol	11.6	13.0	24.0	29.7	29.7
Nitroethane	19.0	13.0	0	23.0	22.7
NMP	16.5	10.4	13.5	23.7	23.1
Pyridine	17.6	10.1	7.7	21.7	21.9
TCE	11.7	14.0	4.4	18.8	18.8
THF	13.3	11.0	6.7	18.5	18.6

In general, the total solubility parameters based on Hansen and Hoy parameters are close to each other. The exception is nitroethane, for which δ_t based on the Hoy solubility parameters is more than 10 % greater than δ_t based on the Hansen solubility parameters. On the other hand, the

differences between Hansen and Hoy values are more significant in individual parameters. It can be noticed in Tables B-1 and B-2 that there exist pairs of solvents (TCE and THF, pyridine and DMAC), for which the Hildebrand parameters are similar while the Hansen and Hoy parameters are quite different. This is not surprising considering that Hansen and Hoy used different approaches for the estimation of their parameters [Barton, 1983]. Except for nitroethane, Hansen δ_d parameters are larger than Hoy δ_d parameters. Consequently, Hoy δ_p and δ_h parameters are generally larger than Hansen δ_p and δ_h parameters. The Hoy dispersion parameters are considered less reliable than the Hansen dispersion parameters, whereas for the hydrogen bond components the situation is opposite [Barton, 1983]. The Hoy solubility parameters for DMAC and DMF are not available. In general, the Hansen solubility parameters cover a more comprehensive list of solvents than the Hoy solubility parameters.

In this study the Hansen solubility parameters were chosen for the evaluation of polymer-solvent interactions. It should; however, be emphasized that the choice of the Hansen parameters over the Hoy parameters is based on the availability of the former parameters for a wider spectrum of solvents.

B.2 Polymers

Hildebrand and Hansen solubility parameters have been determined experimentally for a limited number of polymers. For most polymers these parameters are estimated using a group contribution approach. This method requires decomposition of the repeat unit of polymer into functional groups. In case of HSPPO, the repeat unit can be divided into

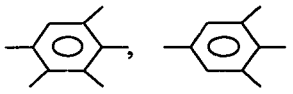 , , —CH_3, —SO_3H, and —O— .

The sulfonic group can further be divided into SO_2 and OH groups. Table B-3 shows the components of the repeat unit of HSPPO along with the cohesion parameters and molar volumes for each group. The numerical values presented in this table are based on the data listed by Matsuura (1993).

Cohesion parameters listed in Table B-3 are used for calculation of the Hildebrand and Hansen solubility parameters. Van Krevelen (1976) proposed the following equations

$$\delta = \sqrt{\sum E_{coh,i} / V_i} \quad \text{(B.2)}$$

$$\delta_d = \sum F_{d,i} / V_i \quad \text{(B.3)}$$

$$\delta_p = \sqrt{\sum F_{p,i}^2} / V_i \quad \text{(B.4)}$$

$$\delta_h = \sqrt{\sum E_{h,i} / V_i} \quad \text{(B.5)}$$

where $E_{coh,i}$, is the structural component of the overall solubility parameter and $F_{d,i}$, $F_{p,i}$, $E_{h,i}$ are the dispersion force, the dipole force, and the hydrogen bonding force components of the solubility parameter, respectively.

Table B-3 Group contributions to the Hildebrand (V_i and $E_{coh,i}$) and Hansen ($V_{i,g}$, $F_{i,d}$, $F_{p,i}$, and $E_{h,i}$) solubility parameters [Matsuura, 1993].

Group	Frequency	V_i cm^3/mol	$E_{coh,i}$ J/mol	$V_{g,i}$ cm^3/mol	$F_{d,i}$ J$^{1/2}$cm$^{3/2}$ /mol	$F_{p,i}$ J$^{1/2}$cm$^{3/2}$ /mol	$E_{h,i}$ J/mol
benzene[a]	*DS*	- 4.6	31,925	72.9	1,368	111	0
benzene[b]	1-*DS*	14.4	31,925	72.9	1,368	111	0
-CH_3	2	33.5	4,707	23.9	419	0	0
-O-	1	3.8	3,347	10.0	100	401	3,000
-SO_2-	*DS*	23.6	39,121	31.8	591	-	13,490
-OH	*DS*	10.0	29,791	9.7	211	458	19,987

a 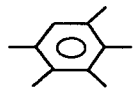 benzene ring with 5 substitutions

b 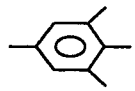 benzene ring with 4 substitutions

It can be noticed that for each group there are two different molar volumes. The Hildebrand parameter is calculated from Eq. (B.2) using the molar volume denoted as V, while the components of the Hansen solubility parameter are calculated from Eqs. (B.3)–(B.5) using the molar volume denoted as V_g [Matsuura, 1993].

The contribution to the polar component of SO_2 group is not available. Hence, Eq. (B.4) cannot be used for the calculation of the polar component of the solubility parameter of HSPPO. Rearranging Eq. (B.1), the polar component of the solubility parameter can be calculated from

$$\delta_p = \sqrt{\delta^2 - \delta_d^2 - \delta_h^2} \quad \text{(B.6)}$$

The summary of the Hildebrand solubility parameter and the components of the Hansen solubility parameter for HSPPO of different *IEC* values are presented in Table B-4.

Table B-4 Hildebrand solubility parameter and components of Hansen solubility parameter for HSPPO of different *IEC*.

IEC[a] meq/g	*DS*	δ $MPa^{1/2}$	δ_d $MPa^{1/2}$	δ_p $MPa^{1/2}$	δ_h $MPa^{1/2}$
0	0	22.90	17.65	13.78	4.79
0.72	0.092	24.27	17.70	15.19	6.72
1.01	0.132	24.84	17.72	15.76	7.38
1.37	0.185	25.54	17.75	16.48	8.14
1.80	0.252	26.40	17.77	17.32	8.98

[a] The relationship between *IEC* and *DS* is given by Eq. (5.1)

It is evident from Table B-4 that both Hildebrand and Hansen solubility parameters increase with an increase in *IEC* of polymer. This increase is not the same for all parameters. For example, when *IEC* increases from 0 to 1.80 meq/g, δ_d increases only by 0.7%, while δ increases by 15%. The maximum increase of 87% is observed for δ_h, which is not surprising considering that sulfonic groups are very electrophilic and have a strong tendency to form hydrogen bonds via OH groups.

It should be emphasized that δ_p of PPO shown in Table B-2 was calculated in the same way as the polar component of the Hansen solubility parameter of HSPPO, that is by using Eq. (B.6). On the other hand, δ_p of PPO can also be calculated directly from Eq. (B.4). The polar component of the solubility parameter of PPO calculated from Eq. (B4) is equal to 3.19 $MPa^{1/2}$, whose value is much smaller than the value listed in Table B2 (13.78 $MPa^{1/2}$). This difference illustrates the uncertainty associated with the estimation of the solubility parameters for polymers.

Appendix C

Prediction of Density and Permeability of HSPPO

The experimental density and permeability of HSPPO obtained in this study have been compared to the values predicted by the modified free volume model proposed recently by Park and Paul (1997). In this appendix the details of the model along with the relevant calculations are presented.

There are two new features in the modified free volume model: (1) introduction of a group dependent constant in the equation for specific volume of polymer, (2) allowing the fractional free volume of the polymer to be different for different gases in the polymer.

C.1 Prediction of Density

The molar volume of polymer (V) is predicted by Eq. (2.24)

$$V = \sum_{k=1}^{K} \beta_k (V_W)_k \tag{2.24}$$

where β_k is a constant depending on the type of group and $(V_W)_k$ is the van der Waals volume for group k.

Table C-1 presents the groups contributing to the repeat unit of HSPPO and the values of β_k and $(V_W)_k$ for these groups. The frequency of occurrence of given group in the repeat unit of HSPPO is given in column 2 within Table C-1.

Table C-1. Group constants for prediction of molar volume of HSPPO.

Group	frequency	V_W, cm^3/mol	β
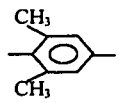	1	65.6	1.66
-SO_2-	*DS*	20.3	1.21
-O-	1+*DS*	5.5	0.772
-H	*DS*	3.44	0.400

Knowing the molar volume of the repeat unit, the density (ρ) of the polymer is calculated by

$$\rho = \frac{M}{V} \tag{C.1}$$

Molecular weight (M) of the repeat unit of HSPPO depends on the degree of sulfonation of polymer

$$M = 120 + 80DS \tag{C.2}$$

where 120 is the molecular weight of the PPO repeat unit and 80 is the molecular weight of the sulfonic group.

Table C-2 presents the summary of density calculations for HSPPO of different *IEC* values. The values of the density from Table C-2 have been plotted along with the values of the experimentally measured densities in Figure 6-1.

Table C-2. Effect of *IEC* on the density of HSPPO determined by the modified free volume model.

IEC,[a] meq/g	*DS*	*M*, g/mol	*V*, cm^3/mol	ρ, g/cm^3
0	0	120.0	113.1	1.061
0.72	0.092	127.3	115.9	1.099
1.01	0.132	130.4	117.1	1.114
1.37	0.185	134.8	118.7	1.135
1.80	0.252	140.0	120.7	1.160

[a] The relationship between *IEC* and *DS* is given by Eq. (5.1)

C.2 Prediction of Permeability

Permeability (P) of polymer for a given gas is predicted by the following equation

$$P = A_p \exp\frac{-B_p}{(FFV)_n} \tag{C.3}$$

where A_p and B_p are the constants depending on the gas and $(FFV)_n$ is the fractional free volume of polymer for a given gas. Eq. (C.3) has a similar form as the equation proposed by Lee (1980) (Eq. 2.22), except for it requires the values of *FFV* rather than the values of *SFV*. The constants A_p and B_p for the gases considered in this study are presented in Table C-3.

Table C-3. Constants A_p and B_p for determination of permeability by the fractional free volume of polymer.

	N_2	O_2	CH_4	CO_2
A_p	112	379	114	1750
B_p	0.914	0.839	0.967	0.860

The fractional free volume for a given gas is calculated from the following equation

$$(FFV)_n = \frac{V - (V_o)_n}{V} \tag{C.4}$$

where V is the molar volume of polymer, which is calculated by Eq. (C1) and $(V_o)_n$ is the molar volume of polymer chains, which is seen by a given gas. The value of $(V_o)_n$ is determined from Eq. (2.25)

$$(V_o)_n = \sum_{k=1}^{K} \gamma_{nk} (V_W)_k \tag{2.25}$$

where $(V_W)_k$ is the van der Waals volume for group k and γ_{nk} represents the set of empirical factors depending on a given gas n and group k. The values of $(V_W)_k$ for the groups contributing to the HSPPO repeat unit have been presented in Table C-1. The values of γ_{nk} for the groups contributing to the repeat unit of HSPPO and the gases considered in this study are presented in Table C-4.

Table C-4 Set of empirical parameters for determination of the specific volume occupied by HSPPO chains seen by different gases.

Group	frequency	$\gamma(N_2)$	$\gamma(O_2)$	$\gamma(CH_4)$	$\gamma(CO_2)$
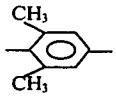	1	1.17	1.17	1.16	1.16
$-SO_2-$	*DS*	0.715	0.708	0.703	0.738
-O-	1+*DS*	2.43	2.51	2.51	2.68
-H	*DS*	0.520	0.526	0.551	0.513

Table C-5 summarizes predicted permeabilities of HSPPO of different *IEC* values for the gases considered in this study.

Table C-5. Effect of *IEC* on predicted permeabilities of HSPPO for different gases[a].

IEC, meq/g	$P(N_2)$	$P(O_2)$	$P(CH_4)$	$P(CO_2)$
0	1.255	5.935	1.029	22.31
0.72	1.135	5.374	0.900	19.58
1.01	1.088	5.153	0.850	18.52
1.37	1.026	4.860	0.784	17.13
1.80	0.956	4.530	0.713	15.59

[a] All permeabilities in Barrer

Appendix D

Permeability Through Series of Membranes

Some membranes under investigation were defective. In order to seal the defects in the membrane structure, the membranes were laminated with a silicone rubber film. Permeation rate, which is measured from the laminated membrane, cannot be used directly for the calculation of the membrane permeability, because of the influence of the laminating layer. Gas permeation through a laminated membrane represents the example of gas permeation through a series of membranes. Figure D-1 shows the schematic representation of gas permeation through two membranes in series.

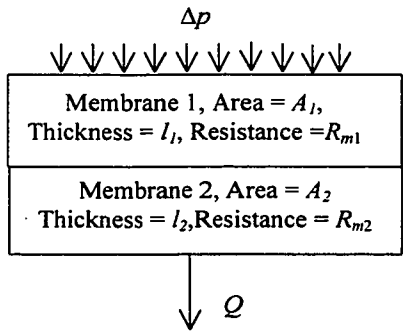

Figure D-1. Gas permeation through a series on membranes

Gas permeation rate is proportional to the pressure gradient (Δp) and inversely proportional to the membrane resistance (R_m)

$$Q = \frac{\Delta p}{R_m} \tag{D.1}$$

The membrane resistance is proportional to the membrane thickness (l) and inversely proportional to the membrane permeability (P) and membrane area (A)

$$R_m = \frac{l}{PA}. \tag{D.2}$$

The total resistance for the membrane in series is the sum of individual resistances

$$R_m = R_{m1} + R_{m2}. \tag{D.3}$$

Dividing both sides of Eq. (D.3) by Δp yields

$$\frac{R_m}{\Delta p} = \frac{R_{m1}}{\Delta p} + \frac{R_{m2}}{\Delta p}. \tag{D.4}$$

Substituting Eqs. (D.1) and (D.2) into Eq. (D.4) yields

$$\frac{1}{Q} = \frac{l_1}{P_1 A_1 \Delta p} + \frac{l_2}{P_2 A_2 \Delta p}. \tag{D.5}$$

Assuming that $A_1 = A_2 = A$, Eq. (D.5) can be rearranged to calculated P_2

$$P_2 = \frac{Q l_2 P_1}{P_1 A \Delta p - Q l_1}. \tag{D.6}$$

Therefore, knowing permeability of one membrane permeability of the other membrane can be determined by measuring gas permeation rate through the series of two membranes. Eq. (D.6) also requires thicknesses of the membranes, pressure gradient across the membrane and the area of the membrane. These parameters can be easily measured.

Silicone rubber (dimethyl siloxane) used in this study had thickness equal to 50.8 μm. Gas permeabilities of silicone rubber were provided by the manufacturer (General Electric Company, Selkirk, NY). These values are presented in Table D-1.

Table D-1. Permeabilities of various gases through the silicone rubber membranes.

Gas	N_2	O_2	CH_4	CO_2
P, Barrer	25	50	80	270